

EXPERIMENTAL DETERMINATION OF PRESTRESSING WIRE BOND AND SPLITTING  
PROPENSITY CHARACTERISTICS THROUGH TENSIONED PULLOUT TESTS

by

JOSEPH ROBERT HOLSTE

B.S., Kansas State University, 2008  
M.S., Kansas State University, 2010

AN ABSTRACT OF A DISSERTATION

submitted in partial fulfillment of the requirements for the degree

DOCTOR OF PHILOSOPHY

Department of Civil Engineering  
College of Engineering

KANSAS STATE UNIVERSITY  
Manhattan, Kansas

2014

## **Abstract**

This dissertation describes a testing program to evaluate the bond and splitting propensity characteristics of 5.32-mm-diameter prestressing wires. Prestressing wire reinforcement is used primarily in the production of prestressed concrete railroad ties. Twelve different 5.32-mm-diameter wires were tested in this study in order to measure bonding characteristics of the reinforcement. Establishment of the bond-slip characteristics of these reinforcement at both transfer of prestress (transfer bond) and under flexural loading (flexural bond) is necessary to enable the accurate modeling of these ties using finite elements. Transfer bond and flexure bond of various indent patterns were tested using tensioned pullouts. Specimens of various sizes with single or multiple wires were tested to determine the effects of cover and wire number on bond. Indents were machined on smooth prestressing wires to accurately compare indent geometries. Lateral expansion was tested to determine which wires have higher propensity to cause cracking or splitting. Crossties were instrumented to compare resulting lateral expansion with results found in the laboratory.

The results from the testing program showed that the tensioned pullout test was able to be used to predict the transfer length of prisms made with the same reinforcement. The results also showed that the indent geometries were able to be used to predict the splitting of specimens based on the amount of slip the wire had experienced. The testing also showed the importance of concrete cover with the relation to splitting potential.

EXPERIMENTAL DETERMINATION OF PRESTRESSING WIRE BOND AND SPLITTING  
PROPENSITY CHARACTERISTICS THROUGH TENSIONED PULLOUT TESTS

by

JOSEPH ROBERT HOLSTE

B.S., Kansas State University, 2008  
M.S., Kansas State University, 2010

A DISSERTATION

submitted in partial fulfillment of the requirements for the degree

DOCTOR OF PHILOSOPHY

Department of Civil Engineering  
College of Engineering

KANSAS STATE UNIVERSITY  
Manhattan, Kansas

2014

Approved by:

Major Professor  
Dr. Robert J. Peterman

# **Copyright**

JOSEPH ROBERT HOLSTE

2014

## **Abstract**

This dissertation describes a testing program to evaluate the bond and splitting propensity characteristics of 5.32-mm-diameter prestressing wires. Prestressing wire reinforcement is used primarily in the production of prestressed concrete railroad ties. Twelve different 5.32-mm-diameter wires were tested in this study in order to measure bonding characteristics of the reinforcement. Establishment of the bond-slip characteristics of these reinforcement at both transfer of prestress (transfer bond) and under flexural loading (flexural bond) is necessary to enable the accurate modeling of these ties using finite elements. Transfer bond and flexure bond of various indent patterns were tested using tensioned pullouts. Specimens of various sizes with single or multiple wires were tested to determine the effects of cover and wire number on bond. Indents were machined on smooth prestressing wires to accurately compare indent geometries. Lateral expansion was tested to determine which wires have higher propensity to cause cracking or splitting. Crossties were instrumented to compare resulting lateral expansion with results found in the laboratory.

The results from the testing program showed that the tensioned pullout test was able to be used to predict the transfer length of prisms made with the same reinforcement. The results also showed that the indent geometries were able to be used to predict the splitting of specimens based on the amount of slip the wire had experienced. The testing also showed the importance of concrete cover with the relation to splitting potential.

# Table of Contents

List of Figures .....	ix
List of Tables .....	xvii
Acknowledgements.....	xviii
Chapter 1 Introduction .....	1
1.1 Background.....	1
1.2 Objectives .....	2
1.3 Scope.....	3
Chapter 2 Literature Review.....	5
2.1 Railroad Tie Background and Production .....	5
2.2 Transfer Length.....	8
2.3 Pullouts .....	10
2.4 Wire Geometries .....	14
2.5 Experimental Measurement Devices .....	16
2.6 Splitting and Cracking Behavior.....	18
2.7 Crack Splitting and Bond Modeling .....	19
2.8 Cyclic Loading.....	21
Chapter 3 Testing Frame Setup.....	22
Chapter 4 Wire Reinforcements.....	28
Chapter 5 Concrete Mix Details .....	31
5.1 Mix A Details.....	34
5.2 Mix B Details.....	35
5.3 Batching Procedure.....	35
Chapter 6 Preliminary Testing to Determine Bond Length .....	45
Chapter 7 Transfer Bond Testing.....	49
7.1 Transfer Bond Test Setup .....	49
7.2 Transfer Bond Test Results.....	54
Chapter 8 Flexural Bond Testing.....	62
8.1 Flexural Bond Test Setup .....	62

8.2 Flexural Bond Test Results.....	62
Chapter 9 Confinement and Cover Tests .....	68
9.1 Confinement and Cover Test Setup .....	68
9.2 Confinement and Cover Test Results .....	74
Chapter 10 2-inch-Diameter Specimen Splitting Tests .....	79
10.1 2-inch-Diameter Specimen Splitting Test Setup .....	79
10.2 2-inch-Diameter Specimen Splitting Test Results.....	80
Chapter 11 Expansion Testing .....	84
11.1 Non-Contact Lasers .....	84
11.2 LVDTs .....	86
11.3 Surface Mounted Strain Gauges .....	90
11.4 Internal Vibrating-Wire Strain Gauges.....	93
11.5 VWSG Results.....	99
Chapter 12 Machined Wire Testing.....	107
12.1 Machined Wire Test Setup .....	107
12.2 Machined Wire Test Results.....	109
Chapter 13 4-Wire vs Single Wire Testing.....	132
13.1 Unreinforced 4-Wire Test Setup.....	132
13.2 Unreinforced 4-Wire Results .....	136
13.3 Reinforced 4-Wire Test Setup .....	145
13.4 Reinforced 4-Wire Results.....	149
Chapter 14 Crosstie Manufacturing Plant Instrumentation .....	156
14.1 Instrumentation of Crossties .....	156
14.2 Crosstie Production.....	162
14.3 VWSG Results.....	170
Chapter 15 Conclusions .....	172
Bibliography .....	175
Appendix A Confinement and Cover Additional Tests .....	182
Appendix B 2-inch Diameter Cylinder Results .....	198
Appendix C VWSG Test Graphs .....	202
Appendix D 4-Wire vs. Single Wire Test Graphs .....	207

Appendix E Plant readings..... 209



## List of Figures

Figure 3.1 Frame setup involving a screw jack at the top of the frame .....	23
Figure 3.2 Frame setup involving screw jacks on top and bottom of frames .....	23
Figure 3.3 Screw jack and S-type load cell arrangement.....	24
Figure 3.4 Plate load cell attached to bottom screw jack.....	25
Figure 3.5 Plate load cell attached to top screw jack.....	25
Figure 3.6 LVDT setup to measure end-slip.....	26
Figure 3.7 Data acquisition system for recording measurements .....	27
Figure 4.1 Wires used in the study (Courtesy Matthew Arnold).....	29
Figure 4.2 Five wires used for a majority of testing (Left to Right: WA, WE, WG, WH, WK)..	30
Figure 5.1 Fine aggregate used in the study .....	32
Figure 5.2 3/8-inch coarse aggregate used in the study .....	33
Figure 5.3 #57 coarse aggregate used in the study .....	33
Figure 5.4 Mixer used in the study .....	36
Figure 5.5 Strength cylinders being vibrated.....	37
Figure 5.6 Test specimen being vibrated .....	37
Figure 5.7 Test specimen after top was finished.....	38
Figure 5.8 Finished test specimen covered with plastic .....	38
Figure 5.9 Smaller test specimen being rodded .....	39
Figure 5.10 Strength cylinders curing next to test specimens .....	40
Figure 5.11 Air-conditioned box used to match-cure .....	41
Figure 5.12 Temperature of test specimen and strength specimen during cure.....	41
Figure 5.13 Compression cylinder being tested.....	42
Figure 5.14 Split tensile specimen after testing .....	43
Figure 5.15 Close-up of split tensile specimen after failure .....	43
Figure 6.1 2-inch bond length test setup.....	46
Figure 6.2 4-inch bond length test setup.....	46
Figure 6.3 6-inch bond length test setup.....	47
Figure 6.4 Top force vs. bottom force of WF with various bond lengths.....	47

Figure 6.5 Top force vs. bottom force of WH with 2.5-inch bond length .....	48
Figure 7.1 Bond break and straw on wire .....	49
Figure 7.2 Metal split molds used.....	50
Figure 7.3 LDVTs mounted to the top of the specimen .....	51
Figure 7.4 LVDTs mounted to the bottom of the specimen .....	52
Figure 7.5 Top jack shaft being turned during testing .....	53
Figure 7.6 Bond stress vs. bottom slip relationship for WA (smooth) .....	54
Figure 7.7 Bond stress vs. bottom slip relationship for WE (spiral).....	55
Figure 7.8 Bond stress vs. bottom slip relationship for WG (chevron) .....	56
Figure 7.9 Bond stress vs. bottom slip relationship for WH (chevron) .....	56
Figure 7.10 Bond stress vs. bottom slip relationship for WK (four-dot).....	57
Figure 7.11 Average bond stress vs. bottom slip relationship for all five wires.....	58
Figure 7.12 Correlation of bond stress at 0.1 inches of bottom slip vs. transfer length .....	59
Figure 7.13 Correlation of bond stress at 0.05 inches of bottom slip vs. transfer length .....	59
Figure 7.14 Correlation of bond stress at 0.025 inches of bottom slip vs. transfer length .....	60
Figure 7.15 Correlation of bond stress at 0.01 inches of bottom slip vs. transfer length .....	60
Figure 8.1 Bond stress versus top slip results for WA (smooth) .....	63
Figure 8.2 Bond stress versus top slip results for WE (spiral).....	64
Figure 8.3 Bond stress versus top slip results for WG (chevron) .....	65
Figure 8.4 Bond stress versus top slip results for WH (chevron) .....	65
Figure 8.5 Bond stress versus top slip results for WK (four-dot).....	66
Figure 8.6 Bond stress vs. top slip results for the five reinforcements .....	67
Figure 9.1 Various cylinder sizes used in this study.....	68
Figure 9.2 4-inch-diameter specimen mold .....	69
Figure 9.3 2-inch-diameter specimen mold .....	70
Figure 9.4 2-inch-diameter specimen after being cast .....	70
Figure 9.5 2-inch-diameter specimen covered with plastic after casting.....	71
Figure 9.6 4-inch-diameter unconfined specimen before testing.....	72
Figure 9.7 4-inch-diameter confined specimen before testing.....	72
Figure 9.8 2-inch-diameter confined specimen before testing.....	73
Figure 9.9 2-inch-diameter unconfined specimen before testing.....	73

Figure 9.10 Confined and unconfined bond stress versus slip relationship for WA .....	74
Figure 9.11 Confined and unconfined bond stress versus slip relationship for WE.....	75
Figure 9.12 Confined and unconfined bond stress versus slip relationship for WG .....	76
Figure 9.13 Confined and unconfined bond stress versus slip relationship for WH .....	77
Figure 9.14 Confined and unconfined bond stress versus slip relationship for WK .....	78
Figure 9.15 Cracked 2-inch-diameter unconfined specimen after testing .....	78
Figure 10.1 Metal mold prior to casting .....	79
Figure 10.2 2-inch-diameter specimen after testing .....	80
Figure 10.3 Bond force versus bottom slip relationship for various indent patterns.....	81
Figure 10.4 Correlation findings from SAS program between bottom slip and indent depth .....	82
Figure 11.1 Laser head setup to measure lateral expansion.....	84
Figure 11.2 Laser head used to measure lateral expansion.....	85
Figure 11.3 Lateral expansion measured with lasers on 2-inch diameter WH specimen .....	85
Figure 11.4 Invar ring setup location on specimen.....	86
Figure 11.5 Lateral expansion measured with invar ring for WH specimen .....	87
Figure 11.6 WH specimen after testing with cracking .....	88
Figure 11.7 Lateral expansion measured on WA specimen .....	89
Figure 11.8 WA specimen after testing without cracking .....	89
Figure 11.9 Strain gauge location on specimen .....	91
Figure 11.10 Strain gauge specimen prior to testing .....	91
Figure 11.11 Comparison of surface strains on WH and WA specimens .....	92
Figure 11.12 Cracked WH specimen after testing.....	93
Figure 11.13 VWSG used in the study .....	94
Figure 11.14 VWSG specimen dimensions .....	95
Figure 11.15 Bond length and base taped before casting .....	95
Figure 11.16 Aluminum insert to secure VWSG in position.....	96
Figure 11.17 VWSG location prior to casting .....	97
Figure 11.18 Spacers used to keep cross section constant.....	97
Figure 11.19 Specimen after mold was removed.....	98
Figure 11.20 Specimen prior to testing.....	98
Figure 11.21 Bond stress and lateral expansion relationship with bottom slip for WA .....	99

Figure 11.22 WA specimen after testing .....	100
Figure 11.23 Bond stress and lateral expansion relationship with bottom slip for WE.....	101
Figure 11.24 Cracked WE specimen after testing .....	101
Figure 11.25 Bond stress and lateral expansion relationship with bottom slip for WG .....	102
Figure 11.26 WG specimen after testing .....	103
Figure 11.27 Bond stress and lateral expansion relationship with bottom slip for WH.....	104
Figure 11.28 Cracked WH specimen after testing.....	104
Figure 11.29 Bond stress and lateral expansion relationship with bottom slip for WK.....	105
Figure 11.30 Cracked WK specimen after testing.....	106
Figure 12.1 Machined indent patterns (Courtesy Mark Haynes).....	108
Figure 12.2 Machined wire before casting .....	109
Figure 12.3 Bond stress and lateral expansion relationship for shallow 15-degree indent.....	110
Figure 12.4 Shallow 15-degree indent specimen after testing.....	110
Figure 12.5 Bond stress and lateral expansion relationship for deep 15-degree indent .....	111
Figure 12.6 Deep 15-degree indent specimen after testing.....	112
Figure 12.7 Bond stress versus bottom slip relationship for both 15-degree indents.....	112
Figure 12.8 Bond stress and lateral expansion relationship for shallow 30-degree indent.....	113
Figure 12.9 Shallow 30-degree indent specimen after testing.....	114
Figure 12.10 Bond stress and lateral expansion relationship for deep 30-degree indent .....	115
Figure 12.11 Deep 30-degree indent specimen after testing.....	115
Figure 12.12 Bond stress versus bottom slip relationship for both 30-degree indents.....	116
Figure 12.13 Bond stress and lateral expansion relationship for shallow 45-degree indent.....	117
Figure 12.14 Shallow 45-degree indent specimen after testing.....	117
Figure 12.15 Bond stress and lateral expansion relationship for 45-degree deep indent .....	118
Figure 12.16 Deep 45-degree indent specimen after testing.....	119
Figure 12.17 Bond stress versus bottom slip relationship for both 45-degree indents.....	119
Figure 12.18 Bond stress and lateral expansion relationship for shallow 60-degree indent.....	120
Figure 12.19 Shallow 60-degree indent specimen after testing.....	121
Figure 12.20 Bond stress and lateral expansion relationship for deep 60-degree indent .....	122
Figure 12.21 Deep 60-degree indent specimen after testing.....	122
Figure 12.22 Bond stress versus bottom slip relationship for both 60-degree indents.....	123

Figure 12.23 Bond stress and lateral expansion relationship for shallow 75-degree indent.....	124
Figure 12.24 Shallow 75-degree indent specimen after testing.....	124
Figure 12.25 Bond stress and lateral expansion relationship for deep 75-degree indent .....	125
Figure 12.26 Deep 75-degree indent specimen after testing.....	126
Figure 12.27 Bond stress versus bottom slip relationship for both 75-degree indents.....	126
Figure 12.28 Bond stress and lateral expansion relationship for shallow 90-degree indent.....	127
Figure 12.29 Shallow 90-degree indent specimen after testing.....	128
Figure 12.30 Bond stress and lateral expansion relationship for deep 90-degree indent .....	129
Figure 12.31 Deep 90-degree indent specimen after testing.....	129
Figure 12.32 Bond stress versus bottom slip relationship for both 90-degree indents.....	130
Figure 12.33 Bond stress versus bottom slip relationship for all shallow indents.....	131
Figure 12.34 Bond stress versus bottom slip relationship for all deep indents.....	131
Figure 13.1 4-wire and single wire frame setup .....	132
Figure 13.2 4-wire specimen before casting.....	133
Figure 13.3 Single wire specimen before casting .....	134
Figure 13.4 Bottom LVDT locations for 4-wire specimen test .....	135
Figure 13.5 Top LVDT locations for 4-wire specimen test.....	135
Figure 13.6 Bond stress vs. bottom slip comparison for 4-wire and single wire test with WA .	136
Figure 13.7 WA 4-wire specimen after testing.....	137
Figure 13.8 WA single wire specimen after testing.....	137
Figure 13.9 Bond stress vs. bottom slip comparison for 4-wire and single wire test with WE..	138
Figure 13.10 WE 4-wire specimen after testing .....	139
Figure 13.11 WE Single wire specimen after testing .....	139
Figure 13.12 Bond stress vs. bottom slip comparison for 4-wire and single wire test with WG	140
Figure 13.13 WG 4-wire specimen after testing.....	141
Figure 13.14 Bond stress vs. bottom slip comparison for 4-wire and single wire test with WH	142
Figure 13.15 WH 4-wire specimen after testing.....	143
Figure 13.16 Bond stress vs. bottom slip comparison for 4-wire and single wire test with WK	144
Figure 13.17 WK 4-wire specimen after testing.....	145
Figure 13.18 Three 3/32-inch-diameter steel rods on prestressed wire .....	146
Figure 13.19 Three 1/8-inch-diameter steel rods on prestressed wire .....	146

Figure 13.20 Three 1/8-inch diameter rods on wire in forms .....	147
Figure 13.21 Three 3/32-inch diameter rod cage off wire .....	147
Figure 13.22 Three 3/33-inch diameter rod cage in forms .....	148
Figure 13.23 Glass fiber mesh around prestressing wires .....	148
Figure 13.24 Glass fiber mesh in forms.....	149
Figure 13.25 Results of three 3/32-inch diameter rods located on the wire .....	150
Figure 13.26 Cracking of specimen with three 3/32-inch diameter rods located on the wire ....	150
Figure 13.27 Results of three 1/8-inch diameter rods located on the wire .....	151
Figure 13.28 Cracking of specimen with three 1/8-inch diameter rods located on the wire .....	152
Figure 13.29 Results of three 3/32-inch diameter rod located off the wire .....	153
Figure 13.30 Cracking of specimen with three 3/32-inch diameter rods located off the wire ...	153
Figure 13.31 Results of glass fiber mesh located off the wire.....	154
Figure 13.32 Cracking of specimen with glass fiber mesh located off the wire.....	155
Figure 14.1 Cross section showing gauge location 1.25 inches from crosstie end.....	157
Figure 14.2 Cross section showing gauge location 8 inches from crosstie end.....	157
Figure 14.3 Crosstie forms with wire tensioned .....	158
Figure 14.4 Close-up of gauges mounted to wires .....	159
Figure 14.5 Close-up of gauge orientation .....	159
Figure 14.6 Gauges mounted at one end of a crosstie .....	160
Figure 14.7 Gauges mounted to wires .....	161
Figure 14.8 Gauges mounted to wires .....	161
Figure 14.9 Crosstie being cast.....	162
Figure 14.10 Crosstie after being cast.....	163
Figure 14.11 Wires exiting the crosstie after curing.....	164
Figure 14.12 Crossties after forms had been removed .....	165
Figure 14.13 Wires taped before going through saw cutting process.....	166
Figure 14.14 Crossties after being cut and loaded onto pallets .....	167
Figure 14.15 Crossties strapped to pallets and wire boxes installed .....	168
Figure 14.16 Wires placed into protective boxes.....	169
Figure 14.17 Crossties ready for shipment .....	170
Figure A.1 Confined and unconfined bond stress versus slip relationship for WA .....	182

Figure A.2 Confined and unconfined bond stress versus slip relationship for WA .....	183
Figure A.3 Bond stress versus slip relationship of confined 2-inch diameter for WA.....	183
Figure A.4 Bond stress versus slip relationship of unconfined 2-inch diameter for WA.....	184
Figure A.5 Bond stress versus slip relationship of confined 4-inch diameter for WA.....	184
Figure A.6 Bond stress versus slip relationship of unconfined 4-inch diameter for WA.....	185
Figure A.7 Confined and unconfined bond stress versus slip relationship for WE.....	185
Figure A.8 Confined and unconfined bond stress versus slip relationship for WE.....	186
Figure A.9 Bond stress versus slip relationship of confined 2-inch diameter for WE .....	186
Figure A.10 Bond stress versus slip relationship of unconfined 2-inch diameter for WE .....	187
Figure A.11 Bond stress versus slip relationship of confined 4-inch diameter for WE .....	187
Figure A.12 Bond stress versus slip relationship of unconfined 4-inch diameter for WE .....	188
Figure A.13 Confined and unconfined bond stress versus slip relationship for WG (5,500 psi) 188	
Figure A.14 Confined and unconfined bond stress versus slip relationship for WG .....	189
Figure A.15 Bond stress versus slip relationship of confined 2-inch diameter for WG.....	189
Figure A.16 Bond stress versus slip relationship of unconfined 2-inch diameter for WG.....	190
Figure A.17 Bond stress versus slip relationship of confined 4-inch diameter for WG.....	190
Figure A.18 Bond stress versus slip relationship of unconfined 4-inch diameter for WG.....	191
Figure A.19 Confined and unconfined bond stress versus slip relationship for WH .....	191
Figure A.20 Confined and unconfined bond stress versus slip relationship for WH .....	192
Figure A.21 Bond stress versus slip relationship of confined 2-inch diameter for WH.....	192
Figure A.22 Bond stress versus slip relationship of unconfined 2-inch diameter for WH.....	193
Figure A.23 Bond stress versus slip relationship of confined 4-inch diameter for WH.....	193
Figure A.24 Bond stress versus slip relationship of unconfined 4-inch diameter for WH.....	194
Figure A.25 Confined and unconfined bond stress versus slip relationship for WK .....	194
Figure A.26 Confined and unconfined bond stress versus slip relationship for WK .....	195
Figure A.27 Bond stress versus slip relationship of confined 2-inch diameter for WK.....	195
Figure A.28 Bond stress versus slip relationship of unconfined 2-inch diameter for WK.....	196
Figure A.29 Bond stress versus slip relationship of confined 4-inch diameter for WK.....	196
Figure A.30 Bond stress versus slip relationship of unconfined 4-inch diameter for WK.....	197
Figure B.1 Bond stress versus slip relationship of 2-inch diameter specimen for WB .....	198
Figure B.2 Bond stress versus slip relationship of 2-inch diameter specimen for WD .....	199

Figure B.3 Bond stress versus slip relationship of 2-inch diameter specimen for WF.....	199
Figure B.4 Bond stress versus slip relationship of 2-inch diameter specimen for WI.....	200
Figure B.5 Bond stress versus slip relationship of 2-inch diameter specimen for WJ .....	200
Figure B.6 Bond stress versus slip relationship of 2-inch diameter specimen for WL .....	201
Figure B.7 Bond stress versus slip relationship of 2-inch diameter specimen for WM .....	201
Figure C.1 Bond stress and lateral expansion relationship with bottom slip for WA .....	202
Figure C.2 Bond stress and lateral expansion relationship with bottom slip for WE.....	203
Figure C.3 Bond stress and lateral expansion relationship with bottom slip for WE.....	203
Figure C.4 Bond stress and lateral expansion relationship with bottom slip for WG .....	204
Figure C.5 Bond stress and lateral expansion relationship with bottom slip for WG .....	204
Figure C.6 Bond stress and lateral expansion relationship with bottom slip for WH .....	205
Figure C.7 Bond stress and lateral expansion relationship with bottom slip for WH .....	205
Figure C.8 Bond stress and lateral expansion relationship with bottom slip for WK .....	206
Figure D.1 Bond stress vs. bottom slip comparison for 4-wire and single wire test with WE...	207
Figure D.2 Bond stress vs. bottom slip comparison for 4-wire and single wire test with WH (single wire specimen had hairline crack).....	208



## List of Tables

Table 4.1 Wire properties .....	28
Table 5.1 Type III Cement Chemical and Physical Properties .....	31
Table 5.2 Grain size distribution of fine aggregate (Courtesy Matthew Arnold).....	32
Table 5.3 Gradation of 3/8-inch aggregate .....	34
Table 5.4 Gradation of #57 aggregate.....	34
Table 5.5 Mix A proportions .....	34
Table 5.6 Mix B proportions.....	35
Table 11.1 Crack width for VWSG tests .....	106
Table 12.1 Indent depth for each indent angle (in mm).....	107
Table 12.2 Crack widths for each indent (in inches) .....	130
Table 13.1 Crack widths for reinforcements on WH wire.....	155
Table 14.1 Average strain for each gauge location (in microstrain).....	171
Table E.1 Strain readings for all gauges (in microstrain) .....	209

## **Acknowledgements**

I would like to thank the Federal Railroad Administration (FRA) for providing a majority of the funding that made this research possible and Dr. Robert Peterman and RJ Peterman & Associates Inc. for donating the use of lab space and equipment. Additionally, LB Foster/CXT Concrete Ties donated extensive resources, including all of the reinforcements, to make the project a success. I would also like to thank Drs. Hailing Yu and David Jeong at the John A. Volpe National Transportation Systems Center for their valuable suggestions and parallel analysis work. Additionally, I wish to thank the Pre-cast/Prestressed Concrete Institute (PCI) for establishing an industry advisory panel to the project, the Kansas State University's University Transportation Center (K-State UTC) for graduate student tuition support, and the Advanced Manufacturing Institute (AMI) for manufacturing services.

I would like to thank Dr. Robert J. Peterman for his help and guidance with this project. I would like to express gratitude to the other three members of my committee: Dr. Kyle Ridding, Dr. Terry Beck, and Dr. Asad Esmaeily.

I would also like to recognize my fellow graduate students that helped with the research project: Naga Bodapati, Robert Schweiger, Mark Haynes, and Matthew Arnold. Thanks to Ryan Benteman for his assistance in helping with fabricating testing equipment.

I would finally like to thank my family, friends, and most importantly my wife, Lea, who has supported me throughout this endeavor.

# Chapter 1 Introduction

Pre-tensioned concrete members have become a profitable and less time consuming method of construction in certain cases. The use of pre-tensioned members allows for member fabrication and casting in an off-site location, thus eliminating the need for formwork at the construction site. The pre-tensioned members are brought to the construction site just prior to setting. The railroad industry has increased use of pre-tensioned concrete members due to their versatility. Increased production of concrete railroad ties has resulted in the emergence of prestressed railroad ties as a primary component of the industry, totaling at least 80 percent of the overall prestressed members produced annually worldwide in 1979 (Hanna, 1979).

## 1.1 Background

In 1884, Joseph Monier designed the first concrete railroad ties in France (Hanna, 1979). These ties were not utilized in the United States, however, until 1893 when only 200 ties were used (Weber, 1969). Because of the scarcity of wood during World War II, prestressed concrete crossties became popular; their use has continued to increase due to their longevity and adaptability (Garay, 1975). Prestressed ties began being produced in the United States as stated by FEC; “The first major use of prestressed concrete ties in the United States was in 1966, when 74,000 were installed on the Florida Coast Railway” (FEC, 1966).

Prestressed concrete railroad ties are produced in concrete tie plants in which the primary type of production involves casting the ties in long prestress beds measuring several hundred feet long. The prestressing reinforcement is tensioned before the ties are cast in forms that act like molds for the ties. After the concrete has cured, the reinforcement is de-tensioned at the ends, leaving a long “beam” of concrete ties. The resulting beam is cut with a diamond-tipped concrete saw to create individual concrete ties. The ties are then loaded on railroad cars and shipped to the field where they will be installed.

The need for larger rail cars and a decrease in adequate timbers for railroad ties have led to the rise of prestressed concrete ties as a viable option for railroad ties (Harris et al., 2011). However, as the railroad industry moves towards the use of concrete railroad ties, several problems must be investigated, including more understanding about transfer bond and flexure

bond of prestressed crossties. Various indent patterns are currently used in prestressing wires in order to achieve better bonding wire. The geometry of the indents can also cause crossties to split and lose prestressing force. Reinforcements must be studied so they do not cause tie failure in the railroad track.

## 1.2 Objectives

The purpose of this research program was to experimentally determine the bond-slip relationship between prestressing wire and concrete. Prestressing wires are mainly used in prestressed concrete railroad ties and at the time of this study, little was known about bond-slip relationships between the wires and concrete. This information was necessary for accurate finite-element modeling and was specifically requested by researchers at the John A. Volpe Center.

Two key types of bond were investigated in this research program. These two types of bond were transfer and flexural bond. Initial tests were modeled after the procedures developed by Abrishami & Mitchell (1993) for 7-wire prestressing strands. However, because of the smaller wire area and potentially better bond of the 5.32-mm-diameter wires, preliminary work had to be conducted to determine the appropriate geometry of the test specimens. Both types of bond are described below along with the steps involved for each test.

Transfer bond-transfer bond is the wire to concrete bond in the transfer length region of a prestressed member that transfers the prestress force from the wire to the concrete. The wire diameter decreases as it is initially stretched and then the diameter gets larger as the wire tension is reduced as it is released into the member due to Poisson's ratio.

Transfer bond test procedure used to evaluate the bond-slip relationship at the time of prestress transfer:

- Tensioned wire to 7,000 pounds (force in wires at prestress transfer)
- Cast concrete specimen
- Wait until concrete reaches a compressive strength of  $4,500 \pm 200$  psi
- Slowly release prestress force into member by reducing the force above the specimen while measuring movement of wire with respect to concrete at top and bottom of specimen

Flexural bond-flexural bond is the wire to concrete bond in the prestressed member that resists the flexural moment during loading of the member. The wire diameter is decreased as the tension in the wire is increased.

Flexural bond test procedure used to evaluate the bond-slip relationship in flexural region of member during loading:

- Tensioned wire to 5,100 pounds (calculated force in concrete ties after long term losses)
- Cast concrete specimen
- Wait until concrete reaches a compressive strength of  $7,000 \pm 200$  psi
- Slowly pull wire through member by increasing the force below the specimen while measuring movement of wire with respect to concrete at top and bottom of specimen

Transfer and flexural bond testing was first done at RJ Peterman & Associates Inc. laboratory due to the availability of testing frames. After the initial testing involving transfer and flexural bond were completed, additional testing frames were fabricated at Kansas State University. These frames were used to investigate the splitting behaviors of the indent types along with the effects of cover and confinement on transfer bond.

### **1.3 Scope**

Chapter 2 describes research methods used to investigate the behavior of prestressed members. It also looks at the use of various prestressing reinforcements and their use in concrete railroad ties. It concludes by examining the details needed to accurately model prestressed members.

Chapter 3 describes the testing frames that were made for the testing of the transfer and flexural bond properties done in this study.

Chapter 4 describes the wire reinforcements that were used in this research program.

Chapter 5 describes the concrete mix and batching procedure that was used to cast the specimens that were tested.

Chapter 6 details the initial testing that was done to determine that appropriate bond lengths to be used in the transfer and flexural bond testing.

Chapter 7 describes the transfer bond testing that was done during this test program.

Chapter 8 details the flexural bond testing that was done during this research program.

Chapter 9 explains the results from testing the effect of confinement and cover on the transfer bond.

Chapter 10 details additional testing done to examine the propensity of splitting for each of the indented wire types.

Chapter 11 describes testing done to investigate the best method to measure the lateral expansion caused by the different wire indent types.

Chapter 12 discusses testing of custom machined indents on smooth wire and the difference in splitting characteristics between them.

Chapter 13 detailed testing done to investigate the effect of multiple wires on transfer bond characteristics.

Chapter 14 details the results from the instrumentation of concrete railroad ties in a manufacturing plant.

Chapter 15 discusses the conclusions that were made from testing that was done during this research program.

## **Chapter 2 Literature Review**

This chapter discusses and summarizes research that has been done with regard to the topics that are investigated in this research program. The background history of concrete railroad ties is explained to show their production is increasing. Prestressing reinforcement testing procedures are also examined to look at the different methods of testing prestressing wire reinforcements. Methods of measuring the wire indent geometries are also explained. Methods of modeling concrete cracking and splitting are also discussed to investigate the variables needed to determine for proper modeling.

### **2.1 Railroad Tie Background and Production**

This section describes the history and background of concrete railroad ties as detailed by many researchers. This history was useful in showing the advancements that have been made in the railroad tie industry.

Hanna (1979) investigated the history, use, and advantages of concrete railroad ties, including their economic value, increased consistency of tie quality, and higher structural strength and durability compared to wood ties. The prestressed concrete tie is currently the primary concrete tie because of its ability to compress the concrete member to withstand a larger load while maintaining a smaller cross section. Hanna also explained the three methods of prestressed tie fabrication: long-line method, stress bench method, and individual form method. The author stated that each method had its reasons of use, but the predominant method used by tie producers in the United States is the long-line method which allows the most ties to be produced with the fewest number of man hours. The large initial capital investment for the long-line method is justified by the fact that the stress bench and individual form methods cannot efficiently or uniformly produce the large numbers of required ties. Hanna also emphasized the need for high quality materials in prestressed tie production. High strength concrete and prestressing tendons stress-relieved with a tensile strength over 225 ksi lead to lower prestress losses and higher flexural strength of the tie. Reinforcement greater than 3/8-inch was not recommended, In addition, the use of indented wires or strands were explained in order to increase reinforcement bond. Freeze-thaw durability was also a concern that was recommended

to be addressed by using air-entraining admixtures. Hanna asserted the vital need for quality control testing of the ties to ensure success of the prestressed concrete tie. The author concluded by explaining the advantages of concrete ties over wood ties, including higher stiffness, better settlement uniformity, lower chance of derailment due to misalignment, fewer irregularities, and longer service life.

Magee (1978) discussed early testing of prestressed concrete ties. In 1959 and 1960, Florida Prestressed Concrete produced prestressed concrete ties using the long-bed method. The concrete ties, intended to replace commonly used 7-inch x 9-inch treated red oak ties, were designed to have a larger bearing area due to higher compressive strength, so the base of the tie was 12 inches wide. The author participated in the design process, so he was able to explain issues pertaining to the design of the tie center in order to resist the negative moment from loading. These ties were placed in a one-quarter mile test track in which researchers utilized a wedge type of shape in the center of the track. The cross section performed well in laboratory testing but demonstrated some issues in the field. The ballast and wedge shape of the tie caused the tie to behave differently than it was designed. The design was modified and additional testing produced a more viable design. The tie used in the test section also included cast-in inserts and bearing pads that were first generation design variations of the types used in current production. These early tests were important in the development of a suitable cross section for prestressed concrete ties.

Harris et al. (2011) investigated ways to optimize concrete railroad tie design. Researchers studied the effects of geometry, reinforcement size and type, and concrete strength on concrete tie strength. The crosstie has two critical design regions: the center of the tie and the locations under the rail seat. These regions experience negative and positive moments, so design of the tie must provide adequate strength at each design region. Variable change at one location can adversely affect the other location due to change in reinforcement eccentricity. The authors concluded that concrete strength increased design capacity by increasing allowable service stresses and decreasing prestress losses. The authors also concluded that smaller reinforcements required larger numbers to provide effective prestressing identical to larger diameter reinforcements.

A majority of crosstie manufacturers incorporate cast-in inserts to connect the track and the tie. These inserts vary between threaded or thread-less, and each type is used with a distinct



fastener system depending on the manufacturer (Hanna 1981). Fasteners, which are necessary to secure the track to the crosstie, have four primary functions: “maintain gage and alignment, restrain longitudinal rail movements, provide resilience, and assure electrical insulation” (Hanna, 1981). Crossties must have adequate tensile and compressive strength so cast-in inserts are well secured and do not become dislodged from the tie during repeated loadings.

Rao et al. (1984) discussed track modernization in India. The authors stated that the increase in prestressed concrete railroad ties was caused by several factors, including reduced timber supply and structural superiority of concrete compared to wood. Concrete ties can haul heavier loads and are better equipped to be used with welded tracks. Because of their rigidity, concrete ties also allow trains to travel at higher speeds. In addition, fasteners used with concrete ties were identified as important features for maintaining constant track alignment. Researchers discussed the nationwide implementation of concrete railroad ties throughout India. This modernization required large amounts of concrete railroad ties, thereby requiring that the crossties be made correctly and tested in the laboratory to verify their strength. Prestressing concrete ties with electrothermal techniques was also discussed. This method utilizes deformed reinforcing bars, heated by electricity, which are placed in forms. The ends of the bars were anchored so the bars could not return to their original length, thus allowing the bars to be tensioned without high tensile prestressing reinforcement. The authors stated that laboratory testing verified that electrothermal prestressing was a possible way to decrease production costs. The authors explained that reinforcement is responsible for 40% of the total cost of concrete ties; therefore, this new method would allow manufacturers to use less expensive steel to achieve prestressing, consequently lowering the cost of production.

Hanna (1986) discussed concrete use in high-speed rail systems. He asserted that concrete is a better choice than wood for high-speed tracks because concrete can withstand higher loads, concrete fasteners used help maintain track alignment, and the weight of concrete prevents it from moving as much as wooden ties, thereby preserving lateral stability. Hanna explained that many countries use some sort of concrete system for railroad tracks, but some countries have begun to use a concrete slab for track foundation. The slabs are precast like the ties, but the slab is replacing many ties because ties are supported by ballast and can demonstrate elevation irregularities. Slabs provide all the advantages of ties, but they can remove the need for ballast and improve track alignment. The slab is also heavier, thus providing stiffer anchorage for

the track. Hanna concluded that a slab track is more expensive to construct, but its long-term maintenance advantages may cause it to be a favorite for high-speed rail construction.

## 2.2 Transfer Length

Transfer length in a concrete beam is the distance it takes to fully transfer the prestress force to the beam through bond. It is also called transmission length in some countries. The value of this length is critical when determining beam performance. In order for the prestress force to be fully effective, the transfer length must be less than the distance from the tie end to the rail seat. Murphy (2012) discovered that the average crosstie produced in the U.S. commonly has a rail seat 21 inches from the end of the tie, closer to 24 inches for specialty ties. These specialty ties include ties used in railway switches.

Surface strain measurements have been successfully used to determine the transfer length location of concrete crossties. Zhao et al. (2013a) developed a method for analyzing data found by measuring transfer length. The new method is called the Zhao-Lee (ZL) method. This method utilizes an algorithm statistically developed to quickly calculate transfer length of crossties. The ZL method was compared to the 95% Average Max Method used in the prestressing industry for years and experimental results determined the ZL method was a quick, unbiased approach to determine transfer length. This method was used with an automated laser speckle imaging (LSI) sensor which was computer-controlled and capable of measuring surface strains along a crosstie in intervals selected by the user. The Whittemore gauge was also used to measure surface strain measurements by recording the change in length between imbedded insert points. The LSI system noted measurements faster than the traditional Whittemore gauge method. Transfer lengths of the crossties were calculated using the ZL method and the 95% Average Max Method, using both types of strain measurements.

Bodapati et al. (2013b) conducted an experiment to determine the effect of wire indents and concrete parameters on the transfer length of prisms. The authors measured transfer lengths of 96 pre-tensioned concrete prisms which were 3.5 inches square with a length of 69 inches. Each prism had four prestressing wires tensioned up to 7,000 pounds. The wires were 5.32 mm in diameter. The experimental program consisted of casting the prisms using concrete with a 6-inch slump, and de-tensioning the prisms at 4,500 psi. Transfer lengths were measured by embedded gauge points and a Whittemore gauge. Twelve reinforcements were utilized in the

experiment, and each reinforcement had a unique smooth, chevron, spiral, or dot indent pattern. Indent types and patterns greatly influenced measured transfer lengths. Data from the experimental program indicated that the indent types, including spiral, chevron, and diamond, provided lower transfer lengths than smooth or dot patterns. The average transfer length of all reinforcement types ranged from 7.4 to 18.7 inches, which is below the 21 inches necessary for occur before the rail seat (Murphy, 2012).

Bodapati et al. (2013a) compared transfer length results from laboratory testing to results found at a concrete crosstie plant. One-hundred-twenty transfer lengths were measured in a laboratory at Kansas State University (KSU), Manhattan, Kansas. The prisms were 3.5, 4.5, or 5.5-inches square cross sections with a length of 69 inches. Fifteen reinforcements were used, including 5.32-mm-diameter wires, 5/16-inch-diameter 3-wire-strand, and 3/8-inch-diameter 7-wire strand for each cross section size, respectively. Each prism was fabricated with four wires or strands evenly spaced in the cross section. The concrete mix included Type III cement with a 0.32 water-to-cement ratio, similar in composition to the mix used at the crosstie plant. Prestress was transferred at a concrete strength of  $4,500 \pm 200$  psi in the laboratory tests. Compressive cylinders were match-cured to ensure identical curing temperature as the prisms. In the laboratory, transfer lengths were measured using inserted brass points with a Whittemore gauge to identify surface strain. At the crosstie plant, each of the 15 reinforcements was used to manufacture crossties. Prestress force was released after the de-tensioning crew finished preparing the bed, so concrete strengths for match-cured specimens at the crosstie plant ranged from 5,063 psi to 6,650 psi. Transfer lengths for each set of ties were measured using a Whittemore gauge with brass inserts and the LSI device, as described by Zhao (2013a). Fifty transfer lengths were measured for each set of reinforcements; these values were compared to laboratory values. The authors used the bilinear method as described by Zhao (2013a) and the 95% Average Max Method to find transfer lengths. Scatter found in the transfer lengths was higher at the concrete plant than in the laboratory, attributed to the fact that, in the laboratory, test beams for each reinforcement were poured with the identical concrete batch and crossties at the plant were poured with 14 batches due to crosstie bed length. When reinforcement averages from the laboratory and the crosstie plant were compared, high correlation was found. These results indicated that prisms used in laboratory testing behaved similarly to manufactured

cross-ties. The authors also concluded that “the best-bonding wires had the most pronounced indentations” (Bodapati, 2013a).

Bodapati et al. (2013b) also studied the effects of concrete strength and slump on transfer lengths. Sixty prisms were cast using slumps of 3, 6, or 9 inches; all prisms had a water-to-cement ratio of 0.32. Five of the twelve wires used in the previous experiment were used in this phase of the program. Prisms were de-tensioned at three release strengths (3,500 psi, 4,500 psi, and 6,000 psi) and transfer lengths were measured. Results indicated that transfer length decreased as concrete strength at release increased. The change in slump did not noticeably impact transfer length.

Rao et al. (1977) studied the effects of ribbed bars on transmission length, also known as transfer length. Researchers cast concrete specimens prestressed with four 5-mm diameter plain wires or two 10-mm diameter ribbed bars. Specimen sizes were 10-mm by 10-mm by 250-mm. A Pfender mechanical strain-gauge measured transmission length by recording surface strain of the concrete specimens before and after transfer. End slip measurements were also taken after release of the prestress. Researchers found that ribbed bars had a transfer length approximately 30 times the diameter of the bar, whereas the plain wire had a transfer length approximately 120 times the diameter of the wire. The ribs created a large decrease in specimen transfer lengths.

Liu et al. (2009) studied the effects of helical ribs on transmission length of prestressed members. Twenty-eight specimens were cast using reinforcement with diameters of 7 mm, 9 mm, or 11 mm. Surface strain was measured by a mechanical measuring device that was accurate to 0.001 mm, and surface strain readings were measured at 1 hour, 1 day, 3 days, 7 days, and 28 days time intervals after prestress transfer. Results were graphed and transmission length was calculated. Surface strains were found to increase over time while maintaining transmission length. Researchers found that ribs on the bars improved bar bonding capacity and decreased the measured transmission length.

### **2.3 Pullouts**

This section discusses findings from research done to investigate bond characteristics of prestressing reinforcements through pullout tests. Pullout tests are used to measure how different

prestressing reinforcements bond to concrete and have been shown to be a determiner of the bond characteristics of prestressing reinforcements.

Rose and Russell (1997) investigated the use of tensioned and un-tensioned pullout tests to determine bond characteristics of 0.5-inch diameter strand and end slip measurements. The authors compared pullout and end slip results with transfer length data found in the experimental program. Concrete that was used had a slump ranging from 7 to 8 inches and used a Type I cement. The authors also tested strands with various surface conditions, including as-received, cleaned, weathered, and silane-treated. Transfer length beam specimens were fabricated with a length of 17 feet and a cross section dimension of 6 inches x 12 inches. The specimens were reinforced with two 0.5-inch diameter strands 2 inches from the bottom and two #6 rebar on the top with a clear cover of .75 inches with #2 smooth bars used as stirrups. The beams were instrumented with detachable, mechanical strain gauge (DEMEC) points after the forms were removed. These points were used to measure transfer length according to surface strain. End slip measurements were also compared to transfer length data. Un-tensioned or “simple” pullout specimens were cast in a 4-ft x 3-ft block measuring 2 feet high. Strands were placed in a square grid so they were 9 inches apart with an embedment length of 18 inches. A total of 12 strands were tested per block. After three days, the strands were tested by a hydraulic ram which pulled the strand until it slipped 1 inch on the free end. Force and end slip data were recorded throughout the entire test. Tensioned pullout test specimens were 12 inches long with a cross section of 5.5 inches square. Unlike the vertical position used by Abrishami and Mitchell (1993), these specimens were cast in a horizontal position. A strand, which ran through the center of the cross section, was initially tensioned before the concrete was placed in forms. After the concrete had cured, tension on one side of the specimen was reduced. Strand force on each side of the specimen and the amount of strand slip was measured. Researchers found correlation between “simple” pullout test data and transfer lengths without including silane-treated strands. Pullout strength at 0.005 inches of end slip was plotted with transfer length values to find a correlation of 0.945. They found that higher pullout values matched up with shorter transfer lengths. When silane-treated strands were included, the correlation dropped to 0.02. End slip measurements strongly correlated to transfer length values. Tensioned pullout data was found to be lower than un-tensioned pullout values. In some cases, the values were 50% of the un-tensioned values. Correlation between tensioned pullout strength at 0.005 inches of slip and transfer lengths from

the beams was found to be 0.45. Researchers concluded that the end slip measurement is the most accurate method of determining transfer length. Since the end slip was measured on the same specimen that the transfer length was measured, no additional comparison was needed. Untensioned pullout tests demonstrated higher correlation even though they were cast in different specimens with unique dimensions. Tensioned pullout values were inconsistent; differences in specimen sizes could have been a factor. Smaller specimens cure slower than larger beams, so addition curing details must be addressed. Vertical orientation of the un-tensioned pullout specimens' strand correlates with values from the horizontal strand orientation of the beams. However, similar to the beams, the tensioned pullout specimen strand was horizontal in orientation, but this did not lead to any correlation indicating that strand orientation may not be a consistent factor unless sufficient cover is present. The end slip test was recommended as the easiest and most accurate test to verify strand bond performance. Based on results of silane-treated strands, the simple pullout test was not recommended as an accurate test to predict bond performance. Tensioned pullout tests also were not recommended because of inconsistent results and complex testing procedure and setup.

Abrishami (1994) used a tensioned strand to test the bond of prestressing strand. Test setup included a tensioned 7-wire prestressing strand and a concrete specimen cast around the strand. The setup tested transfer and flexure bond properties of the strand based on how the test was conducted. For a transfer bond stress test, the strand was tensioned to the load in the strand after jacking losses, and then the specimen was cast around the strand. After the concrete had reached release strength, tension in the strand above the specimen was reduced using a jacking mechanism. The strand slip on the top and bottom of the specimen and the force in each strand section was measured during the test. For the flexure bond test, the strand was tensioned to the load experienced after all prestress losses. The specimen was then cast and allowed to cure. After the specimen had a strength comparable to the long-term strength of a prestressed member, tension below the specimen support was increased. Identical measurements were recorded as in the transfer bond test program. Specimens cast for each test were 150-mm diameter cylinders with a height of 300 mm. Bond length for the test procedure was 300-mm, or the total height of the specimen. The author also tested bond stress of rebar using a similar setup.

Abrishami and Mitchell (1993) reported that transfer bond values were higher than flexural bond values by a magnitude ranging from 1.5 to 2.3, depending on strand diameter.

They also reported that, in both testing setups, peak load was reached before slip was measured on the opposite side of the specimen. Displacement control during the test helped produce a complete curve without being affected by force reduction after slip was recorded. Abrishami and Mitchell (1992) reported that the testing procedure could be used for pullout and splitting tests and that the test setup enabled researchers to study the bond-slip relationship for any reinforcement type, including epoxy-coated rebar and prestressing strand. Because of their work in bond modeling development, Abrishami and Mitchell (1996) also found that many variables influence predicted bond stress distribution. These variables include specimen size, reinforcement size, embedment length, and properties of concrete used to cast the specimen.

Arnold et al. (2013) tested twelve indented prestressing wires using an un-tensioned pullout test. The wires were cast in 4-inch x 8-inch cylinder specimens with a mortar mix. Six-inch bond length was achieved by placing a 1-inch bond break on wires at the top and bottom of the specimens, and the specimens were tested when mortar cubes reached a compression strength of 4,500 psi. Wires were pulled out of the specimens by a force-controlled servo hydraulic system. End slip measurements and pullout forces were recorded. The author tabulated the data and found direct correlation between the maximum pullout force at 0.1 inches of slip and the transfer length measured by Bodapati (2013b) for each wire. The correlation showed that the un-tensioned pullout test can be related to the expected transfer length of the various reinforcements.

Filho et al. (2008) tested bond behavior of self-compacting concrete, or flowable concrete able to fill forms without requiring vibration. The research procedure involved testing pullout strength of 10-mm and 16-mm diameter ribbed bars and beam tests with the same diameter bars. Self-compacting concrete and regular concrete requiring vibration was used. Pullout tests were un-tensioned and slip and force were measured during the test. For the beam test, end slip on each side of the beam was measured during loading. Researchers found that self-compacting concrete specimens demonstrated similar results compared to regular vibrated concrete. Pullout test results had low variability, so researchers concluded that they are a better choice for testing because beam tests demonstrate high variability.

Rose and Russell (1995) stated that, “Adhesion, Hoyers’ effect, and mechanical interlocking are three mechanisms which contribute to the bond performance of a prestressing tendon.” The authors explained that these three mechanisms, however, are not all tested in an un-tensioned pullout test. The strand diameter decreases during the test, thus removing the Hoyers’

effect on the bond. Tensioned pullout tests provide a wedging action necessary to fully understand bond performance.

Malvar (1991) investigated the effect of confinement on bond slip relationships of rebar. The study consisted of twelve specimens being tested with various amounts of confinement. No. 6 rebar was used having rib angles of 68 and 90 degrees. Three-inch diameter specimens were cast having a height of four inches. The rebar was pulled out of the specimen while various amounts of confining pressure were applied to the outer surface of the specimen. The bond slip relationship for each of the different confining pressures were found and compared to each other. The author found that the increase in confinement caused an increase in the bond capacity of the rebar during the testing. The angle of the ribs also seemed to have an effect on the bond characteristics. The ribs that were at 90 degrees from the bar surface were found to create higher bond forces and also produce more severe cracking of the specimen.

Barbosa et al. (2008) studied the effect that rib area had on the bond stress of reinforcing bars. The authors tested various diameters of bars that ranged from 12.5 to 25.0-mm and had rib angles from 45 to 50 degrees. The concrete strength of the test specimens was varied from 20 to 100 MPa. The test results showed that the 47 degree angle rib had the highest capacity of bond stress. The authors also concluded that the concrete strength influenced the bond stress that was found from the experiments.

Hamad (1995) conducted experiments using rebar with different rib geometries. The rib angles varied from 30 to 90 degrees and the height of the ribs were also varied. The author machined the ribs to create the various angles. The bars were tested using an un-tensioned pullout test. The concrete strength of the specimens was also varied between different test setups. The author found that the higher angle ribs had higher pullout forces. The higher concrete strengths also produced higher pullout values.

## **2.4 Wire Geometries**

Prestressing wires differ from prestressing strands in that, unless altered in the manufacturing process, the wire is smooth. A majority of prestressing strand bond capabilities can be attributed to the fact that prestressing strands are composed of several wires stranded together. The stranding effect causes the strands to perform well in prestressed locations. Prestressing wires are manufactured with several different surface characteristics to potentially



increase their bond capacity. Research has measured these characteristics and correlated them to the bonding ability of prestressing wires.

Haynes (2012) developed a non-contact measuring device to measure the size and orientation of surface characteristics, including smooth wire, spiral wire, dot pattern indents, and chevron pattern indents. Twelve reinforcement types were used to measure these different surface characteristics. The researcher built a device that utilized a commercial Keyence scanning head to measure the surface of each wire type, or the distance of the wire from the laser as the wire was turned. Wire orientation and wire distance from the laser were recorded. The device also could move the laser in a vertical plane, so the vertical orientation was combined with the previous two measurements to create a three-dimensional coordinate system of measurements. The device could measure 1,000 data points per second, a necessary speed because the device required 17 minutes to measure 1 cm of wire. In addition, this device could measure far more than basic geometry measurements required by the American Society for Testing and Materials (ASTM). Design guidelines (A881/A881M) require only depth and edge slope indent measurements (ASTM International, 2010), but the device developed by Haynes provided a 3D wire mapping processed by computer algorithms. Algorithms allowed the author to plot a 3D model of the wires and thoroughly study the indents, including indent geometry differences.

As described by Haynes (2013c), data from selected prestressing wires collected with the non-contact device (Haynes, 2012) were used to correlate prestressing wire indent geometries to transfer length. Ten prestressing wires were used in this study, including nine with chevron indent patterns and a smooth wire to act as a baseline for the measurements. The chevron pattern was chosen because it is the primary pattern used by prestressing wire manufacturers and it provides the most number of specimens to compare with each other. Eighteen indent geometry characteristics were measured and compared with transfer length data from railroad crossties found by Murphy (2012). The researcher utilized all possible linear regression analysis to find possible geometrical features that correlated with transfer lengths. The author found that a model with three variables, including projected surface area per unit length, ellipsoidal width, and indent edge triangular facet surface area, produced the highest correlation between transfer lengths. A Bond Index Number (BIN) predictor was developed using these measurements to predict the measured transfer length that reinforcements would produce.

Additional research by Haynes (2013a) indicated possible use of three-dimensional mapping of prestressing wires. A device similar to the one used by Haynes was developed to measure surface indents (Haynes, 2012). Indents for each wire were measured and the indent patterns were processed by computer algorithms. Information recorded from the three-dimensional mapping detected irregularities between indents on the same wire. In addition to the new measuring device, algorithms and real-time analysis could be used to measure prestressing wire as it is manufactured (Haynes, 2013b). Algorithms allow the system to increase the rate at which it measures and computes indent patterns. Since most prestressing wire surface does not include an indent, removal of non-indent measurements from recorded data decreases the amount of processed data points. This technology and computer programming could allow prestressing wire manufacturers to monitor their product as it is produced, thus providing information regarding the amount of wearing present in the production rollers (Haynes, 2013b). Wire manufacturers could also use this real-time analysis to determine high-bonding reinforcement by calculating the BIN of prestressing wire reinforcement (Haynes, 2013c). This new measurement technology could be very beneficial to prestressed wire manufacturers. The use of this data with proposed testing could potentially predict the splitting propensity of certain reinforcements. This predictor could be merged into the BIN calculation to be an overall predictor of ideal prestressed wire reinforcement that bonds well and has low propensity to cause concrete tie splitting.

## **2.5 Experimental Measurement Devices**

This section examines different measurement systems that were used in testing of concrete members by different researchers. This information was needed to properly determine what testing equipment would perform better for this research project.

Zhao et al. (2013b) explained the development of a system which utilizes five cameras to measure transfer length of railroad crossties. Unlike the time consuming method of having cast-in inserts measured with a Whittemore gauge, the five-camera system is completely automated, thus allowing the system to be used on a larger scale than what is possible with Whittemore gauge points. The five-camera system is also a large advancement on the LSI (Zhao, 2013a) measurement system because five cameras are mounted above the crosstie. During production, the bottom of the tie faces upwards, exposing the surface to be measured. The cameras photograph the tie surface at five distinct locations. After the ties are cut, the cameras

rephotograph the same tie locations. Computer software previously developed and utilized with the LSI system (Zhao, 2013a) uses the images to calculate change in length. The five-camera system then plots strain along the beam for those four sections. The produced graph is statistically matched to other transfer length data to show that transfer length can be accurately determined by just four points. This new measurement system will allow crosstie manufacturers to measure large numbers of transfer lengths during production and enable those manufacturers to have better quality assurance.

Yuan et al. (2002) compared the use of a fiber optic extensometer to a conventional extensometer. The fiber extensometer was mounted to concrete specimens with epoxy or was embedded in the specimens during casting. A protective gauge coating prevented the gauge from bonding exactly to the concrete, causing a need for an experimentally calculated correction. This correction factor was approximately 0.758 for the surface-mounted gauge with epoxy and 0.556 for the gauge cast in the specimen. The gauge reading was divided by the correction factor to find the change in concrete length. An LED light source with a wavelength of 1,300 nm was used for the study. The fiber optic extensometer measured the change in distance of light traveling through the gauge length of fiber; the change in distance was approximately 4 inches. Two mirrors at each end of the fiber, a specialized light-detecting device, and a computer were used to measure the change in distance. The fiber optic extensometer proved to measure deformation of tested concrete specimens as accurately as a conventional extensometer gauge.

The fiber optic extensometer had several challenges requiring correction if intended to be used in this study. First, protective coating of the fiber optic gauge causes the gauge to experience lower strain readings than the specimen actually experiences because the coating is less ridged than the glass gauge. A correction factor would need to be found experimentally. Second, the fiber optic gauge used by Yuan et al. (2002) had a gauge length of 4 inches, which is larger than the diameter of specimens measured in this present study.

Lahnert et al. (1986) tested the use of magnetoresistors to measure slip between steel and concrete. Researchers developed a testing mechanism that included principles proposed by Nies (1979) regarding magnetic fields. Researchers used a coil, which was embedded into a steel bar, to produce a measurable magnetic field. As the steel bar was moved, the measured magnetic field also changed, as long as the device measuring the field remained in place. Researchers calibrated the testing device and then used it to test the slip of #8 bars with a 2-inch length of

embedment. Testing results matched predicted values and dial gauges used to verify measurements. However, the testing procedure was susceptible to temperature and must be calibrated at the same temperature as which it would be used for testing. Researchers concluded that the testing procedure was acceptable but was labor intensive and expensive. Test sensitivity required a short distance between the bar and measuring device, thus limiting the amount of applications that warrant use of this device.

## **2.6 Splitting and Cracking Behavior**

This section investigates the findings from research done on the splitting behavior of concrete. These findings were looked at to discover what variables play a role in the cracking of concrete members. The information found was used to provide a better understanding of the splitting behavior of the concrete specimens.

Gambarova et al. (1989b) discussed test results of steel to concrete bond. The authors described four stages involved in the bonding of steel reinforcement to concrete. The first stage is chemical bonding between the concrete and steel. The breaking of that bond leads to the second stage involving ribs of the bar creating friction with the concrete as the bar slips. Researchers also explained that, because of wedging from the ribs, microcracks begin to develop during this stage. The third stage is characterized by the presence of the first crack; these cracks increase as the concrete fails in tension. The fourth stage, which happens quickly if no transverse reinforcement is present, occurs when cracks continue to the surface and the bond stress is zero. Researchers found that by confining the concrete or using transverse reinforcement, bond stress levels increase and are less likely to fail by splitting. Reinforcement with ribs has been predicted to have slip happen when the ribs crush concrete that is in direct contact with the ribs and by the shearing action of the concrete between the ribs (Gambarova, 1989a).

Additional research has studied the effects of splitting on bond. The effect of confinement on bond strength has been identified as a linear function of the confinement amount (Gambarova, 1996). This finding emphasizes the importance of confinement, leading to the need for better understanding of bond behavior that does not have confinement. Researchers have also discovered that when confinement is present, the presence of a crack decreases bond strength (Gambarova, 1989a).

Quihua et al. (1996) investigated the cause of concrete railroad tie cracking. Prestressed ties had six groups of hooped steel bars to act as stirrups. The ties were placed in a track between Nanjing and Shanghai, China. Of the 13,200 studied ties, 3,623 ties demonstrated longitudinal cracking. The cause of cracking was investigated by differential thermal analysis, SEM/EDAX analysis, visual examination, petrographic examination, and study of aggregate alkali-reactivity. Testing showed high alkali content of 5.2-6.2 kg/m<sup>3</sup>. The presence of cement and water reducing admixture typically cause the alkali value to remain below 3.0 kg/m<sup>3</sup>. The resulting high alkali content was determined to be a possible cause of cracking because the ties have high alkali-silica reactions, causing the concrete to expand and crack. This investigation discussed one potential reason for concrete tie failure which can be prevented by using aggregates that are not alkali-silica reactive.

Inderwick (1997) detailed the need for quality control in concrete tie production and explained legal actions that can be filed against tie manufacturers if poor products are produced. Concrete ties can fail in the field, resulting in train derailments. Inderwick cited several legal cases from the 1980s in which tie manufacturers were held responsible for faulty ties and sued for damages. Consequent investigations led to millions of dollars of lawsuit expenses. One tie manufacturer stated that the cement used for the ties caused the failures and the lawsuit was subsequently expanded to include the cement manufacturer. Inderwick identified the need for manufacturers to be conscious of their product and emphasized that concrete tie manufacturers will be held legally responsible if their product is determined to be inadequate. This particular case was concluded with the affirmation that an alkali-silica reaction caused the failures but that better tie testing and reinforcements are necessary to ensure proper tie performance.

## **2.7 Crack Splitting and Bond Modeling**

This section describes research that was done to model the cracking and splitting of concrete. The information needed to correctly model each of these behaviors was investigated to determine what properties needed to be found in this research program.

Chen and Chen (1975) discussed nonlinear analysis performed on concrete splitting tests. The authors used plasticity theory and numerical analysis to model concrete cylinder behavior during a split tensile test. The effect of local cracking was studied to determine stress behavior

during split tensile tests. The authors concluded that split-cylinder tensile behavior could be predicted by the linear elastic solution.

Vecchio and DeRoo (1995) discussed the use of smeared-crack modeling to predict the behavior of concrete splitting by tension. Smear-crack modeling was described as an effective method to predict reinforced-concrete behavior. The authors compared test results from other researchers and used the results to develop a finite element model. After its development, the model was compared to experimental data, demonstrating its ability to predict parts of the test behavior, but not all of it. Researchers blamed this incompleteness on the effects of tension splitting which cause secondary cracks. Modeling showed that the smeared-crack model could predict tension splitting after additional in-depth research and programming has been completed.

Chanvillard (1999) explained the development of a model to predict the behavior of steel fiber pullouts. Fibers have been used in structural concrete to provide additional tension reinforcement, but the author developed a model able to model cohesion and friction during the pullout test. Chanvillard concluded that the model could be used to model newer types of fibers in order to potentially alter fiber geometry and behavior.

Yu et al. (2011) discussed the development of a finite element concrete crosstie model which could predict tie behavior regarding the ballast, subgrade, and track. The model used a plasticity model to predict concrete behavior. In addition, the strand and concrete interaction was modeled by bond-slip relationships. The authors concluded that the crosstie model was a good foundation that could be built on after additional experiments were conducted.

Galvez et al. (2010) discussed a cohesive-frictional model used to predict the bond and splitting action of prestressing wire. A finite element model was developed to incorporate steel and concrete interaction and reproduce results determined through experimental results. The authors concluded that the model was able to predict the splitting action of prestressed concrete members but stated that further research was necessary to improve the model before it was used on a large scale.

Oh et al. (2006) discovered a non-linear behavior of specimen splitting and the amount of cover in the specimen. The findings showed the presence of confinement from the additional cover prevented the specimen from splitting. Modeling of the behavior was used to show adequate cover would prevent cracking.

Choi et al. (2010) modeled the bearing angle of rebar ribs to determine the bond properties of the ribs. The authors used information from experimental research to predict the model behavior. The model found that higher amounts of confinement with an increase in rib height caused the ribs to pullout before splitting. The lower confinement and rib height lead to splitting before pullout.

## **2.8 Cyclic Loading**

This section looked at the testing that was done with cyclic loading of prestressed concrete members. This information was needed to determine if the prestressing wires would perform differently under cyclic loading conditions like the ones that a concrete railroad tie experiences.

Gessner and Hegger (2012) discussed a test setup designed to determine the behavior of prestressing strand through cyclic loading. Bond behavior through the development of a testing procedure that tested prestressed girders under cyclic loading was presented. Pullout tests were performed using cyclic loading to develop bond behavior used in girder design. Researchers found that the anchorage zone of the girder is an important feature for cyclic loading because the anchorage zone includes the transfer length and part of the flexural part of the girder. Since transfer length can vary, its length and flexural bond properties must be accurately predicted in order to properly design anchorage length. Researchers described a method for testing cyclic behavior of the bond-slip relationship that can be used to test cyclic bond properties of prestressing strand and wire.

Kaar and Hanson (1975) studied the cyclic response of one-hundred-eight concrete crossties. The crossties were loaded at various locations along the tie length, and the load that created a crack of 0.001 inches was recorded. Findings from the study showed that crossties must have load applied away from the transfer length in order for the tie to withstand three million cycles of loading. The distance from the transfer length was found to be 2.2 times the transfer length for severely loaded crossties reinforced with smooth strand. Researchers concluded that transfer lengths for prestressed crossties should be short in order to provide acceptable fatigue life.

## Chapter 3 Testing Frame Setup

This section details design of testing frames used for the research explained in this paper. Frame setup was altered for flexural bond test and 4-wire tests, explained in later chapters, but this section describes general frame setup. Frames were used to accurately measure tensioned pullout behavior of 5.32-mm-diameter prestressing wires at KSU. Testing frames used in this research consisted of a wire tensioned between two points while a location was provided between wire ends in order to cast a concrete specimen.

Tensioned pullout frames were fabricated to enable wire testing. Because the wire must stay tensioned during casting and pouring, screw jacks were used to tension wires instead of a servo hydraulic system. Screw jacks enabled the use of multiple frames without multiple servo valves. Utilized screw jacks had a gear ratio of 200 revolutions per inch. The jacks, which provided a displacement controlled test, were able to hold force in the wire without monitoring.

Five frames were set up to be used throughout this study. Each frame included two 5-inch tall, 10-ft long I-beams that acted as support columns. Near each end of the frames, 8-inch channels were bolted on each side of the I-beams to create a frame, and a base plate was attached to the channels to provide a location to anchor the wire. A 50-kip screw jack was attached to the top base plate and the bottom plate, depending on the test setup. The center shaft of the jacks was drilled out to allow passage of the wire. A pair of 12-inch channels was bolted to the beams near the middle of the I-beam section height, and a base plate was attached to the top of the channels to provide a location to cast the specimen. Holes were drilled into the base plates to allow the wire to continue through the entire frame. One side of the 12-inch channel was plasma cut to enable setup of the LVDT's as seen in Figure 7.4, and load cells were connected to the jacks and base plates at each end of the frame. Figure 3.1 shows frame setup consisting of one screw jack attached to the top of the frame, and Figure 3.2 shows frame setup involving a screw jack on the top and bottom of the frames.





**Figure 3.1** Frame setup involving a screw jack at the top of the frame



**Figure 3.2** Frame setup involving screw jacks on top and bottom of frames

Load cells were used to measure the amount of reinforcement force as the wire was tensioned. Two types of load cells were used: two plate-type load cells that the reinforcement pushed against or two S-type load cells attached to the reinforcement with chucks and pulled in tension. S-type load cells rated for 15,000 pounds were attached to both ends of the frame and a wire chuck was attached to the load cell to provide secure anchorage for the wire. Figure 3.3 shows the S-type load cell attached to the top screw jack. Figure 3.4 and Figure 3.5 show plate load cells attached to the bottom and top screw jacks, respectively.

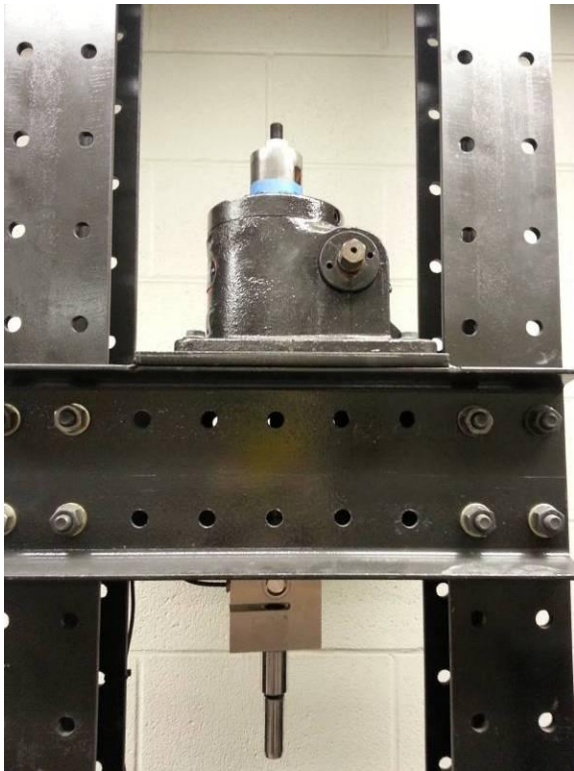


**Figure 3.3 Screw jack and S-type load cell arrangement**



**Figure 3.4 Plate load cell attached to bottom screw jack**



**Figure 3.5 Plate load cell attached to top screw jack**

Linear Variable Differential Transducers were attached to the reinforcement to measure the amount of reinforcement slip. LVDTs were attached by a custom bushing connected to the reinforcement at a single point so that elastic shortening of the reinforcement could be calculated and removed from end-slip measurements. Figure 3.6 shows the LVDT setup. The load cells and LVDTs were calibrated and connected to a data acquisition system to record measurements during testing. Figure 3.7 shows a data acquisition system used for recording measurements.



**Figure 3.6 LVDT setup to measure end-slip**



**Figure 3.7 Data acquisition system for recording measurements**

Portions of the preceding chapter were originally published here:

Transfer Bond Test Used To Predict Transfer Length Of Concrete Railroad Ties, by Joseph R. Holste, M.S., Robert J. Peterman, PhD, PE, Naga Narendra B. Bodapati, B. Terry Beck, Chih-Hang John Wu, Proceedings of the ASME 2013 Rail Transportation Division Fall Technical Conference, RTDF2013-4726. Copyright 2013 American Society of Mechanical Engineers.

Tensioned Pullout Test Used To Investigate Wire Splitting Propensity in Concrete Railroad Ties, by Joseph R. Holste, M.S., Mark Haynes, M.S., Robert J. Peterman, PhD, PE, B. Terry Beck, PhD, Chih-Hang John Wu, PhD, Proceedings of the 2014 Joint Rail Conference, JRC2014-3833, Copyright 2014 American Society of Mechanical Engineers.

## Chapter 4 Wire Reinforcements

This section discusses various reinforcement types used in research for this dissertation. Reinforcements were selected based on bonding and characteristics found in research conducted at KSU by Arnold (2013) and Bodapati et al. (2013b). Reinforcements consisted of prestressing wires used by concrete crosstie manufacturers. Wire names were developed to maintain wire manufacturer confidentiality. Prestressing wires used in this study were 5.32-mm in diameter, and twelve wires were investigated with ultimate tensile capacities ranging from 268 to 293 ksi. The wire properties can be seen in Table 4.1. The wire indent geometries were measured by Mark Haynes and the indent depth and indent angle were found according to ASTM A881. These measurements can be seen in Table 4.1.

**Table 4.1 Wire properties**

Wire	Ultimate Tensile Force (lbf)	Ultimate Tensile Strength (ksi)	Diameter (in.)	Area (in <sup>2</sup> )	Indent Type	Indent Depth (mm)	Indent Angle (Deg)
A	10184	293.5	0.2102	0.0347	N.A.	N.A.	N.A.
B	9712	281.7	0.2095	0.0345	chevron	0.155	27.3
D	9696	275.5	0.2117	0.0352	chevron	0.192	17.4
E	9258	268.6	0.2095	0.0345	spiral	0.295	16.5
F	9280	269.2	0.2095	0.0345	chevron	0.154	25.1
G	9376	271.0	0.2099	0.0346	chevron	0.096	20
H	9438	271.2	0.2105	0.0348	chevron	0.233	19.5
I	9389	279.5	0.2068	0.0336	chevron	0.132	14.5
J	9702	276.9	0.2112	0.0350	chevron	0.164	11
K	9839	284.6	0.2098	0.0346	4-dot	0.107	9.7
L	9711	280.9	0.2098	0.0346	2-dot	0.161	9.1
M	N.A.	N.A.	N.A.	N.A.	chevron	0.126	18

All but one wire were manufactured with indent patterns pressed into the wires in order to increase bond capacity on the wires. The remaining wire was a smooth wire with no surface indentations. Wires used for the study consisted of a smooth wire (WA), a spiral-patterned wire (WE), four- and two-dot indented wires (WK and WL), respectively, and eight chevron-patterned indented wires (WB, WD, WF, WG, WH, WI, WJ, and WM). The variety of indent

patterns was used to test indent ability to cause specimen splitting and to investigate various bonding capacities of the indents. Figure 4.1 shows wires used in the study.

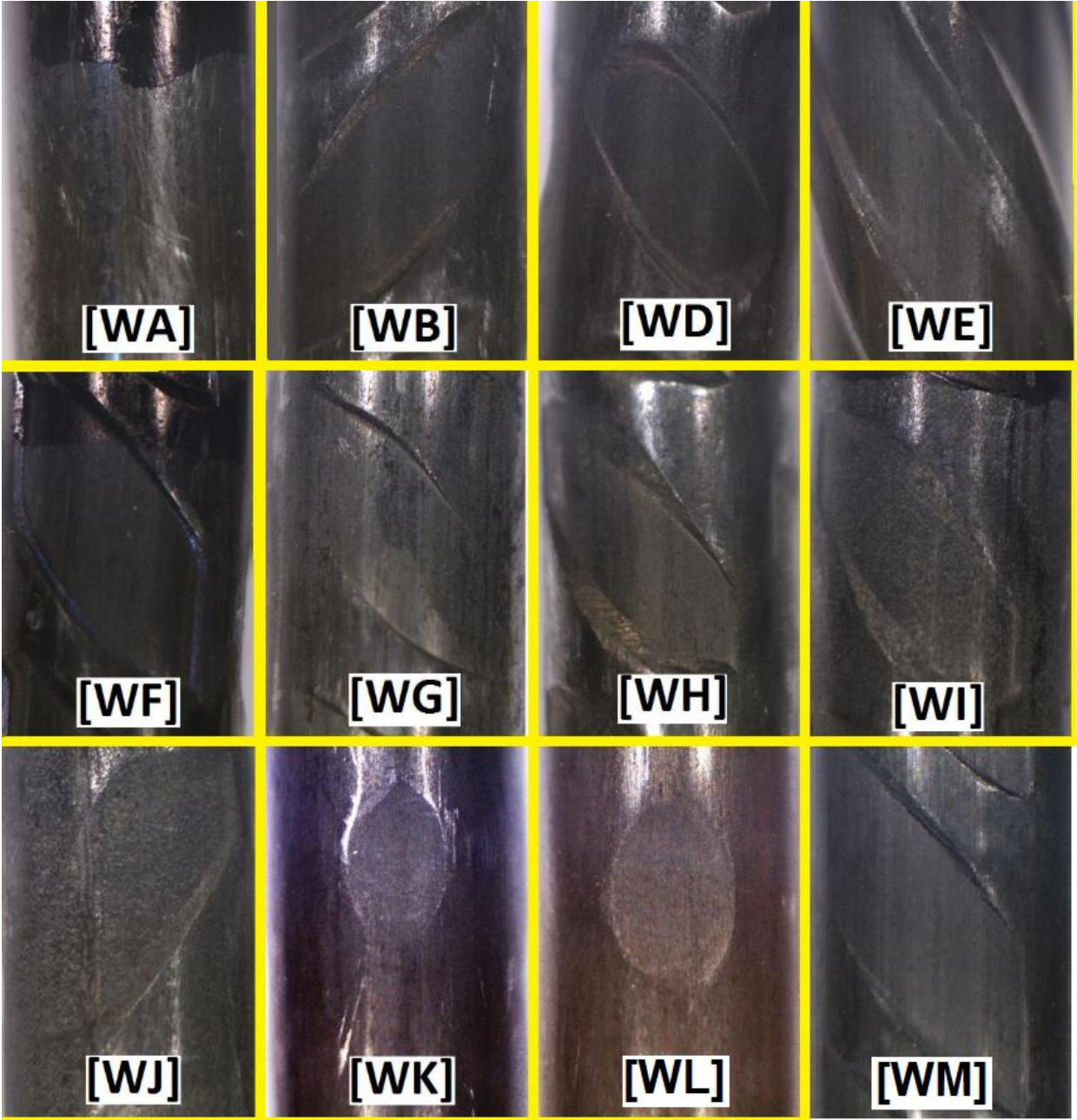


**Figure 4.1 Wires used in the study (Courtesy Matthew Arnold)**

Wire reinforcements selected for a majority of the testing setups described in this dissertation were WA, WE, WG, WH, and WK. These reinforcements, based on research data from Bodapati et al. (2013b), were chosen because of pattern type and transfer length differences of each wire type. Figure 4.2 shows the various wires used for a majority of the testing.



**Figure 4.2 Five wires used for a majority of testing (Left to Right: WA, WE, WG, WH, WK)**

Portions of the preceding chapter were originally published here:

Transfer Bond Test Used To Predict Transfer Length Of Concrete Railroad Ties, by Joseph R. Holste, M.S., Robert J. Peterman, PhD, PE, Naga Narendra B. Bodapati, B. Terry Beck, Chih-Hang John Wu, Proceedings of the ASME 2013 Rail Transportation Division Fall Technical Conference, RTDF2013-4726. Copyright 2013 American Society of Mechanical Engineers.

Tensioned Pullout Test Used To Investigate Wire Splitting Propensity in Concrete Railroad Ties, by Joseph R. Holste, M.S., Mark Haynes, M.S., Robert J. Peterman, PhD, PE, B. Terry Beck, PhD, Chih-Hang John Wu, PhD, Proceedings of the 2014 Joint Rail Conference, JRC2014-3833, Copyright 2014 American Society of Mechanical Engineers.



## Chapter 5 Concrete Mix Details

This section discusses concrete mixes used during this research project. Two mixes, based on the mix used by Bodapati et al. (2013b) at KSU, were used due to different testing setups.

The five components used in the concrete batches were water, cement, fine aggregate, two course aggregates, and a high range water reduced (HRWR). The cement used was a Type III cement which produced a high strength gain within the same day of casting. Table 5.1 shows the composition properties on the Type III cement used in the testing.

**Table 5.1 Type III Cement Chemical and Physical Properties**

Silicon dioxide	21.78
Ferric oxide	3.40
Aluminum oxide	4.27
Calcium oxide	63.21
Magnesium oxide	1.95
Sulphur trioxide	3.18
Loss on ignition	2.64
Free lime	0.99
Sodium oxide	0.21
Potassium oxide	0.52
Alkalies (equiv.)	0.55
Blaine Surface Area	5590
Tricalcium silicate	49.20
Dicalcium silicate	25.30
Tricalcium aluminate	5.60
Tetracalcium aluminoferrite	10.30

The fine aggregate used was local sand similar to sand used at the concrete crosstie plant, as shown in Figure 5.1. Table 5.2 shows the grain size distribution of the fine aggregate. The two course aggregates were supplied by the tie manufacturer and included a 3/8-inch gradation pea gravel and a #57 aggregate. Figure 5.2 shows the 3/8-inch aggregate and Figure 5.3 shows the larger #57 aggregate. Table 5.3 shows the gradation of the 3/8-inch aggregate and Table 5.4 shows the gradation of the #57 aggregate. The HRWR matched the same type used at the crosstie plant. The mixes were designed to have a target slump of 6 inches by varying the amount of HRWR for each mix.

The aggregates were dried in an oven at 200 degrees Fahrenheit for more than 24 hours to ensure the moisture content was zero. After drying, the aggregates were stored in a dry storage container until they were used for batching. Twenty-four hours before mixing, the materials were weighed and stored in air-tight buckets in a temperature-controlled room until the concrete was batched. Material storage in the temperature-controlled environment provided consistency in batch temperature and slump from day to day.



**Figure 5.1 Fine aggregate used in the study**

**Table 5.2 Grain size distribution of fine aggregate (Courtesy Matthew Arnold)**

Sieve #	Opening (mm)	% Passing
4	4.75	95
8	2.38	80
16	1.2	50
30	0.599	25
50	0.297	12
100	0.152	2



**Figure 5.2 3/8-inch coarse aggregate used in the study**



**Figure 5.3 #57 coarse aggregate used in the study**

**Table 5.3 Gradation of 3/8-inch aggregate**

Sieve	% Passing
3/8"	100.0
#4	25.6
#8	0.5
#16	0.0
#50	0.0

**Table 5.4 Gradation of #57 aggregate**

Sieve	% Passing
1"	100.0
3/4"	78.1
1/2"	31.3
3/8"	9.2
#4	0.0

## 5.1 Mix A Details

Mix A was similar to the mix used by Bodapati et al. (2013b). Mix proportions were identical except for the HRWR dosage. Mix A was used for initial testing and transfer and flexural bond testing with 8-inch tall cylinders. Table 5.5 shows the mix proportion used for this testing procedure.

**Table 5.5 Mix A proportions**

<i>Material</i>	<i>Quantity per Batch (0.5 ft<sup>3</sup>)</i>
Type-III Cement	18 lbs.
Sand	24 lbs.
3/8" Aggregate	12 lbs.
#57 Aggregate	20 lbs.
Water	5.76 lbs.
Type-F HRWR	36 ml

## 5.2 Mix B Details

Mix B used similar materials to Mix A, but the mix was altered by removing the larger #57 aggregate, leaving a maximum aggregate size of 3/8-inch because the specimen size was smaller and the distance (clear cover) between the wire and molds was close to 7/8-inch. The HRWR amount increased because of additional aggregate surface area due to removal of the larger #57 aggregate. The sand and 3/8-inch aggregate quantities were altered to replace the larger aggregate and to provide a consistent mix. This mix was used for all testing with 2.5-inch tall specimens. Mix design proportions used in this experimental program are shown in Table 5.6.

**Table 5.6 Mix B proportions**

<i>Material</i>	<i>Quantity per Batch (0.25 ft<sup>3</sup>)</i>
Type-III Cement	9 lbs.
Sand	16 lbs.
3/8" Aggregate	12 lbs.
Water	2.88 lbs.
Type-F HRWR	25 ml

## 5.3 Batching Procedure

The concrete batching procedure was uniform throughout the research to provide a consistent mix. Batching consisted of the addition of half the aggregates to the mixer. Next, HRWR was added to 3/4 of the water which was consequently added to dry aggregates in the mixer. The mixer ran for 15 seconds and then cement was added to the mixer. After all the cement was added, the remaining water was added to the mixer. After allowing the mixture to blend for an additional 15 seconds, the remaining aggregates were added to the mixer; it ran for three additional minutes after which the mixer was stopped. The mixture was allowed to rest for two minutes while the mixer sides were scrapped to ensure no cement or aggregates were caked to the sides of the mixer. Next, the mixer ran for three additional minutes and then the concrete was dumped into a pan. The mixture slump was measured according to ASTM C143. Figure 5.4 shows the mixer used in the batching procedure.



**Figure 5.4 Mixer used in the study**

Concrete compression strength in this study was determined by testing 4-inch-diameter x 8-inch-tall cylinders that were cast according to ASTM C192; Figure 5.5 shows the cylinder vibration. Test specimens were filled and rodded or vibrated depending on specimen size. The 8-inch tall specimens were vibrated, but the smaller specimens were rodded because the specimen size did not allow for vibrator use. Figure 5.6 shows specimen vibration and Figure 5.7 shows a finished specimen. The specimen tops were finished and covered with plastic wrap to prevent moisture loss, as seen in Figure 5.8. Figure 5.9 shows the rodding of a smaller specimen.



**Figure 5.5 Strength cylinders being vibrated**



**Figure 5.6 Test specimen being vibrated**



**Figure 5.7 Test specimen after top was finished**



**Figure 5.8 Finished test specimen covered with plastic**





**Figure 5.9 Smaller test specimen being rodded**

Strength specimens were cured by one of two methods, depending on the test specimen size. For the 8-inch tall specimens cast with Mix A, identical strength specimens were cast and tested to determine compressive strength of the specimens. Figure 5.10 shows 4-inch x 8-inch strength specimens cured next to 4-inch x 8-inch test specimens.



**Figure 5.10 Strength cylinders curing next to test specimens**

Testing was done at Kansas State University using Mix B allowed for the use of smaller specimens because of the availability of a match cure system. For the 2.5-inch tall specimens cast with Mix B, the specimens did not have the same volume as the strength cylinders, so additional setup was required because the strength cylinders would heat up more than the test specimens. Because of volume difference between compressive strength specimens and test specimens, the two specimens cured at different rates. To account for this difference in curing temperature, a special cooling box was built in which to place the compressive cylinders as they cured. The box was cooled by an air conditioner to decrease the compressive cylinder temperature below the test specimens. The cylinders were cast in a match-cure mold programmed to heat the cylinder to match the test specimen temperature. The tops of the molds were covered with Styrofoam to insulate the open section of the molds. The box used to cool the molds is shown in Figure 5.11. Figure 5.12 shows the match-cure temperature graph.



Figure 5.11 Air-conditioned box used to match-cure

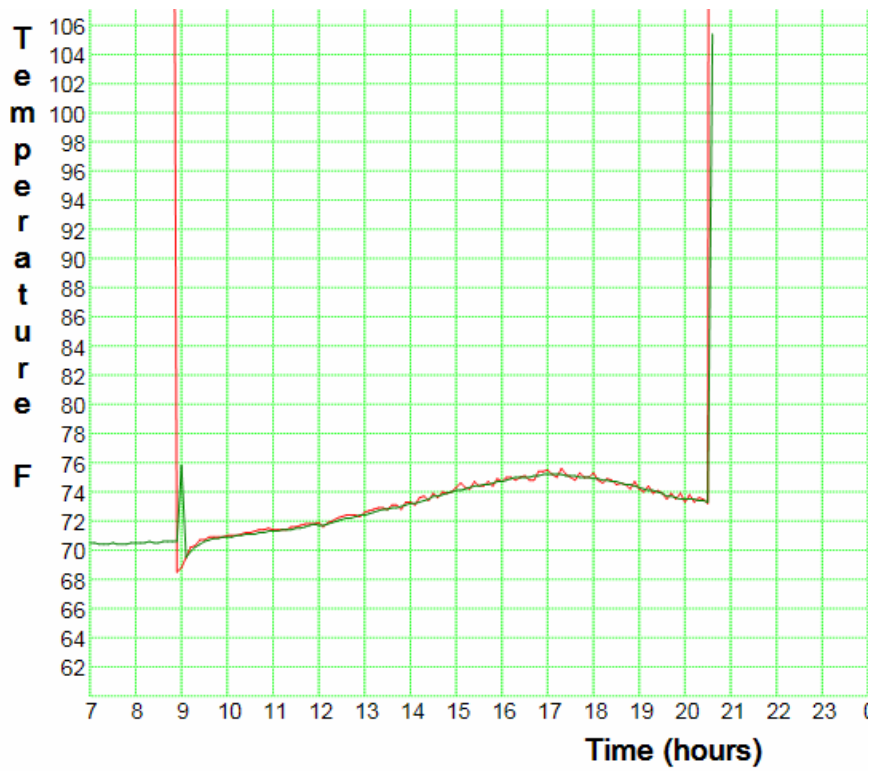


Figure 5.12 Temperature of test specimen and strength specimen during cure

Strength cylinders were tested according to ASTM C39 using a Forney compressive testing machine, as shown in Figure 5.13. Cylinder ends were capped with sulfur for tests using Mix A and neoprene compression caps were used for cylinders cast with Mix B. The average cure time to achieve a compressive strength of 4,500 psi ranged from 12 to 13 hours for all the testing. Split tensile capacity of Mix A and B were found to be 440 psi and 410 psi, respectively, by following ASTM C496. Figure 5.14 shows a split cylinder after test completion. Figure 5.15 shows a split cylinder from Mix B after testing.

Flexure bond testing required a higher compressive strength of 7,000 psi which required an average of 32 hours to achieve.



**Figure 5.13 Compression cylinder being tested**



**Figure 5.14 Split tensile specimen after testing**



**Figure 5.15 Close-up of split tensile specimen after failure**

Portions of the preceding chapter were originally published here:

Transfer Bond Test Used To Predict Transfer Length Of Concrete Railroad Ties, by Joseph R. Holste, M.S., Robert J. Peterman, PhD, PE, Naga Narendra B. Bodapati, B. Terry Beck, Chih-Hang John Wu, Proceedings of the ASME 2013 Rail Transportation Division Fall Technical Conference, RTDF2013-4726. Copyright 2013 American Society of Mechanical Engineers.

Tensioned Pullout Test Used To Investigate Wire Splitting Propensity in Concrete Railroad Ties, by Joseph R. Holste, M.S., Mark Haynes, M.S., Robert J. Peterman, PhD, PE, B. Terry Beck, PhD, Chih-Hang John Wu, PhD, Proceedings of the 2014 Joint Rail Conference, JRC2014-3833, Copyright 2014 American Society of Mechanical Engineers.

## Chapter 6 Preliminary Testing to Determine Bond Length

This section discusses initial testing to determine specimen size and bond length to be used in future tests described in this dissertation. These tests utilized the frame setup described in Chapter 3 with only a single jack located on the frame top.

Various bond lengths were tested using the transfer bond procedure that will be described in Chapter 7. Reinforcement WF was used first due to its high bonding capability discovered by Arnold (2013) of over 6,500 pounds in an eight-inch bond length of concrete. This high bond capacity caused the 12-inch of bond length used by Abrishami and Mitchell (1993) to be reduced for the wire testing. The prestressing strand tested by Abrishami and Mitchell (1993) had a larger amount of area and could be tensioned to a higher load than prestressing wires. The strand pattern also had a lower perimeter area in contact with the concrete with respect to total area of the strand. Therefore, the wires transferred their prestressing force sooner than prestressing strands. Tested bond lengths with WF were 2, 4, and 6 inches by using a plastic straw to act as debond. Debond was used since the specimen size had to remain the same size as the compression strength cylinders (4-inch diameter by 8-inch tall) to provide the same strength gain since a match cure system wasn't available for this part of the testing. Figure 6.1 through Figure 6.3 show the various bond length test setups. Figure 6.4 shows results of the three tests using WF. The top force was plotted with respect to the bottom force to discern if the wire would slip through the specimen and cause a large decrease of force in the bottom section of wire. As demonstrated in the graph, the 2-inch bond length allowed the wire to slip and create a large decrease in the bottom force. This behavior was wanted so that there would be measureable amounts of slip and the bond-slip characteristics of each wire could be seen for large amounts of slip.

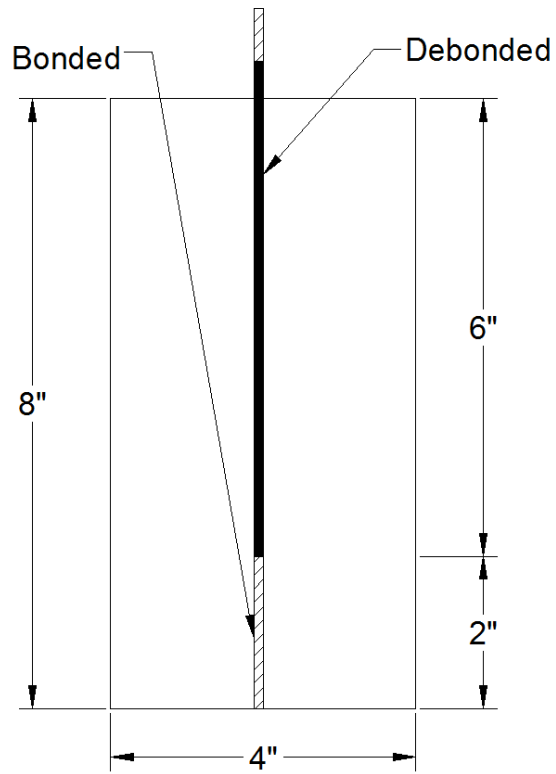


**Figure 6.1 2-inch bond length test setup**

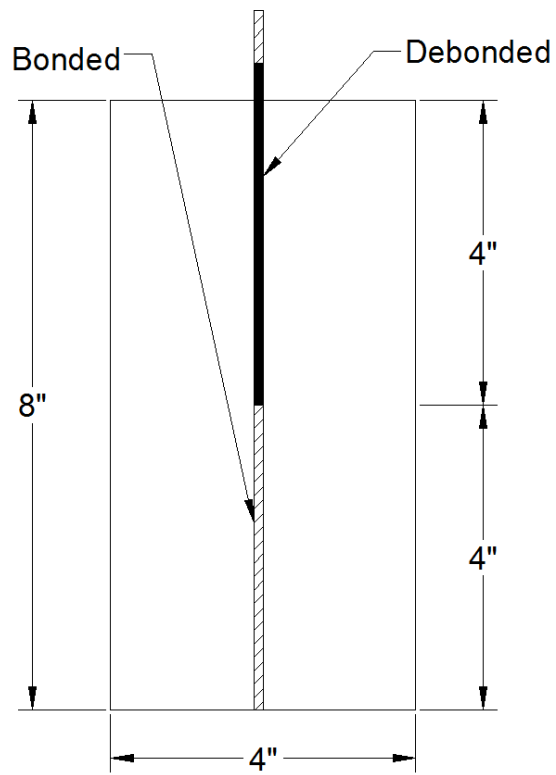


**Figure 6.2 4-inch bond length test setup**



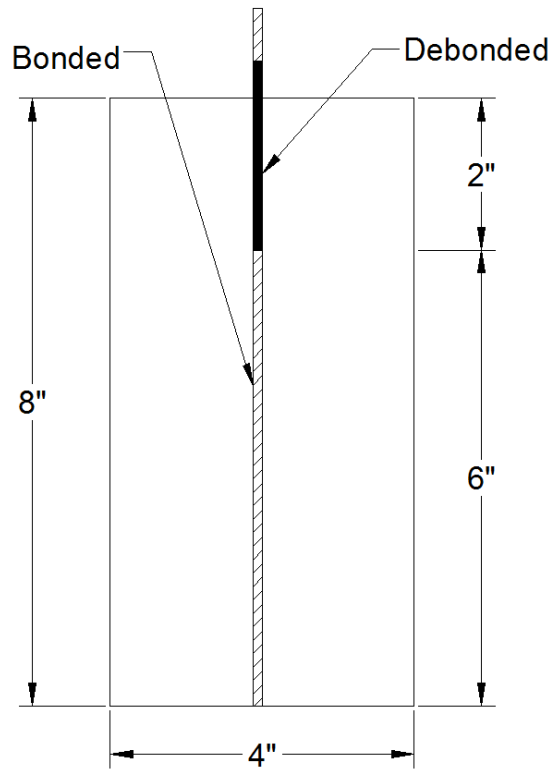


**Figure 6.3 6-inch bond length test setup**

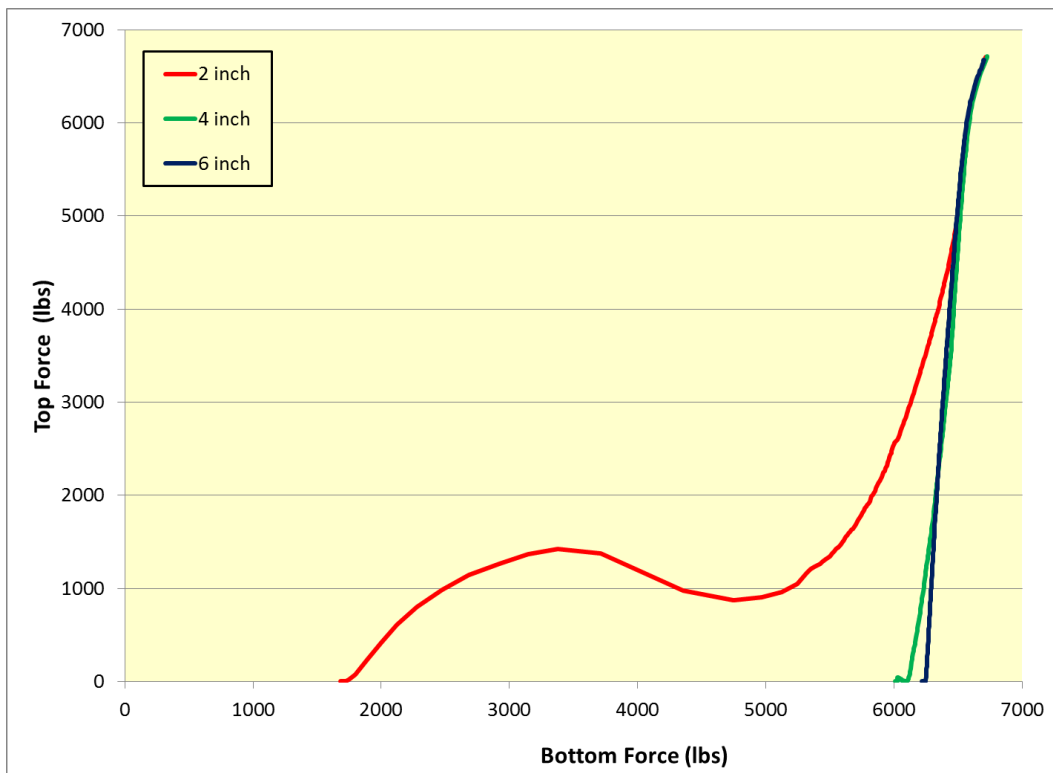


**Figure 6.4 Top force vs. bottom force of WF with various bond lengths**

Next, Wire WH was used to verify bond length for that wire type. A 2.5-inch bond length was chosen based on initial test findings with wire WF. This length was tested; results are presented in Figure 6.5. This amount of bond length allowed measureable amounts of slip to be present for the transfer bond test. The large amounts of slip were wanted to provide more detail about each wire's bond behavior.

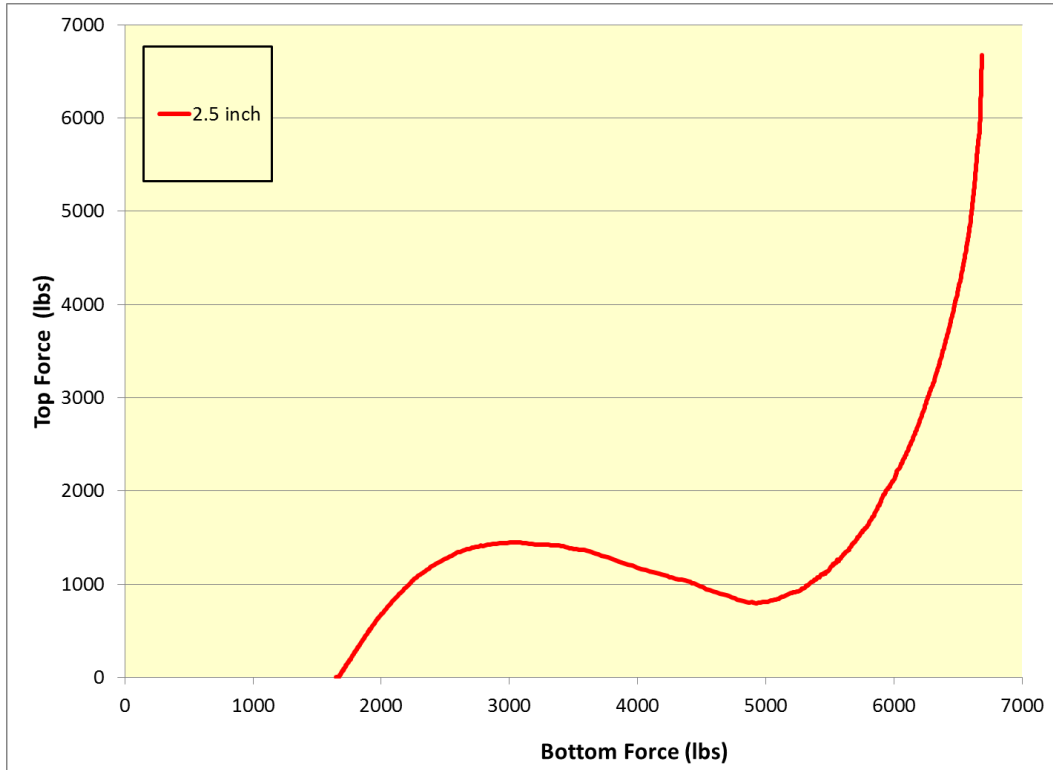


**Figure 6.5 Top force vs. bottom force of WH with 2.5-inch bond length**

## Chapter 7 Transfer Bond Testing

Testing was conducted to measure transfer bond properties of five reinforcements. WA, WE, WG, WH, and WK were selected for this testing phase. The 5.32-mm-diameter reinforcements were tensioned to 7,000 pounds prior to casting the specimens. This load simulated the force present in the wires at transfer in concrete crosstie. Specimens were 4-inch x 8-inch cylinders with a bond length of 2.5 inches. The concrete mix was Mix A. Before testing, the metal form was loosened from the cylinder surface. Each specimen was tested by decreasing wire tension on the top part of the frame. Wire tension on both sides of the specimen and end slip of the wire during loading were measured.

### 7.1 Transfer Bond Test Setup

The cast specimen was a 4-inch x 8-inch cylinder. A clear plastic straw was used as a bond breaker and sleeve for the wire to move through without touching the concrete. Gray tape attached the straw ends to the wire. Figure 7.1 shows the wire setup with 2.5-inch bond length.



**Figure 7.1 Bond break and straw on wire**

Metal split molds allowed the mold to be removed after the specimen had cured but before testing in order to prevent the mold from adding strength to the specimen. Specimens were cast in molds and vibrated to compact the concrete mix. Specimen tops were leveled and a plastic sheet was placed over the specimen to prevent moisture loss. Figure 7.2 shows one of the metal split molds that were used in the testing.

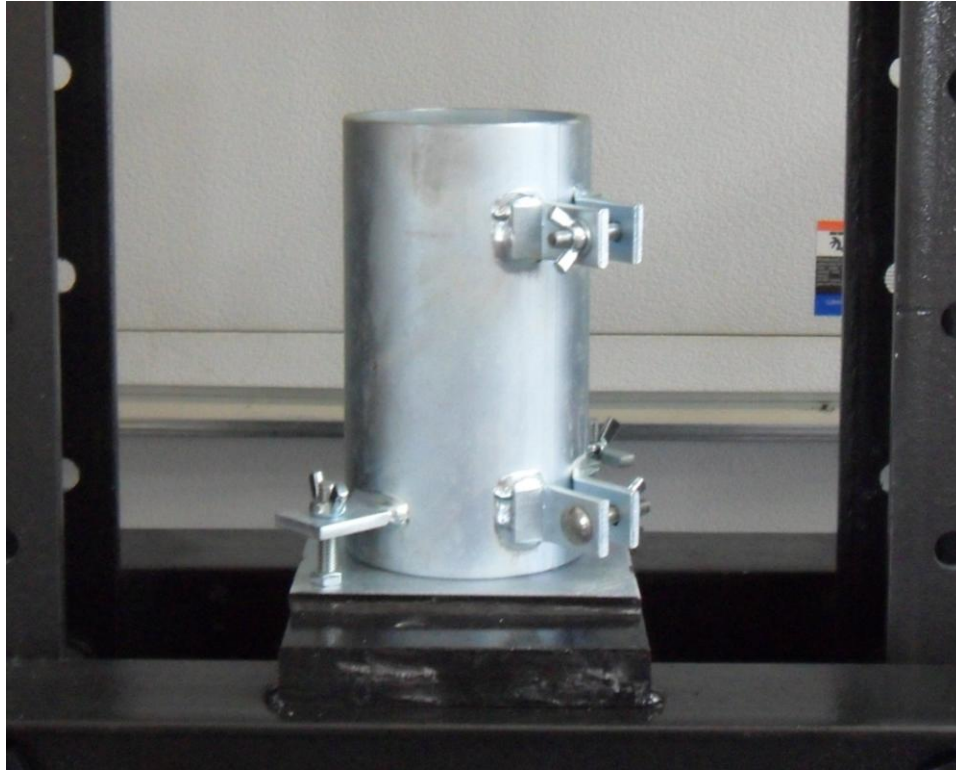


**Figure 7.2 Metal split molds used**

After the specimen had cured and compression strength of the strength cylinders reached  $4,500 \pm 200$  psi, the specimens were tested. To provide a better estimate of each wire's behavior; three different wire types were tested with each pour. The mold was loosened and removed from the specimen. To measure end slip, LVDTs were mounted on the wire on the top and bottom of each specimen using brass tipped screws secured to a specific wire location on the wire. Two LVDTs were used at each location in order to provide two measurements to provide an average reading. Distance between the specimen and screw mount was measured and used to remove elastic shortening effects from LVDT readings by using Equation 1. Figure 7.3 and Figure 7.4 show LDVTs mounted on the top and bottom of the specimen, respectively.

$$\Delta = \frac{PL}{AE} \quad (1)$$

Where:

$\Delta$  is the amount of shortening to remove from end-slip measurements (in inches)

P is the change in force of the wire (in lbs.)

L is the length of wire from the LVDT attachment to the concrete bond (in inches)

A is the cross section of the wire (in inches<sup>2</sup>)

E is the modulus of elasticity of the wire (psi)

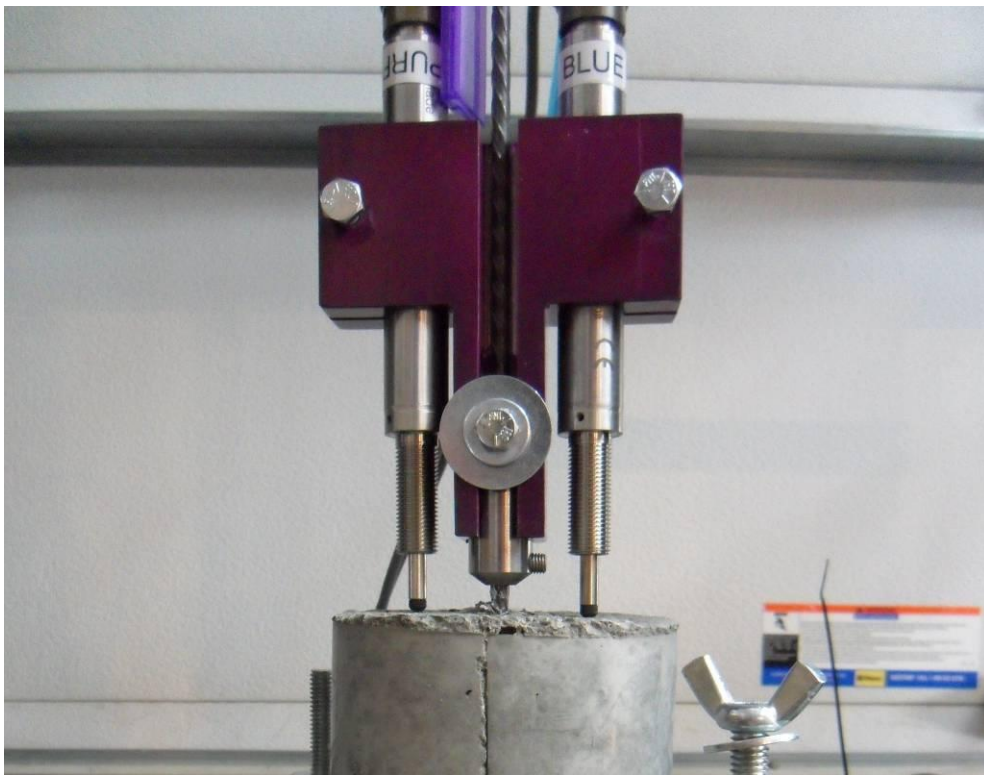


**Figure 7.3 LVDTs mounted to the top of the specimen**

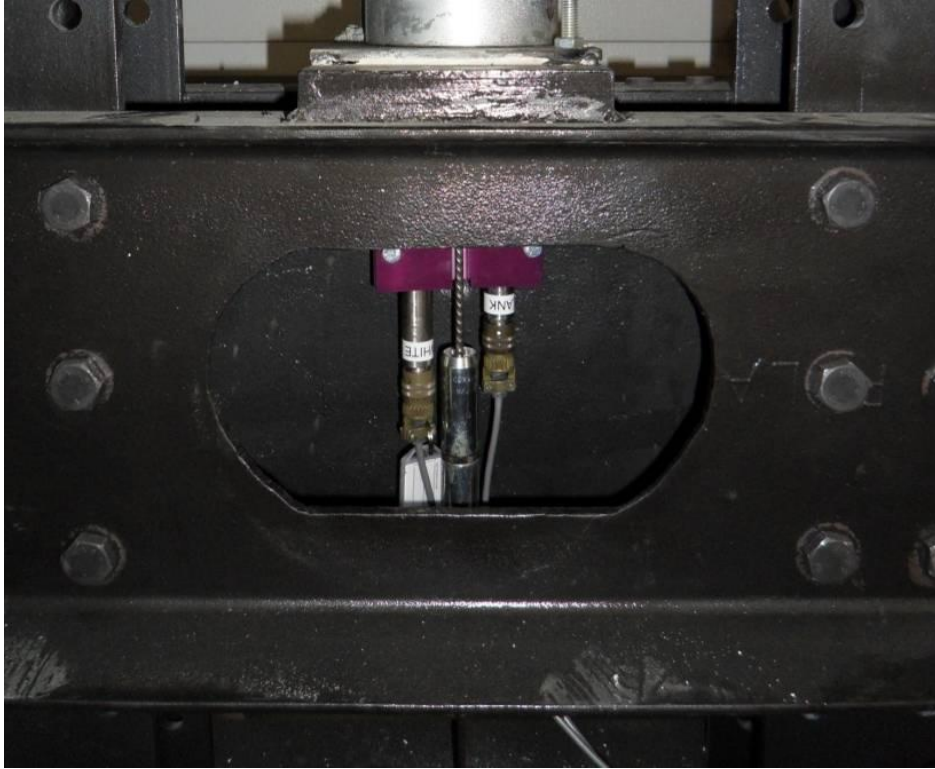


**Figure 7.4 LVDTs mounted to the bottom of the specimen**

The top jack was used to release the prestress force into the specimen. The jack was turned at a speed of 15 revolutions per minute (RPM) with a gear ratio of 200 turns per inch of ram travel. Thus the wire was released at 0.075 inches per minute. The speed of the jack movement was ensured by turning the shaft in sync with a metronome app on a cell phone. Figure 7.5 shows the author turning the top jack shaft during testing.



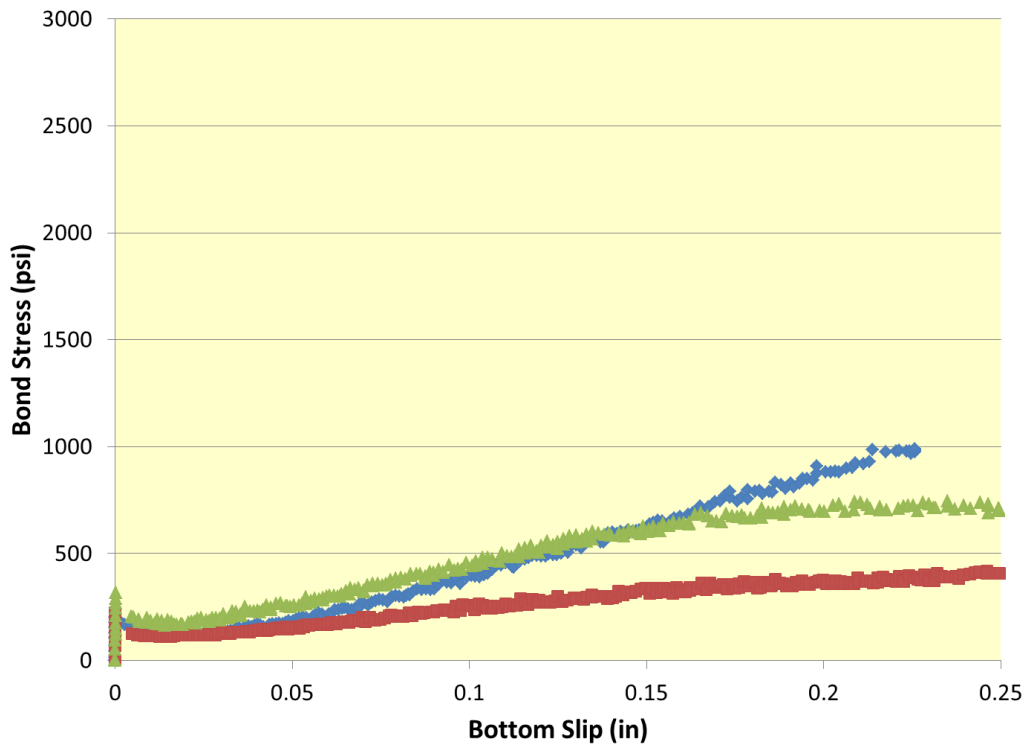
**Figure 7.5 Top jack shaft being turned during testing**

Load cell and LVDT measurements were recorded by a data acquisition system. The data acquisition system used for testing using Mix A was capable of scanning 50 scans per second. The data acquisition system used with Mix B was capable of scanning 2,048 scans per second but was set to record 100 scans per second since the test was quasi-static. Decreased load on the top wire caused the wire to move to the bottom of the specimen in order to maintain identical force in the wire on the bottom of the specimen, but 2.5 inches of concrete bonded to the wire prevented the wire from moving. Depending on the wire that was tested, as the force held by the bond increased, the wire would slip. Two sets of LVDTs measured slip on each side of the specimen, and the data acquisition system measured and recorded end-slip measurements and force in the top and bottom wires. The test was complete when the force in the top wire was zero. The bottom jack was used to release force in the bottom wire in order to remove the specimen after the test.

## 7.2 Transfer Bond Test Results

Data recorded during the test was analyzed to determine the bond relationships. The difference in force between top and bottom load cells was the force carried by the concrete-to-wire bond, labeled as bond force. In order to determine bond stress, the bond force was divided by the area of the 5.32-mm-diameter wire in contact with the concrete, taken as  $1.64 \text{ in}^2$ . The bond stress was plotted with the bottom slip for each wire type. Three specimens were tested each day using three of the five wire types. Each wire type was tested three different times. These tests were conducted on different days using separate concrete batches.

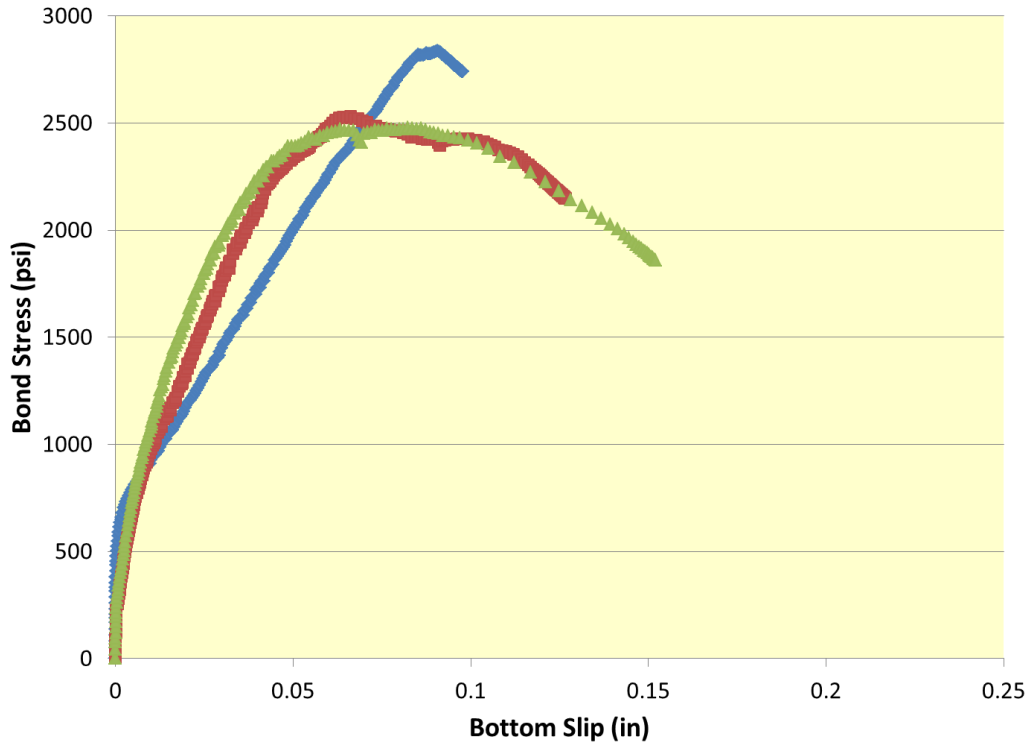
Figure 7.6 shows results from the three tests involving WA. As shown in the graph, bond stress decreased as the wire began to slip and then the bond stress slowly increased due to the expansion of the wire due to Poisson's effect.



**Figure 7.6 Bond stress vs. bottom slip relationship for WA (smooth)**

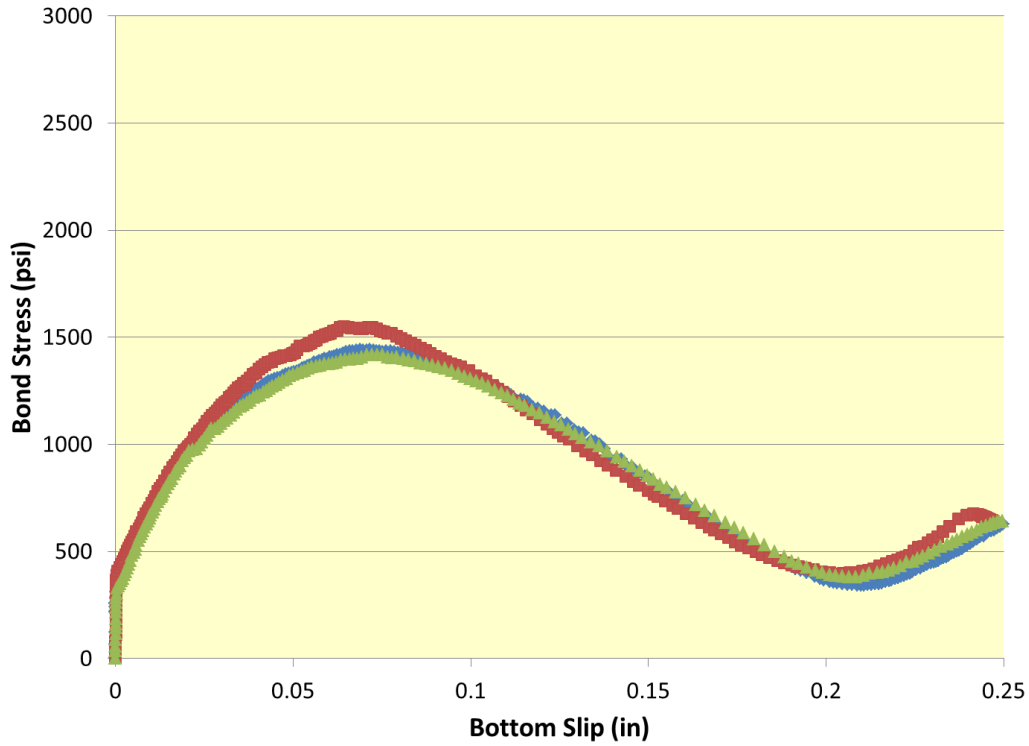
Figure 7.7 shows results from the WE tests. The spiral pattern was able to produce significantly higher bond stresses than the smooth wire.



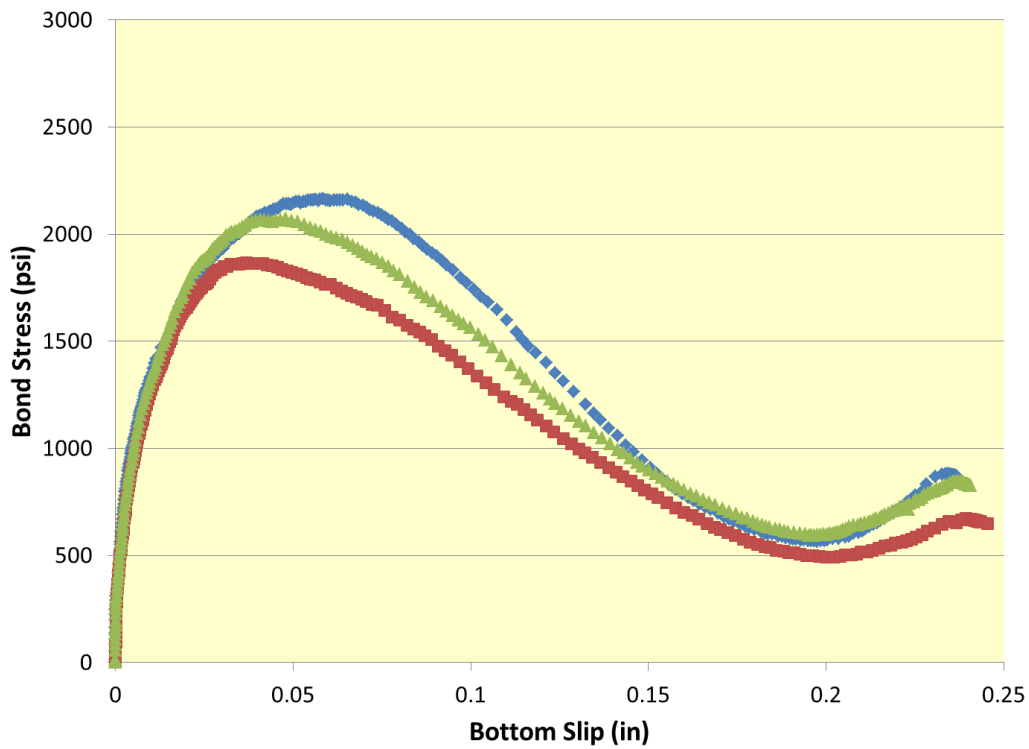


**Figure 7.7 Bond stress vs. bottom slip relationship for WE (spiral)**

Figure 7.8 and Figure 7.9 show results from chevron-indented wires, WG and WH. Both graphs indicate the same trend, but WH shows a larger overall bond stress. Because WH had deeper indents, WH enabled the wire to bond higher than WG.

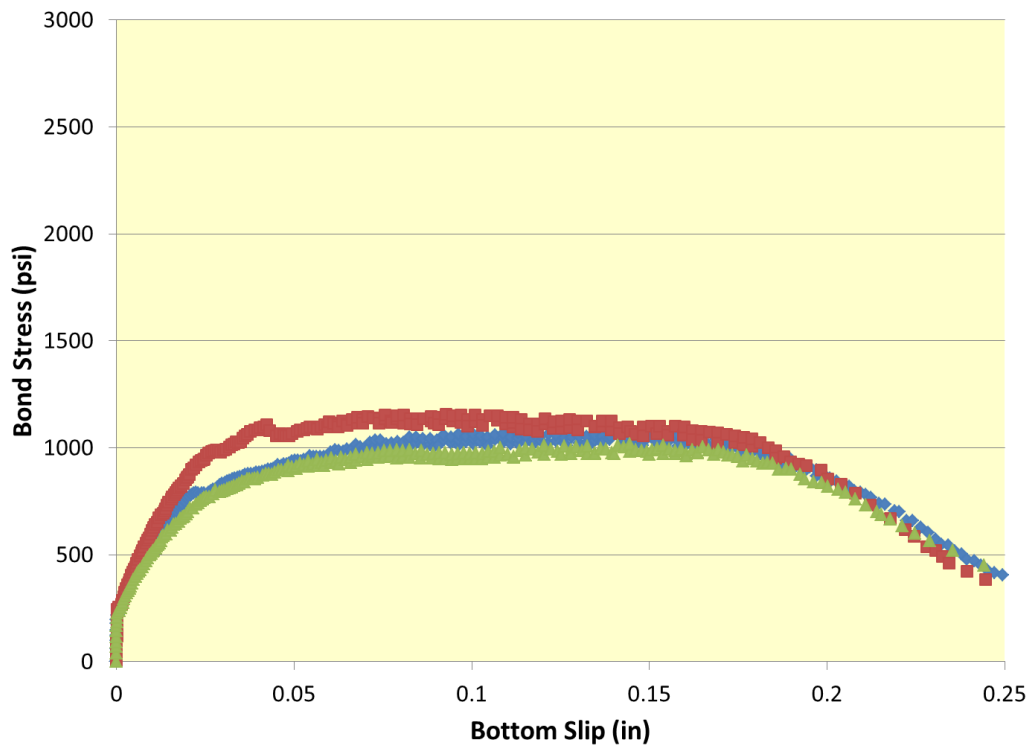


**Figure 7.8 Bond stress vs. bottom slip relationship for WG (chevron)**



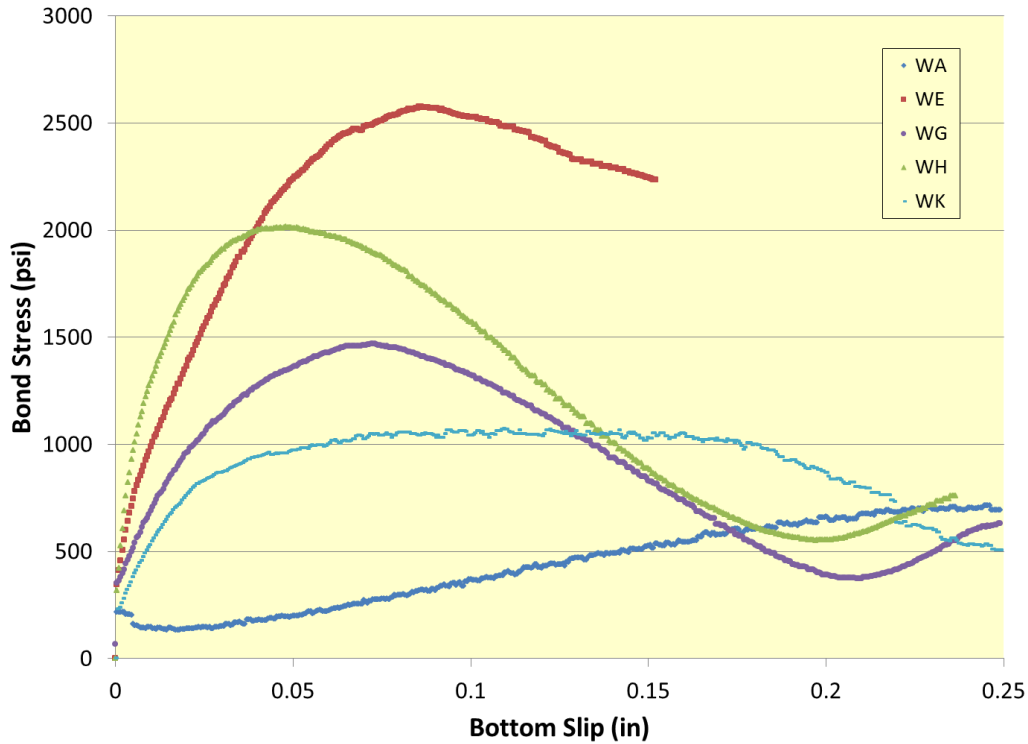
**Figure 7.9 Bond stress vs. bottom slip relationship for WH (chevron)**

Figure 7.10 shows results from the three tests involving WK. The four-dot pattern provides some bonding ability, but it is still lower than all the wires except WA.



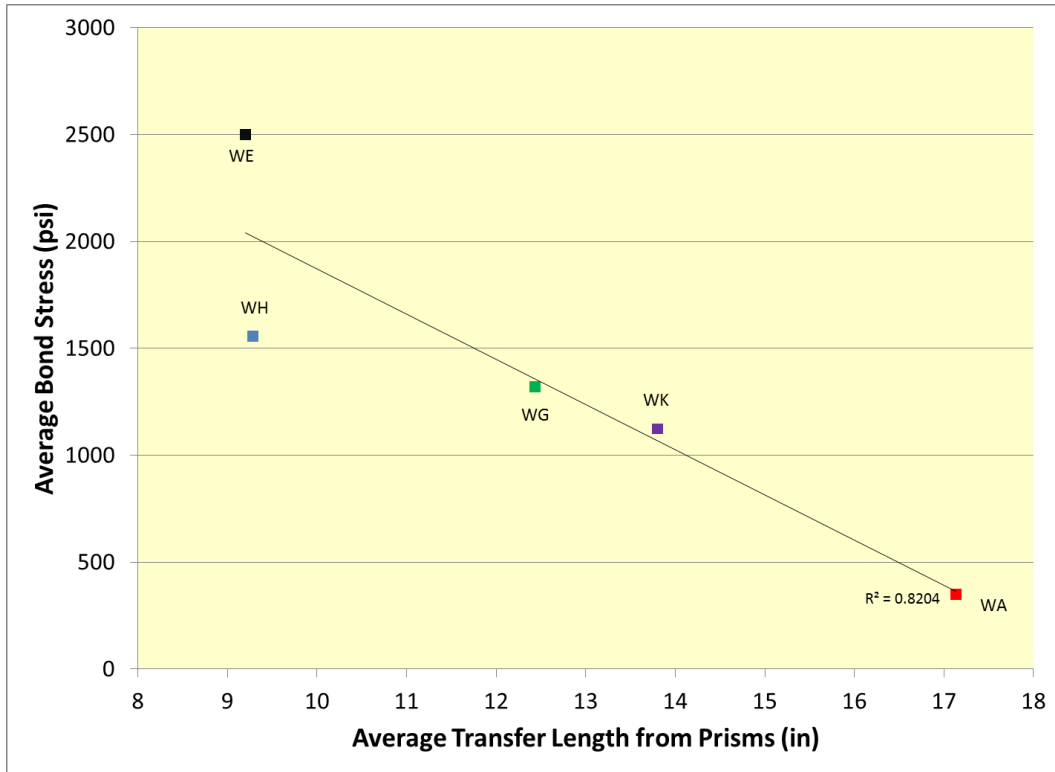
**Figure 7.10 Bond stress vs. bottom slip relationship for WK (four-dot)**

Figure 7.11 shows the average of the five wire behaviors plotted on the same graph.



**Figure 7.11 Average bond stress vs. bottom slip relationship for all five wires**

Each of the five reinforcements exhibited a unique bond-slip relationship as the wire was released and slipped through the specimen. Wires with indent patterns caused bond stress to increase faster than with smooth wire. This increase in bond behavior was also observed by Bodapati et al. (2013b); therefore, bond stress at various slip values was plotted with transfer lengths from Bodapati et al. (2013b). Transfer lengths from the prisms were matched with the three tests for each wire. The average of these values were plotted to find correlation between bond stress at different slip values and transfer length, as shown in Figure 7.12 through Figure 7.15. The coefficient of determination was found to be greater than 0.9 for slip values of 0.01, 0.025, and 0.05 inches. Arnold (2013) found that the maximum force at 0.10 inches of slip provided the highest correlation for un-tensioned pullouts.



**Figure 7.12 Correlation of bond stress at 0.1 inches of bottom slip vs. transfer length**

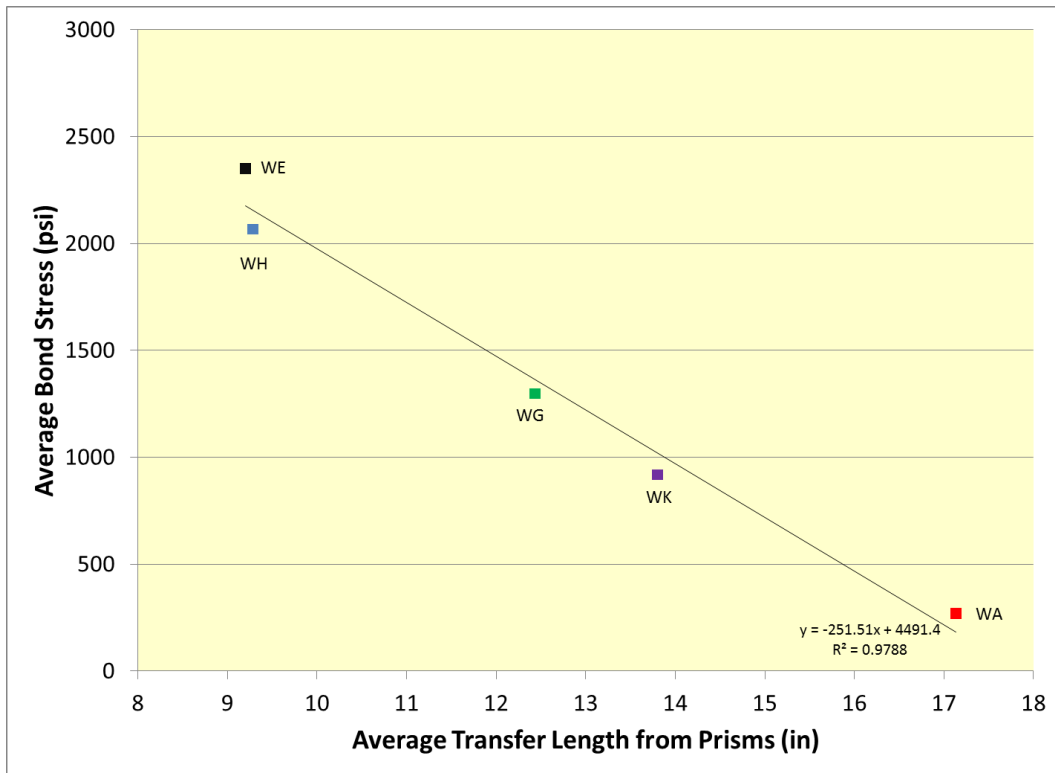


**Figure 7.13 Correlation of bond stress at 0.05 inches of bottom slip vs. transfer length**

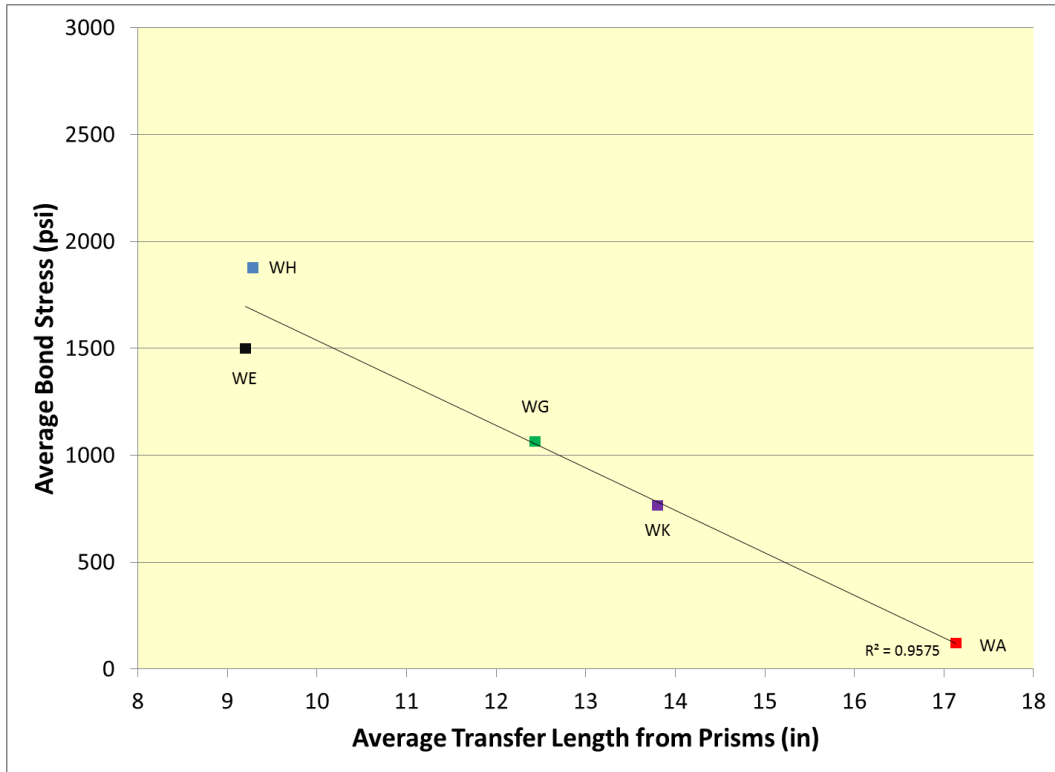


**Figure 7.14 Correlation of bond stress at 0.025 inches of bottom slip vs. transfer length**

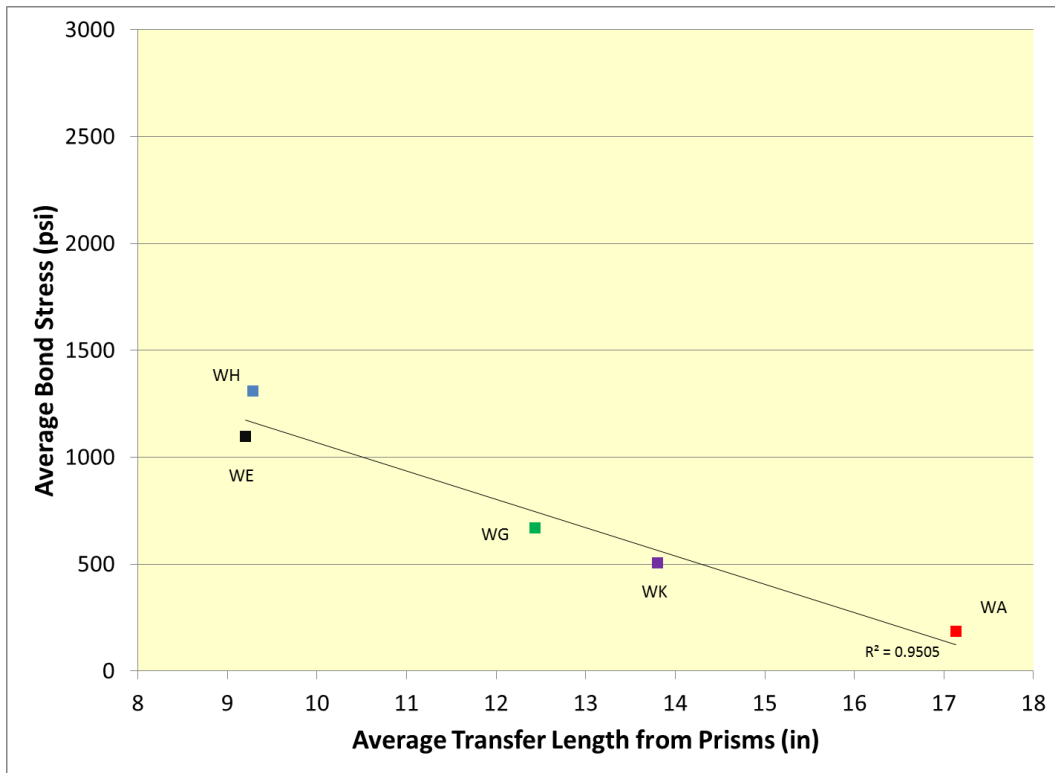


**Figure 7.15 Correlation of bond stress at 0.01 inches of bottom slip vs. transfer length**

Data analysis revealed that bond stress at 0.05 inches of bottom slip had the highest correlation with transfer length data when using a concrete mix similar to the one used to fabricate the prisms. Therefore, this test could be used to predict transfer length ( $L_t$ ) of prestress wire based on bond stress at 0.05 inches using Equation 2.

$$L_t = 17.86 - (BS / 251.51) \quad (2)$$

Where:

$L_t$  is the transfer length (in inches)

BS is the bond stress at 0.05 inches of bottom slip (in psi)

Portions of the preceding chapter were originally published here:

Transfer Bond Test Used To Predict Transfer Length Of Concrete Railroad Ties, by Joseph R. Holste, M.S., Robert J. Peterman, PhD, PE, Naga Narendra B. Bodapati, B. Terry Beck, Chih-Hang John Wu, Proceedings of the ASME 2013 Rail Transportation Division Fall Technical Conference, RTDF2013-4726. Copyright 2013 American Society of Mechanical Engineers.

Tensioned Pullout Test Used To Investigate Wire Splitting Propensity in Concrete Railroad Ties, by Joseph R. Holste, M.S., Mark Haynes, M.S., Robert J. Peterman, PhD, PE, B. Terry Beck, PhD, Chih-Hang John Wu, PhD, Proceedings of the 2014 Joint Rail Conference, JRC2014-3833, Copyright 2014 American Society of Mechanical Engineers.

## Chapter 8 Flexural Bond Testing

This section discusses flexural bond tests performed using prestressing wire. This test simulated bond behavior of prestressing wire in the region that is in the flexural bond part of a concrete crosstie. A concrete specimen was cast around a tensioned wire, and bond-slip behavior was tested after the concrete had cured by increasing the tension in the bottom wire. Five wire types (WA, WE, WG, WH, and WK) were tested during this procedure.

### 8.1 Flexural Bond Test Setup

Test setup consisted of the frame setup described in Chapter 3, which involved a screw jack mounted on the top and bottom sides of the frame. Load cells were attached to each jack to provide a load reading above and below the specimen. The wire was tensioned to a stress of 148 ksi, which, as found by Murphy (2012), was the average stress present in the concrete crosstie after all losses. The specimens used were 4-inch x 8-inch cylinders with a bond length of 2 inches. This length was shorter than the transfer bond length due to higher strength of the concrete. The concrete mix was Mix A, as described in Chapter 5. Before testing, the metal form was loosened from the cylinder surface. After the specimen was cast and cured to a compressive strength of 7,000 psi, the specimen was tested. End-slip measurement devices consisting of LVDTs were attached above and below the specimen. Specimen testing consisted of increased force in the wire below the specimen by turning the screw on the bottom jack. A data acquisition system recorded end-slip measurements and load during testing. A metronome allowed for the operator to achieve a constant load rate for each test. To prevent wire breakage, the test ended when force in the bottom load cell reached 90% of the  $f_{pu}$  of the reinforcement.

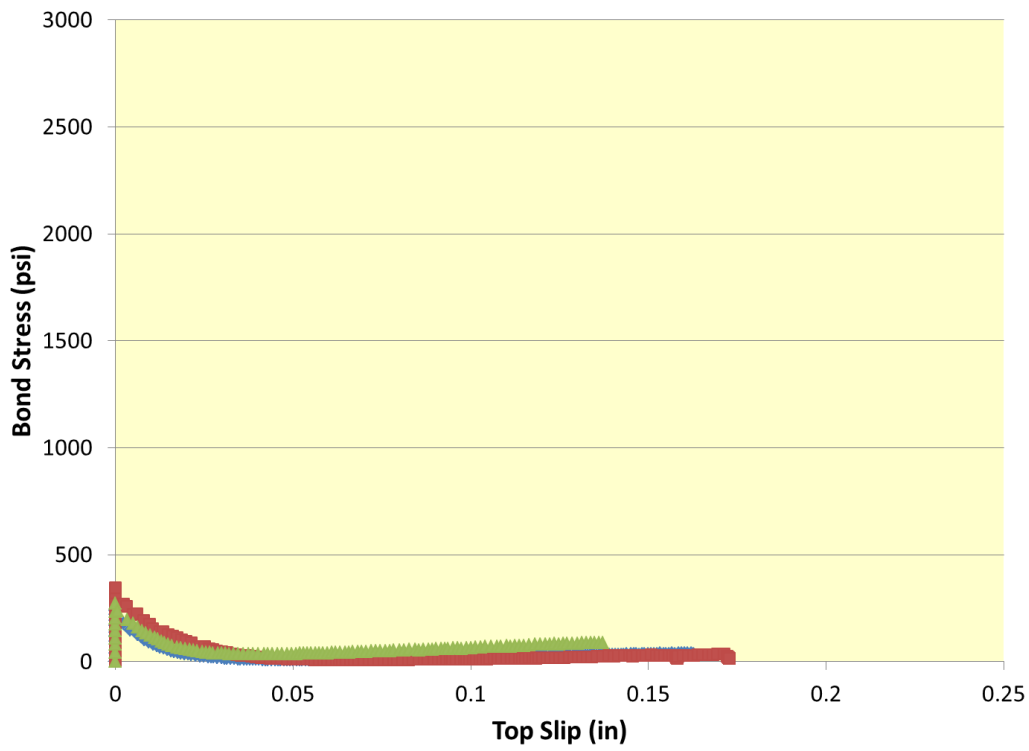
### 8.2 Flexural Bond Test Results

The five wire types were tested three times with the flexural bond test. Results were tabulated and a graph of each wire reinforcement type behavior was created. These graphs showed behavior differences for each wire type. Bond stress was the amount of force held by the specimen divided by the perimeter area of the tested wire. The amount of force held by the specimen was the difference between top and bottom load cells.

Figure 8.1 shows bond stress versus top slip relationship for WA. WA loses all bonding capabilities as the wire slips because WA does not have any indents; therefore, when the wire

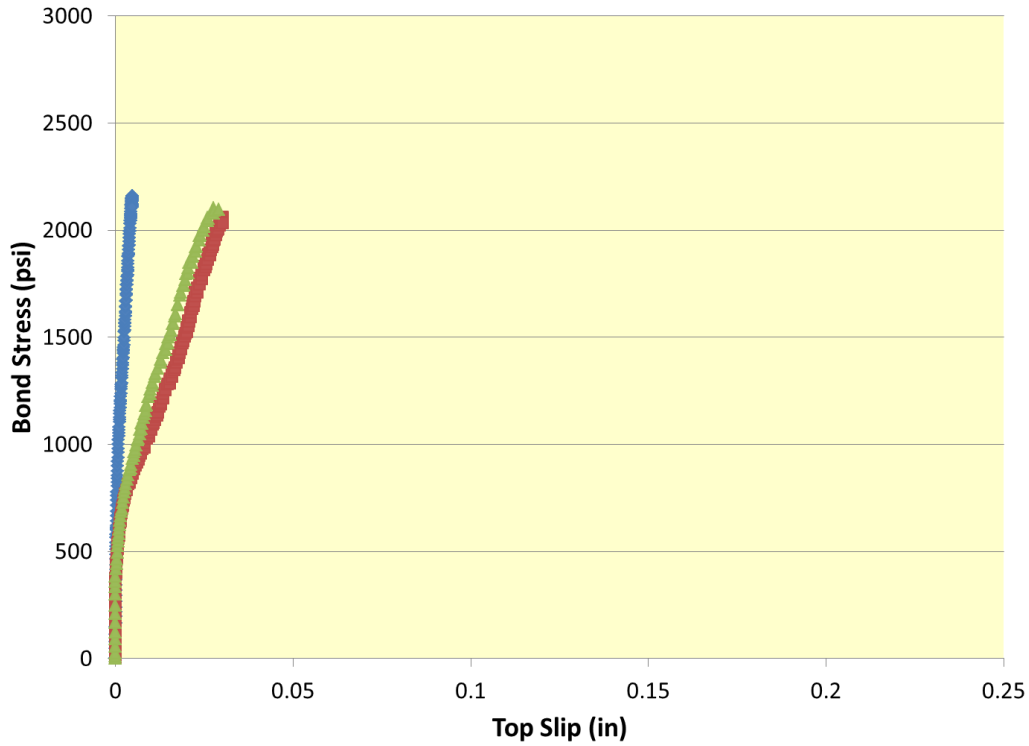


slips, surface friction is the only way that the wire can hold force. Since the wire increases in tension during loading, it decreases in cross section, causing surface friction to decrease.



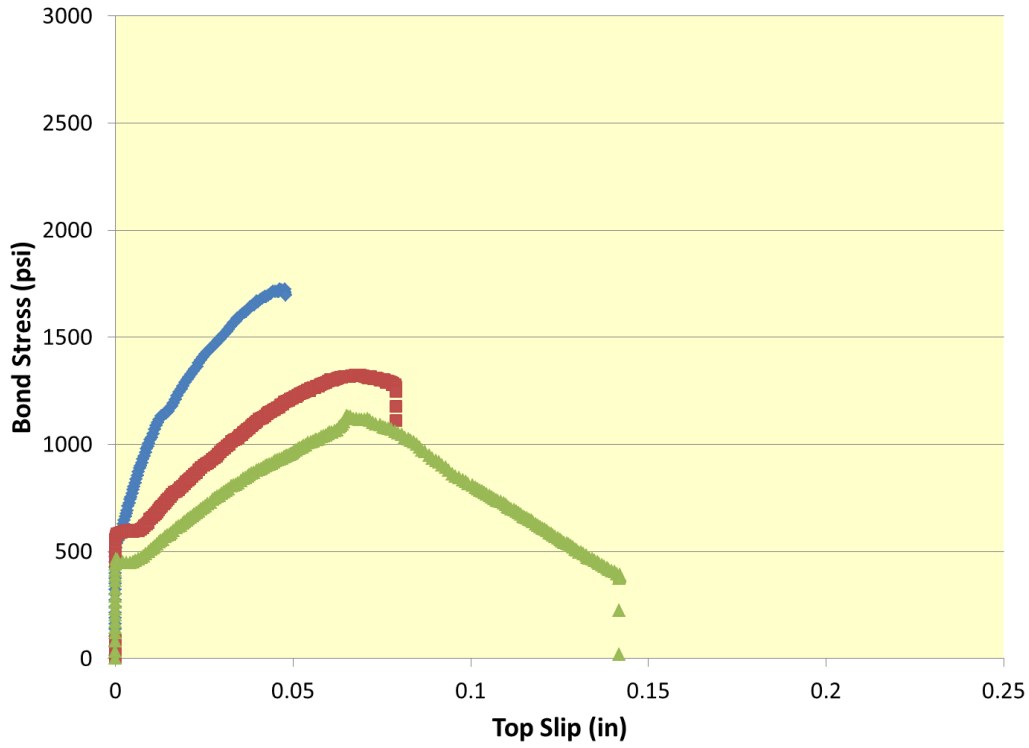
**Figure 8.1 Bond stress versus top slip results for WA (smooth)**

Figure 8.2 shows the bond versus slip relationship for WE. The spiral pattern of the wire causes the bond stress to increase as the wire slips. All WE tests were stopped before a large amount of end-slip occurred since the wire bond was high enough to hold additional load.

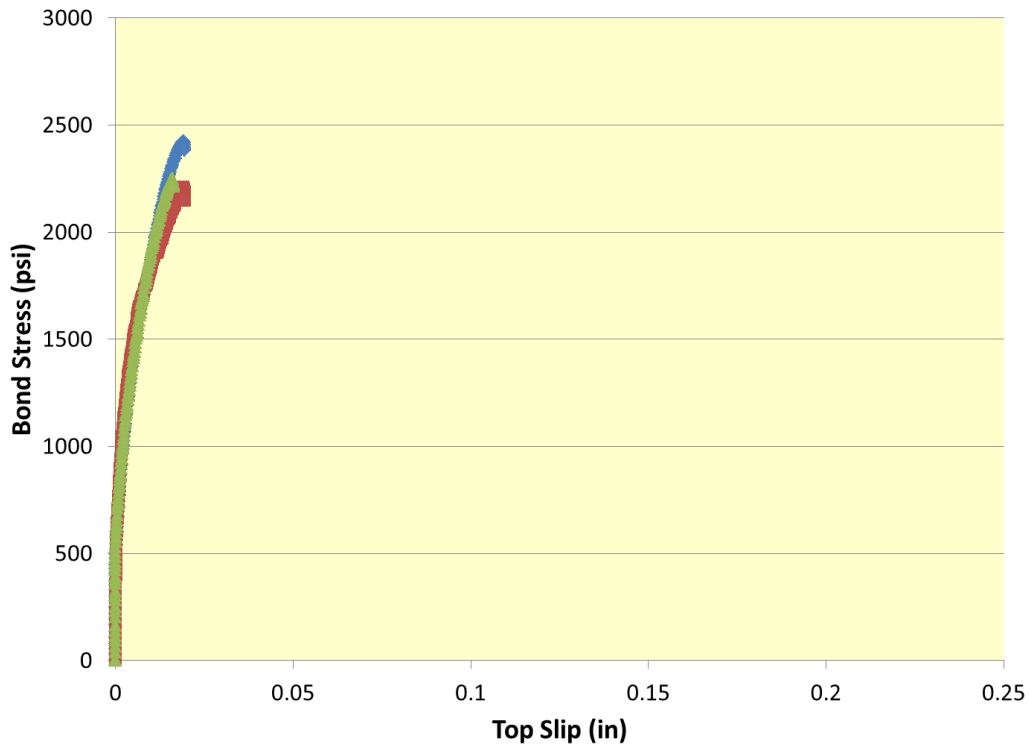


**Figure 8.2 Bond stress versus top slip results for WE (spiral)**

Figure 8.3 and Figure 8.4 show results for two chevron-patterned indents, WG and WH, respectively. The deeper indent of WH causes bond stress to increase at a higher rate than WG. WG's shallow indent causes increased bond stress until a peak is reached and then bond stress decreases and the wire slipped more. Similar to WE, WH bonded very well and the test was stopped before a large amount of slip occurred.

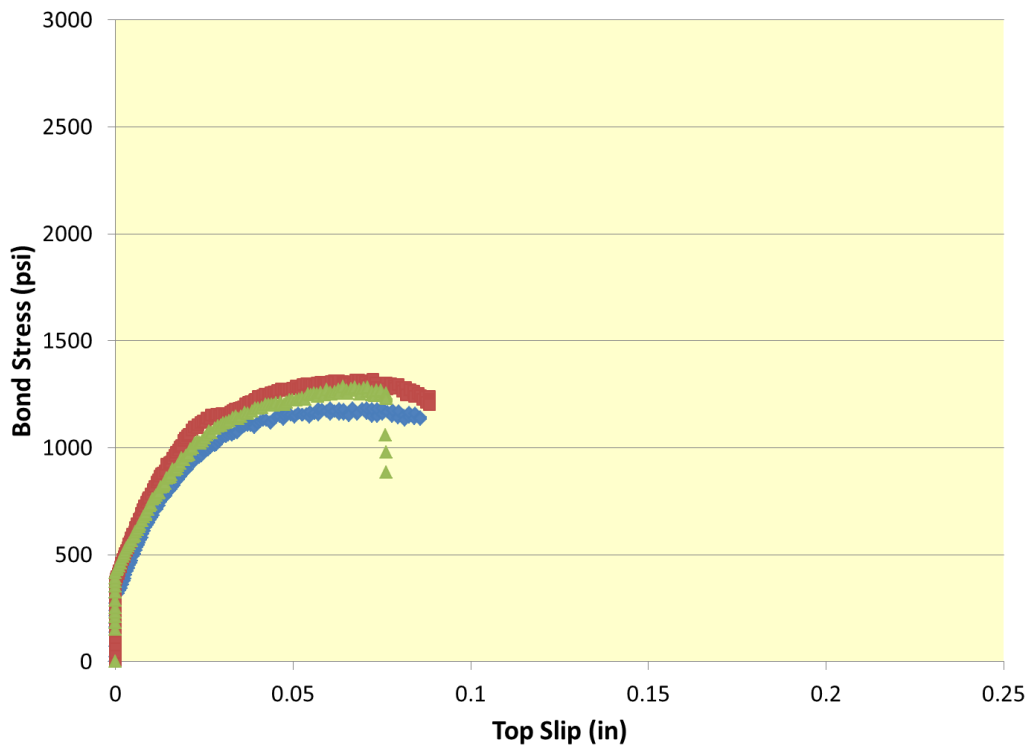


**Figure 8.3 Bond stress versus top slip results for WG (chevron)**



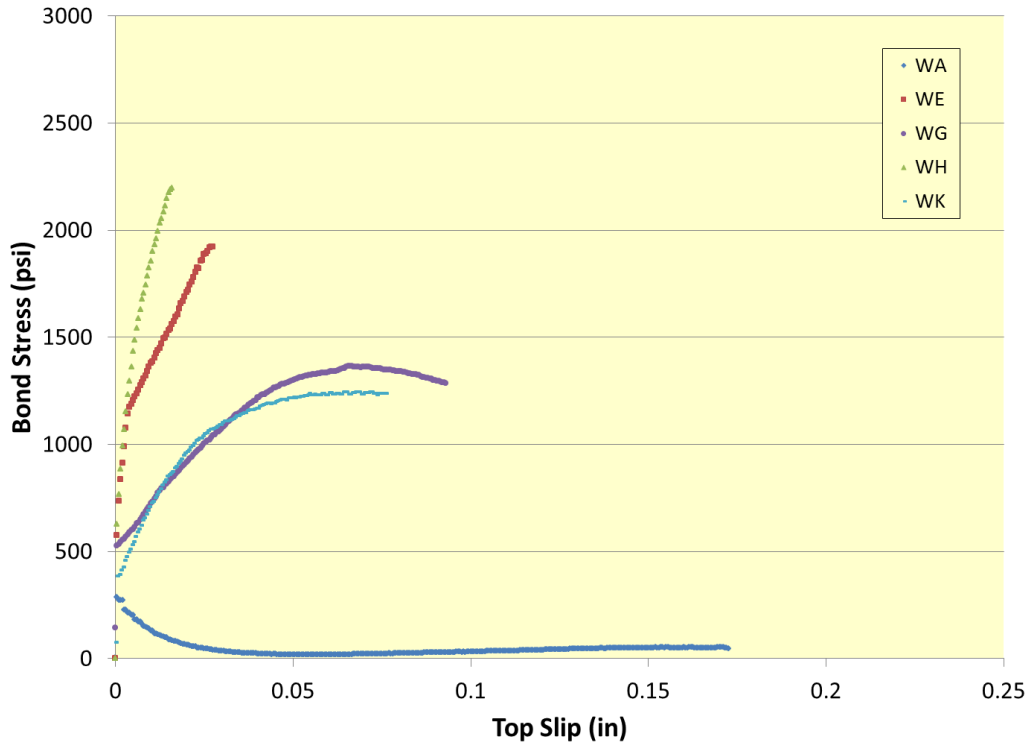
**Figure 8.4 Bond stress versus top slip results for WH (chevron)**

Figure 8.5 shows results from testing involving WK. Results show that WK behaved similarly to WG, but the bond stress value never dropped during the testing.



**Figure 8.5 Bond stress versus top slip results for WK (four-dot)**

Figure 8.6 shows results from the five wires plotted on one graph, indicating variation in flexural bond capacity between various wire reinforcement types.



**Figure 8.6 Bond stress vs. top slip results for the five reinforcements**

Flexural bond testing showed that various indent patterns provide varying amounts of bond during the test. Because of lack of indents, the smooth wire (WA) lost all bond as the wire began to slip. WH and WE showed large amounts of bond stress as the slip increased, demonstrating that either wire type provides a large amount of flexural bond capacity. WG and WK showed lower amounts of bond capacity, but bond stress initially increased, demonstrating that indents provide additional flexural bond capacity.

## Chapter 9 Confinement and Cover Tests

This section discusses results of testing which investigated the behavior of cover and confinement on the bond-slip relationship of prestressing wires. The testing procedure included specimens with two different diameters that were tested using a transfer bond test described in Chapter 7. Five wire types were used during this testing procedure.

### 9.1 Confinement and Cover Test Setup

Two and 4-inch-diameter specimens were tested to examine the effect of cover and confinement on the bonding capacity of prestressing wires. The two specimen diameters provided approximately 1 and 2 inches of cover each for the various test setups. Figure 9.1 illustrates the two cylinder sizes used in this section.

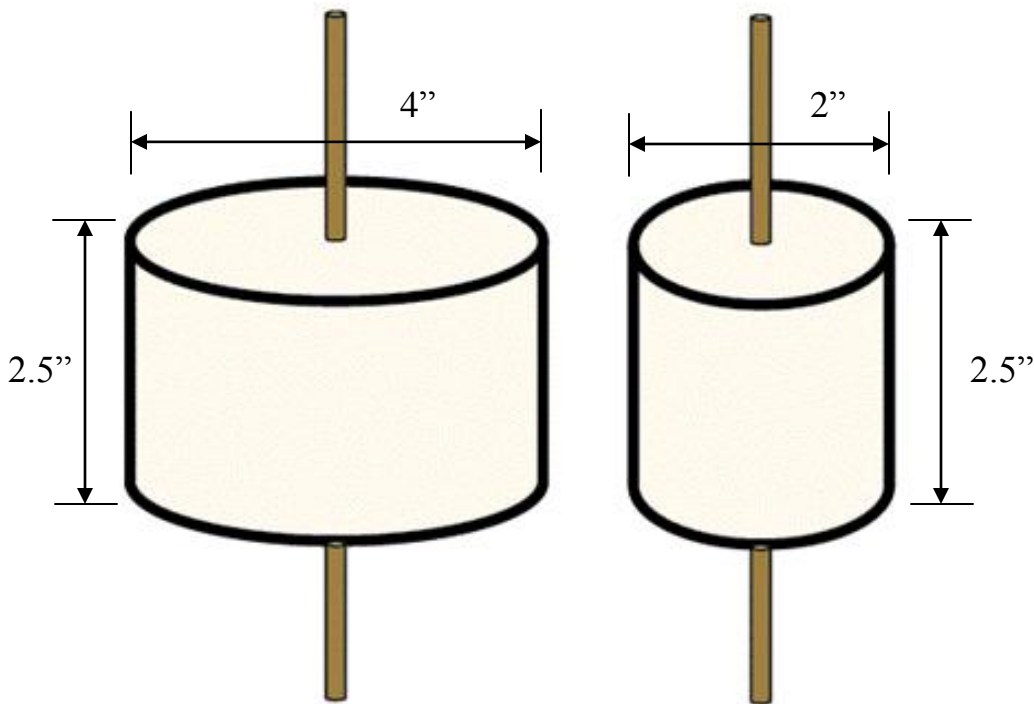


**Figure 9.1** Various cylinder sizes used in this study

Reinforcements used in this portion of the study were WA, WE, WG, WH, and WK, as described in Chapter 4. These reinforcements provided a variety of indent types for testing. The concrete mix that was used was Mix B, as described in Chapter 5. Specimens were cast in metal

molds with a height of 2.5 inches, which produced the same bond length as the initial transfer bond tests. Figure 9.2 and Figure 9.3 show the two different diameter molds used during testing. Both steel mold sizes had wall thicknesses of 0.25 inches and were clamped using one 0.375-inch-diameter steel bolt. Bond break was attached to the wire to ensure a bond length of exactly 2.5 inches, and the base of the mold was sealed to the wire to prevent concrete loss during casting. Figure 9.4 shows the 2-inch-diameter specimen after casting. The specimens were covered with plastic to prevent moisture loss, as shown in Figure 9.5.



**Figure 9.2 4-inch-diameter specimen mold**



**Figure 9.3 2-inch-diameter specimen mold**



**Figure 9.4 2-inch-diameter specimen after being cast**





**Figure 9.5 2-inch-diameter specimen covered with plastic after casting**

The metal mold was removed from unconfined specimens prior to testing, whereas the mold was left on the specimen for confined tests and LVDTs were mounted on each specimen. Based on findings from the transfer bond testing, one LVDT was used for each top and bottom slip measurement instead of two. Figure 9.6 shows the unconfined 4-inch-diameter specimen prior to testing. The confined 4-inch-diameter specimen is shown in Figure 9.7. Figure 9.8 and Figure 9.9 show the 2-inch-diameter confined and unconfined before testing, respectively. Once the specimen strength reached  $4,500 \pm 200$  psi, the specimens were tested using the procedure explained in Chapter 7. Each wire type was cast three times for each specimen type. Four frames were used to allow for the four different specimen types to be cast with one concrete batch using the same wire type. The specimens were then tested within ten minutes of each other to prevent any difference in compressive strength between the four specimens.

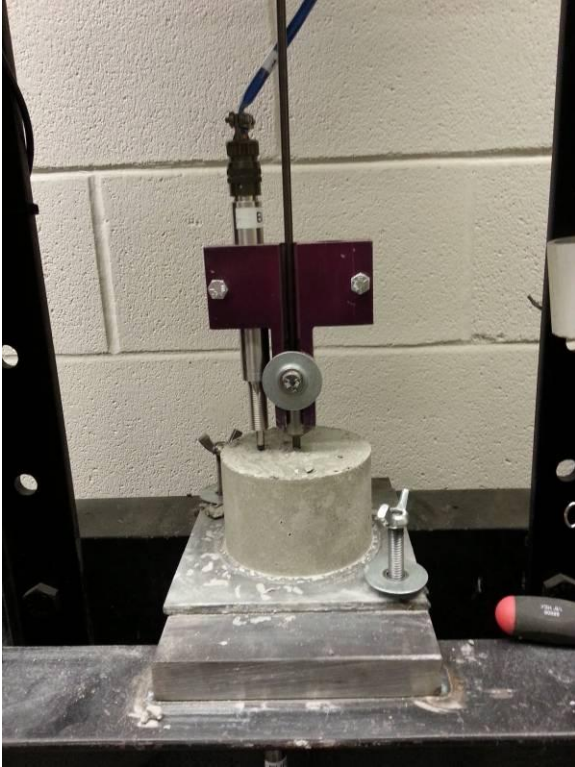


**Figure 9.6 4-inch-diameter unconfined specimen before testing**

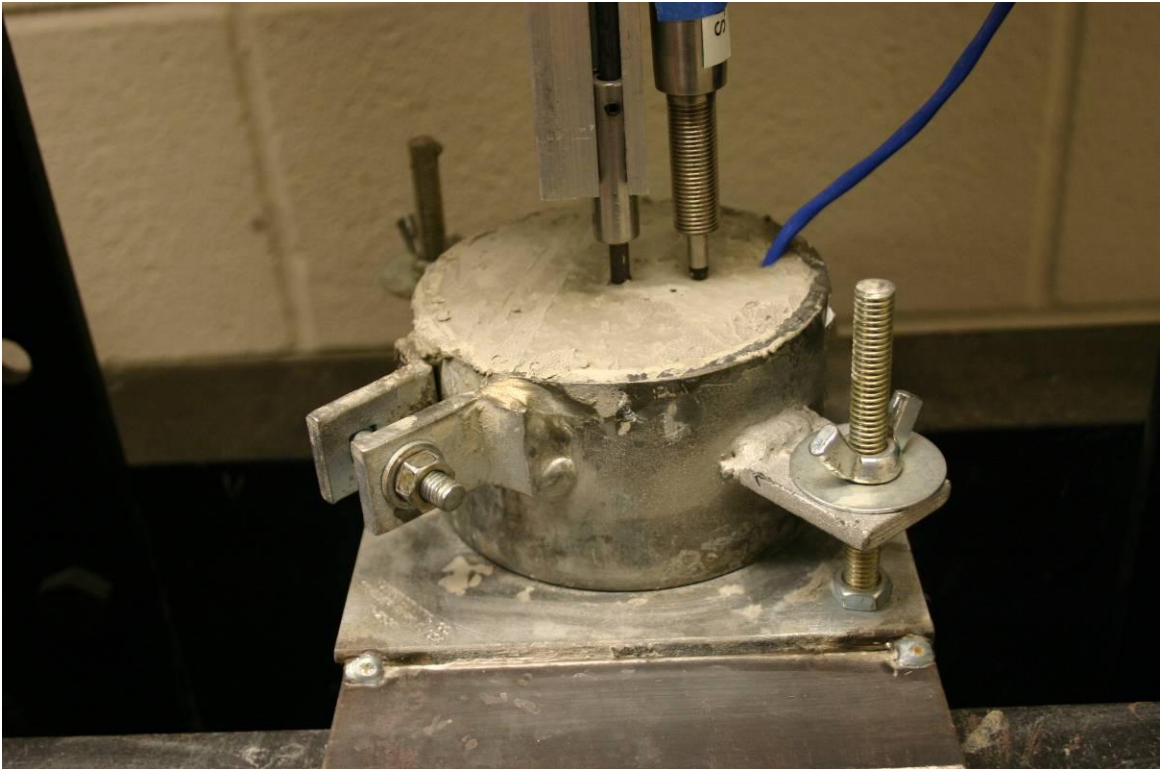


**Figure 9.7 4-inch-diameter confined specimen before testing**



**Figure 9.8 2-inch-diameter confined specimen before testing**

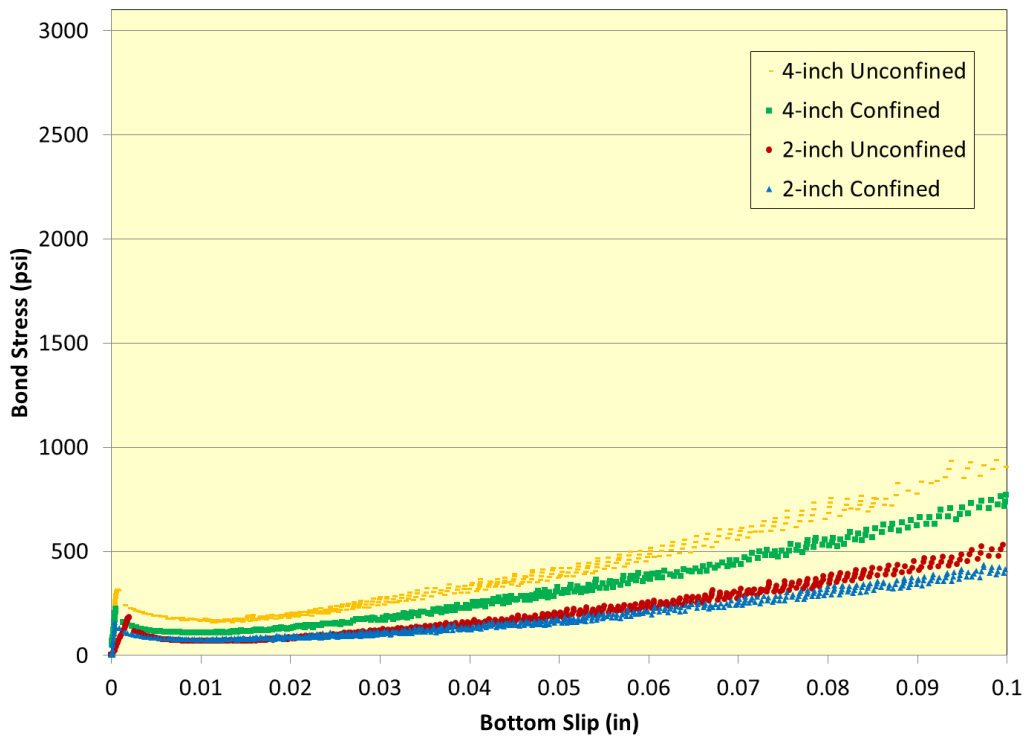


**Figure 9.9 2-inch-diameter unconfined specimen before testing**

## 9.2 Confinement and Cover Test Results

Results from the confinement and cover investigation were compared for the five reinforcement types. Test data from the two 4-inch-diameter specimens (confined and unconfined) were plotted with data from the two 2-inch-diameter specimens (confined and unconfined) for each wire type.

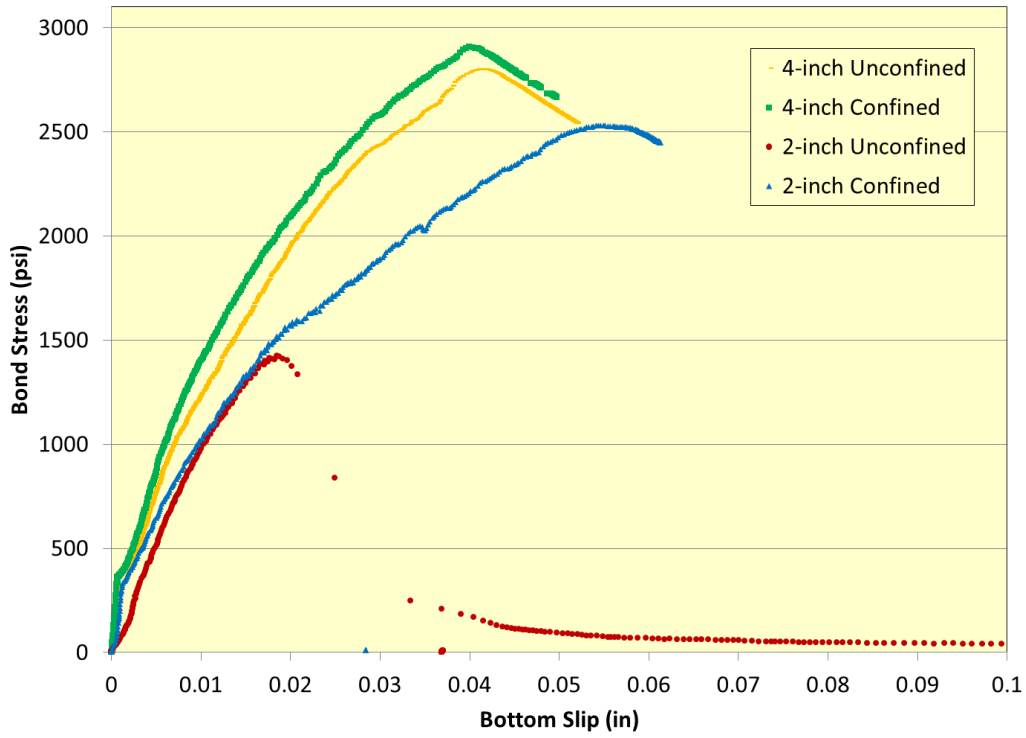
Figure 9.10 shows one plot of the four tests for WA. The other two plots are presented in Figure A.1 and Figure A.2. All three plots show that the two sizes and amounts of confinement for WA specimens did not impact smooth wire behavior. No 2-inch-diameter specimens cracked during testing. Figure A.3 through Figure A.6 show the combined results for the four different test setups with WA.



**Figure 9.10 Confined and unconfined bond stress versus slip relationship for WA**

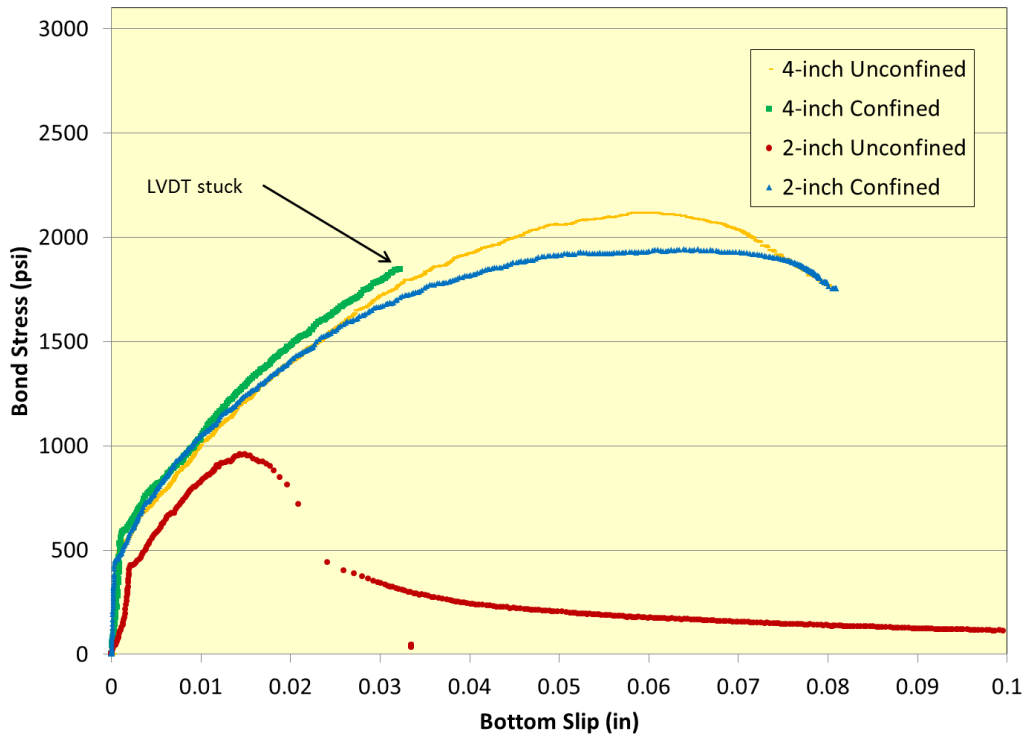
Figure 9.11 shows results of a comparison test performed during this portion of the program. The remaining two test results are presented in Figure A.7 and Figure A.8. Figure A.9 through Figure A.12 show the combined results for the four different test setups with WE. Unlike the WA specimens, all 2-inch-diameter unconfined specimens cracked during testing, as indicated in the plotted data by the decreased bond stress for the unconfined 2-inch-diameter.

The 2-inch-diameter confined specimens had a lower peak than the two 4-inch-diameter specimens.



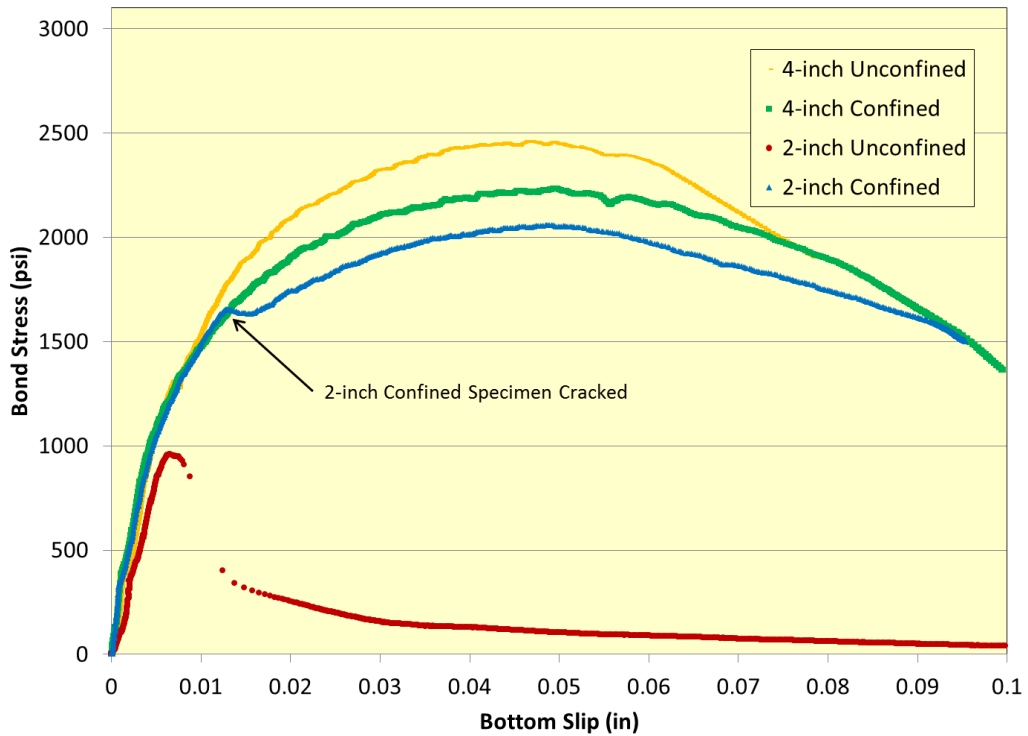
**Figure 9.11 Confined and unconfined bond stress versus slip relationship for WE**

Figure 9.12 shows results from the first test conducted with WG. The other two tests are presented in Figure A.13 and Figure A.14. Figure A.15 through Figure A.18 show the combined results for the four different test setups with WG. Due to an unexpected increase in the laboratory temperature, specimens for Figure A.13 were tested at 5,500 psi, resulting in higher bond stress. The LVDT for the 4-inch-diameter confined specimen stuck during testing, as shown in Figure 9.12 but reached a max bond stress of 2,215 psi. Similarly to tests for WE, all WG 2-inch-diameter unconfined specimens cracked during testing, as shown in each plot. The 2-inch-diameter confined specimens behaved closely to 4-inch-diameter specimens that what was found with Wire WE.



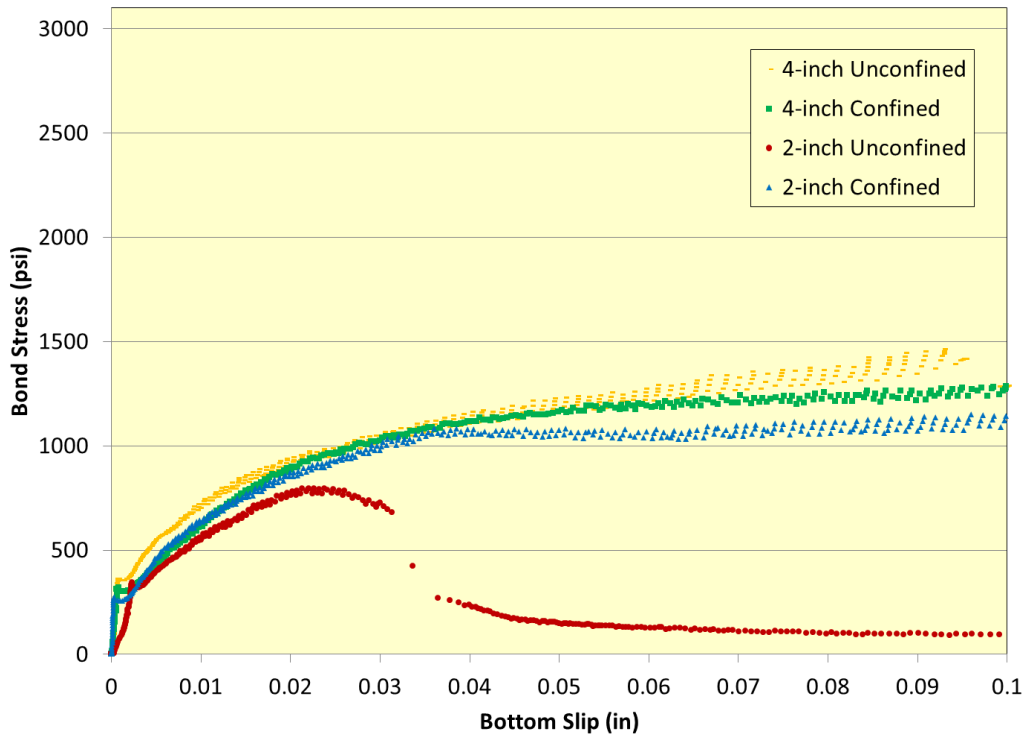
**Figure 9.12 Confined and unconfined bond stress versus slip relationship for WG**

Figure 9.13 shows results from testing WH. Both 2-inch-diameter specimens cracked during testing, as shown in the graph. The 2-inch-diameter unconfined specimen produced a hairline crack due to confinement of the mold, thus preventing the crack from opening. Figure A.19 and Figure A.20 show results from two other WH tests. Figure A.21 through Figure A.24 show the combined results for the four different test setups with WH. Similar to WG and WE, all 2-inch-diameter unconfined specimens cracked. The 4-inch-diameter confined specimen for the second test had showed poor bonding, resulting in the erroneous plot, as shown in Figure A.19.



**Figure 9.13 Confined and unconfined bond stress versus slip relationship for WH**

Figure 9.14 shows results from the first WK test, and Figure A.25 and Figure A.26 show results from the second and third tests. Two of the three 2-inch-diameter unconfined specimens cracked during testing, as shown in the plotted data. Figure A.27 through Figure A.30 show the combined results for the four different test setups with WA. Indents for the WK did not produce as much splitting potential as the other reinforcements. Figure 9.15 shows a 2-inch-diameter unconfined specimen after cracking.



**Figure 9.14 Confined and unconfined bond stress versus slip relationship for WK**



**Figure 9.15 Cracked 2-inch-diameter unconfined specimen after testing**



## Chapter 10 2-inch-Diameter Specimen Splitting Tests

This section discusses results of using a tensioned wire pullout test to correlate the amount of slip needed to split a specimen with different wire geometry parameters. Twelve 5.32-mm-diameter wires with distinct indent patterns, as described in Chapter 4, were used in this program. Each wire reinforcement was tested in three specimens.

### 10.1 2-inch-Diameter Specimen Splitting Test Setup

Specimens cast in this test were 2.5 inches tall with a diameter of 2 inches. Initial testing with a 4-inch diameter specimen showed that the cylinder did not split; therefore, a 2-inch-diameter specimen was chosen to provide a low amount of cover to exacerbate cracking behavior of the indents. Bond breaker was attached to the wire at the top of the molds to provide a 2.5-inch bond length, and the hole in the support was also covered with gray tape to seal the bottom of the mold. Figure 10.1 shows the mold prior to specimen casting.



**Figure 10.1 Metal mold prior to casting**

The specimens were cast in molds in two lifts and rodded for compaction. Mix B was used for specimen casting, as described in Chapter 5. Four wire types were tested with each pour to prevent one erroneous pour from causing misleading data, a potentiality if only one wire type was tested per batch. Specimens were tested using the transfer bond test procedure described in Chapter 7. Figure 10.2 shows a cracked specimen.

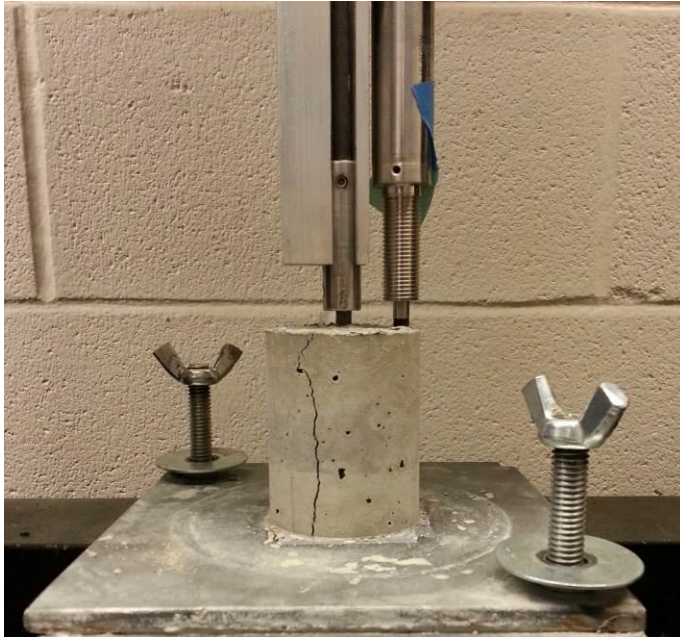


**Figure 10.2 2-inch-diameter specimen after testing**

## **10.2 2-inch-Diameter Specimen Splitting Test Results**

Data from tensioned pullout tests was tabulated to discern bond force and end-slip measurement values. Load cell measurements were used to determine the amount of bond force carried by the concrete bond with the wire. Bond force was determined by calculating the difference between the two load cells on each frame (i.e., top and bottom). LVDT readings were used to determine the amount of wire slip present on the top and bottom ends of the specimen. Elastic shortening effects were accounted for in end-slip value calculations by using Equation 1 from Chapter 7.

The indent patterns provided distinct bond force versus end-slip behaviors. The indent patterns also caused some specimens to split during testing while others did not split. The smooth wire (WA) did not cause the specimen to split. Other wire indent patterns that did not cause splitting were the 2-dot (WL) and 4-dot (WK) patterns; however one of the three WK specimens split during testing. The spiral-patterned wire (WE) caused splitting but because the wire did not

have indents, it was removed from this section of testing. All chevron-patterned indent wires caused the specimen to split during testing; however, each reinforcement exhibited distinct bond behaviors prior to splitting.

Data from chevron-indented specimen tests were examined to discern the correlation between indent geometries and the cause for specimen splitting. As shown in Figure 9.3, specimens achieved a maximum bond force and then bond decreased as the specimen began to split. Individual test results for each wire type are shown in Appendix B. Top and bottom slip values at the maximum bond force were found for each test. Each value corresponded to when the specimen began cracking; these values were averaged for each wire type and compared to geometrical wire measurements found by Haynes et al (2013b).

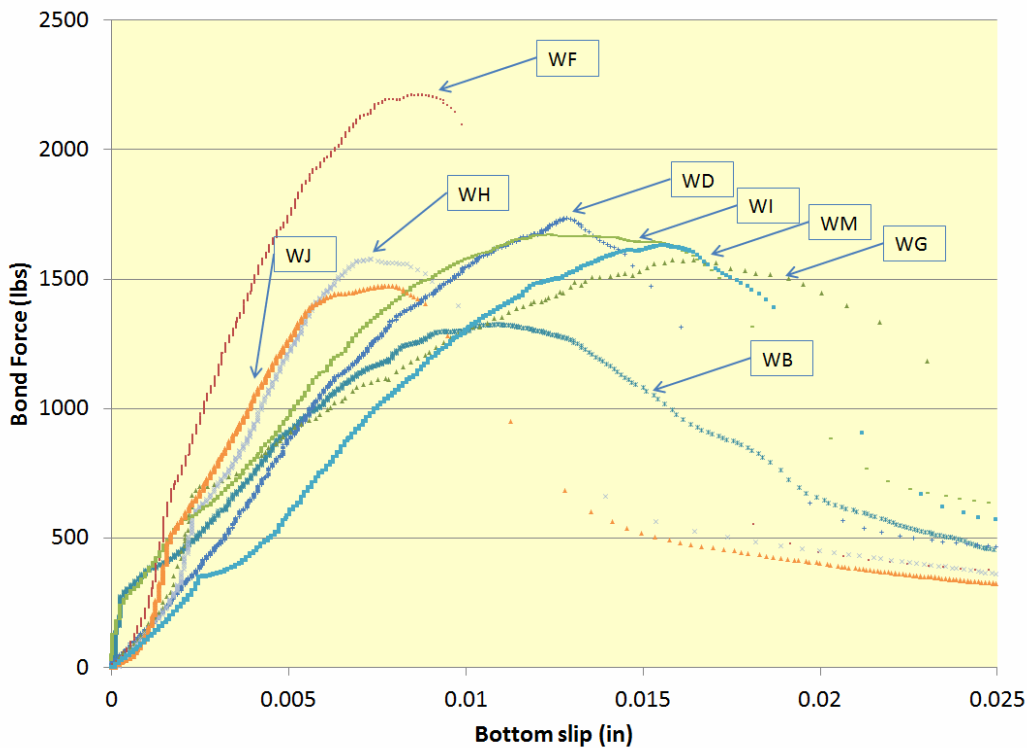


**Figure 10.3 Bond force versus bottom slip relationship for various indent patterns**

Bottom slip values provided the highest correlation with geometrical measurements of the various indent patterns but top slip values showed correlation lower than bottom slip values. Maximum load values showed lowest correlation with geometries. Indent depth was a primary geometrical feature able to be correlated with the bottom slip at splitting. Figure 10.4 shows model findings with indent depth.

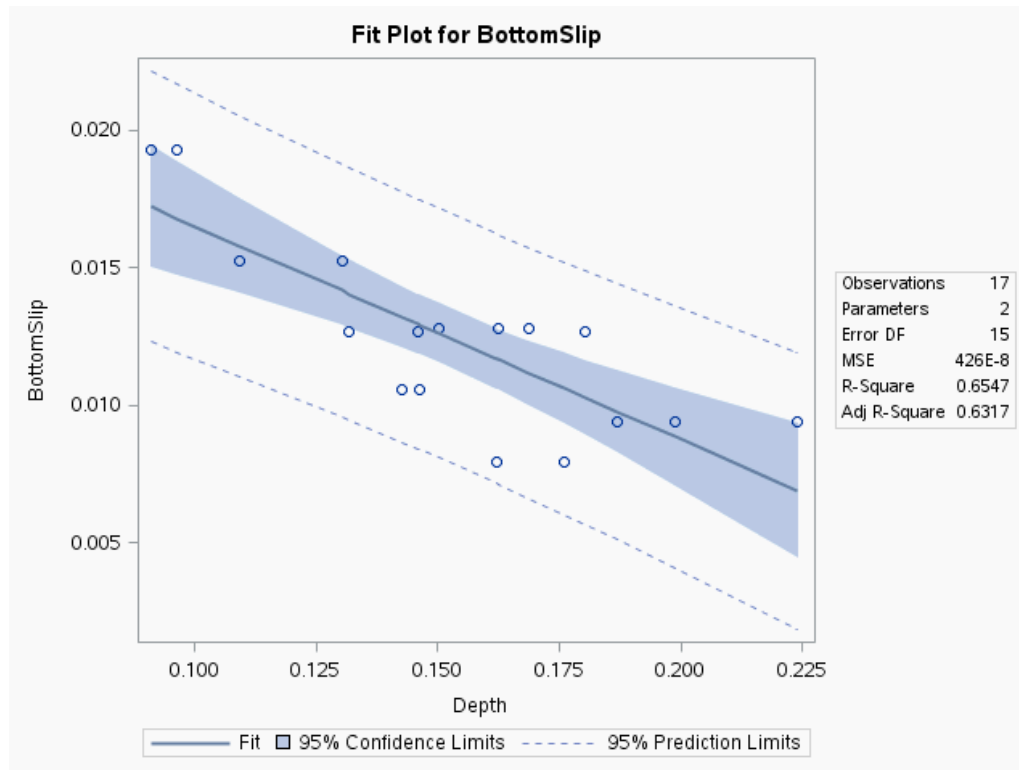


**Figure 10.4 Correlation findings from SAS program between bottom slip and indent depth**

Statistical Analysis Software (SAS) was used to correlate multiple features; three features were found to predict the bottom slip (BS) at splitting with an  $R^2$  of 80% and a p-value  $<.0001$ . These features included indent depth, projected surface area of the indent, and volumetric void of the indent. Equation 3 revealed that these variables were related to the bottom slip at splitting.

$$BS=0.07081+0.01756*VV-0.33870*D-0.00314*PSA \quad (3)$$

Where:

- BS is bottom slip at splitting (in inches)
- VV is volumetric void of indent (in  $\text{mm}^3$ )
- D is indent depth (in mm)
- PSA is projected surface area of indent (in  $\text{mm}^2$ )

Tensioned pullout tests showed that geometrical features of the indents caused the test specimens to split. The bottom slip that the specimens split at was correlated to geometrical

features of the indents. An absence of indents did not cause splitting as seen with the smooth wire (WA). Lower amounts of indents also demonstrated a lower probability of splitting, as seen with the 2-dot indented wire (WL) which did not split and the 4-dot indented wire (WK) which split one of the three tested specimens.

Findings from this test program showed that geometry of the indent pattern can determine at what slip value the reinforcement would cause a specimen to split. Higher bonding wire patterns showed a lower slip value in order to split the specimen.

Portions of the preceding chapter were originally published here:

Tensioned Pullout Test Used To Investigate Wire Splitting Propensity in Concrete Railroad Ties, by Joseph R. Holste, M.S., Mark Haynes, M.S., Robert J. Peterman, PhD, PE, B. Terry Beck, PhD, Chih-Hang John Wu, PhD, Proceedings of the 2014 Joint Rail Conference, JRC2014-3833, Copyright 2014 American Society of Mechanical Engineers.

## Chapter 11 Expansion Testing

This section details attempted methods to measure lateral strain produced from the five indent types (WA, WE, WG, WH, and WK). Several methods were investigated to determine the most suitable method for measuring lateral strain in concrete specimens during the transfer bond test, as described in Chapter 7. Investigative methods included two non-contact lasers heads, externally mounted strain gauges, externally mounted LVDTs, and embedded Vibrating Wire Strain Gauges (VWSGs). Each method setup and results are described in the following sections.

### 11.1 Non-Contact Lasers

Two non-contact lasers, placed on each side of the specimen, were tested to measure lateral expansion of the specimens. The lasers were capable of measuring distance to the specimen in a range of 20 mm with 0.025 microns of accuracy, so two lasers allowed the author to measure specimen expansion as the average of the two laser readings. Laser measurements, force, and end-slip measurements were input into the data acquisition system.

The specimen tested using non-contact lasers was a 2-inch-diameter cylinder 2.5 inches tall, which was the same cylinder size used in Chapter 9. Mix B was used because of the specimen's size. WH was used to investigate this option due to its cracking of specimens in Chapter 9. Figure 11.1 shows a schematic of the laser head setup. Figure 11.2 shows one of the lasers used to measure lateral expansion.

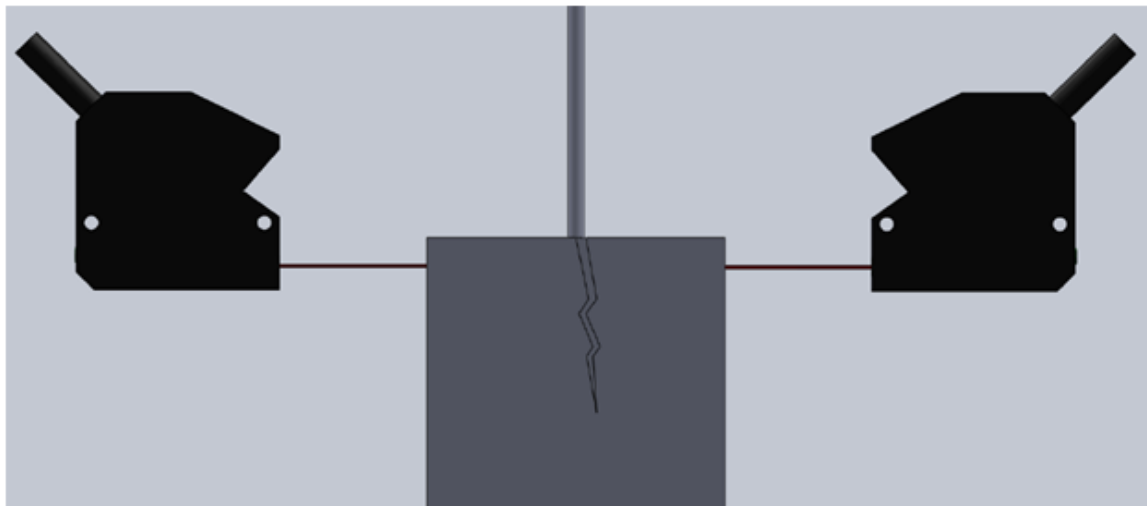


**Figure 11.1 Laser head setup to measure lateral expansion**

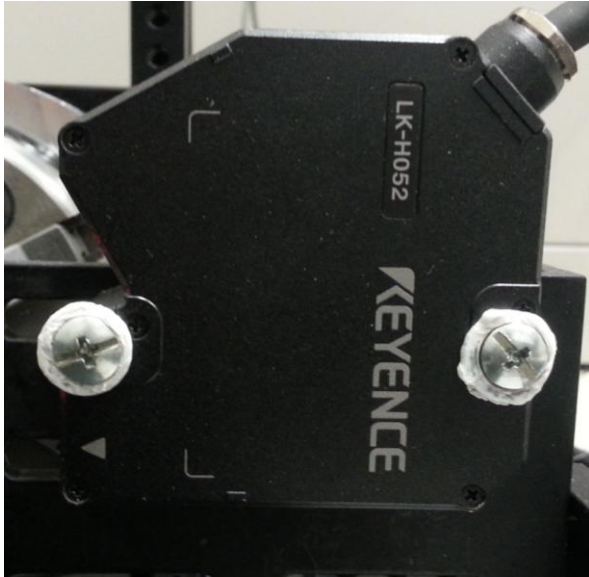


**Figure 11.2 Laser head used to measure lateral expansion**

Figure 11.3 shows results from the lateral expansion test setup with laser heads. Focal points of the lasers were determined to be too small and surface roughness of the specimen produced inconstant results. In addition, the lasers could not measure any noticeable displacement prior to cracking.

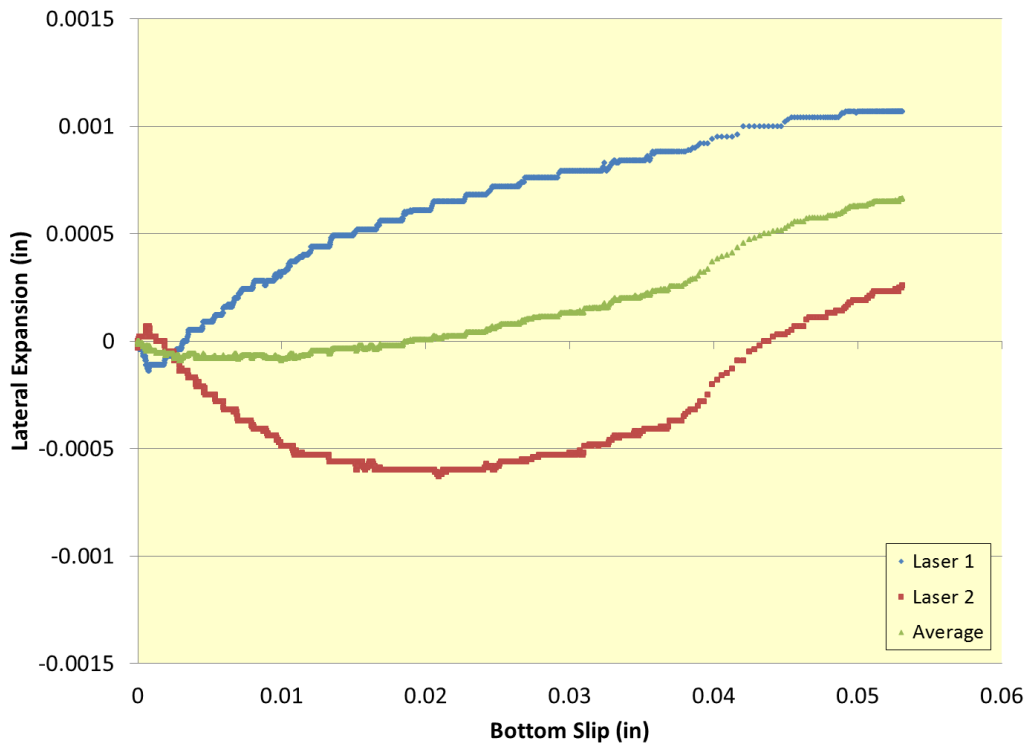


**Figure 11.3 Lateral expansion measured with lasers on 2-inch diameter WH specimen**

## 11.2 LVDTs

The second method to measure lateral expansion of a concrete specimen was a custom-made invar ring equipped with four LVDTs. LVDTs were mounted to the ring in order to measure specimen expansion. The same concrete mix and specimen size were used as with the non-contact laser setup previously described. WH and WA were tested to identify expansion differences between the two wire types.

An invar ring was fabricated to mount around the cylinder during testing. Invar was chosen because of its low coefficient of thermal expansion of  $1.2 \times 10^{-6} \text{ } ^\circ\text{C}^{-1}$ ; therefore, this material is very stable with temperature changes preventing erroneous measurements due to temperature change. The ring was equipped with four LVDTs to measure expansion, readings were measured during testing, and data were recorded. The LVDTs were positioned to measure expansion 0.5 inches from the top surface of the specimen. Figure 11.4 shows invar ring setup.

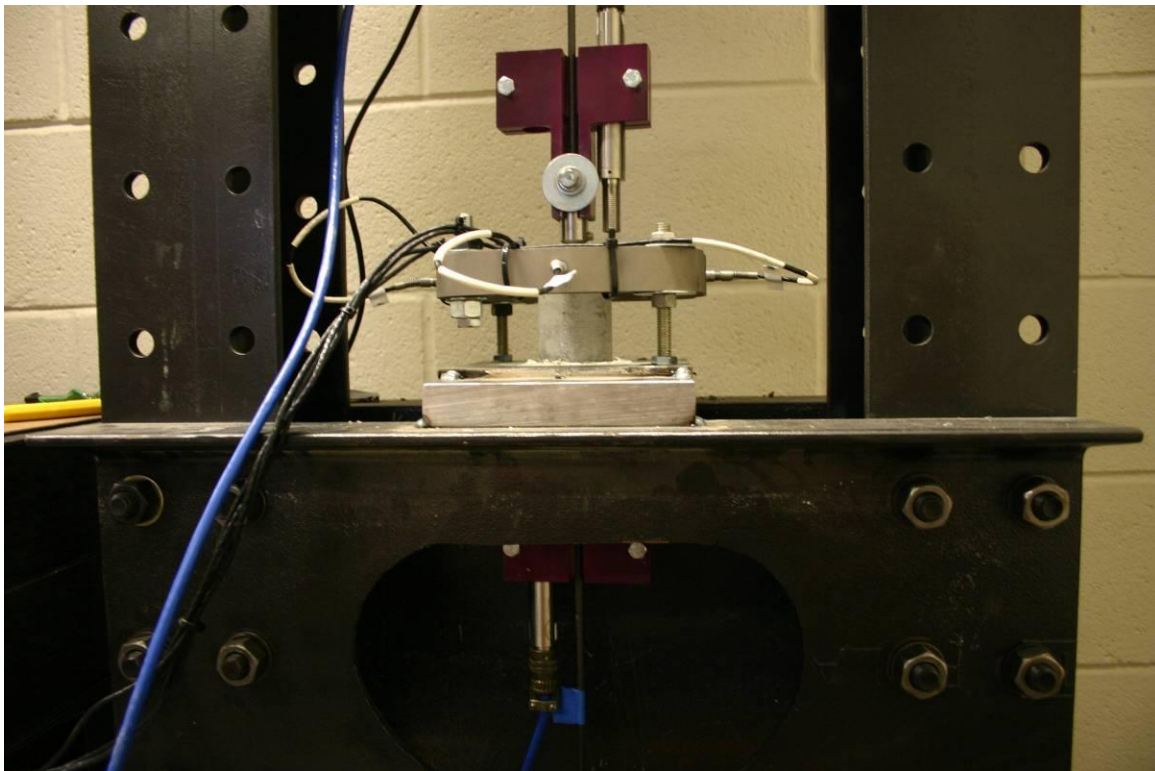


**Figure 11.4 Invar ring setup location on specimen**

The setup with the invar ring was used to obtain expansion of the concrete surface as the prestress force was introduced. However, no appreciable expansion was measured prior to specimen splitting. The LVDTs were numbered one through four with number one located



directly opposite number three. Therefore, the two measurements were averaged in order to determine expansion. The procedure was repeated for the two even LVDTs, and then resulting averages were averaged to determine the overall average. Figure 11.5 shows results from the test using WH. Splitting during the test was observed only after the specimen cracked. Figure 11.6 shows the cracked WH specimen after testing.

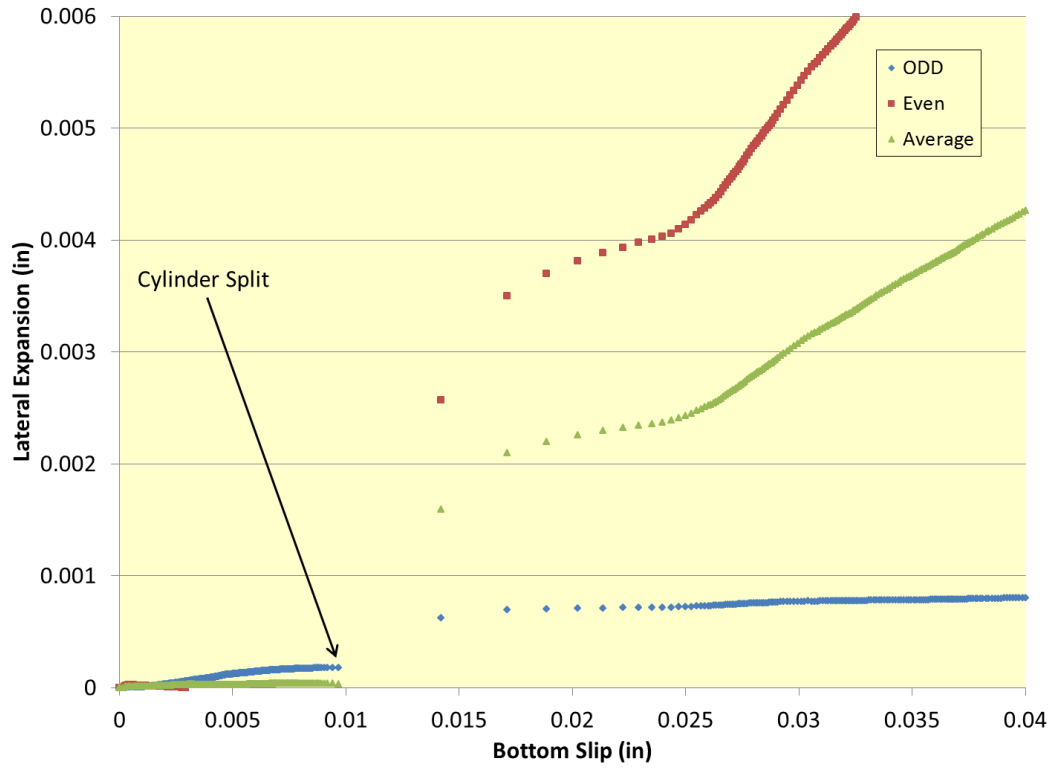


**Figure 11.5 Lateral expansion measured with invar ring for WH specimen**



**Figure 11.6 WH specimen after testing with cracking**

The WA specimen failed to crack during testing but demonstrated a slightly higher average lateral expansion than the WH specimen prior to cracking, as seen in Figure 11.7. Figure 11.8 shows the WA with no cracks after testing.

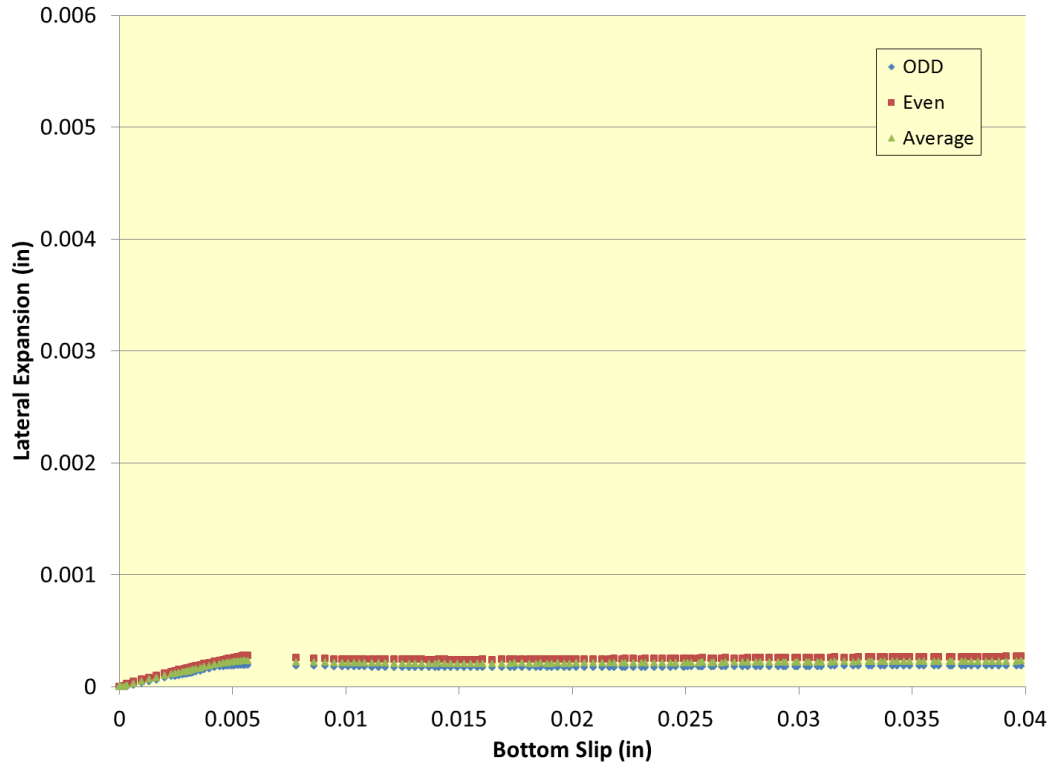


**Figure 11.7 Lateral expansion measured on WA specimen**

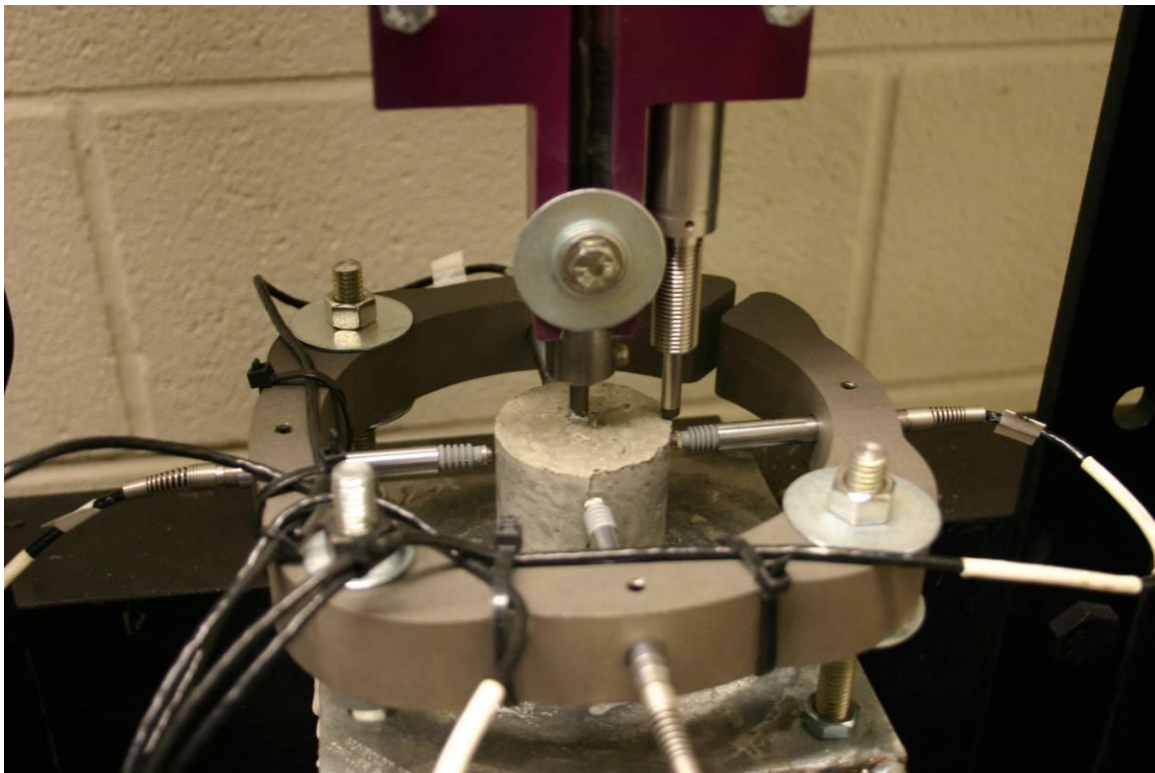


**Figure 11.8 WA specimen after testing without cracking**

The LVDT ring setup effectively measured lateral expansion after the specimen cracked, but it did not identify any consistent expansion before cracking. The WH specimen cracked and caused an overall higher average lateral expansion, but it had a lower average value than the WA specimen before cracking.

### **11.3 Surface Mounted Strain Gauges**

The third method used to measure lateral expansion involved externally mounted strain gauges. Two gauges were mounted near the top of each test cylinder, and WA and WH wires were used for this test setup. Strain gauges were connected to the data acquisition system, and strain was measured during the release of tension in the wires. Specimen size and concrete mix matched the ones used in the previous two sections.

Strain gauges were used to measure surface strain caused by lateral expansion of the reinforcements. After the specimens had cured for 10 hours, the molds were removed so the concrete surface could dry because evaporating moisture from the concrete surface would inhibit the bonding agent. After 30 minutes of drying, two 2-inch long strain gauges were mounted to the surface of the specimen 0.5 inches from the top surface. Figure 11.9 shows the mounted gauges on the specimen. The gauges were connected to P3500s to allow gauge reading. The strain reading was output from the P3500s as voltage and was into the data acquisition system, thus allowing strain readings to be recorded simultaneously with force and end-slip measurements. Figure 11.10 shows a specimen prior to testing.

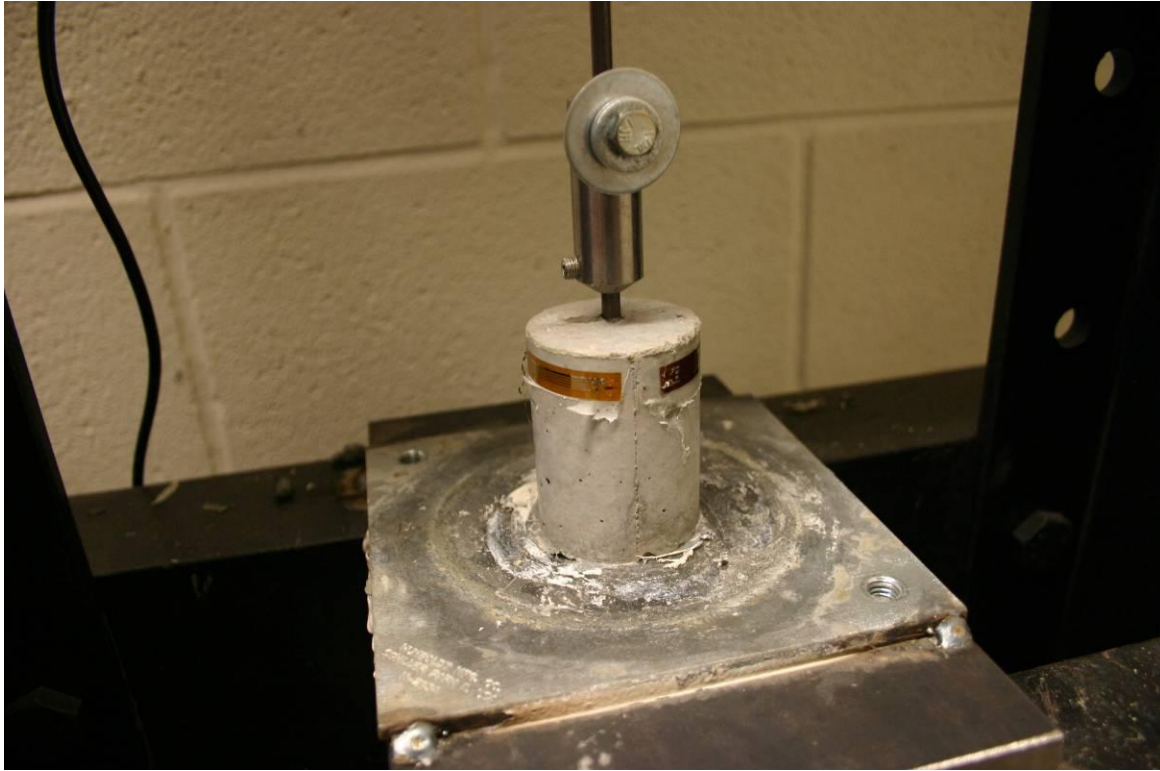


**Figure 11.9** Strain gauge location on specimen

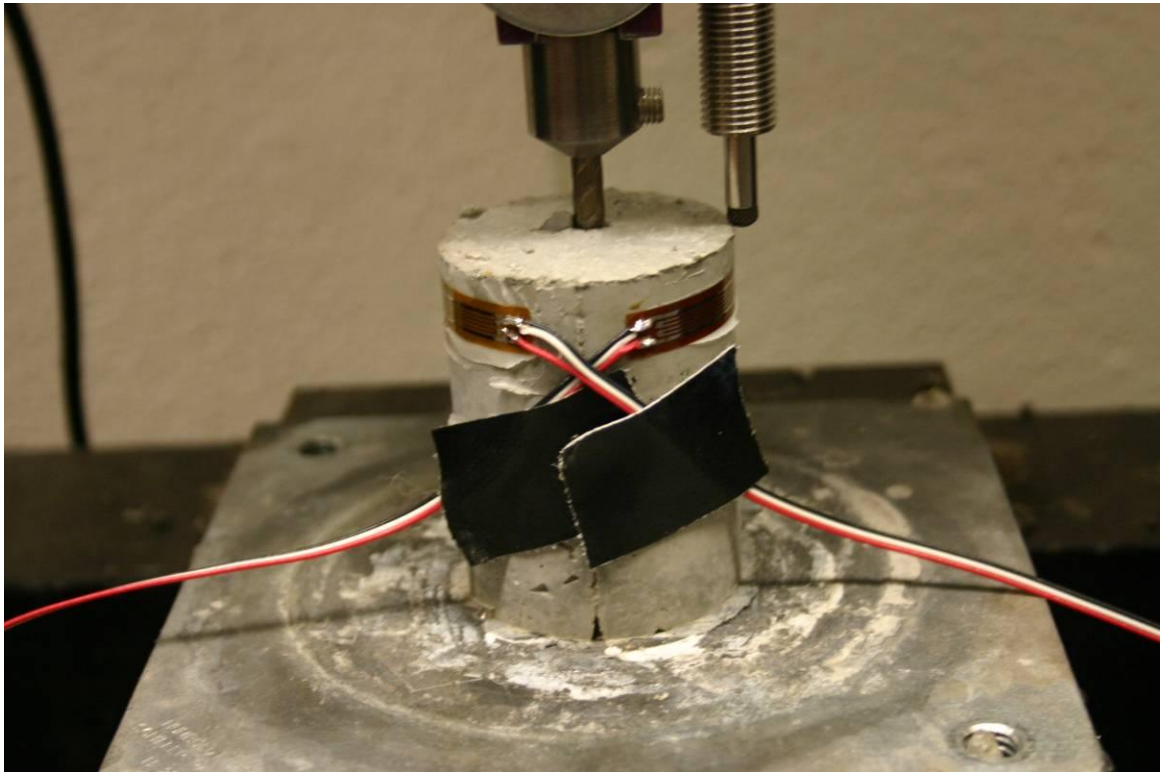


**Figure 11.10** Strain gauge specimen prior to testing

The WH cylinder split during testing, but the WA cylinder remained intact. Strain readings were plotted versus bottom slip values for each test. Figure 11.11 shows data from both tests on one graph. Strain readings from the WH cylinder indicate a steep increase in perimeter strain with respect to bottom slip values. After the specimen cracked, the strain gauge was unusable, so post cracking data was unobtainable. Figure 11.12 shows the cracked WH specimen after testing. The strain reading for the WA wire increased almost to the same amount present in the WH prior to cracking; however, these results seem unlikely compared to results in Chapter 9. The amount of strain recorded for each test was low compared to the range the gauge was able to measure. These readings could be erroneous due to incomplete bonding of the strain gauge to the concrete surface. Because of the limited time available until the specimens gained strength at a rapid rate, the bonding agent was fast-setting. Other bonding agents could have been used, but they require additional time and heat, consequently altering specimen strength. Readings found with this setup were determined inconclusive.

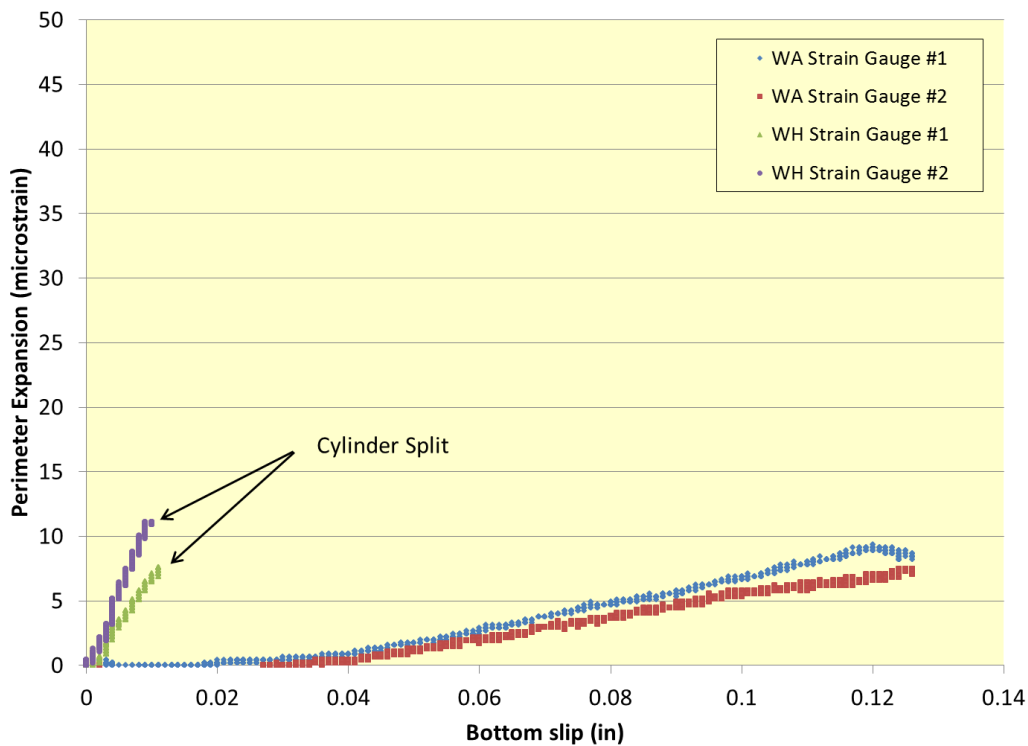


**Figure 11.11 Comparison of surface strains on WH and WA specimens**

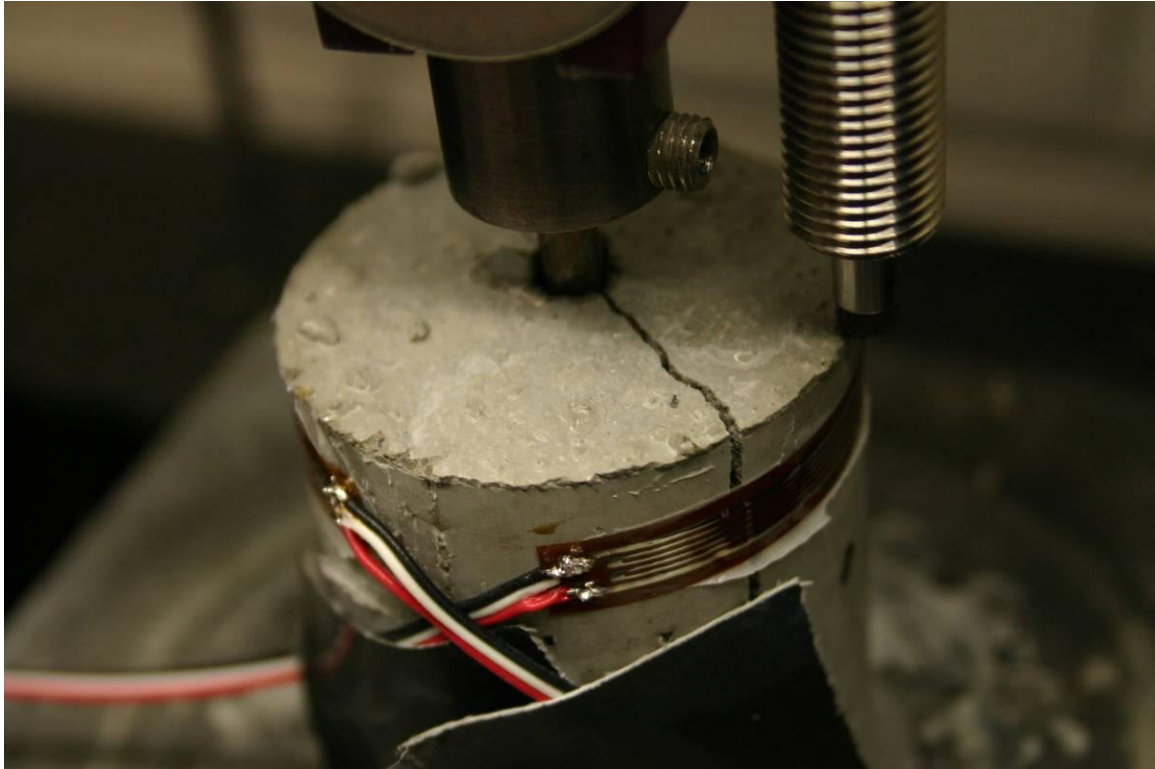


**Figure 11.12 Cracked WH specimen after testing**

#### **11.4 Internal Vibrating-Wire Strain Gauges**

Vibrating-wire strain gauges (VWSGS) were also utilized to measure lateral expansion of the specimens. Gauges were embedded into concrete when the specimen was cast, enabling the author to observe lateral expansion near the wire reinforcement instead of the exterior of the specimen. Figure 11.13 shows one gauge.



**Figure 11.13 VWSG used in the study**

The specimen size chosen for this testing was a 1.75-inch by 3.5-inch rectangle 2.5-inches tall. These dimensions provided a smaller cross section that allowed knowledge of the crack location. Figure 11.14 shows the dimensions of the VWSG specimen. A single wire was located near the center of the specimen with a bond length of 2.5-inches. Figure 11.15 shows specimen bond length and the taped base plate to prevent the specimen from bonding to the plate.



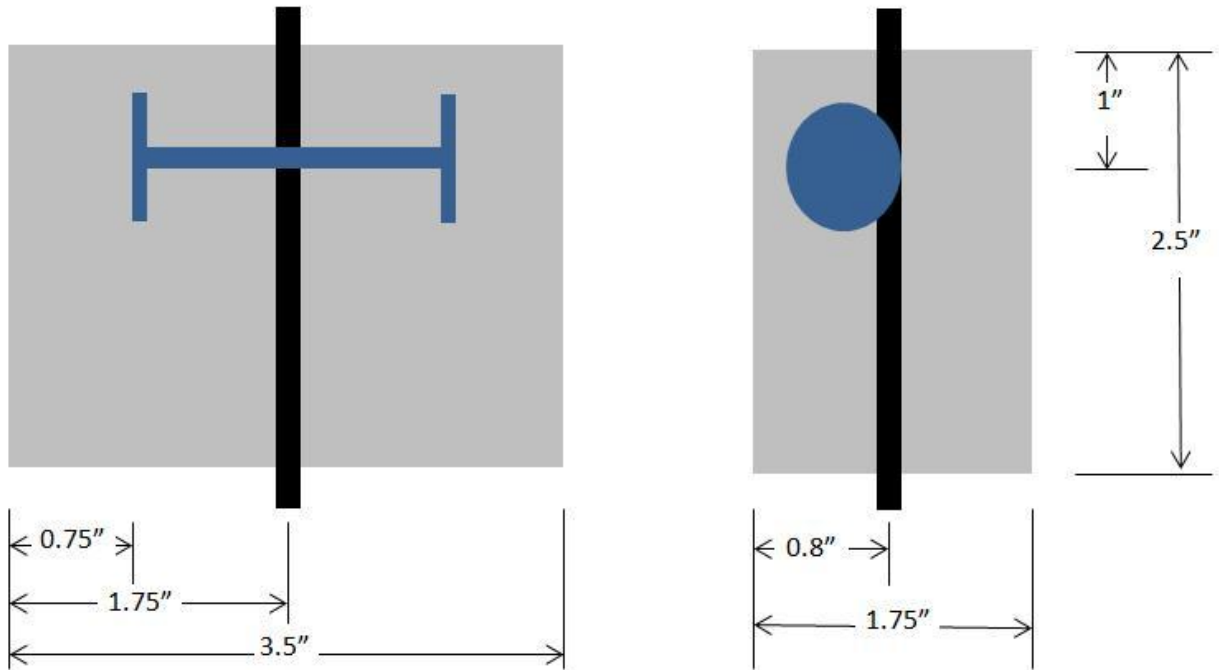


**Figure 11.14 VWSG specimen dimensions**

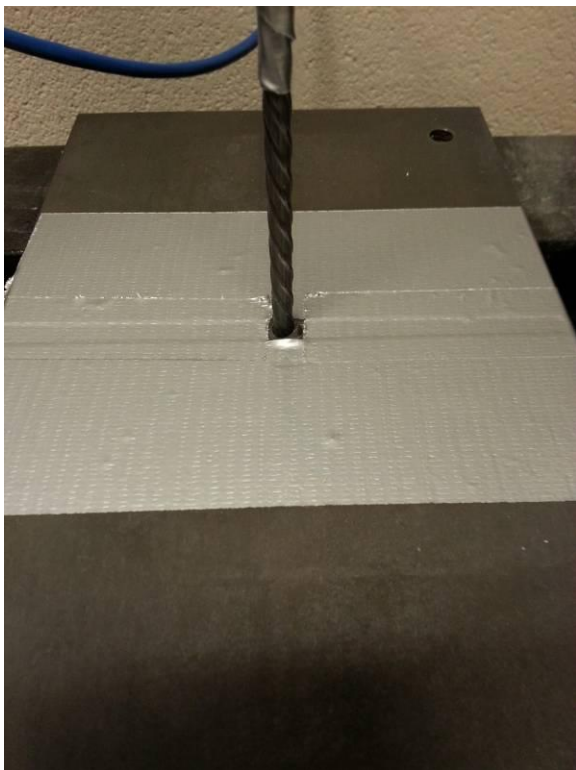


**Figure 11.15 Bond length and base taped before casting**

Aluminum inserts were used to mount a VWSG to the side of the forms. The inserts provided a rigid support for the VWSG but allowed the gauge to rotate and slide back and forth before casting. A hole was drilled into the inserts to allow the gauge ends to fit, allowing this movement. Figure 11.16 shows one insert mounted to the molds.



**Figure 11.16 Aluminum insert to secure VWSG in position**

A rectangular shape specimen was chosen so that the crack location could be predicted, unlike circular specimens previously discussed which cracked along random vertical planes. The VWSG was located 0.75 inches from the side of the form, and a gauge block was used to ensure that the wire edge was located 0.7 inches from the side of the form. The VWSG was located on a smaller cross section in order to promote the crack formation to appear on the side with the VWSG. Figure 11.17 and Figure 11.18 show the gauge prior to casting. Figure 11.19 and Figure 11.20 show the specimen before testing.

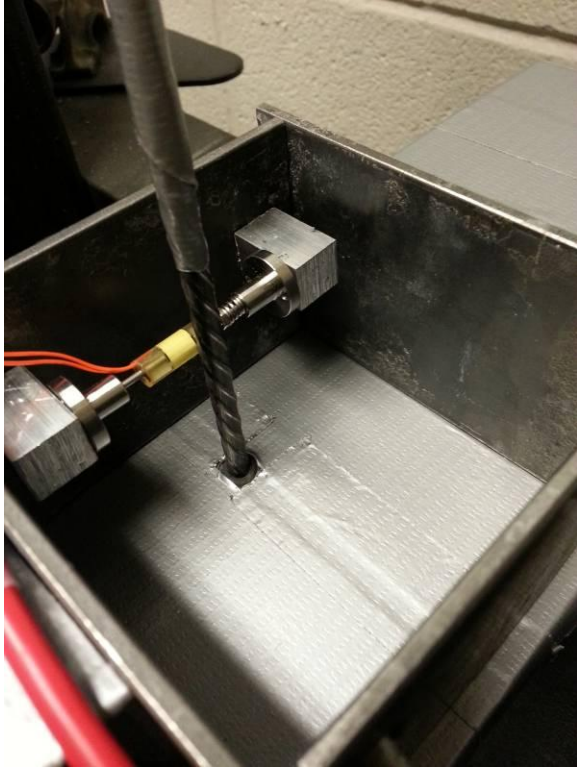


**Figure 11.17 VWSG location prior to casting**

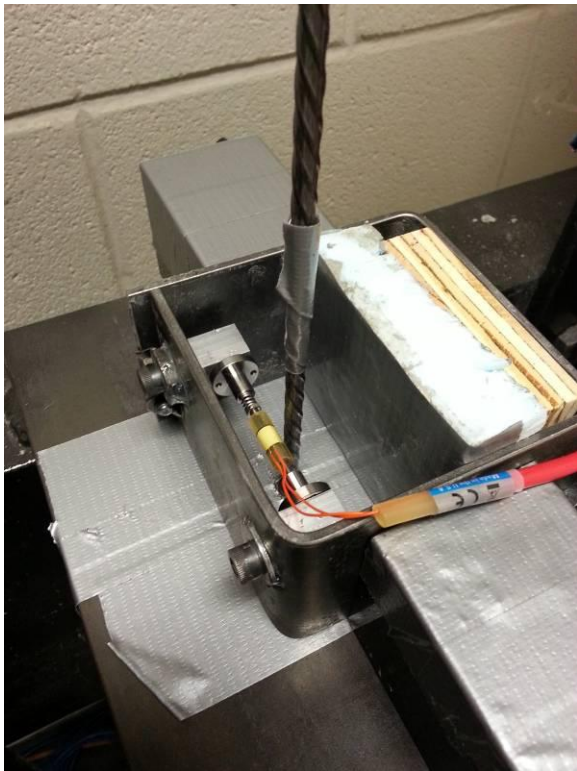


**Figure 11.18 Spacers used to keep cross section constant**



**Figure 11.19 Specimen after mold was removed**

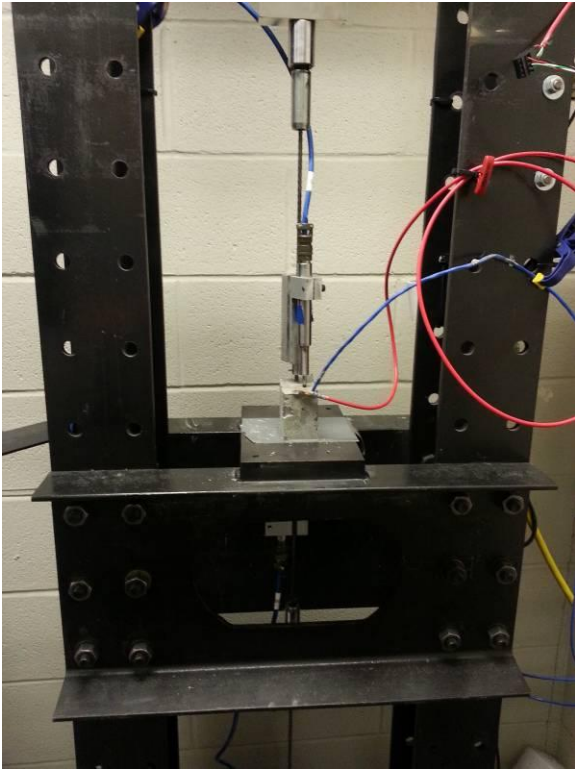


**Figure 11.20 Specimen prior to testing**

## 11.5 VWSG Results

VWSGs were used to test the five wire types (WA, WE, WG, WH, and WK) in order to determine the lateral expansion caused by each wire type. Load cell readings and end-slip measurements were recorded during testing. The VWSG reader could record only one reading per second, so the specimens were tested at a slower rate than previous tests. Readings were entered into the data acquisition system as a linear voltage measurement and this data was used to graph the behavior of each wire type. In addition, bond stress and lateral expansion were graphed versus the bottom slip for each wire type.

Figure 11.21 shows results from the test using WA. As demonstrated in the graph, internal lateral strain reached 20 microstrain. During testing, the wire slipped through the specimen, making audible clicks. This clicking caused some VWSG readings to deviate from the constant reading, as shown by points near the 50 microstrain level. However, the specimen did not crack during testing, as demonstrated in Figure 11.22. A second test was performed using WA, and its results are shown in Figure C.1; however, load cell data was not collected, so only lateral strain versus bottom slip values are plotted.

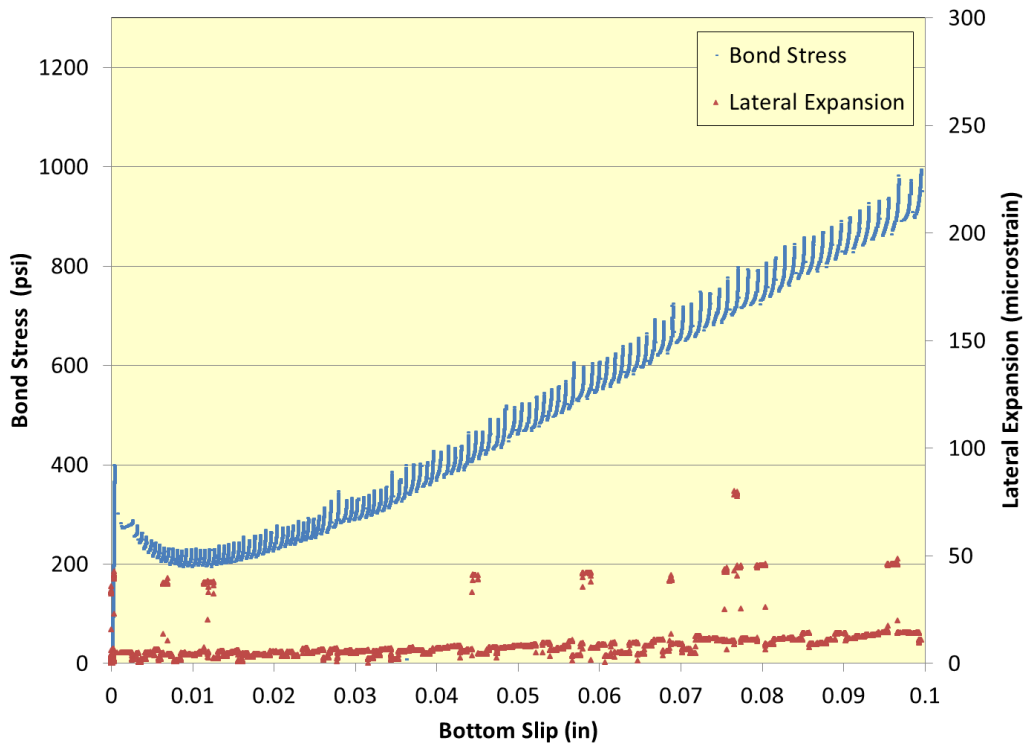
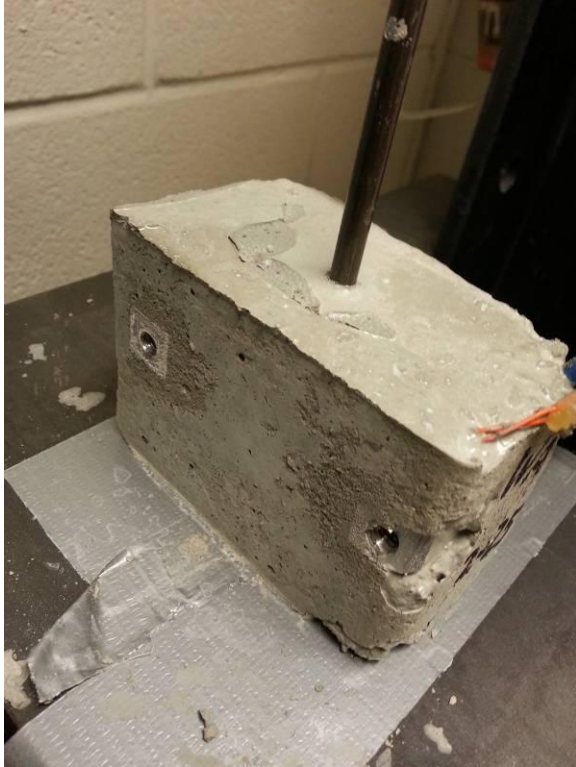
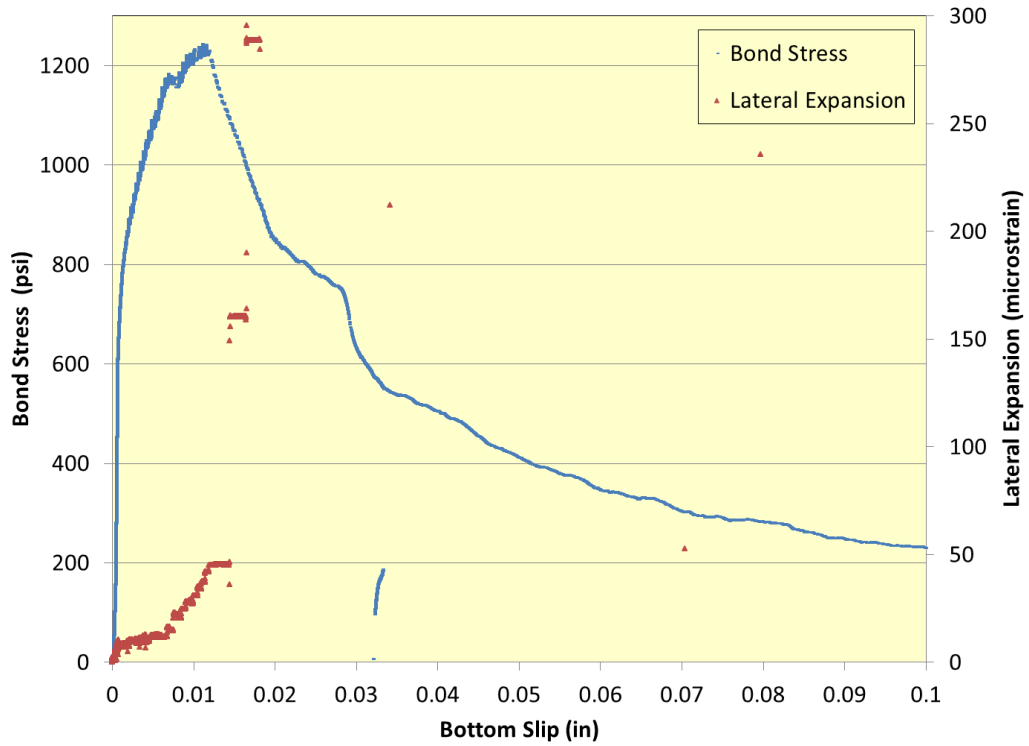


Figure 11.21 Bond stress and lateral expansion relationship with bottom slip for WA



**Figure 11.22 WA specimen after testing**

Figure 11.23 shows results from one of the three tests performed with WE. The other two tests are shown in Figure C.2 and Figure C.3. All three specimens cracked during testing, as shown in plotted data in Figure 11.24. WE bonded very rapidly and then cracked before 0.01 inches of bottom slip.



**Figure 11.23 Bond stress and lateral expansion relationship with bottom slip for WE**

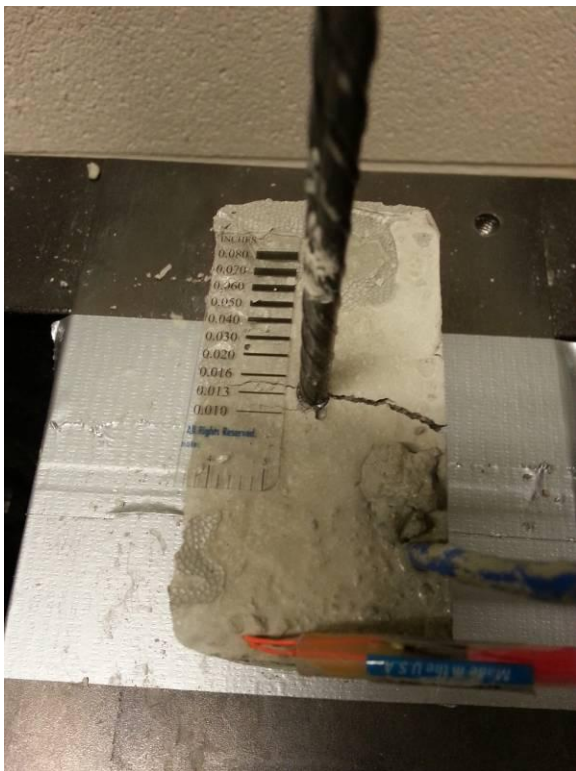


**Figure 11.24 Cracked WE specimen after testing**

Three WG tests were performed and had mixed results. One of the three specimens cracked during testing, but the other two did not crack. Figure 11.25 shows results from one of the tests done using WG. As shown in the graph, the specimen did not crack during testing, as also shown in Figure 11.26. Results from the other two tests with WG are shown in Figure C.4 and Figure C.5. Figure C.4 shows data for the specimen that cracked during testing, and specimen results plotted in Figure C.5 refer to the specimen that did not crack.

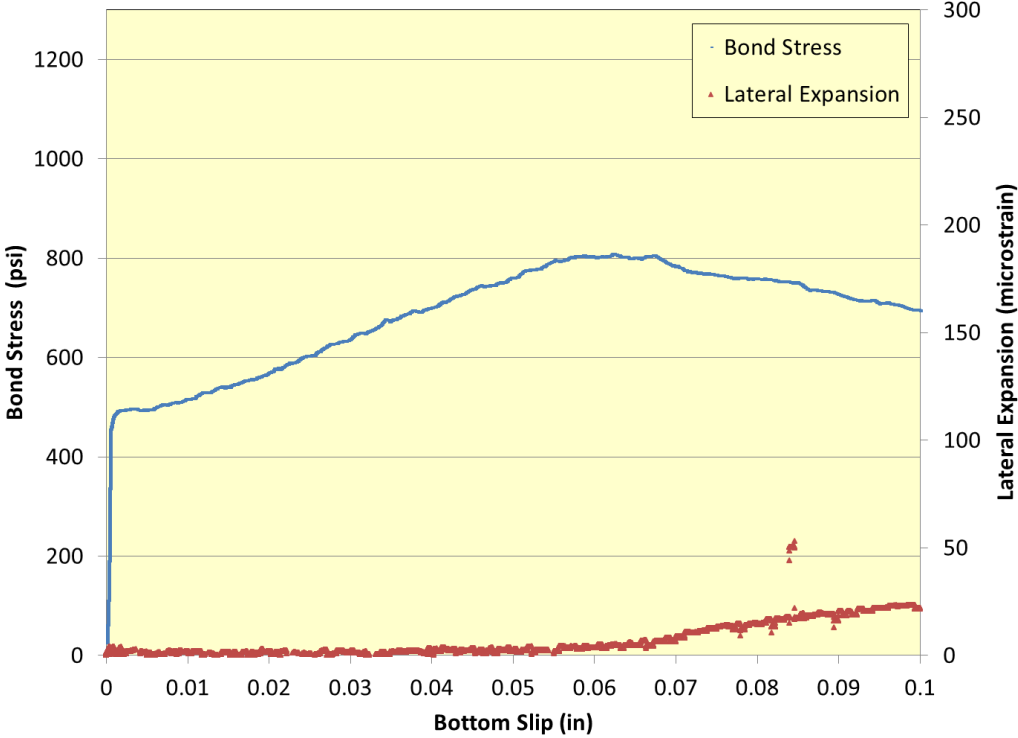


**Figure 11.25 Bond stress and lateral expansion relationship with bottom slip for WG**



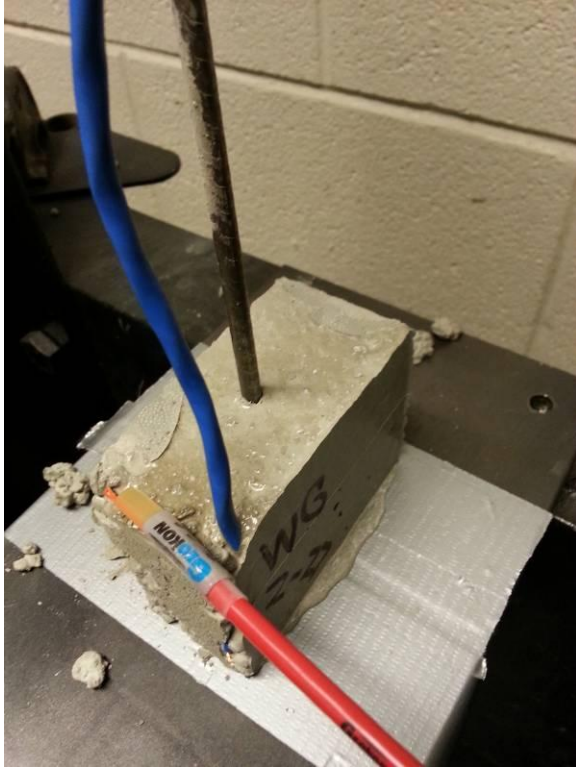


**Figure 11.26 WG specimen after testing**

Figure 11.27 shows results from one of the three tests done using WH, and Figure C.6 and Figure C.7 show results from the other two tests. Similar to WE, all WH specimens cracked during testing and before 0.01 inches of bottom slip. Figure 11.28 shows one cracked WH specimen after testing.

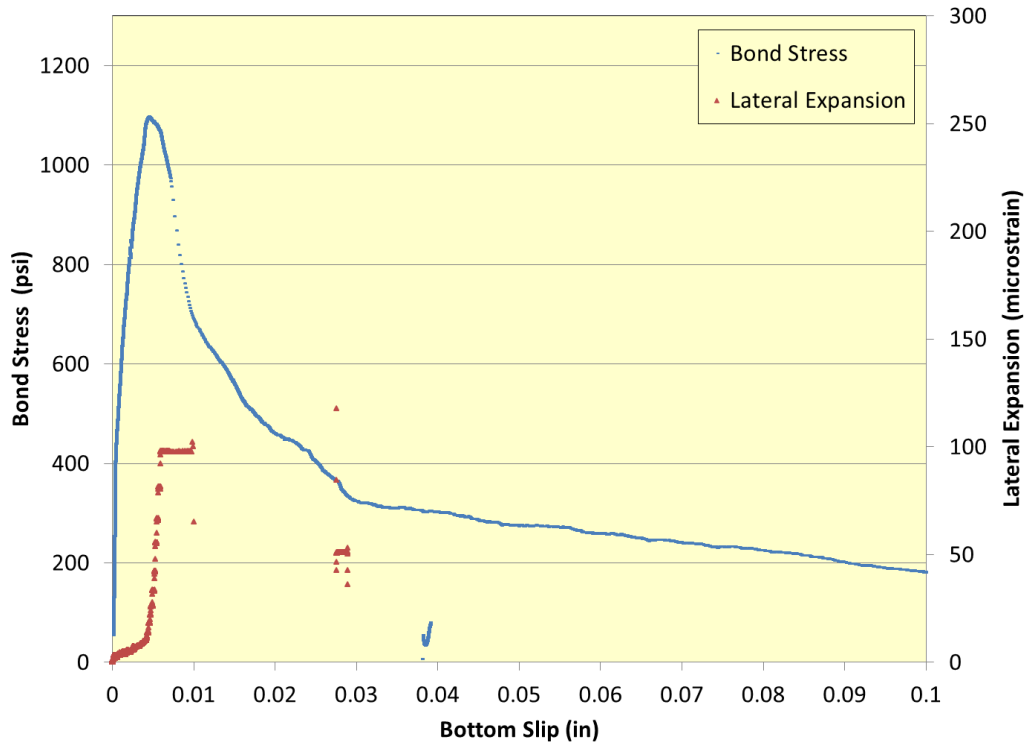


**Figure 11.27 Bond stress and lateral expansion relationship with bottom slip for WH**

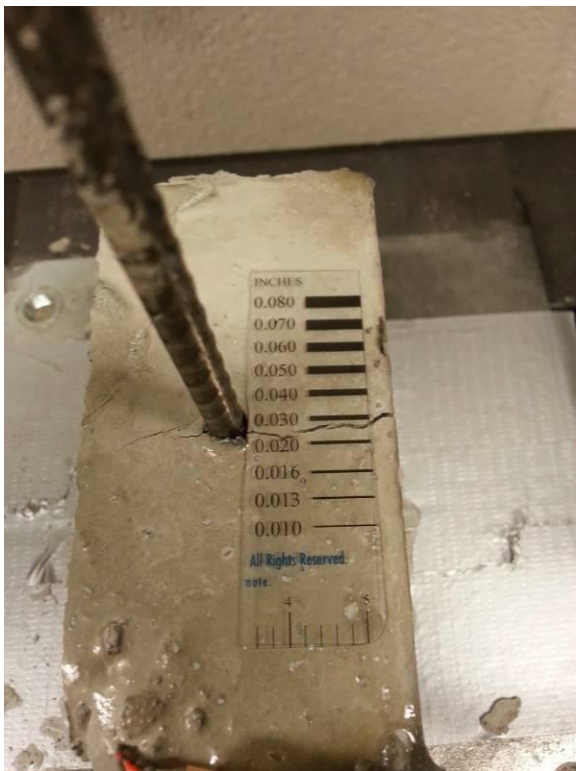


**Figure 11.28 Cracked WH specimen after testing**

Two WK specimens were tested during this part of the project. Figure 11.29 shows results from one specimen and Figure C.8 shows results from the second specimen. Both specimens cracked during loading. One cracked specimen is shown in Figure 11.30.

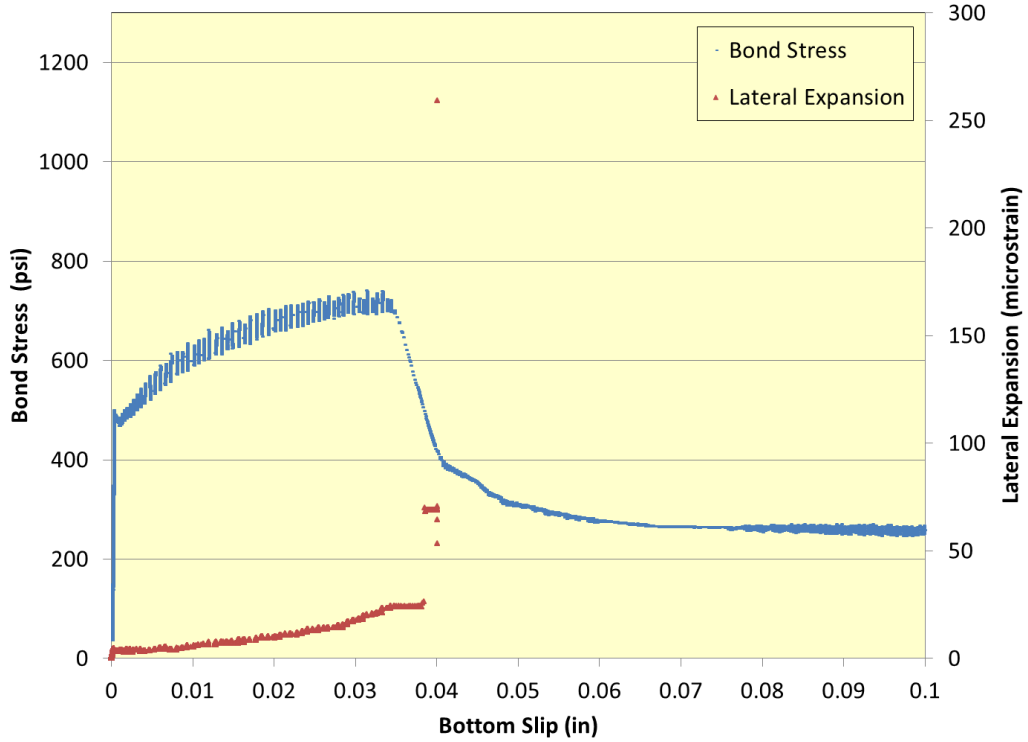


**Figure 11.29 Bond stress and lateral expansion relationship with bottom slip for WK**



**Figure 11.30 Cracked WK specimen after testing**

VWSGs determined lateral expansion in the specimens prior to cracking and they showed the expansion amount in specimens that did not crack. Table 11.1 shows the max crack widths on the top of the specimen for each of the VWSG tests.

**Table 11.1 Crack width for VWSG tests**

Wire	Crack width (in)	Figure plotting test
WA	No Crack	Figure 11.21
WA	No Crack	Figure C.1
WE	0.030	Figure 11.23
WE	0.035	Figure C.2
WE	0.030	Figure C.3
WG	No Crack	Figure 11.25
WG	0.003	Figure C.4
WG	No Crack	Figure C.5
WH	0.020	Figure 11.27
WH	0.016	Figure C.6
WH	0.012	Figure C.7
WK	0.004	Figure 11.29
WK	0.003	Figure C.8

## Chapter 12 Machined Wire Testing

This section investigates indent angle and depth and resulting wire reinforcement bond behavior. Custom wire indents were created for this set of tests, and the testing setup was matched with the setup for VWSGs discussed in Chapter 10. VWSGs were also used to measure lateral strain created by the various indents.

### 12.1 Machined Wire Test Setup

Custom indents were machined into a WA reinforcement by Mark Haynes. A computer numerical control mill equipped with carbide-tipped mill ends was used to machine various types of indents into the smooth reinforcement (WA). The process differed from the conventional method of creating indents since the conventional method involves pressing indent patterns into the wire. This difference in manufacturing could cause a change the bonding characteristics of the wires. Indents were placed 120 degrees from each other in order to match typical orientation found in chevron indent patterns used in other tests in this study.

After indents were machined into the wire, the wires were scanned to measure indent dimensions. Indent depths varied depending on the tooling setup. Twelve indent patterns were machined using six indent wall angles. For each indent wall angle, two different depths of indents were made for each angle. Table 12.1 shows the indent angles and average depth for each indent.

**Table 12.1 Indent depth for each indent angle (in mm)**

	15°	30°	45°	60°	75°	90°
Shallow	0.310	0.158	0.156	0.142	0.286	0.142
Deep	0.400	0.261	0.245	0.245	0.387	0.217

After the wires were scanned, they were tested using the VWSG procedure described in Chapter 10. The concrete mix, Mix B, also matched the mix used in Chapter 10 to ensure consistency between the two tests involving conventionally manufactured indents and custom machined indents. Figure 12.1 shows various indent patterns after machining. Figure 12.2 shows one machined wire prior to casting the specimen.

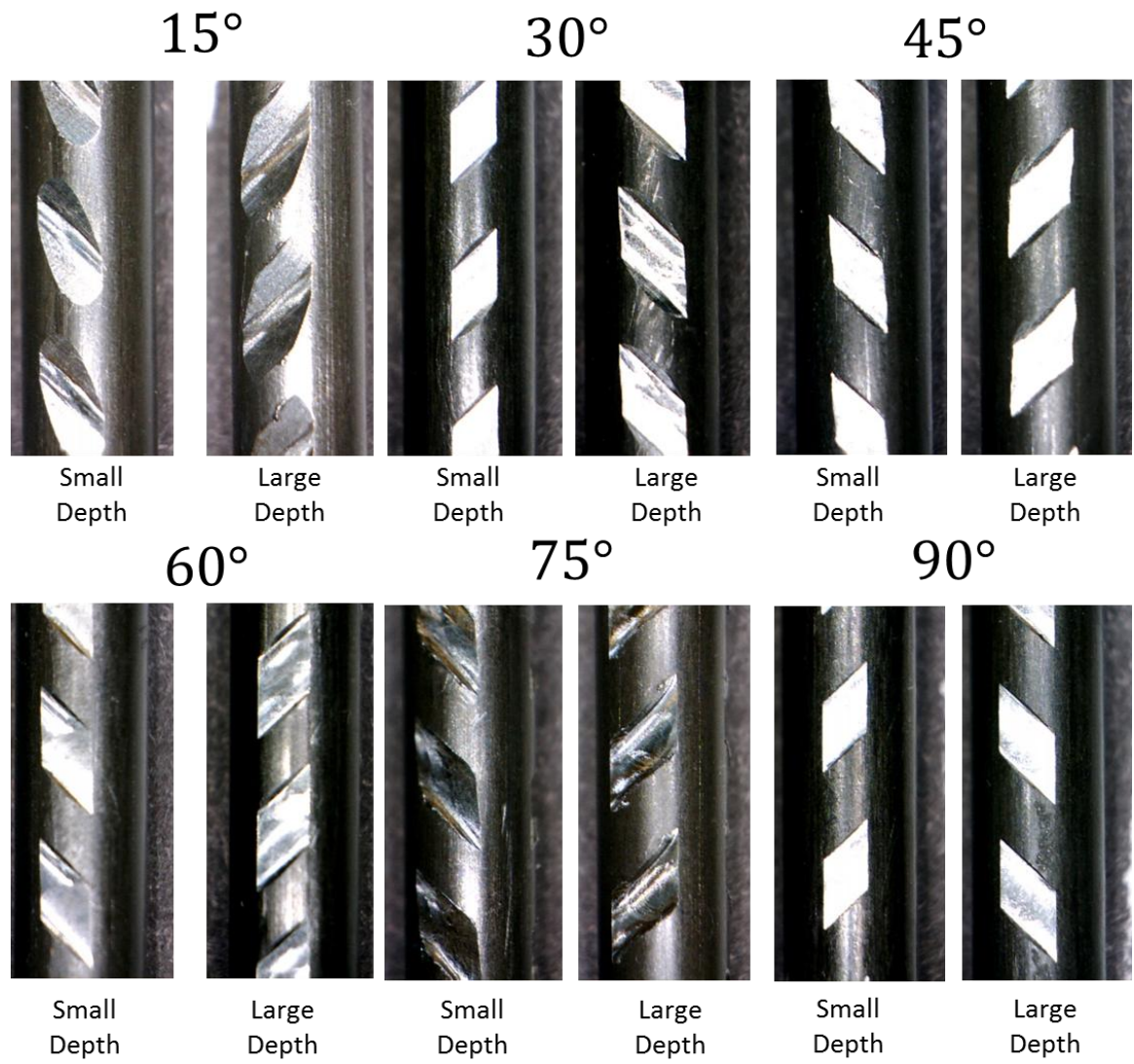


**Figure 12.1 Machined indent patterns (Courtesy Mark Haynes)**

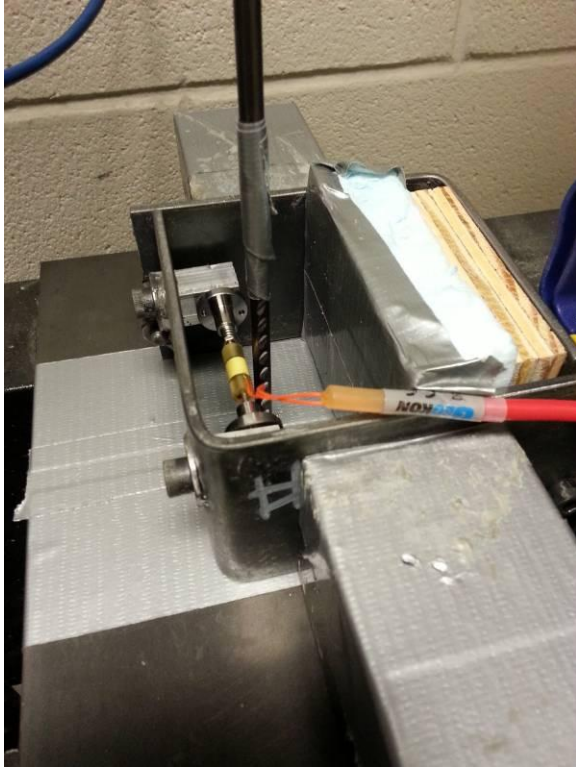


**Figure 12.2 Machined wire before casting**

## **12.2 Machined Wire Test Results**

Bond stress was plotted in relation to the bottom slip for each indent. Lateral expansion was also plotted on the same graph to show lateral expansion change in relation to bond stress.

Figure 12.3 shows the test plot for the 15-degree shallow indent. As shown in the graph, the specimen cracked during testing as seen by the decrease in bond stress and increase in lateral expansion. Figure 12.4 shows the specimen after testing.

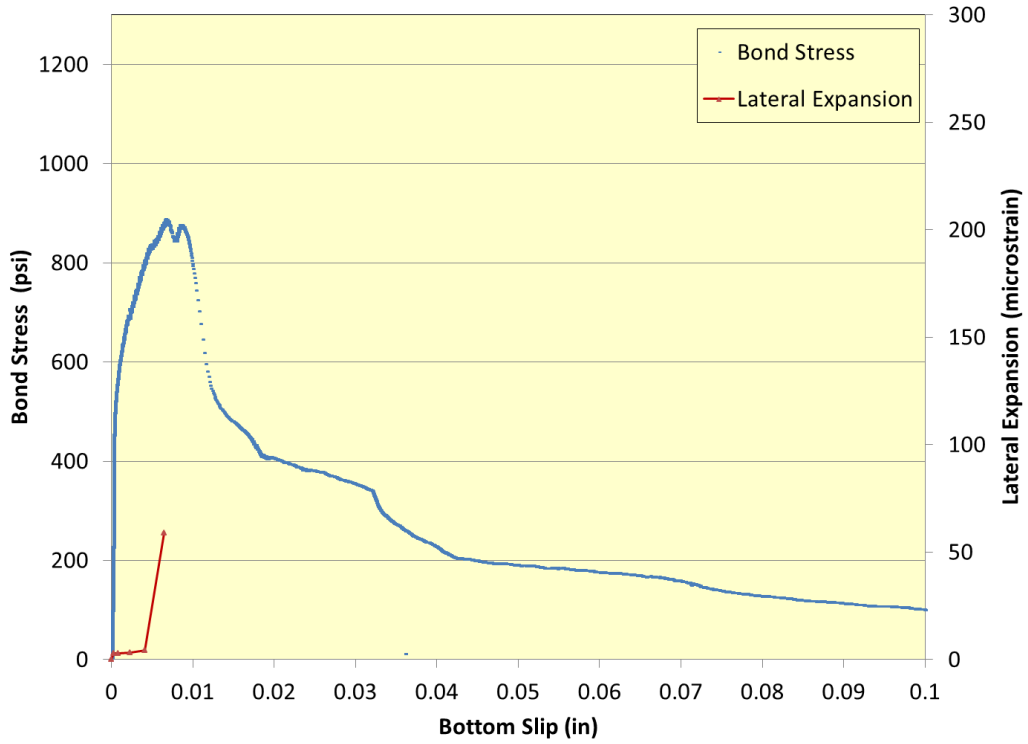


**Figure 12.3 Bond stress and lateral expansion relationship for shallow 15-degree indent**



**Figure 12.4 Shallow 15-degree indent specimen after testing**



Figure 12.5 shows results from the test using the 15-degree deep indent. The specimen cracked during testing, as shown in Figure 12.6. Both 15-degree indents cracked the specimen after only 0.005 inches of bottom slip. Figure 12.7 shows the bond stress versus bottom slip relationship for both indent depths. Increased indent depth may have caused the cracking.

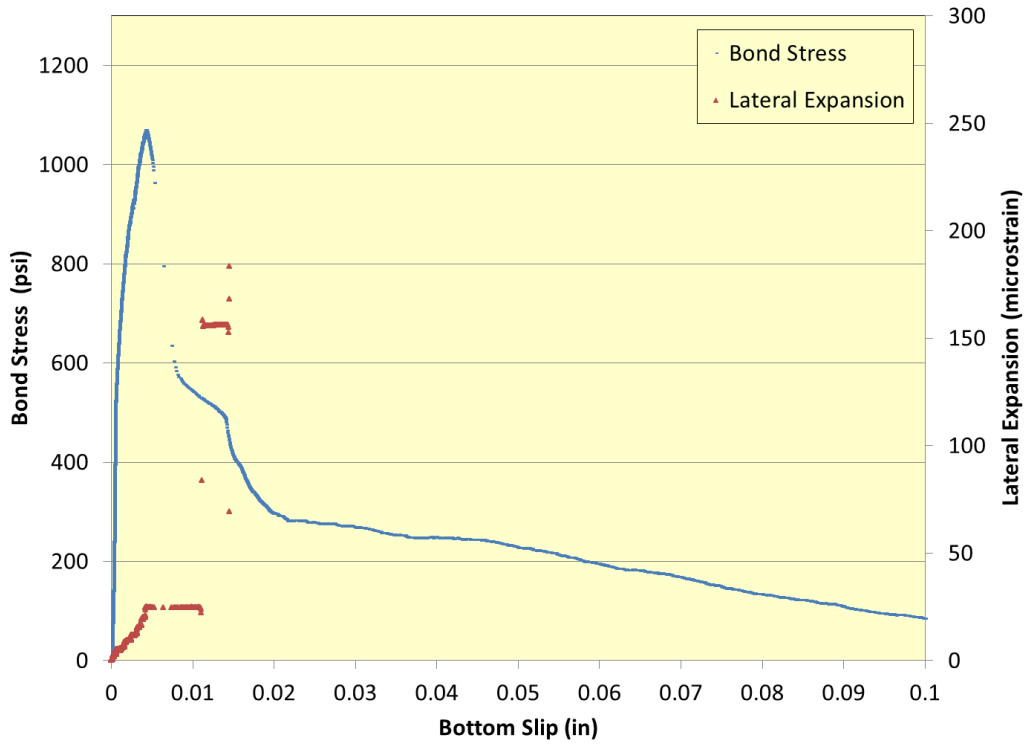


**Figure 12.5 Bond stress and lateral expansion relationship for deep 15-degree indent**



Figure 12.6 Deep 15-degree indent specimen after testing

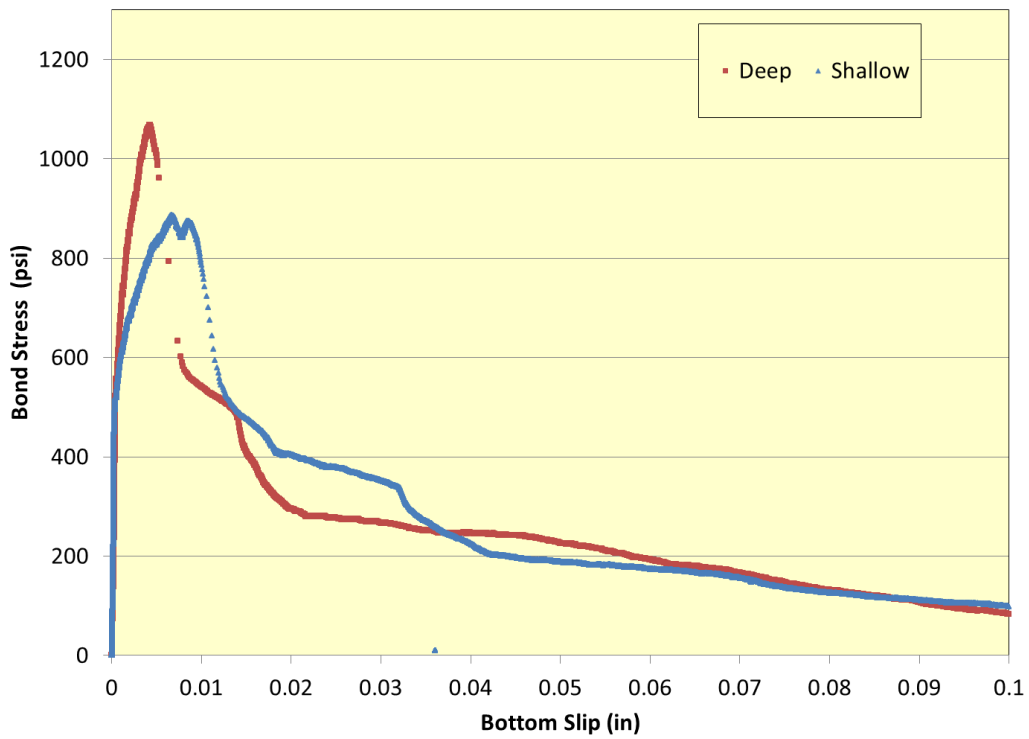
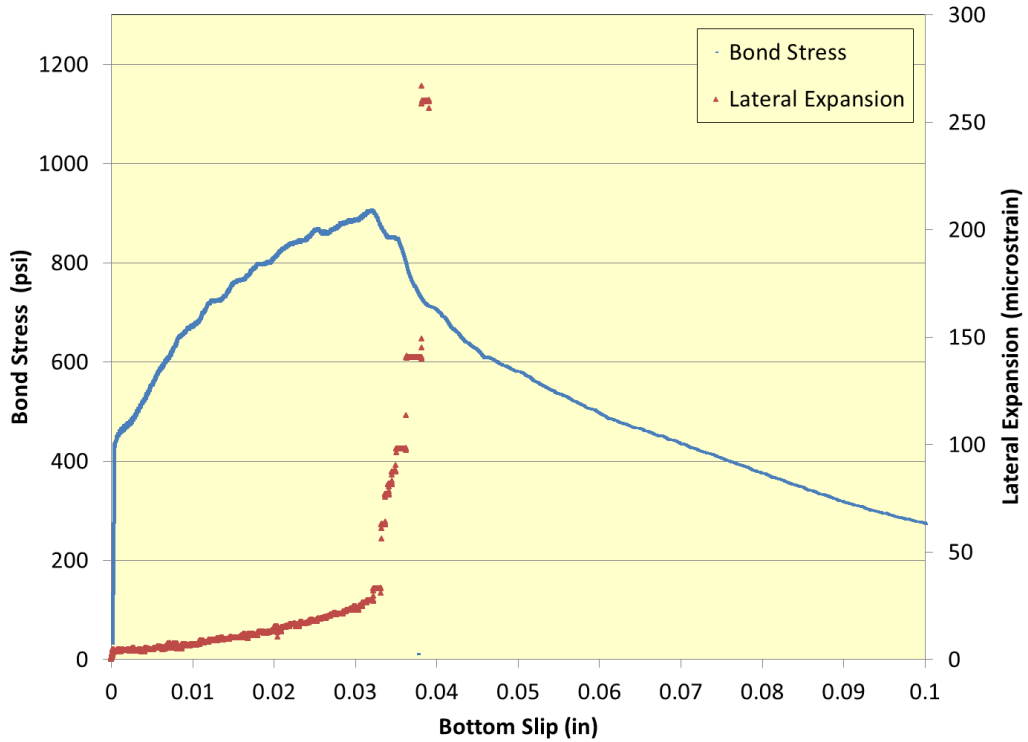


Figure 12.7 Bond stress versus bottom slip relationship for both 15-degree indents

Figure 12.8 shows results from the 30-degree shallow indent. The specimen cracked during testing after 0.03 inches of bottom slip. Figure 12.9 shows the cracked specimen after testing.



**Figure 12.8 Bond stress and lateral expansion relationship for shallow 30-degree indent**



**Figure 12.9 Shallow 30-degree indent specimen after testing**

Figure 12.10 shows results from the 30-degree deep indent. The specimen cracked at approximately half the bottom slip of the 30-degree shallow specimen. The increased indent depth caused the wire to bond faster but created higher lateral expansion. Figure 12.11 shows the specimen after testing. Figure 12.12 shows the bond stress versus bottom slip relationship for both indent depths.

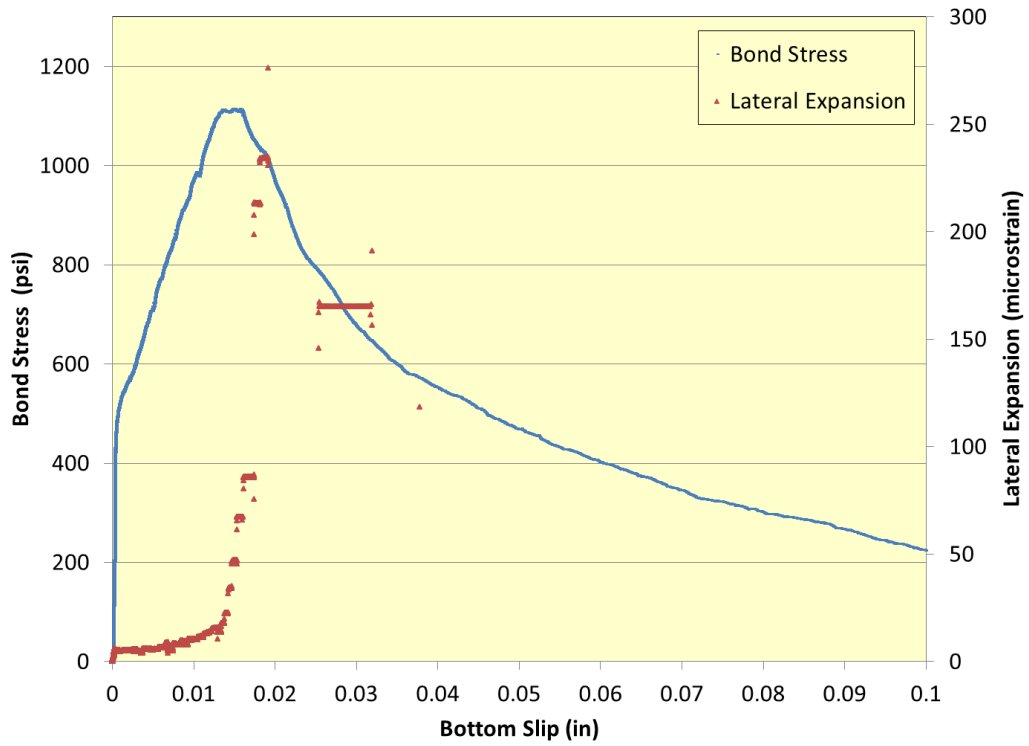


**Figure 12.10 Bond stress and lateral expansion relationship for deep 30-degree indent**

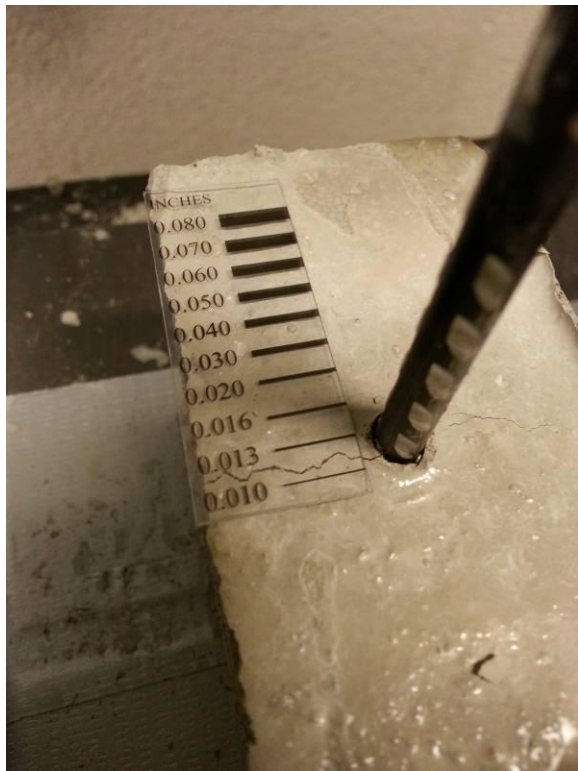


**Figure 12.11 Deep 30-degree indent specimen after testing**

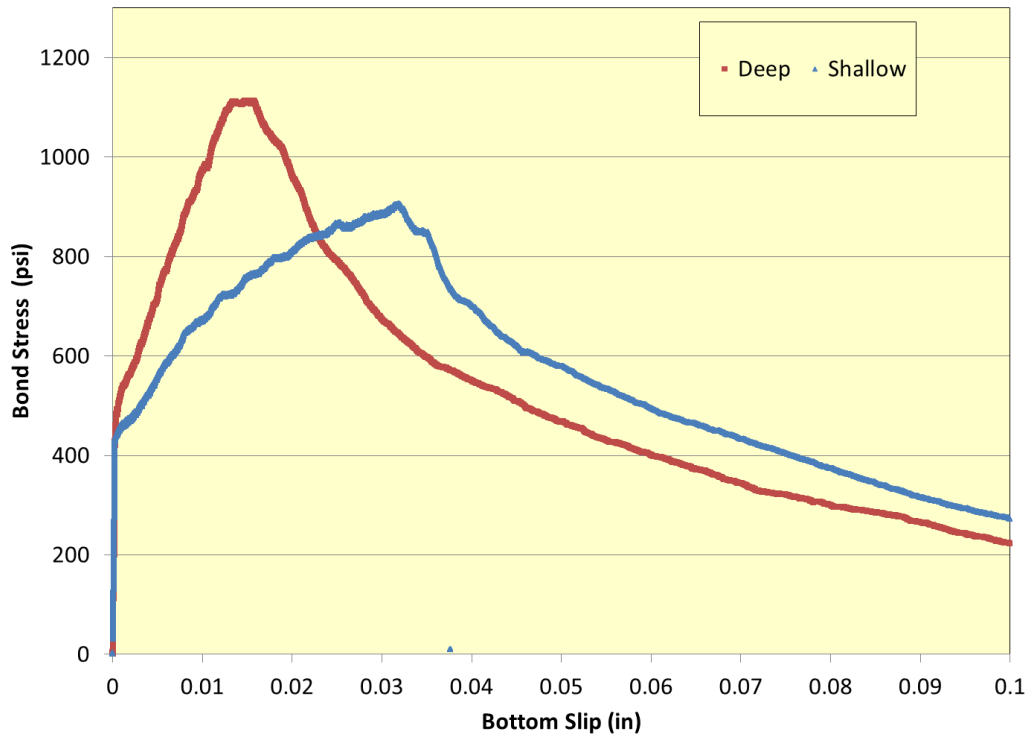


**Figure 12.12 Bond stress versus bottom slip relationship for both 30-degree indents**

Figure 12.13 shows results from the 45-degree shallow indent. The specimen did not crack during the testing, as shown in Figure 12.14, and lateral expansion only reached a maximum between 10 and 20 microstrain.

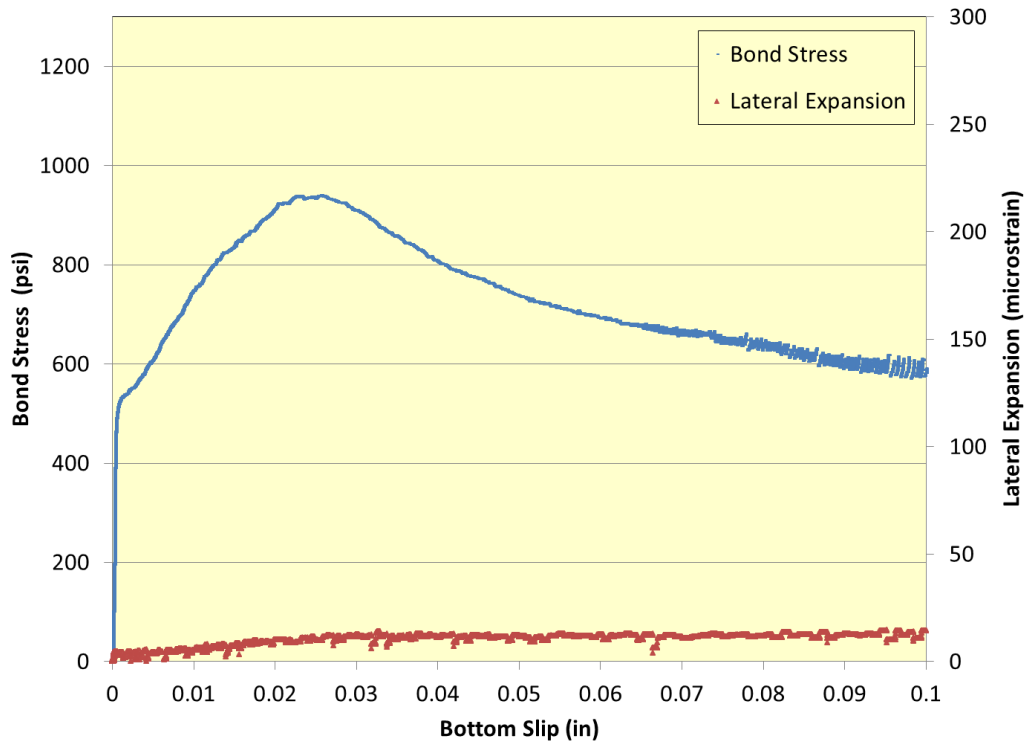


**Figure 12.13 Bond stress and lateral expansion relationship for shallow 45-degree indent**



**Figure 12.14 Shallow 45-degree indent specimen after testing**

Figure 12.15 shows results from the 45-degree deep indent. Unlike the shallow indent, the deep indent cracked during testing. Figure 12.16 shows the cracked specimen. Figure 12.17 shows the bond stress versus bottom slip relationship for both indent depths.

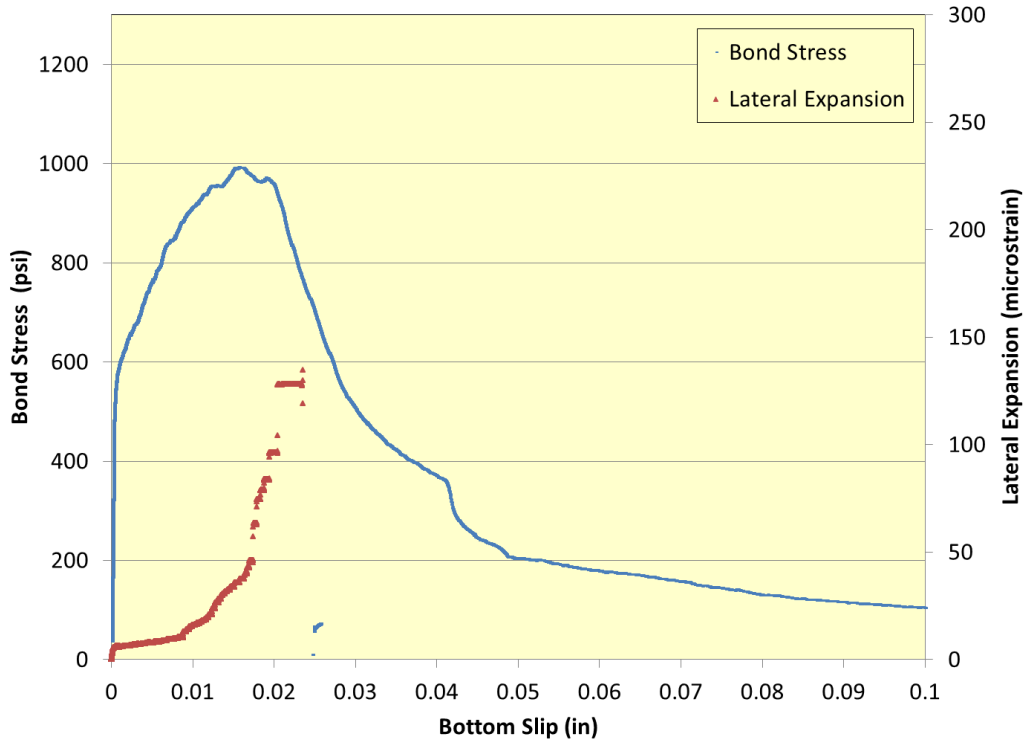


**Figure 12.15 Bond stress and lateral expansion relationship for 45-degree deep indent**





Figure 12.16 Deep 45-degree indent specimen after testing

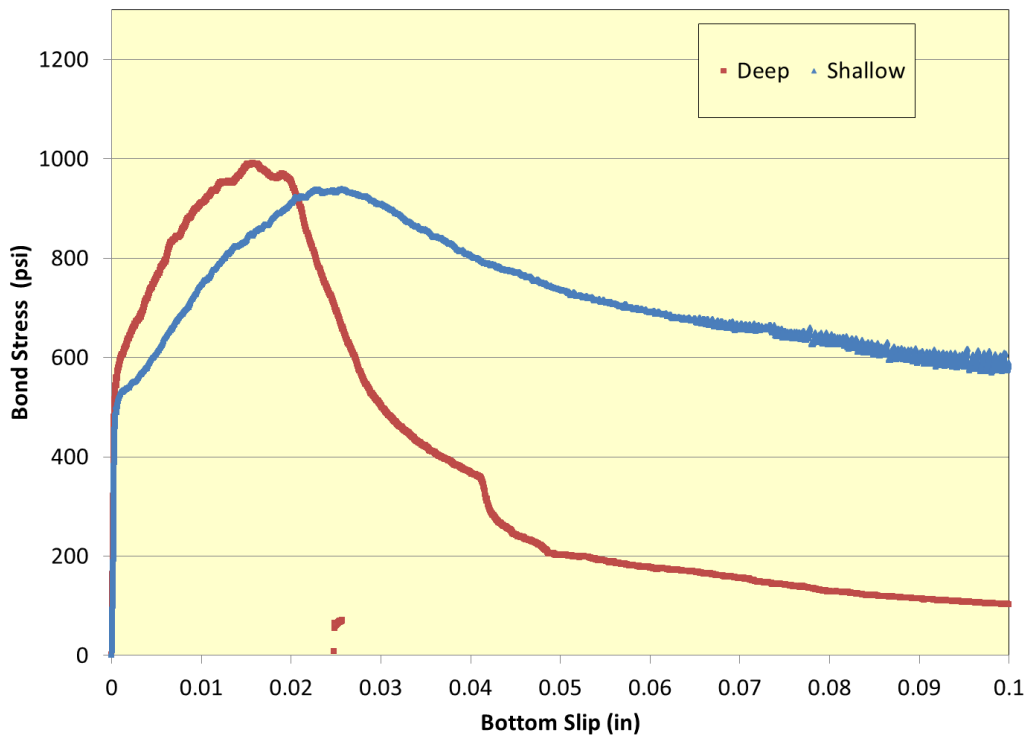
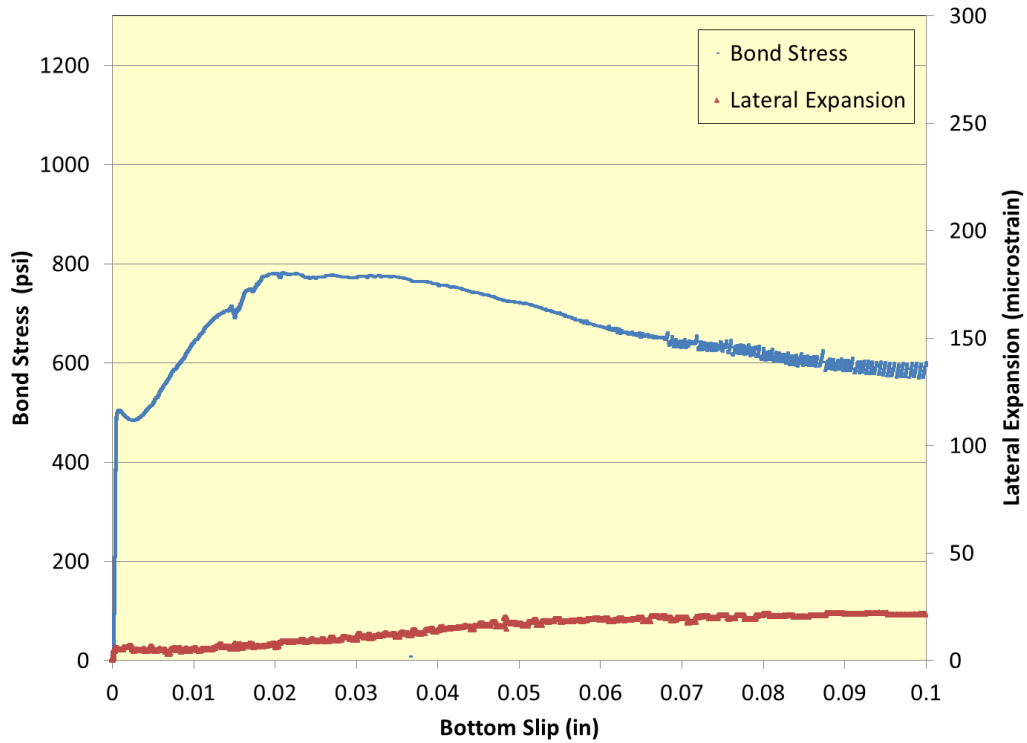
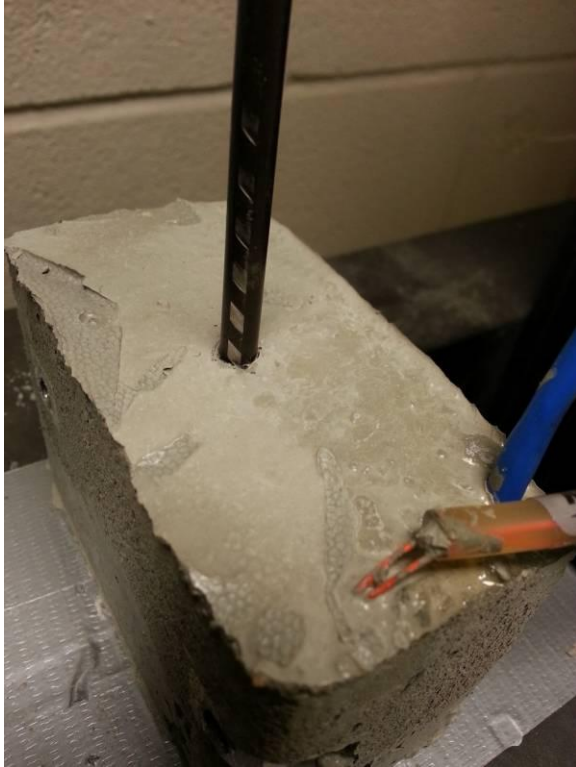


Figure 12.17 Bond stress versus bottom slip relationship for both 45-degree indents

Figure 12.18 shows results from the 60-degree shallow indent. This indent behaved similarly to the 45-degree shallow indent and also did not crack the specimen. However, lateral expansion only reached a maximum of 25 microstrain throughout the test. Figure 12.19 shows the un-cracked specimen.



**Figure 12.18 Bond stress and lateral expansion relationship for shallow 60-degree indent**



**Figure 12.19 Shallow 60-degree indent specimen after testing**

Figure 12.20 shows results from 60-degree deep indent. Similar to the 45-degree deep indent, the specimen had a higher bond than the shallow indent specimen and cracked the specimen during testing. Figure 12.21 shows the cracked specimen. Figure 12.22 shows the bond stress versus bottom slip relationship for both indent depths.

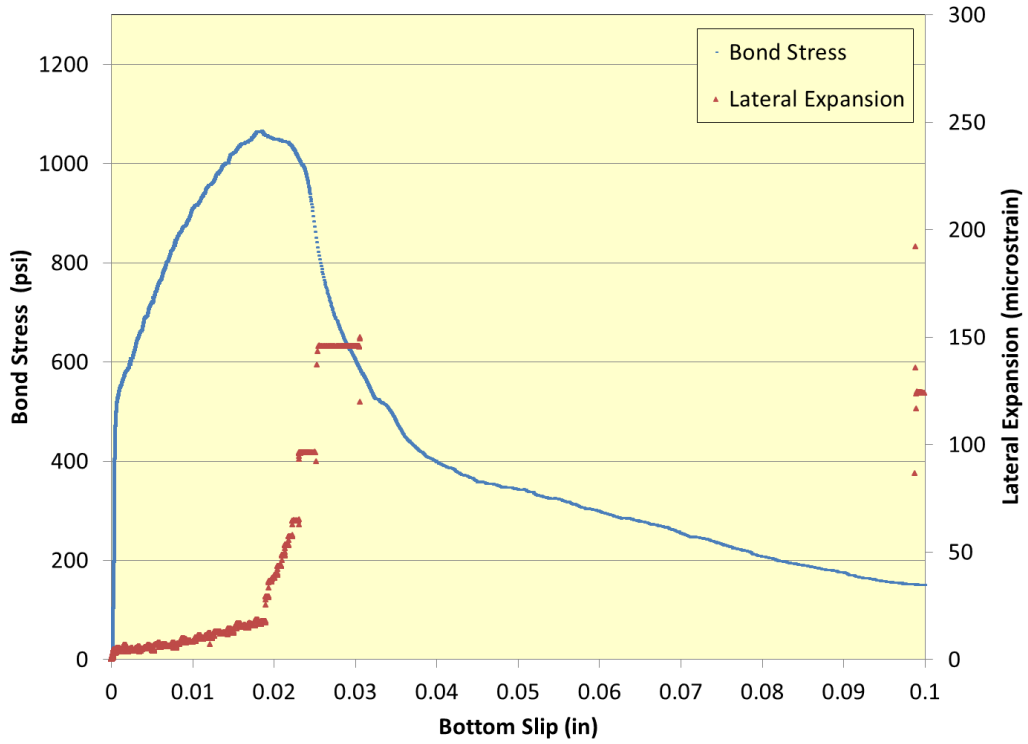


**Figure 12.20 Bond stress and lateral expansion relationship for deep 60-degree indent**



**Figure 12.21 Deep 60-degree indent specimen after testing**

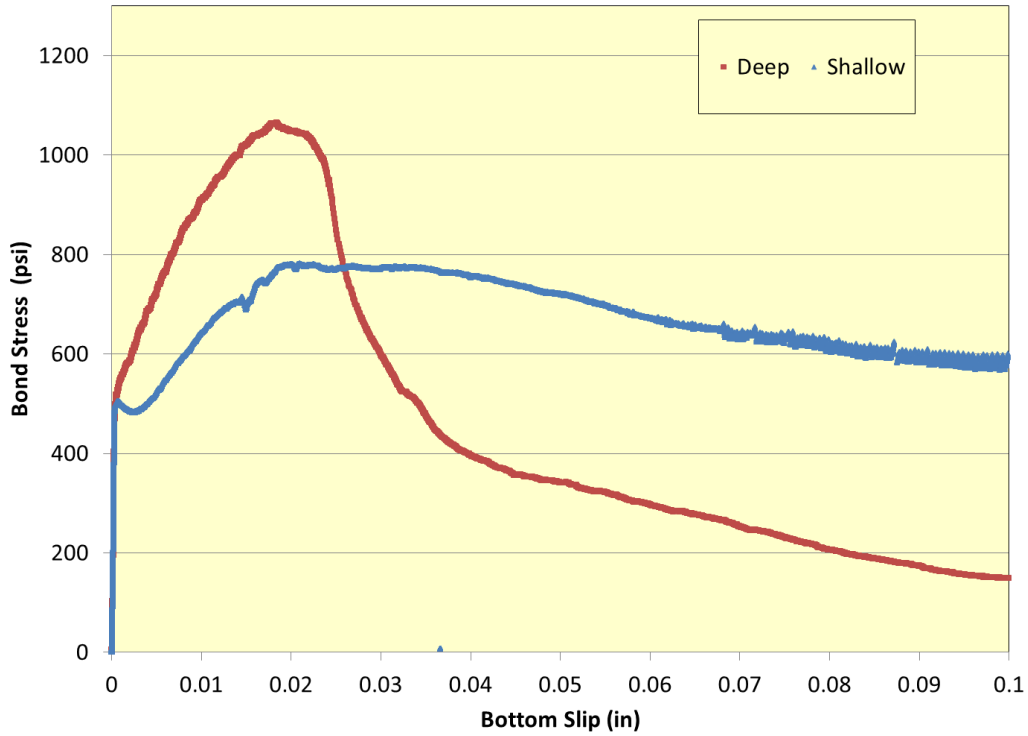


**Figure 12.22 Bond stress versus bottom slip relationship for both 60-degree indents**

Figure 12.23 shows results from the 75-degree shallow indent tests. Similar to the 15-degree indents, the 75-degree indents were deeper than other angle indents, thus causing the specimens to crack since the indent bonded more to the specimen. Figure 12.24 shows the cracked specimen.

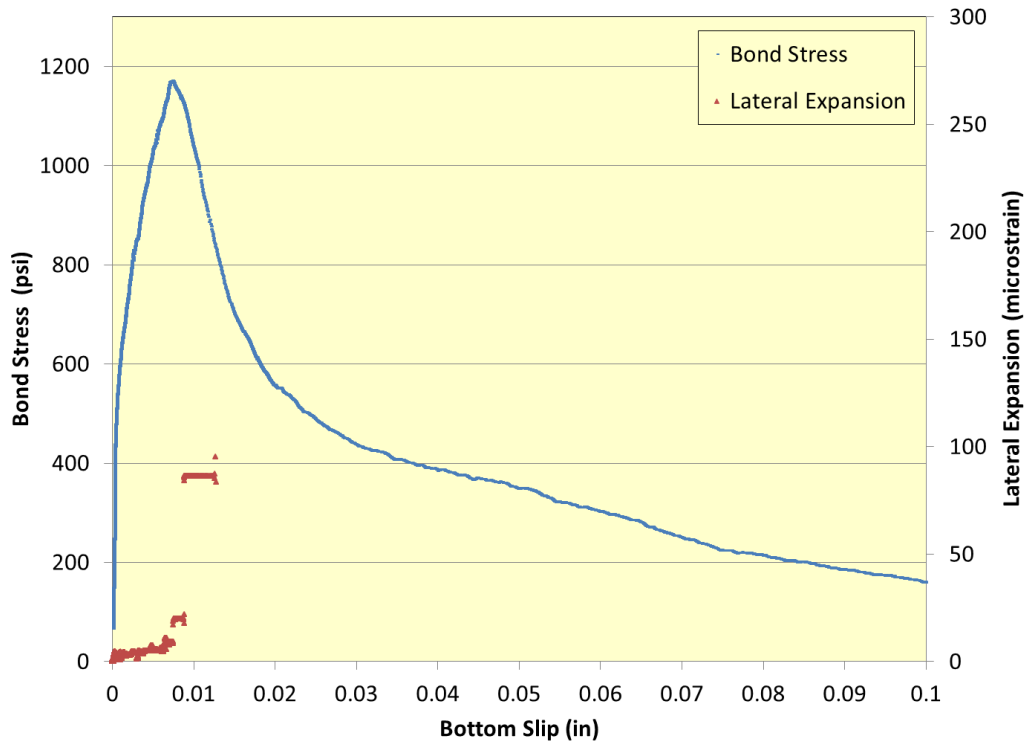


Figure 12.23 Bond stress and lateral expansion relationship for shallow 75-degree indent

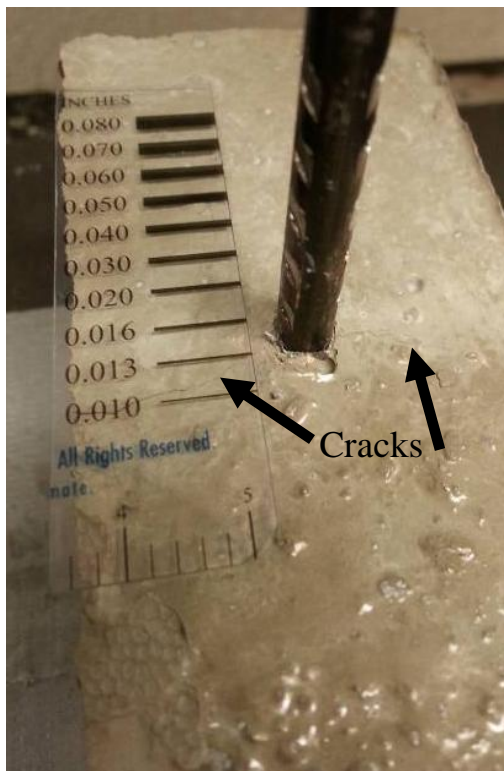
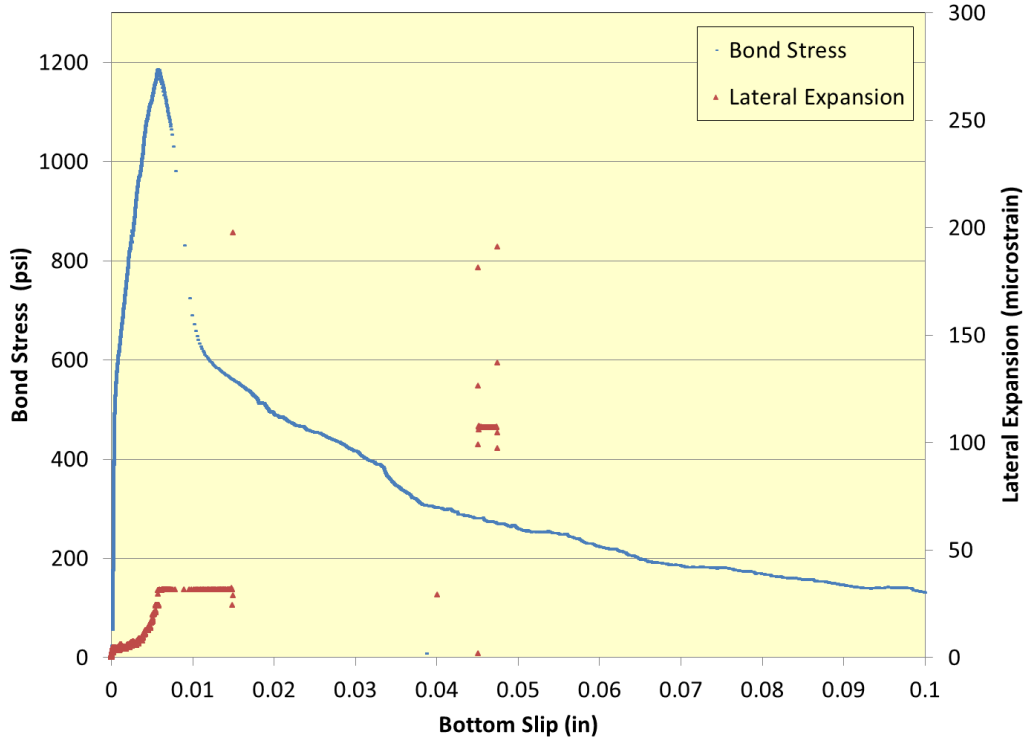


Figure 12.24 Shallow 75-degree indent specimen after testing

Figure 12.25 shows results from the 75-degree deep indent tests. Similar to the shallow indent, the specimen cracked during testing. The deeper indent caused the specimen to crack sooner than the shallow indent. Figure 12.26 shows the specimen after testing. Figure 12.27 shows the bond stress versus bottom slip relationship for both indent depths.



**Figure 12.25 Bond stress and lateral expansion relationship for deep 75-degree indent**

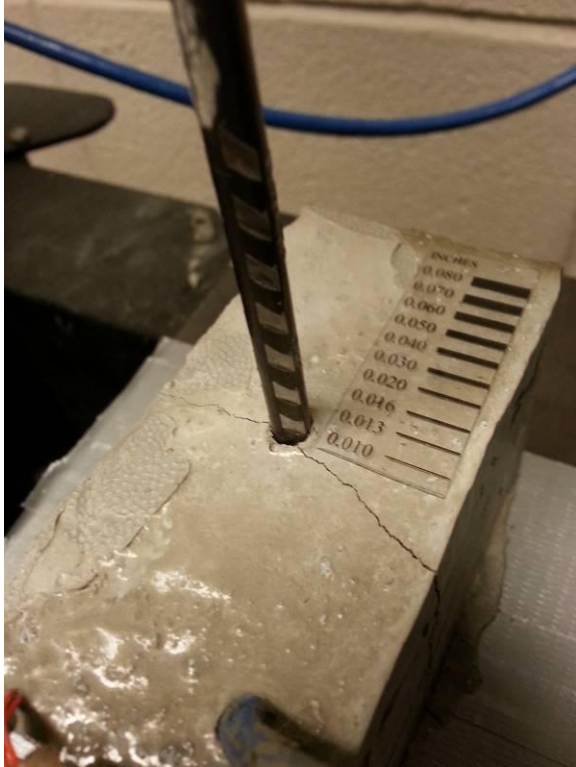


Figure 12.26 Deep 75-degree indent specimen after testing

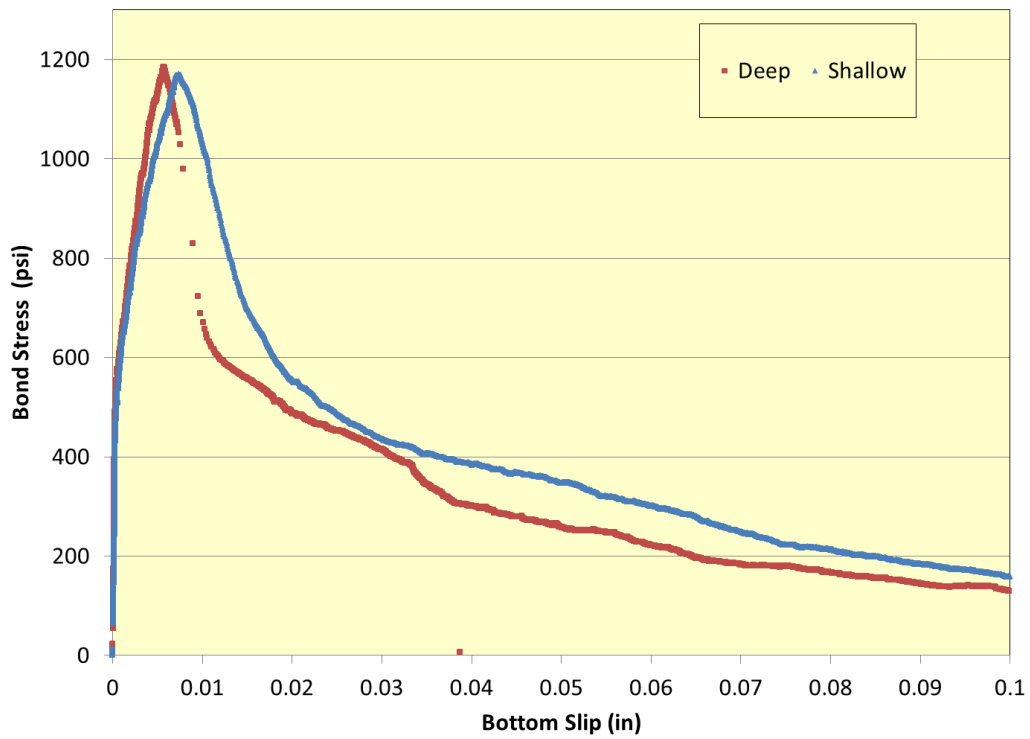
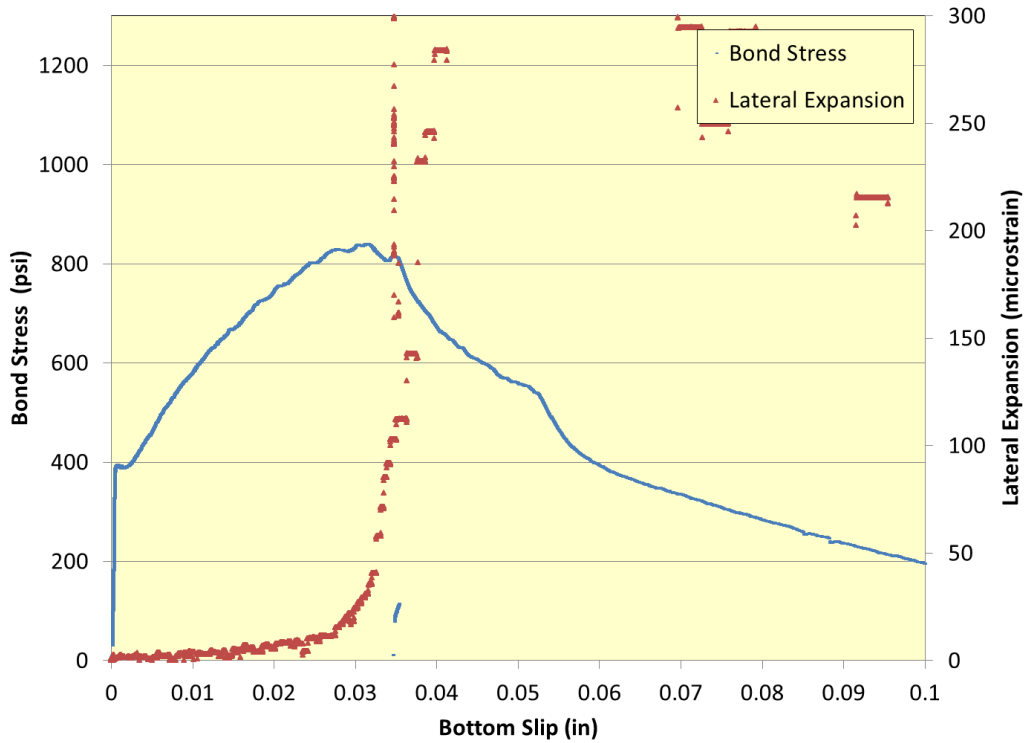


Figure 12.27 Bond stress versus bottom slip relationship for both 75-degree indents



Figure 12.28 shows results from the 90-degree shallow indent test. The graph indicates that bond stress increased after the initial slip until the bond stress peaked and the specimen cracked. The specimen cracked after 0.03 inches of bottom slip, comparable to 30-degree shallow indent results. Figure 12.29 shows the cracked specimen.



**Figure 12.28 Bond stress and lateral expansion relationship for shallow 90-degree indent**



**Figure 12.29 Shallow 90-degree indent specimen after testing**

Figure 12.30 shows results from the 90-degree deep indent. The graph is similar to the 90-degree shallow indent graph except that bond stress was slightly higher and the specimen cracked sooner. Figure 12.31 shows the cracked specimen. Figure 12.32 shows the bond stress versus bottom slip relationship for both indent depths.

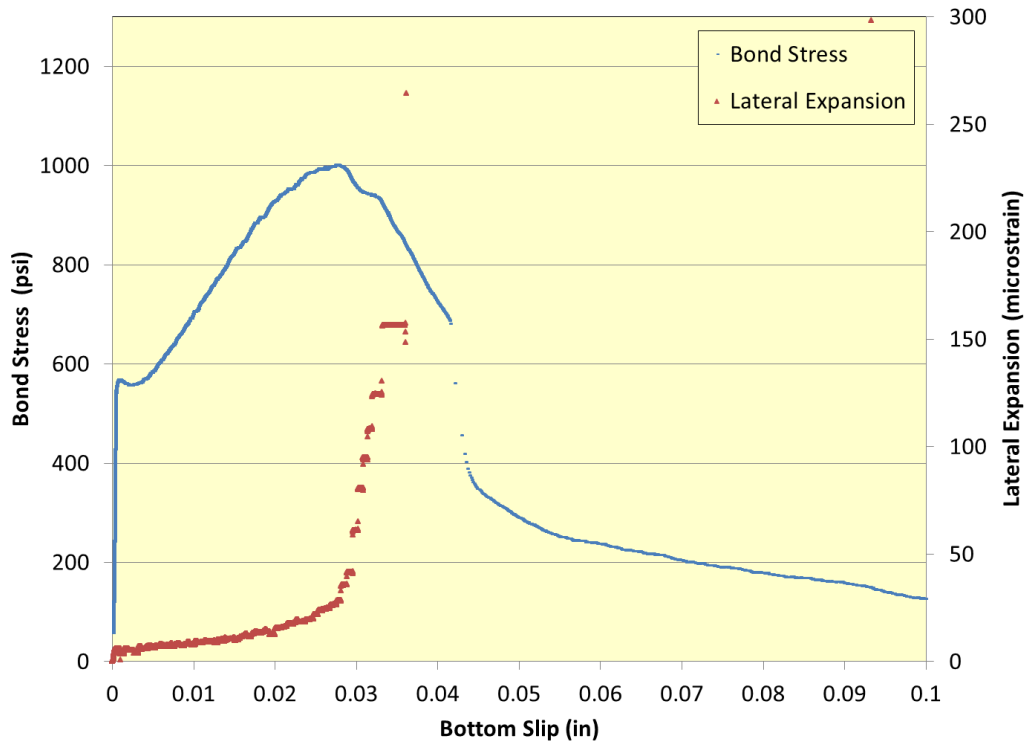


**Figure 12.30 Bond stress and lateral expansion relationship for deep 90-degree indent**



**Figure 12.31 Deep 90-degree indent specimen after testing**

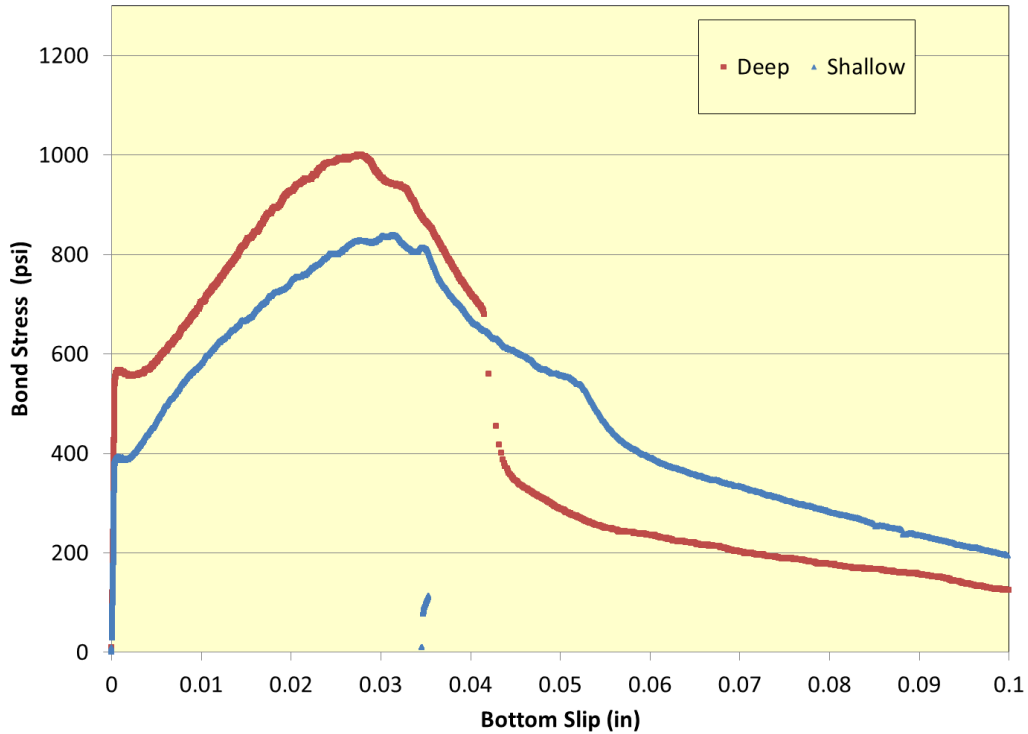


**Figure 12.32 Bond stress versus bottom slip relationship for both 90-degree indents**

Results from all shallow indents were combined and plotted in Figure 12.33, and deep indent results were plotted in Figure 12.34. The two plots illustrate a trend of increased bond stress with increasing indent depth. The graphs also show that deeper indents caused the specimens to crack with less slip than the shallow indents. Table 12.2 shows a summary of the max crack widths on the top of the specimen for each indent.

**Table 12.2 Crack widths for each indent (in inches)**

Angle	Shallow Indent	Deep Indent
15-Degree	0.016	0.025
30-Degree	0.003	0.008
45-Degree	No Crack	0.012
60-Degree	No Crack	0.003
75-Degree	0.005	0.012
90-Degree	0.004	0.008

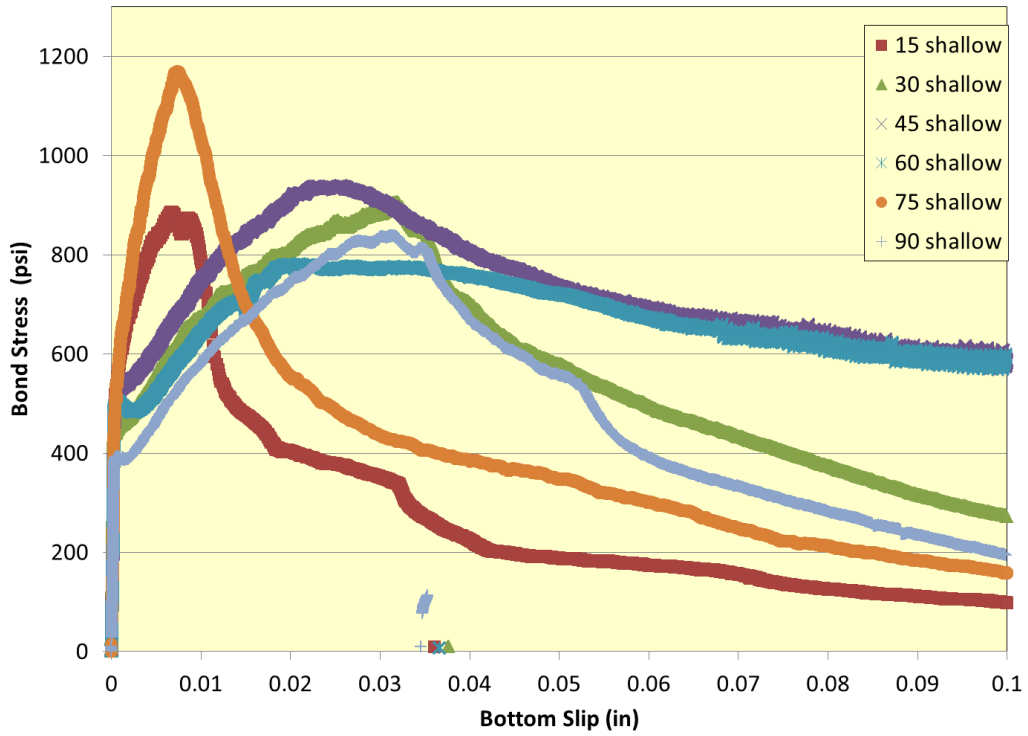


Figure 12.33 Bond stress versus bottom slip relationship for all shallow indents

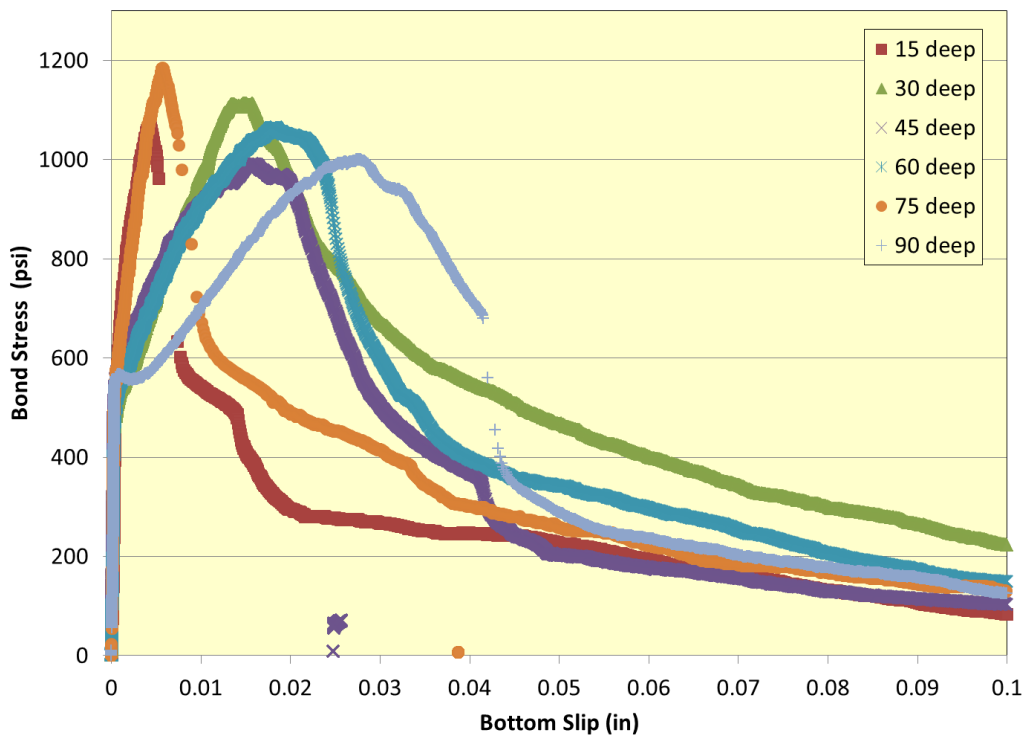


Figure 12.34 Bond stress versus bottom slip relationship for all deep indents

## Chapter 13 4-Wire vs Single Wire Testing

Testing was done to determine the effects of multiple wires in a prism. The specimens used were 3.5-inch square prisms. One set of prisms had a single wire located in the center of the cross section and the other sets of prisms had four wires evenly spaced in the prisms. The specimens were batched using Mix B and tested using the transfer bond procedure described in Chapter 7. Figure 13.1 shows the setup for multiple-wire tests.



**Figure 13.1 4-wire and single wire frame setup**

### 13.1 Unreinforced 4-Wire Test Setup

This section investigated the effect of multiple wires on bond capacity of prestress wires. Concrete railroad ties typically contain 16 to 20 reinforcement wires per tie, so this section determines whether the presence of multiple wires in a specimen alters the bond behavior of the wires.

Specimens cast for this portion of the study were 3.5-inch x 3.5-inch squares with a height of 2.5 inches. This cross section was identical to the cross section used by Bodapati et al. (2013). Two wire locations were chosen for this cross section. The first location matched the

setup of Bodapati et al. (2013) and included four wires equally spaced and 1 inch from the edge of the forms. The second cross section consisted of a single wire located at the same location as one of the wires in the 4-wire setup. Specimens with a bond length of 2.5 inches were tested using the transfer bond setup as described in Chapter 7 and were cast using Mix B as detailed in Chapter 5. The wires used were WA, WE, WG, WH, and WK, as discussed in Chapter 4. Figure 13.2 and Figure 13.3 show setups for the 4-wire and 1-wires setups, respectively.



**Figure 13.2 4-wire specimen before casting**



**Figure 13.3 Single wire specimen before casting**

Figure 13.4 and Figure 13.5 show the 4-wire specimen before testing with LVDTs mounted to each wire.



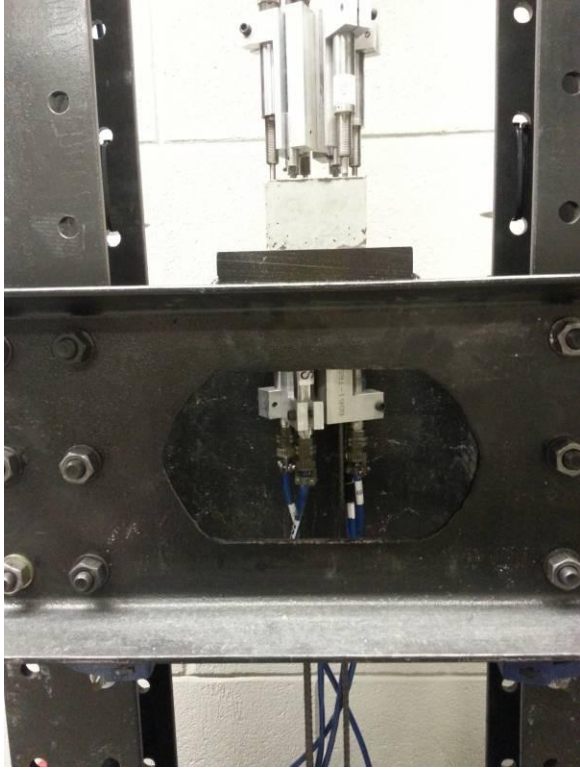


**Figure 13.4 Bottom LVDT locations for 4-wire specimen test**



**Figure 13.5 Top LVDT locations for 4-wire specimen test**

## 13.2 Unreinforced 4-Wire Results

The five wire types were tested to determine bond behavior of each wire. Load cell readings and end-slip measurements were used to plot bond stress versus bottom slip for each reinforcement. The five reinforcements demonstrated distinct behaviors similar to those seen in Chapter 6.

Figure 13.6 shows data from the test using WA. Due to lack of indents, the smooth wire began slipping at a much lower bond stress value than the other four wire types. Bond stress increased as the bottom slip increased because of increased surface friction of the wire as decreased wire tension caused the wire to expand. Figure 13.7 shows the WA specimen after testing; no cracking is present.

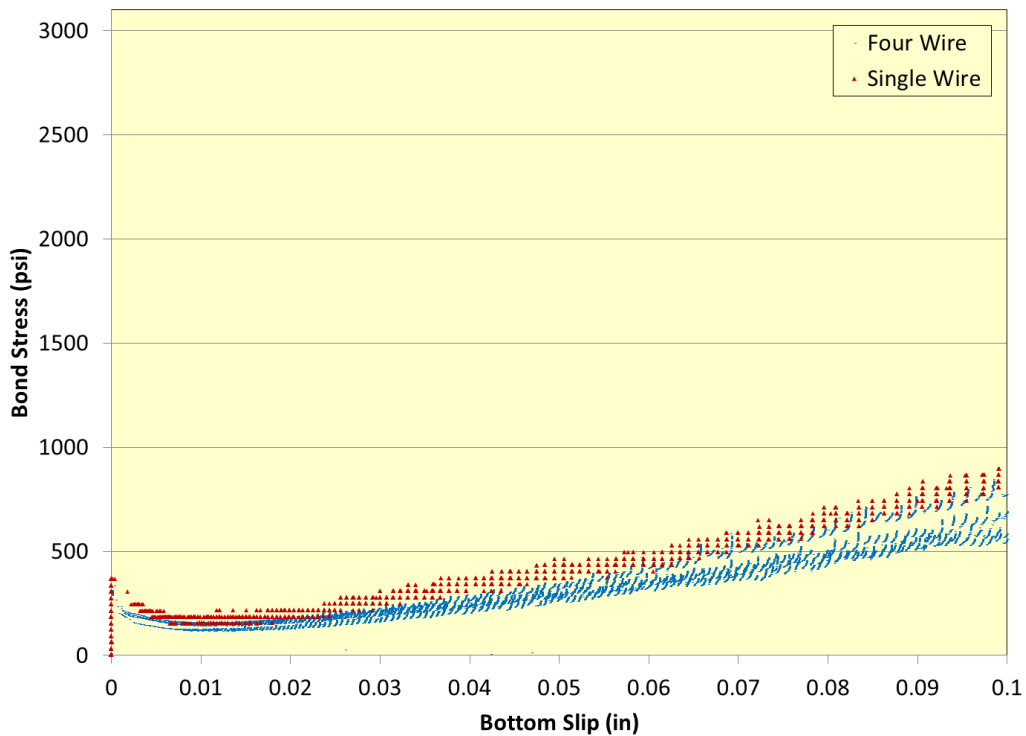


**Figure 13.6 Bond stress vs. bottom slip comparison for 4-wire and single wire test with WA**



**Figure 13.7 WA 4-wire specimen after testing**



**Figure 13.8 WA single wire specimen after testing**

Figure 13.9 displays test results from the WE comparison test. Wires in the 4-wire specimen displayed similar bond versus slip behavior to the wire in a single wire specimen. As shown in Figure 12.9, both test specimens cracked during testing as indicated by the drop in bond stress after the peak was reached. Figure 13.10 shows the cracked WE 4-wire specimen after testing. The single wire specimen also cracked, as shown in Figure 13.11. A second set of tests was performed using WE, and results from that test are shown in Figure D.1. Both specimens demonstrated the same behavior as the first set and they also cracked.

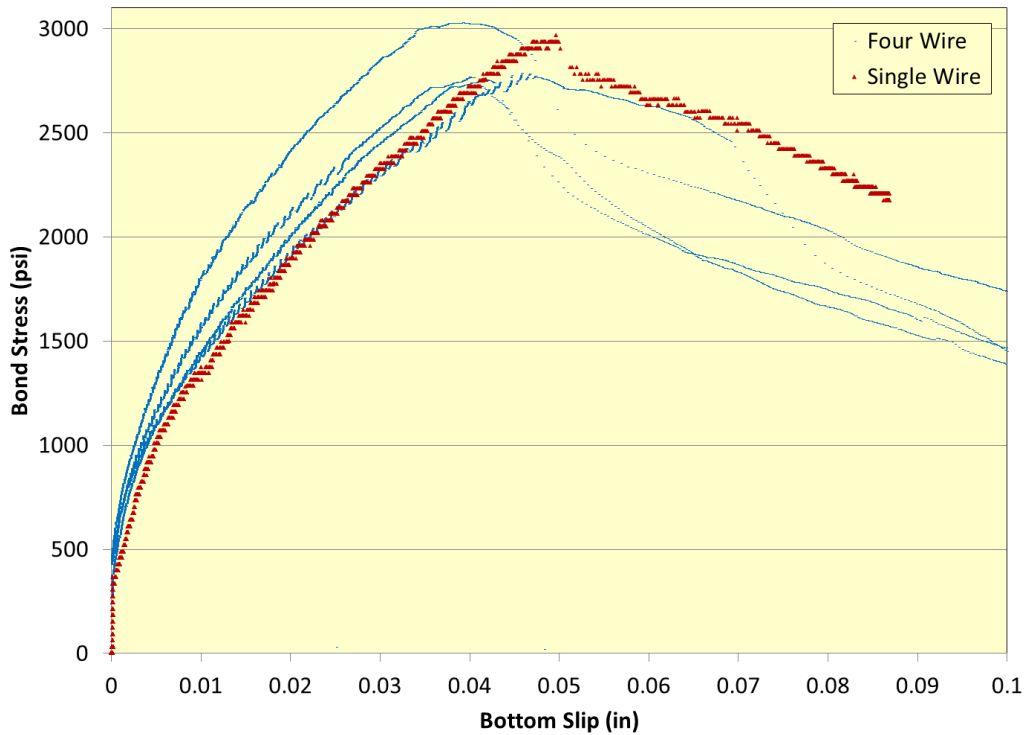


**Figure 13.9 Bond stress vs. bottom slip comparison for 4-wire and single wire test with WE**

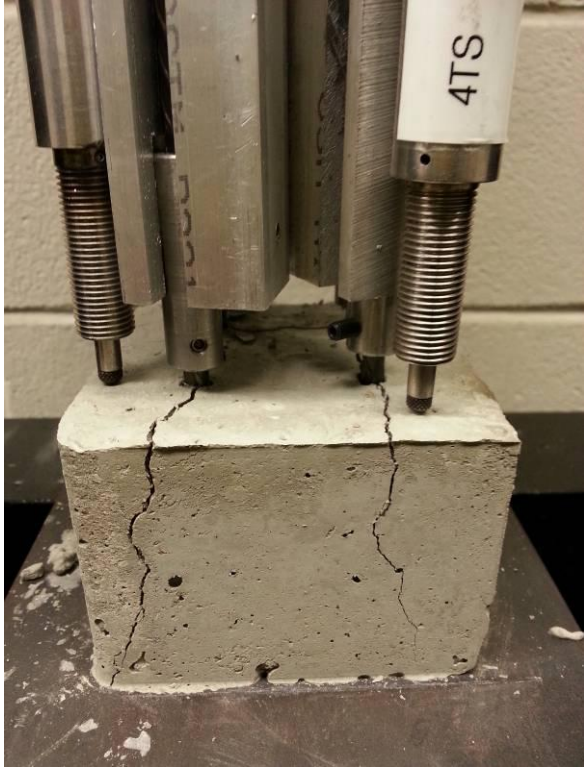


Figure 13.10 WE 4-wire specimen after testing

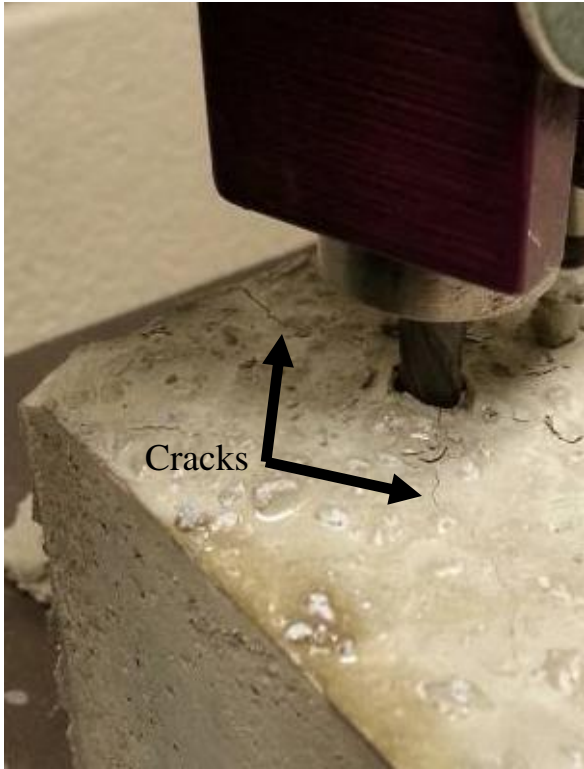
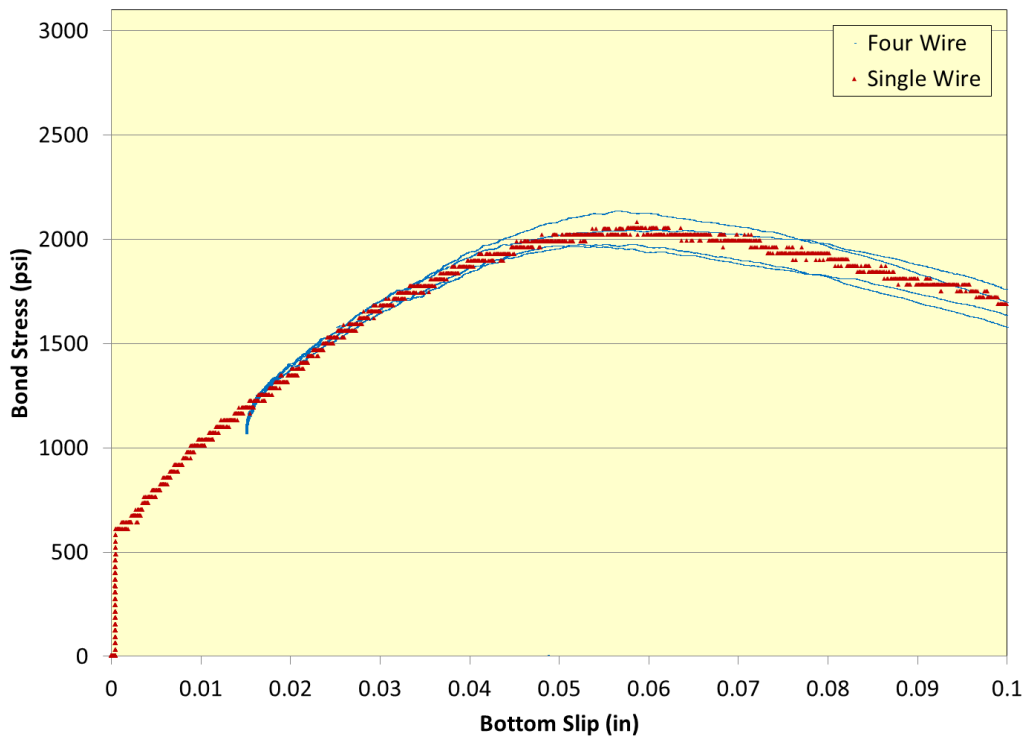


Figure 13.11 WE Single wire specimen after testing

Figure 13.12 shows results for WG specimens. Neither specimen cracked during testing. The 4-wire specimen after testing is shown in Figure 13.13. During the 4-wire WG specimen test, the data acquisition system stopped recording. After restarting the system, testing was completed but a loss of data for the beginning of the test had occurred. Bottom slip data needed to be offset since slip had occurred prior to restarting the data acquisition system.



**Figure 13.12 Bond stress vs. bottom slip comparison for 4-wire and single wire test with WG**



**Figure 13.13 WG 4-wire specimen after testing**

Figure 13.14 shows one test conducted using WH. Both specimens cracked during testing, evidenced by the decrease in bond stress after the peak. Figure 13.15 shows the 4-wire specimen after testing and the cracking that occurred in the specimen. Results from the second set of specimens tested with WH are shown in Figure D.2. Both specimens cracked, however, the single wire specimen only had a hairline crack and maintained high bond stress high throughout the test.

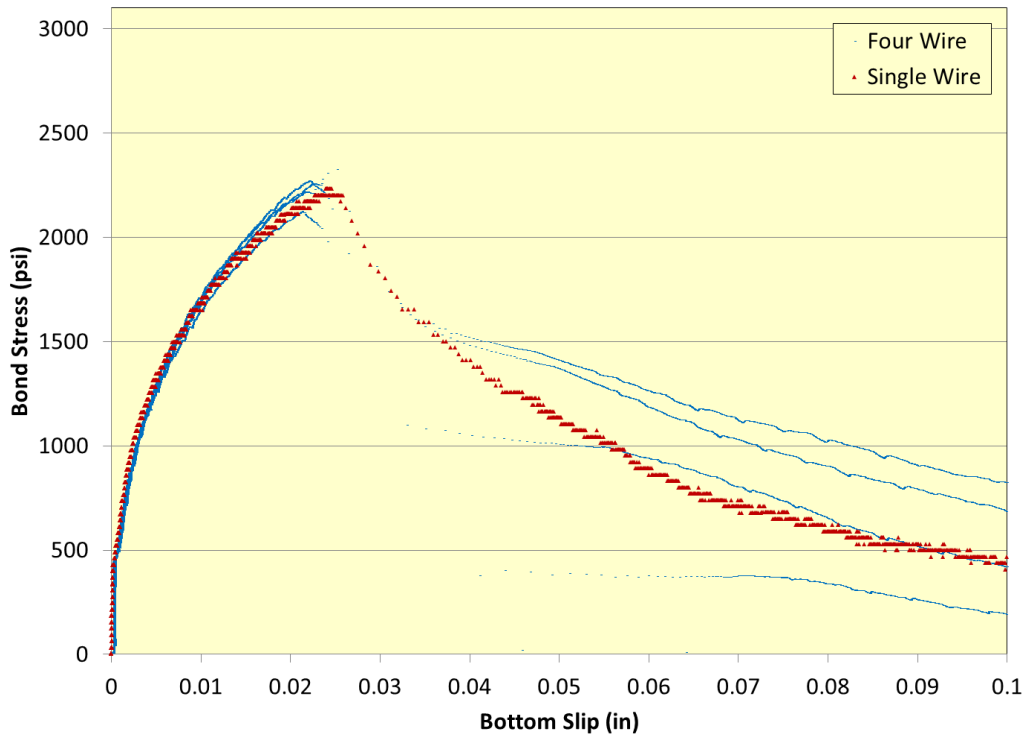


**Figure 13.14 Bond stress vs. bottom slip comparison for 4-wire and single wire test with WH**





**Figure 13.15 WH 4-wire specimen after testing**

Results from the 4-wire versus single comparison test with the WK are shown in Figure 13.16. WK behaved similarly to WA because WK started slipping at a lower stress than other wire types and then gradually increased bond as the slip increased. This increase in bond with respect to slip was due to the increase in surface friction as the wire increased in size due to Poisson's effect. Figure 13.17 shows the WK specimen with no cracking after testing.

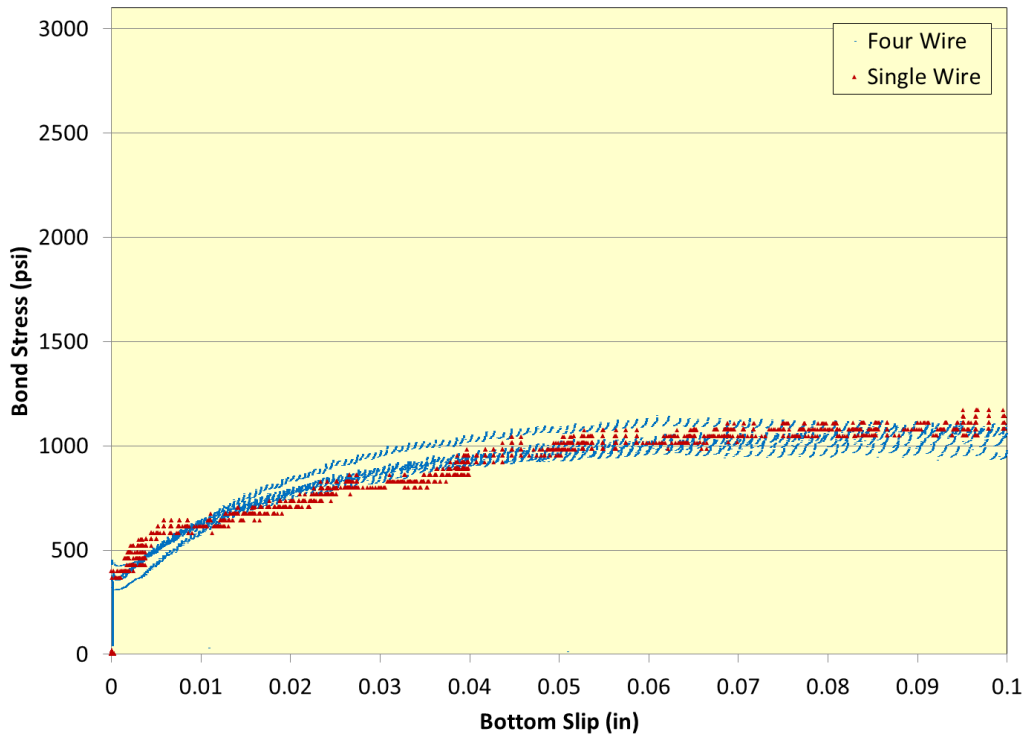


**Figure 13.16 Bond stress vs. bottom slip comparison for 4-wire and single wire test with WK**



**Figure 13.17 WK 4-wire specimen after testing**

### **13.3 Reinforced 4-Wire Test Setup**

After initial testing of the 4-wire specimens and the findings from the confined and unconfined testing described in Chapter 9, experimental testing investigating the effect of reinforcement on cracking reduction was done. Initial testing was conducted to determine if future testing could potentially reduce the cracking propensity.

WH wire was used for this test setup because of its propensity to crack previous test specimens in Chapter 9 and Chapter 13. The test setup included the same frame used for initial 4-wire setup discussed in this chapter. Testing also used Mix B and was identical to the previous 4-wire setup except that various reinforcements were tested to provide different amounts of confinement.

Four reinforcement setups were investigated, two of which were investigated during this study. The first setup involved wrapping three 3/32-inch-diameter steel wires and three 1/8-inch-diameter steel wires around the prestressed wires. The second setup involved two reinforcements placed away from the wire. The first reinforcement was a wire cage made from three 3/32-inch wires (identical to the first setup) and the second reinforcement included a glass fiber mesh.

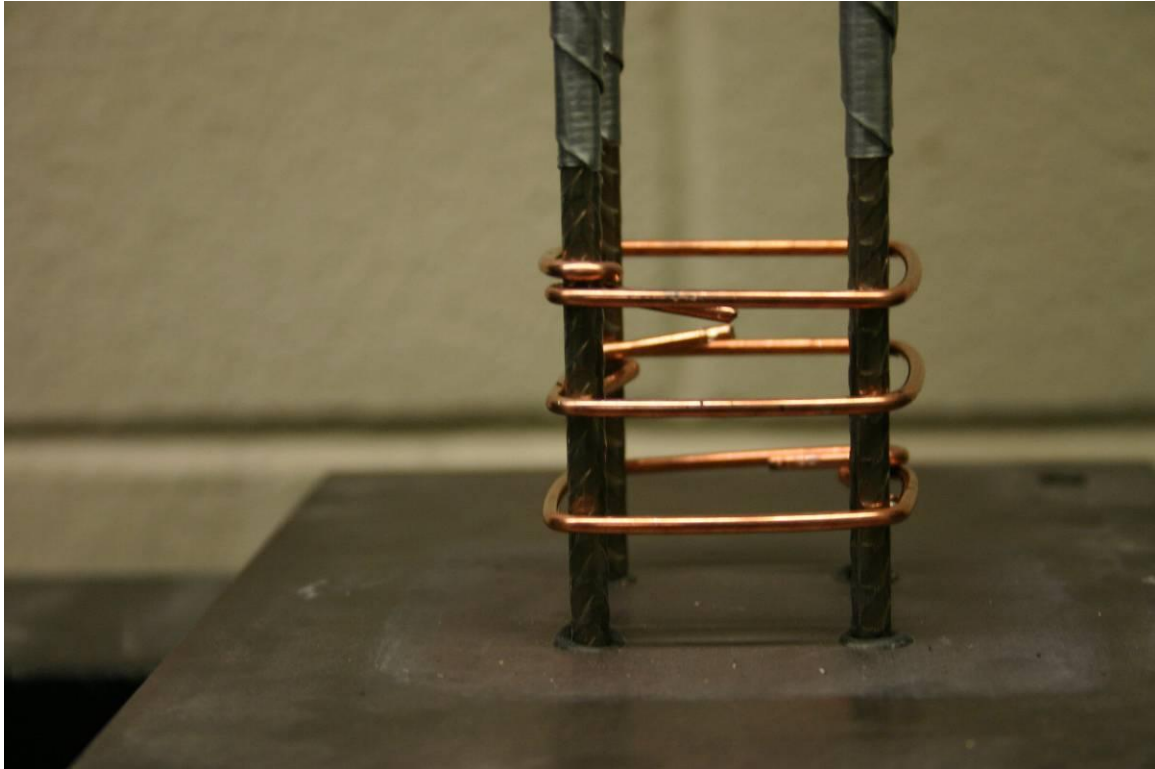


**Figure 13.18** Three 3/32-inch-diameter steel rods on prestressed wire

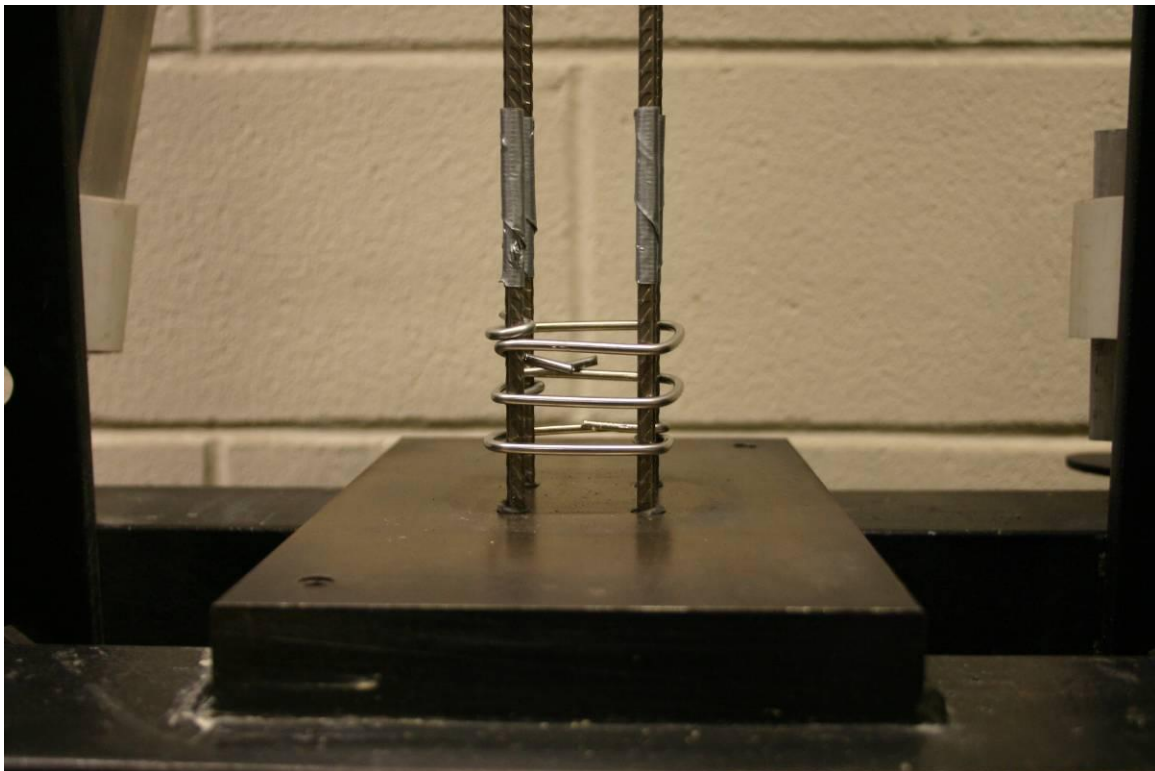


**Figure 13.19** Three 1/8-inch-diameter steel rods on prestressed wire

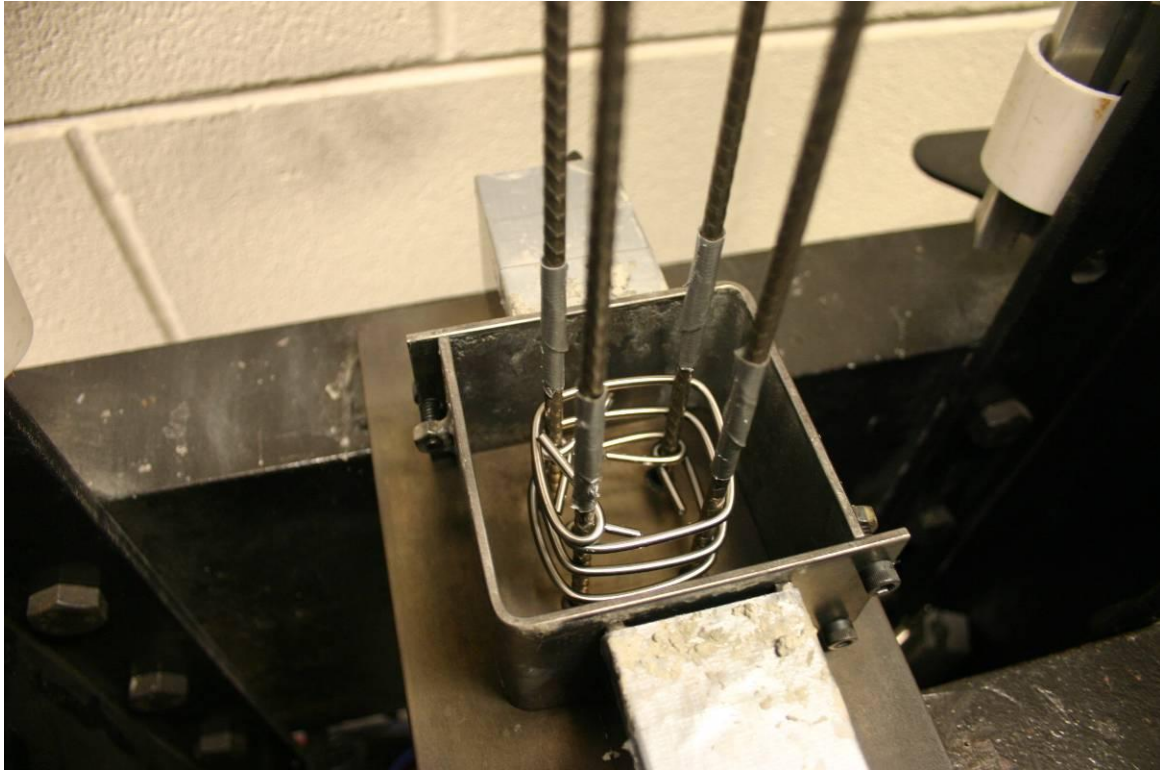


**Figure 13.20 Three 1/8-inch diameter rods on wire in forms**

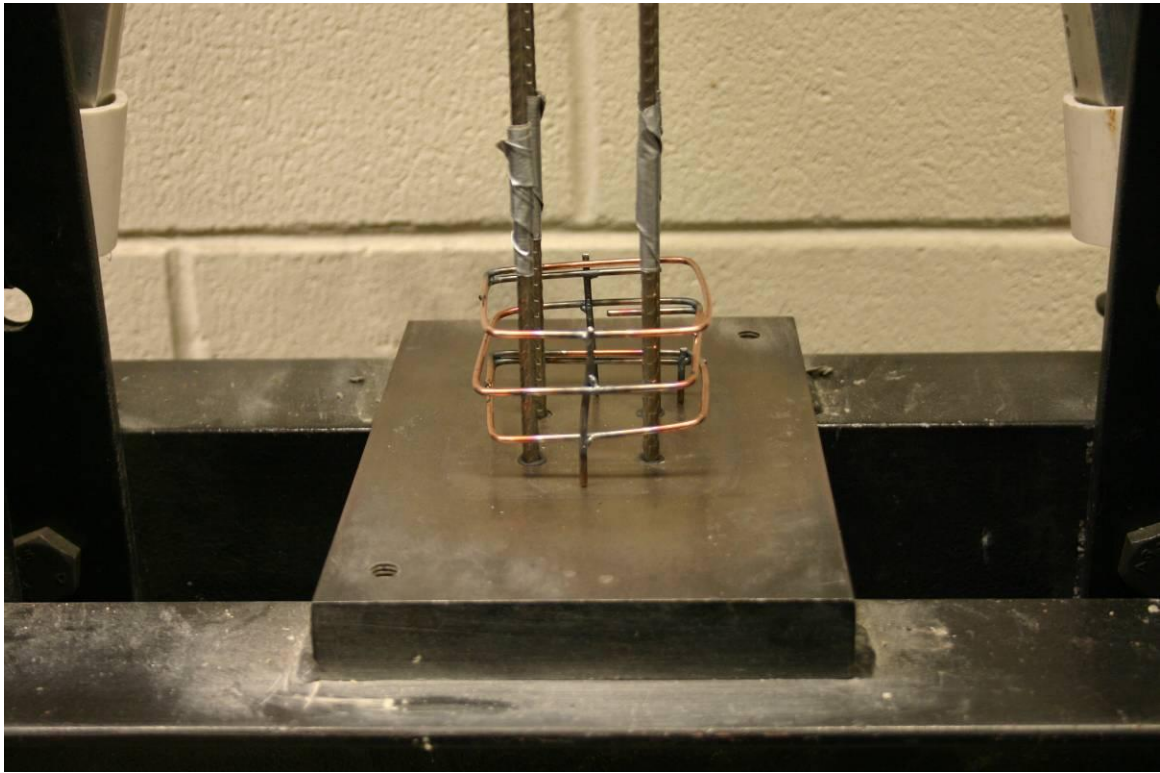


**Figure 13.21 Three 3/32-inch diameter rod cage off wire**

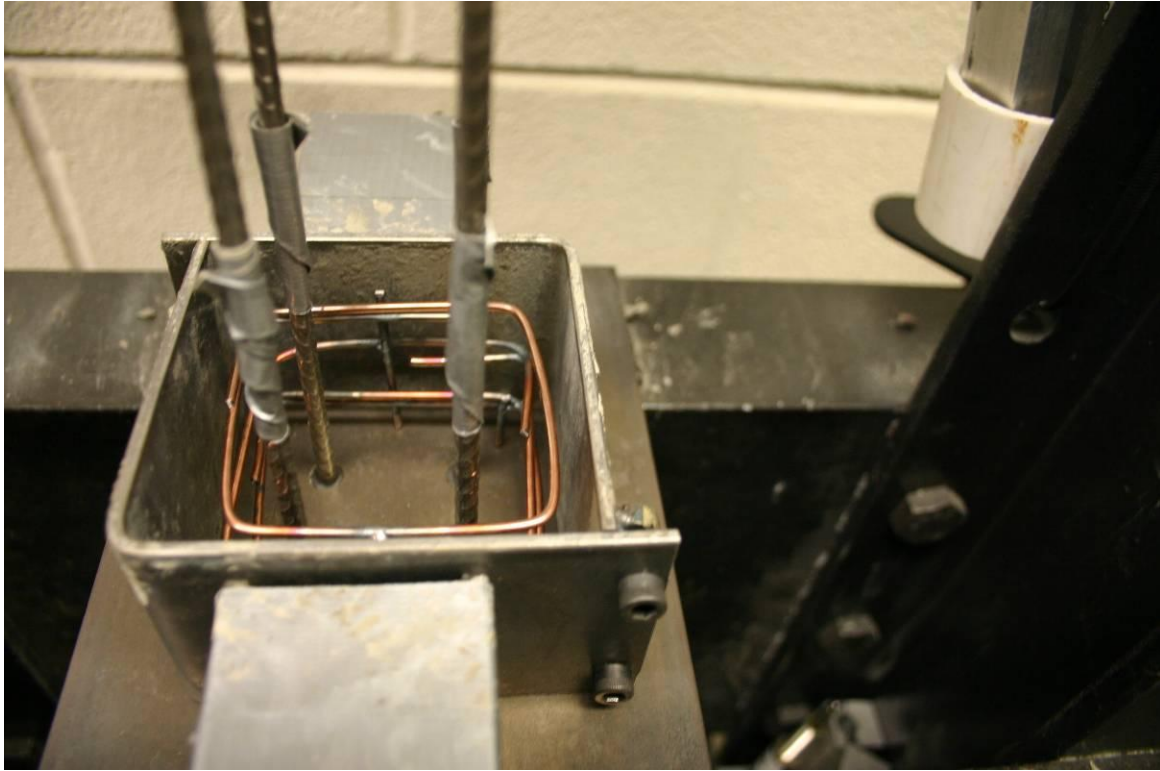


**Figure 13.22 Three 3/33-inch diameter rod cage in forms**

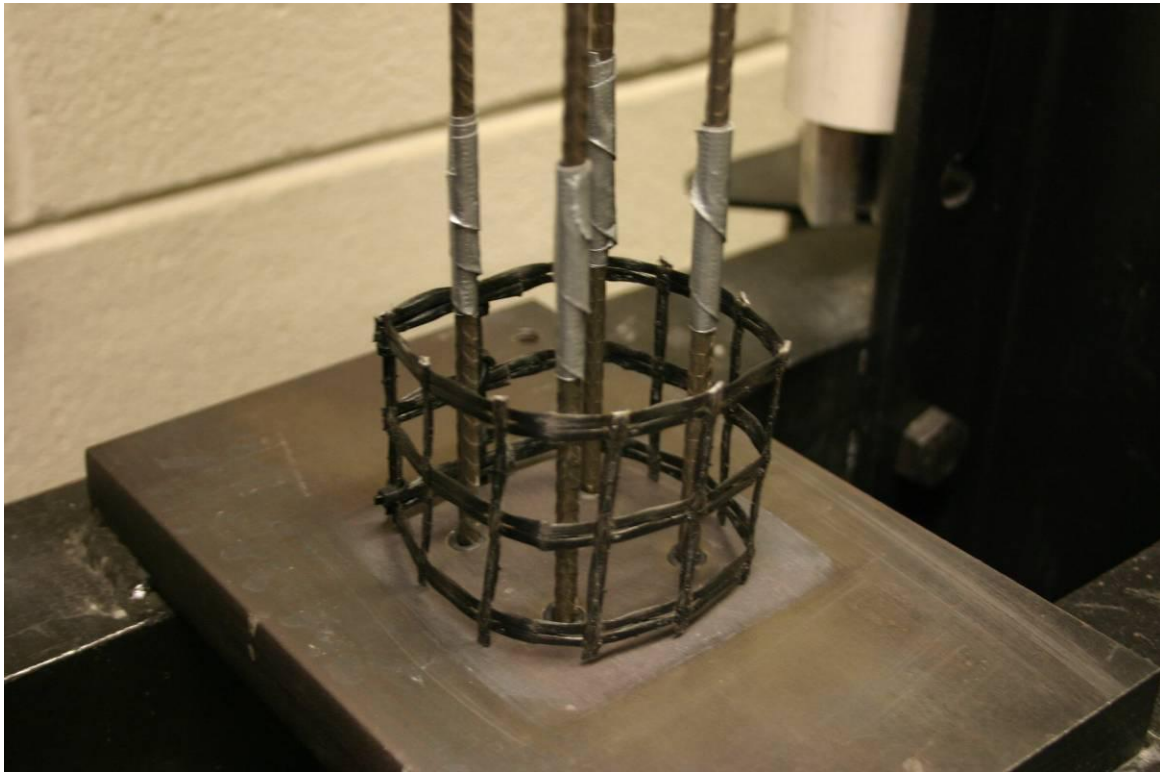


**Figure 13.23 Glass fiber mesh around prestressing wires**

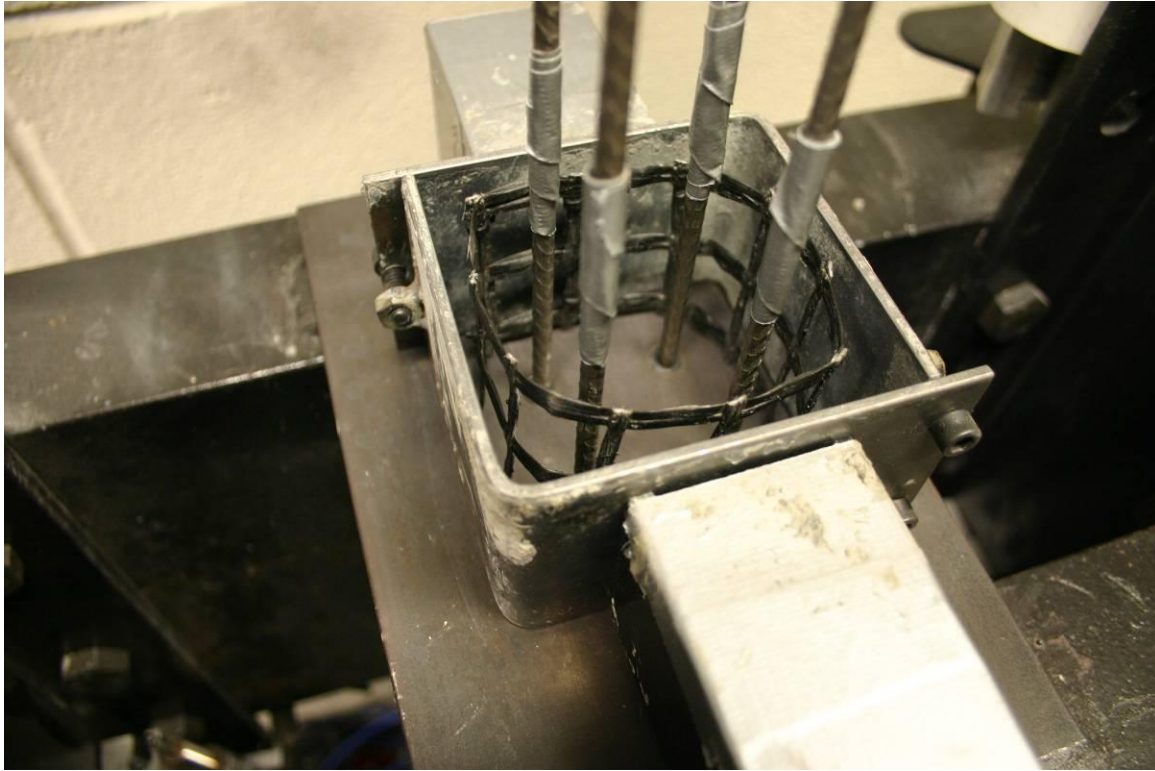
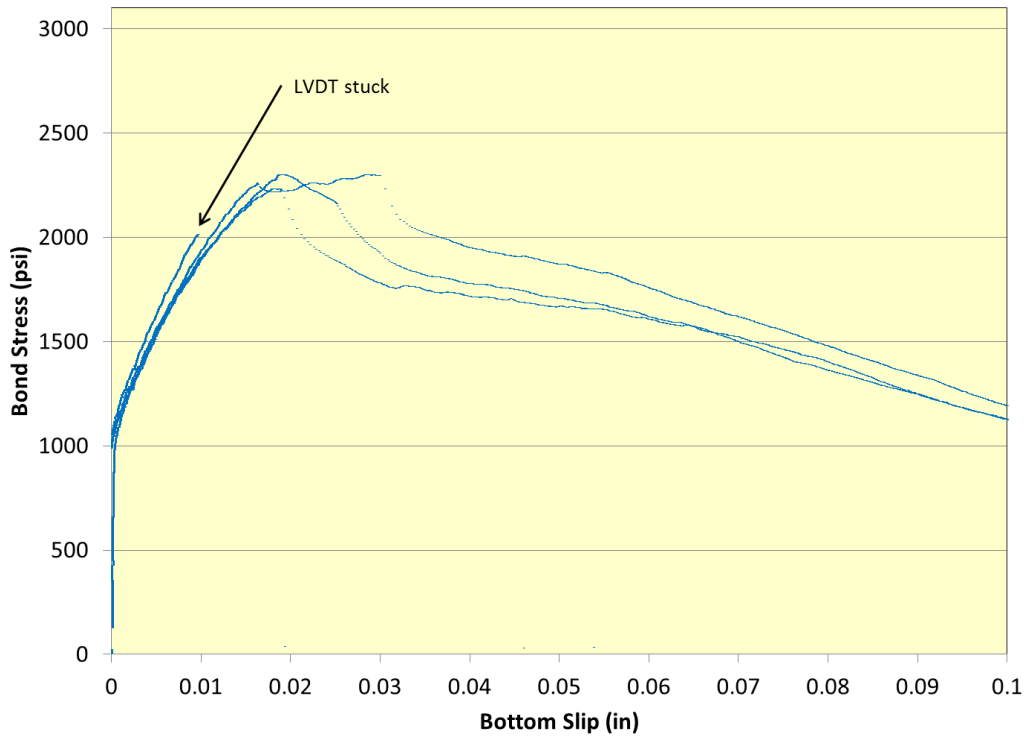


**Figure 13.24 Glass fiber mesh in forms**

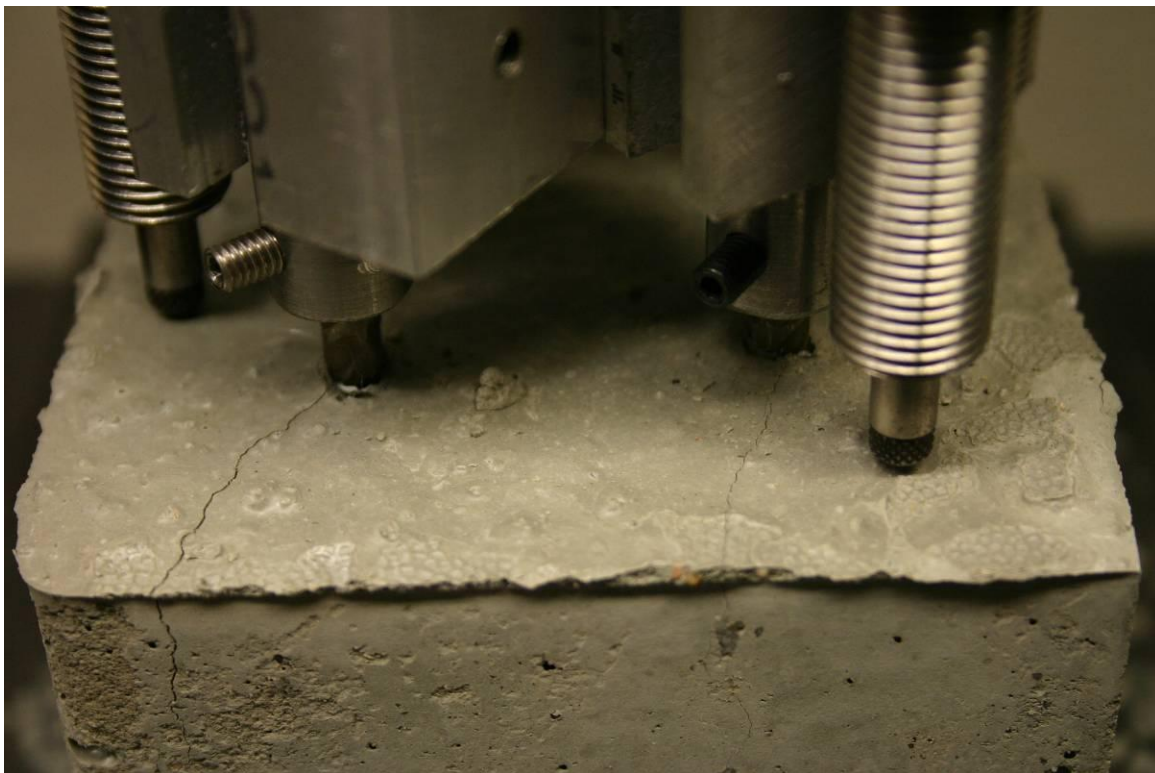
### **13.4 Reinforced 4-Wire Results**

The four reinforcement arrangements were tested and data from the end-slip and load cell readings were tabulated to determine setup effectiveness. Bond stress was graphed in relation to the bottom slip for each test. The amount of surface cracking was also investigated to determine if the various setups led to diverse cracking behaviors.

Figure 13.25 shows the graph of bond stress versus bottom slip of the specimen with three 3/32-inch diameter rods on the wire. The four lines are each associated with an individual prestressing wire used in the test. The bottom slip LVDT stuck during the testing, as shown in the graph. Figure 13.26, which shows the specimen after testing, reveals surface cracking and that it propagates to the side of the specimen even though reinforcement was used. Reinforcement increased bond stress capacity of the specimens compared to unreinforced WH 4-wire specimen results shown in Figure 13.14 and Figure D.2.



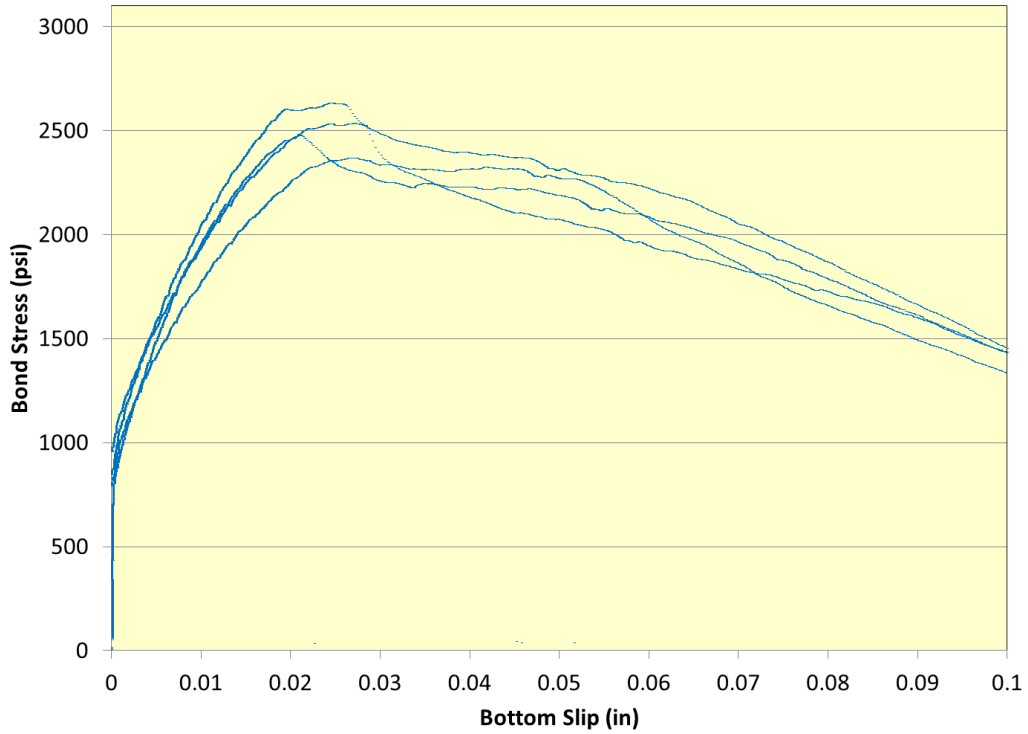
**Figure 13.25 Results of three 3/32-inch diameter rods located on the wire**



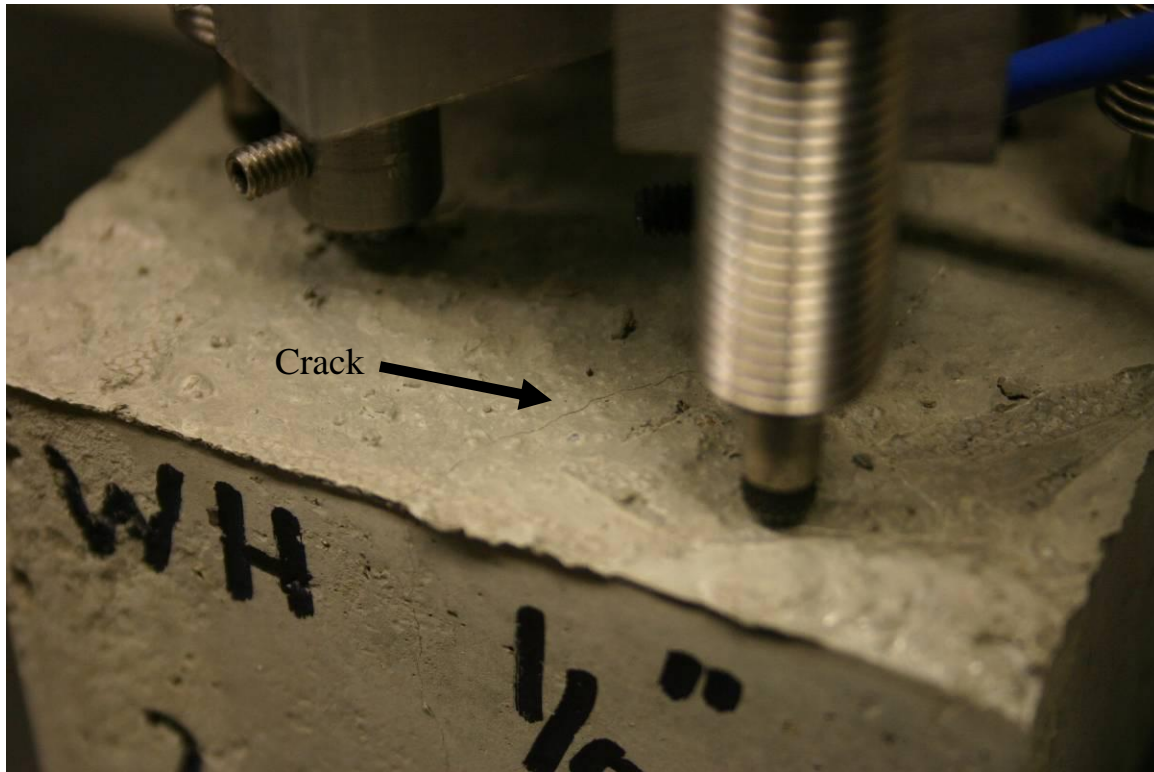
**Figure 13.26 Cracking of specimen with three 3/32-inch diameter rods located on the wire**



Figure 13.27 shows results from the test using three 1/8-inch diameter rods attached to prestressing wires' surfaces. The amount of bond stress held by the specimen was higher than the specimen with three 3/32-inch diameter rods attached to the wires. Figure 13.27 also indicates that bond stress remained higher than the previous test even after specimen cracking. Figure 13.28, which shows the specimen after testing was completed, reveals reduced crack width on the specimen; however, the crack still propagated to the side surface of the specimen.



**Figure 13.27 Results of three 1/8-inch diameter rods located on the wire**



**Figure 13.28 Cracking of specimen with three 1/8-inch diameter rods located on the wire**

Figure 13.29 shows results from three 3/32-inch diameter rods located off the wire. The graph indicates that reinforcement off the wires allowed the specimen to hold a larger amount of bond stress before cracking. Test results are similar to ones using 1/8-inch wire shown in Figure 13.27 but used 50% less reinforcement. This test also included identical amounts of reinforcement as test results shown in Figure 13.25 but higher stresses were developed. Reinforcement location completely confined the wires, differing from the previous two tests that confined part of the wire. Cracks between prestressing wires could escape beyond confining reinforcement. Figure 13.30 shows the cracked specimen, but the crack does not extend to the edge surface of the specimen. This test demonstrated that proper reinforcement placement greatly impacts prestressing wire bond behavior.

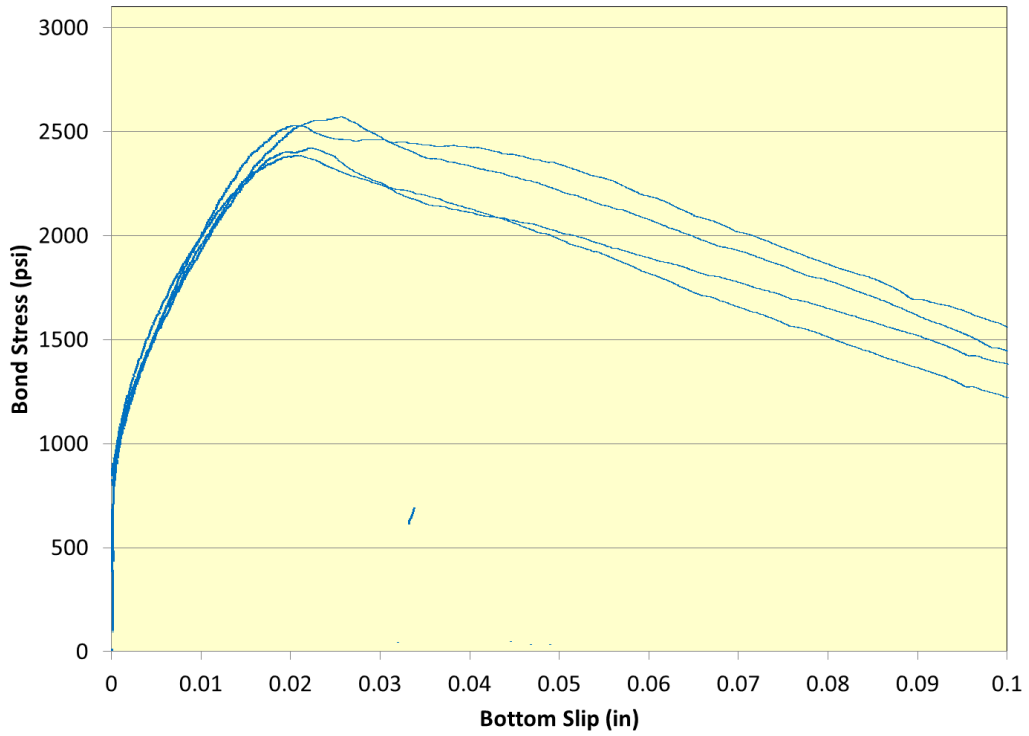


**Figure 13.29 Results of three 3/32-inch diameter rod located off the wire**

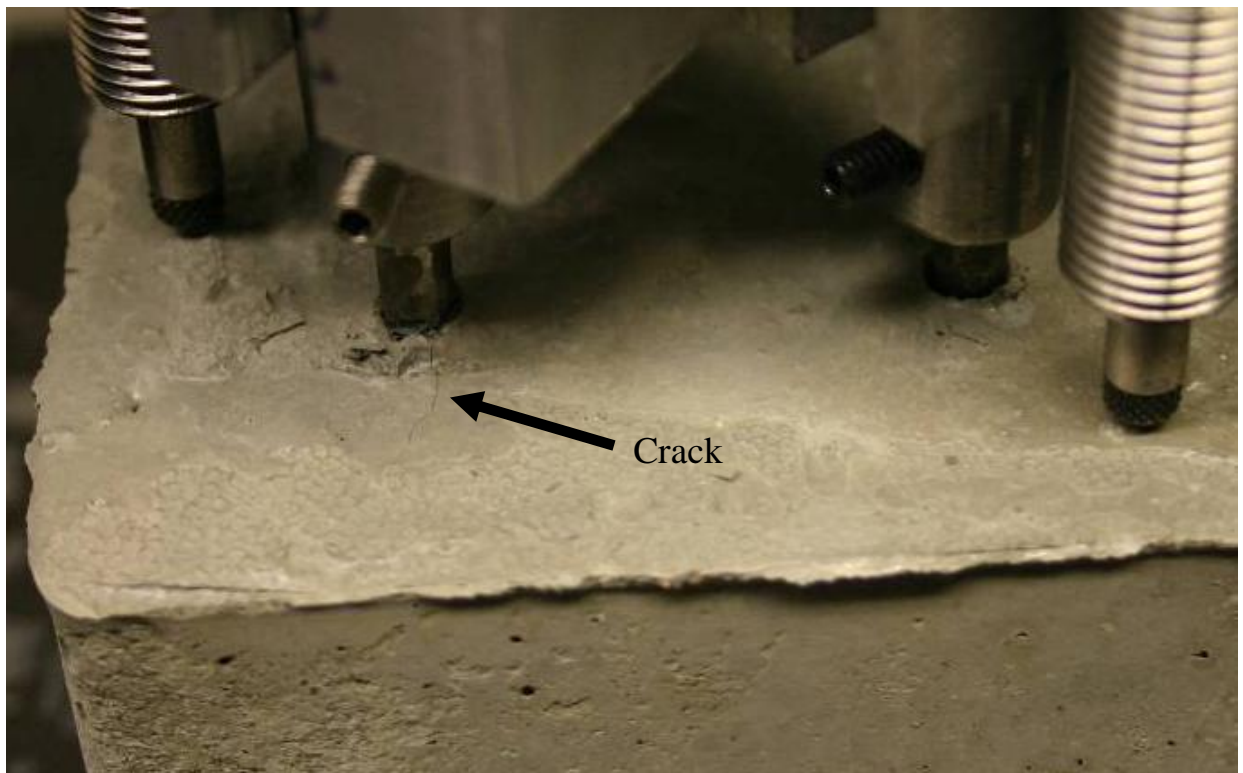


**Figure 13.30 Cracking of specimen with three 3/32-inch diameter rods located off the wire**

Figure 13.31 shows results from a test utilizing glass fiber mesh as a confinement. Results show that the mesh did not provide as much confinement as the steel. The amount of glass mesh must be increased and investigated to determine if additional areas of reinforcement would increase bond strength. Figure 13.32 shows the specimen after testing with large amounts of cracking extending to the edge of the specimen.

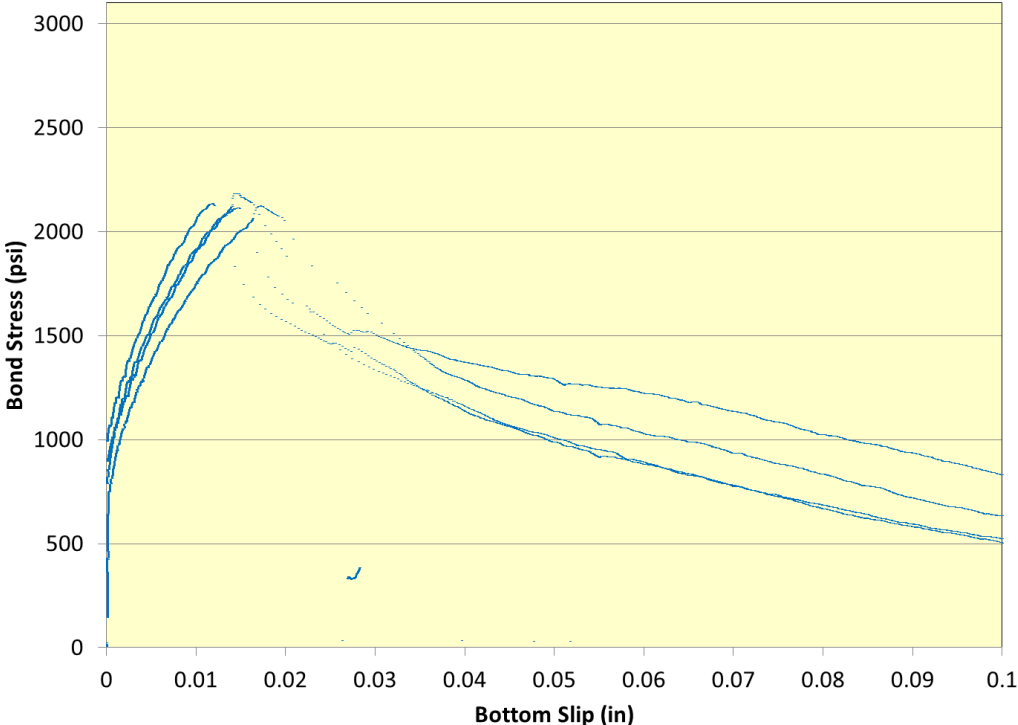


**Figure 13.31 Results of glass fiber mesh located off the wire**



**Figure 13.32 Cracking of specimen with glass fiber mesh located off the wire**

Table 13.1 shows a summary of the crack widths on the top of the specimen for each of the reinforcement types used on the WH specimens.

**Table 13.1 Crack widths for reinforcements on WH wire**

Additional Reinforcement	Crack width at wire (in)	Crack width at edge of specimen (in)
3/32"-diameter steel rod on wire	0.008	0.005
3/32"-diameter steel rod off wire	0.004	No Crack
1/8"-diameter steel rod on wire	0.004	0.004
Glass fiber mesh off wire	0.012	0.008
None	0.016	0.012

## **Chapter 14 Crosstie Manufacturing Plant Instrumentation**

This section details instrumentation of concrete crossties in a precast plant. Crossties were instrumented to determine the amount of lateral expansions various reinforcements cause in the crosstie. Resulting data provided details regarding the amount of strain present in crossties during production.

### **14.1 Instrumentation of Crossties**

Four crossties were instrumented using VWSGs. Two crossties used one type of reinforcement and the remaining two crossties used a different type of reinforcement. The wire pattern was identical for all four ties. The ties were instrumented with eight gauges each, four on each end, and the ends were labeled “dead or live” ends based on orientation on the tie in relation to the jacking end of the prestress bed.

The VWSGs used in the study were identical to the type of gauges used in Chapter 11. Gauges were mounted in various orientations in crosstie cross sections. Four gauges were used for each end of the crosstie. Three gauges were mounted 1.25 inches from the end of the tie and the remaining gauge was located 8 inches from the end of the tie. Figure 14.1 shows gauge locations for gauges mounted 1.25 inches from the end of the crosstie. Figure 14.2 shows gauge location for the gauge located 8 inches from the crosstie end. The gauges were numbered 1 through 4 for each crosstie end and D or L for dead end or live end, respectively. The four crossties were labeled A through D so each individual gauge had a 3-digit code. For example, gauge B-L-3 was gauge #3 from the live end of the B crosstie. Ties A and B had identical reinforcement and C and D had a different reinforcement.

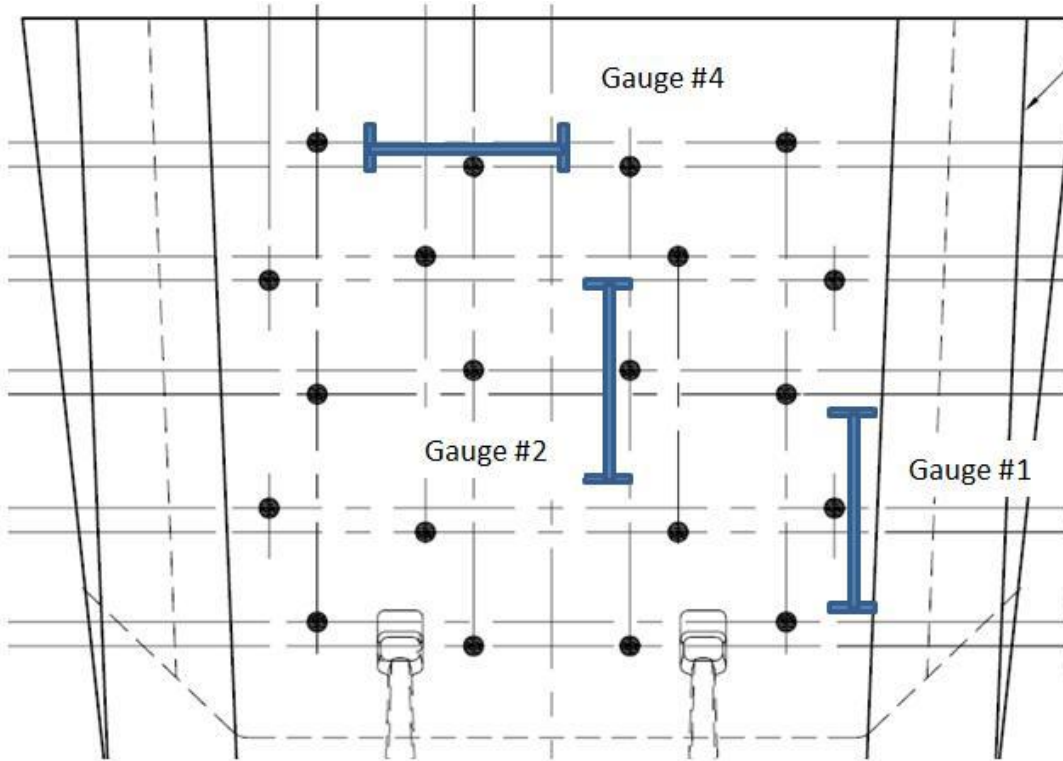


**Figure 14.1 Cross section showing gauge location 1.25 inches from crosstie end**

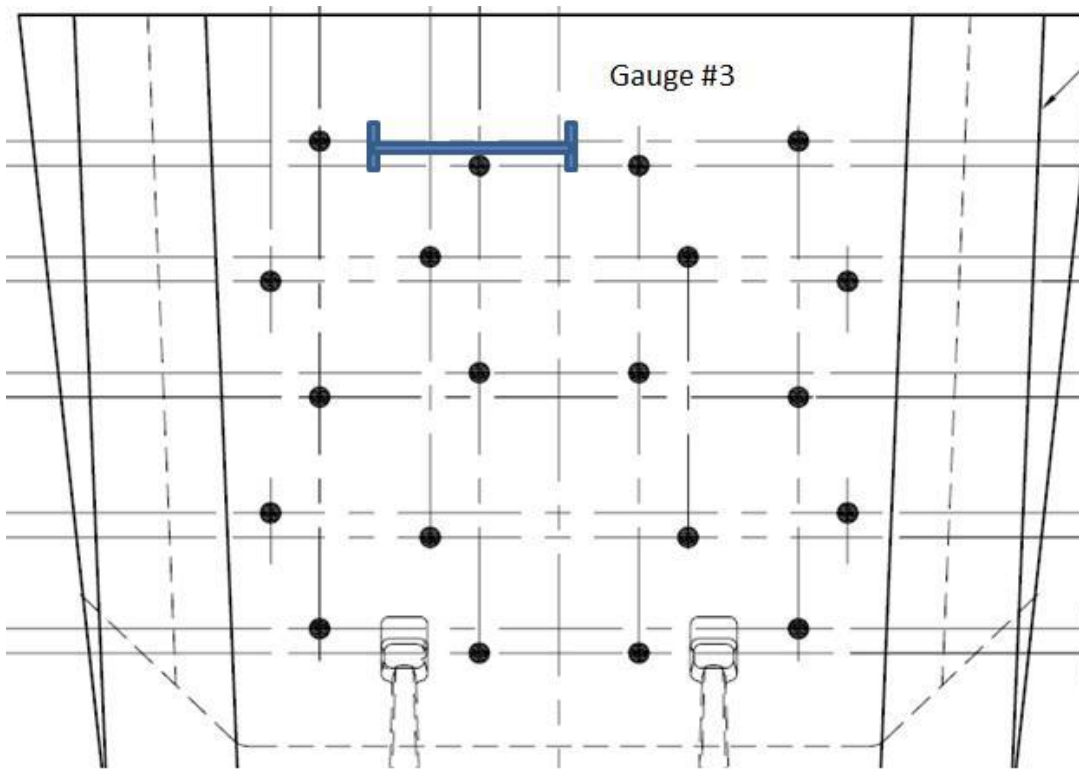


**Figure 14.2 Cross section showing gauge location 8 inches from crosstie end**

Gauges were mounted with wires sleeved in plastic tubing. This tubing prevented the wire from providing additional reinforcement to concrete located near the gauge. The gauges were mounted next to the wires because of findings discussed in Chapter 11. Figure 14.3 shows the forms after the wires had been tensioned and the gauges were mounted.



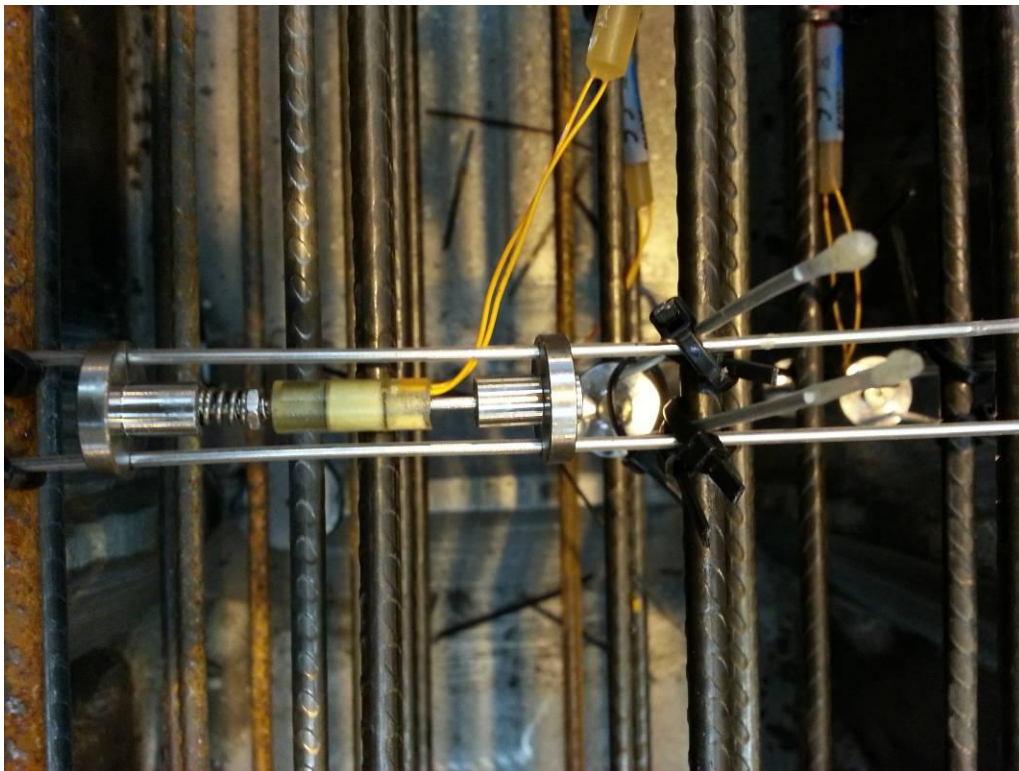
**Figure 14.3 Crosstie forms with wire tensioned**

Figure 14.4 and Figure 14.5 show a close-up of the gauges after being attached to the wire.





**Figure 14.4** Close-up of gauges mounted to wires



**Figure 14.5** Close-up of gauge orientation

Figure 14.6 through Figure 14.8 show the gauges after being attached to the wires. Wires connected to each gauge ran towards the center of the crosstie where they were attached to a wooden frame to allow exit from the tie. The figures also show cables for the gauges as they are routed to the center of the crosstie.



**Figure 14.6 Gauges mounted at one end of a crosstie**

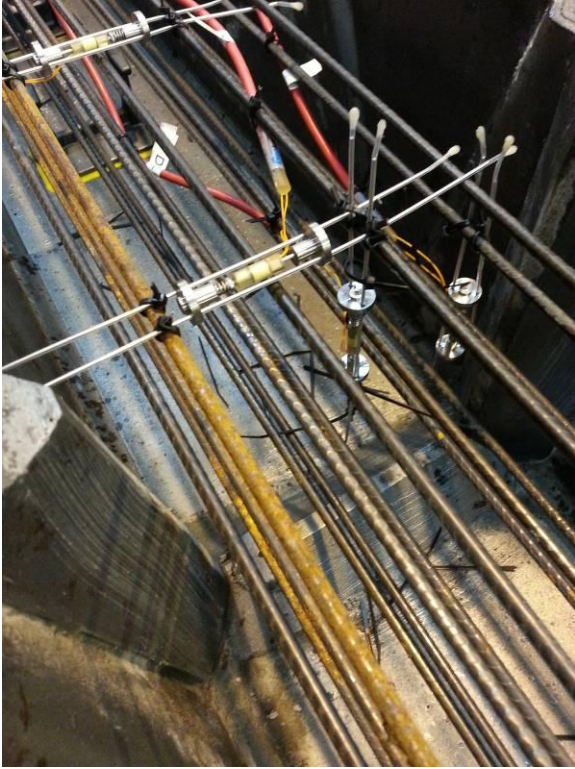


**Figure 14.7 Gauges mounted to wires**



**Figure 14.8 Gauges mounted to wires**

## 14.2 Crosstie Production

Crossties were cast by plant workers and crosstie beds were vibrated as they were filled. Gauges were monitored during casting to prevent movement due to vibration or the surrounding flow of concrete. Figure 14.9 shows the crosstie cast with gauges, and Figure 14.10 shows the finished crosstie after casting. After the crossties were cast, the forms were covered with plastic to prevent moisture loss.



**Figure 14.9 Crosstie being cast**



**Figure 14.10 Crosstie after being cast**

After the ties had cured for eight hours, the wires were removed from the plastic bags in which they had been placed before casting. Gauges were read to obtain initial readings for each gauge. These baseline readings were necessary in order to calculate changes in strain experienced by each gauge. Figure 14.11 shows wires for the gauges after the crosstie had cured.



**Figure 14.11 Wires exiting the crosstie after curing**

Once initial readings were taken, forms of the crossties were removed by the plant workers to prepare the crossties to be separated. Readings were taken after the forms had been removed. Figure 14.12 shows the crossties after removal of the forms.

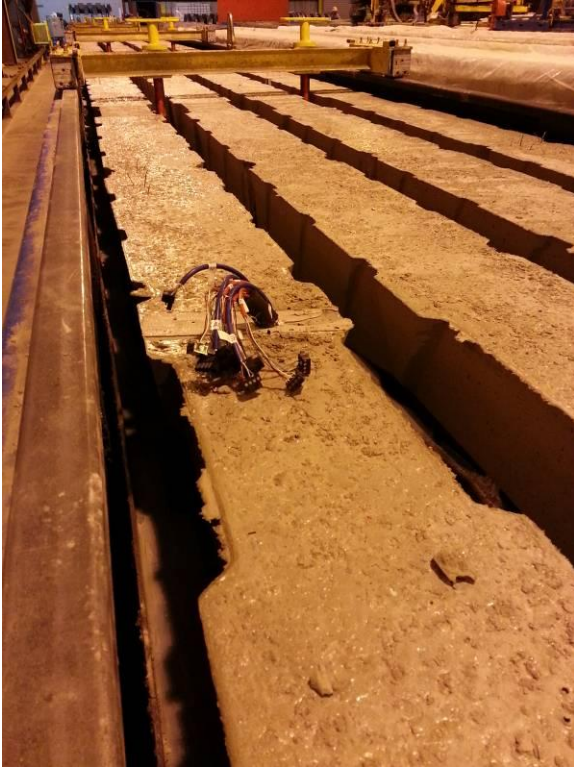


**Figure 14.12 Crosssties after forms had been removed**

Once the concrete reached release strength, the bed was de-tensioned, thus releasing the bed ends and allowing the crosssties to be compressed by prestressed wires. Readings were taken after de-tensioning, but these readings were not final since the crosssties were still connected as a long column. Readings showed resulting compressive forces in the crosssties. An additional set of readings was taken immediately before the crosssties were saw cut in order to obtain a close measurement before and after saw cutting. Then the wires were taped to the crossstie to allow the crossstie to fit in the saw. Figure 14.13 shows the wires after they are taped to the crossstie.



**Figure 14.13 Wires taped before going through saw cutting process**

After the cross-ties were cut, they were moved outside, set on pallets, and kept upside down to allow access to the wires for additional readings. Figure 14.14 shows the ties after they were cut.





**Figure 14.14** Crossties after being cut and loaded onto pallets

The crossties were strapped to the pallets to secure them for shipment and protective boxes were mounted to the crossties to protect the wire and avoid sun exposure. A final set of readings was taken before the wires were placed in the protective boxes. Figure 14.15 shows crossties strapped to the pallets, and Figure 14.16 shows the wires placed in protective boxes.



**Figure 14.15 Crossties strapped to pallets and wire boxes installed**



**Figure 14.16 Wires placed into protective boxes**

After the wires were placed in protective boxes, the boxes were sealed and the cross-ties were ready for shipment to KSU. Figure 14.17 shows cross-ties ready for shipment.



**Figure 14.17 Crossties ready for shipment**

### **14.3 VWSG Results**

Gauge readings were used to calculate change in strain for each gauge. The internal temperature of the gauge was also used to correct for temperature changes in the crosstie. Readings for each gauge are presented in Appendix E.

Readings from each gauge were used to compare the two reinforcements used and locations on the gauges. The average for each gauge location was calculated for the two wire types. Table 14.1 shows a comparison of strains between the two wire types. Wire 2 had overall higher strain values for each reading. Strain readings found for Gauge 3 were higher due to lateral expansion because the Poisson's effect caused by compressive force of the prestressing wires. All strain readings were lower than the tensile capacity of the concrete specimens.

**Table 14.1 Average strain for each gauge location (in microstrain)**

	Gauge	After forms drop	After Detensioning	Before Cutting	After Cutting	Outside on pallets
Wire 1	1	-4	37	28	1	-58
( A and B ties)	2	8	60	56	20	-16
	3	-1	95	96	109	78
	4	11	48	43	44	-5
Wire 2	1	-3	52	42	-7	-67
( C and D ties)	2	-5	92	94	30	-3
	3	-2	140	147	169	144
	4	4	18	3	-12	-77

## Chapter 15 Conclusions

This section discusses conclusions made from preceding tests. Many advances were found regarding bond behavior of prestressing wires. Information was also obtained in relation to the splitting behavior of prestressing wire indents.

1. Transfer bond testing conducted at the beginning of this study effectively advanced understanding of prestressing wire behavior. Tensioned pullout test results accurately predicted transfer length of prisms cast in the laboratory. Unlike Abrishami and Mitchell's (1993) testing of prestressing strands which used peak load, the transfer length of each reinforcement was matched to the bond stress at 0.05 inches of bottom slip with a  $R^2$  of 0.956. This result was similar to findings from Arnold (2013) involving un-tensioned wire pullout tests. Results did conflict, however, with findings from Rose and Russell's (1997) testing of prestressing strands by correlating tensioned pullout tests to transfer length. This study demonstrated that the tensioned pullout setup can predict transfer length of prestressing wires using a concrete mix.
2. Testing conducted with various amounts of cover showed that the amount of cover in a specimen changes bond characteristics of prestressing wires. Small 2-inch diameter cylinders cracked during testing due to a small amount of cover. Cover is necessary to confine prestressing wires as they slip. Without adequate cover, tensile capacity of the concrete is reached and the specimen cracks during testing. Confinement testing using 2-inch and 4-inch diameter cylinders showed that confinement improved bonding capacity of the 2-inch-diameter cylinder by preventing the specimen from cracking. Confined and unconfined 4-inch-diameter cylinders demonstrated identical bond behavior, indicating a limit to the bond amount prestressing wires can achieve through passive confinement. This amount of bond is based primarily on indent geometry. Additional testing involving confinement of 4-wire specimens also reinforced this finding.
3. Testing involving unconfined 2-inch cylinders was beneficial in showing how indent geometries affect the splitting behavior of prestressing wires. Geometrical feature measurements of the indents were able to predict the amount of bottom

slip necessary to split the specimen. These amounts of slip differ from crossties, but the testing procedure can be used to predict the likelihood that an indent will cause crosstie splitting. Deeper indent patterns were shown to bond better, but they caused splitting at lower amounts of slip. Bond ability without producing splitting was investigated further in this study.

4. Lateral expansion testing proved to be a beneficial section of this testing program. VWSGs provided a method to measure lateral expansion inside concrete specimens prior to cracking. This ability was important in determining the amount of strain present in specimens that did not crack during testing. Higher bonding wires demonstrated higher lateral expansion in relation to the amount of slip.
5. Machined wire testing was a crucial section of this research project to investigate variables in indent geometries. Since a majority of indent patterns available to concrete crosstie producers have similar characteristics, the ability to test custom indents provided much needed information. Machined wire testing showed that shallow indents with edge wall angles of 45 and 60 degrees did not cause specimen splitting. This finding shows that shallower indent geometries with those angles are properties a prestressing wire indent with low splitting potential could have.
6. Testing involving different numbers of wires in the specimen showed that the addition of prestressing wires does not change bonding characteristics of individual wires. As long as the wires have the same amount of cover and distance between wires, they exhibit bond behavior identical to a single wire with identical cover and orientation in the specimen. Additional reinforcement improved bonding behavior of multiple-wire specimens. This finding can be a point of future research towards the investigation of other options to increase tensile capacity of concrete crossties.
7. Testing involving instrumentation of concrete crossties at a plant was crucial in determining lateral expansion present in crossties. This step was crucial in order to compare laboratory results to industry results. Findings showed that crossties had little amounts of lateral strain near the tie ends. Strains found from gauges located 8 inches from the tie ends showed higher strains due to compressive force

caused by prestressing wires. Findings also showed that lateral strain values in the cross-ties was lower than tensile strain capacity of the cross-ties, proving that the evaluated cross-ties were adequately equipped to handle tensile stresses caused by indents.

8. Flexural bond testing revealed behaviors of various indents in the flexural region of the cross-tie. Indents provided anchorage during the testing and the decreasing of the wire cross section. The smooth wire demonstrated very little capacity after the cross section of the wire began to decrease with increased tension in the wire.
9. Indents with low splitting potential had shallower geometries with depths below 0.15 mm and edge wall angles of 45 to 60 degrees. High bonding indent geometries had higher splitting potential than the lower bonding geometries. High bonding indent patterns provide a shorter transfer length than shallower indents, but splitting behavior of the indent must be addressed with adequate tensile strength in the concrete. Shallow indent patterns produce larger transfer lengths that must be monitored to ensure they are anchored before the rail seat.

Portions of the preceding chapter were originally published here:

Transfer Bond Test Used To Predict Transfer Length Of Concrete Railroad Ties, by Joseph R. Holste, M.S., Robert J. Peterman, PhD, PE, Naga Narendra B. Bodapati, B. Terry Beck, Chih-Hang John Wu, Proceedings of the ASME 2013 Rail Transportation Division Fall Technical Conference, RTDF2013-4726. Copyright 2013 American Society of Mechanical Engineers.

Tensioned Pullout Test Used To Investigate Wire Splitting Propensity in Concrete Railroad Ties, by Joseph R. Holste, M.S., Mark Haynes, M.S., Robert J. Peterman, PhD, PE, B. Terry Beck, PhD, Chih-Hang John Wu, PhD, Proceedings of the 2014 Joint Rail Conference, JRC2014-3833, Copyright 2014 American Society of Mechanical Engineers.



## Bibliography

1. Abrishami, H. H. (1994) Studies on Bond and Cracking of Structural Concrete. Thesis from McGill University.
2. Abrishami, H.H. & Mitchell, D. (1992). Simulation of Uniform Bond Stress. *ACI Materials Journal*, March-April: 161-168.
3. Abrishami, H. H. & Mitchell, D. (1993). Bond Characteristics of Pretensioned Strand. *ACI Materials Journal*, May-June: 228-235.
4. Abrishami, H. H., & Mitchell, D. (1996). Analysis of Bond Stress Distributions in Pullout Specimens. *Journal of Structural Engineering*, 255-261.
5. Arnold, M. L., Peterman, R. J., Bodapati, N. B., Beck, B. T., & Wu, C.-H. J. (2013). Development of a standardized bond test for indented prestressing wires. Proceedings to Joint Rail Conference.
6. ASTM C39 Standard Test Method for Compressive Strength of Cylindrical Concrete Specimens, 2009.
7. ASTM C143 Standard Test Method for Slump of Hydraulic-Cement Concrete, 2009.
8. ASTM C192 Standard Practice for Making and Curing Concrete Test Specimens in the Laboratory, 2009.
9. ASTM C496 Standard Test Method for Splitting Tensile Strength of Cylindrical Concrete Specimens, 2009.

10. ASTM International Standard Specification for Steel Wire, Indented, Low-Relaxation for Prestressed Concrete Railroad Ties, 2010.
11. Barbosa, M.T.G., Filho, E.S.S., Oliveira, T.M., & Santos, W.J. (2008). Analysis of the Relative Rib Area of Reinforcing Bars Pull Out Tests. *Materials Research*, 453-457.
12. Bodapati, N.B., Peterman, R.J., Zhao, W., Beck, B. T., Wu, C.-H. J., Holste, J., & Arnold, M. (2013a). Transfer-length Measurements on Concrete Railroad ties Fabricated with 15 different Prestressing Reinforcements. Proceedings to PCI Conference.
13. Bodapati, N. B., Peterman, R. J., Zhao, W., Wu, C.-H. J., Beck, B. T., Haynes, M., & Holste, J. (2013b). Influence of Indented Wire Geometry and Concrete Parameters on the Transfer Length in Prestressed Concrete Crossties. 2013 Joint Rail Conference. Knoxville, TN: American Society of Mechanical Engineers.
14. Chanvillard, G. (1999). Modeling the pullout of wire-drawn steel fibers. *Cement and Concrete Research*, 1027-1037.
15. Chen, A. C. T. & Chen, W. F. (1976). Nonlinear analysis of concrete splitting tests. *Computer and Structures*, 451, 457.
16. Choi, O.C., Choi, H.J., & Hong, G.H. (2010). Bearing angle model for bond of reinforcing bars to concrete, *Fracture Mechanics of Concrete and Concrete Structures*, 807-810.
17. FEC's New Main-Track Design: Concrete Ties, Welded Rail. (1966). *Railway Track and Structures*, July: 25.

18. Filho, F. M. A., Debs, M.K.E., & Debs, A.L.H.C.E. (2008). Bond-slip behavior of self-compacting concrete and vibrated concrete using pull-out and beam tests. *Materials and Structures*, 1073-1089.
19. Galvez, J. C., Benitez, J. M., Casati, M. J., Tork, B. S., & Cendon, D. A. (2010). Cohesive-frictional model for bond and splitting action of prestressing wire. *International Journal for Numerical and Analytical Methods in Geomechanics*, 1257-1277.
20. Gambarova, P.G. & Rosati, G. (1996). Bond and splitting in reinforced concrete: test results on bar pull-out. *Materials and Structures*, 267-276.
21. Gambarova, P.G., Rosati, G.P., & Zasso, B. (1989a). Steel-to-concrete bond after concrete splitting: constitutive laws and interface deterioration. *Materials and Structures*, 347-356.
22. Gambarova, P.G., Rosati, G.P., & Zasso, B. (1989b). Steel-to-concrete bond after concrete splitting: test results. *Materials and Structures*, 35-47.
23. Garay, L. L. (1975) Mechanized Production of Railroad Track Ties made of Prestressed Concrete. *Revista IMCYC*, 11-24.
24. Gessner, S. & Hegger, J. (2012). Bond Behavior of Pretensioned Strands under Cyclic Loading. Proceedings to PCI Conference.
25. Hamad, B.S. (1995). Comparative Bond Strength of Coated and Uncoated Bars with Different Rib Geometries. *ACI Materials Journal*, 579-590.
26. Hanna, Amir. N. "Prestressed Concrete ties for North American Railroads." *PCI Journal*, Sept.-Oct. 1979: 32-61

27. Hanna A. N., (1981). Analyzing fastener performance in concrete ties. *Railway Track and Structures*, 30-34.
28. Hanna, A. N. (1986). Modern Track design for High-speed rail. *Railway Track and Structures*, March: 45-46.
29. Harris D. K, Lutch, R. H, Ahlborn, T. M., Duong, P. (2011). Optimization of a Prestressed Concrete Railroad Crosstie for Heavy-Haul Applications. *Journal of Transportation Engineering*, November: 815-822.
30. Haynes, M., Wu, C.-H. J., Beck, B. T., & Peterman, R. J. (2012). Non-contact measurement of Wire Indent Profiles on Prestressing Reinforcement Steel. Areama Conference.
31. Haynes, M., Wu, C.-H. J., Beck, B. T., & Peterman, R. J. (2013a). 3D Non-contact Profilometry for reinforcement Steel Quality Control. Proceedings to the Industrial and Systems Engineering Research Conference.
32. Haynes, M., Wu, C.-H. J., Beck, B. T., & Peterman, R. J. (2013b). Automated Real-Time Search and Analysis Algorithms for a Non-Contact 3D Profiling System. Proceedings of SPIE Conference.
33. Haynes, M., Wu, C.-H. J., Beck, B. T., Bodapati, N. B., & Peterman, R. J. (2013c). Prestressing steel reinforcement wire bond index number. Proceedings to Joint Rail Conference.
34. Inderwick, A.F. (1997). Performance of some Concrete Railway Cross Ties in North America.” *Concrete Precasting Plant and Technology*, 118-122.
35. Kaar, P. H. & Hanson, N. W. (1975). Bond fatigue tests of beams simulating pretensioned concrete crossties. *PCI Journal*, Sept.-Oct.: 65-80.

36. Lahnert, B.J., Houde, J., & Gerstle K. (1986). Direct measurement of slip between steel and concrete. *ACI Journal*, December: 974-982.
37. Liu, L. & Zhongqi, L. (2009). Experimental study on the transmission length of prestressed reinforcement with helical rib in concrete. *Zhengzhou da xue xue bao. Gong xue ban*, December: 11-14.
38. Magee, G. M. (1978). Prestressed concrete tie: The U.S. story from the beginning. *Railway Track and Structures*, August: 16-19.
39. Malvar, L.J. (1991). Bond of reinforcement under controlled confinement. Naval Civil Engineering Laboratory Technical Note.
40. Murphy, Robert L. (2012). Determining the Transfer Length in Prestressed Concrete Railroad Ties Produced in the United States. Master thesis, Kansas State University, Manhattan, Kansas, USA.
41. Nie, W. (1979). A new method for the measurement of local slip between steel and concrete. Ph.D dissertation, Technische Hochschule, Darmstadt.
42. Oh, B.H., Kim, E.S., & Choi, Y.C. (2006). Theoretical analysis of transfer lengths in pretensioned prestressed concrete members. *ASCE Journal of Engineering Mechanics*, 1057-1066.
43. Quihua, J., Min, D., & Sufen, H. (1996). Investigation of Deteriorated Concrete Railway ties. *Cement and Concrete Research*, 999-1006.
44. Rao, A. G. M., Parameswaran, V.S., & Murthy, D.S.R. (1984). Prestressed concrete railroad ties. *Concrete International*, September: 42-50.

45. Rao, P.S., Kalyanasundaram, P., & Sharief, M.F. (1977). Transmission length of ribbed bars in pre-tensioned concrete. *Indian Concrete Journal*, May: 149-159.
46. Rose, D. R. & Russell, B. W. (1995). Measurement of bond performance; correlation of pullout strength with transfer length. Proceedings of Structure Congress, 1474-1477.
47. Rose, D.R., & Russell, B.W. (1997). "Investigation of Standardized Tests to Measure the Bond Performance of Prestressing Strand." *PCI Journal*, 56-80.
48. Vecchio, F. J. & DeRoo, A. (1995). Smeared-Crack modeling of concrete tension splitting. *Journal of Engineering Mechanics*, June: 702-708.
49. Weber, J. W. (1969). Concrete Crossties in the United States. *PCI Journal*, V. 14, No. 1 February: 46-61.
50. Yu, H., Jeong, D., Choros, J., & Sussmann, T. (2011). Finite Element modeling of prestressed concrete crossties with ballast and subgrade support. Proceeding to the International Design Engineering Technical Conference.
51. Yuan. L., Zhou, L., Lau, K.T., Jin, W., & Demokan, M.S. (2002). Fiber optic extensometer for concrete deformation measurements. *Review of Scientific Instruments*, 2469-2474.
52. Zhao, W., B.T. Beck, Peterman, R.J., Murphy, R., Wu, C.-H. J., Lee, G. (2013a). A Direct Comparison of the Traditional Method and a New Approach in Determining 220 Transfer Lengths in Prestressed Concrete Railroad Ties. Proc. 2013 Joint Rail Conference. Paper Reference #JRC2013-2469. Knoxville, TN.

53. Zhao, W., B.T. Beck, Peterman, R.J., Wu, C.-H. J. (2013b). Development of a 5-Camera transfer length measurement system for real time monitoring of railroad crosstie production. Proceedings to the Joint Rail Conference.

## Appendix A Confinement and Cover Additional Tests

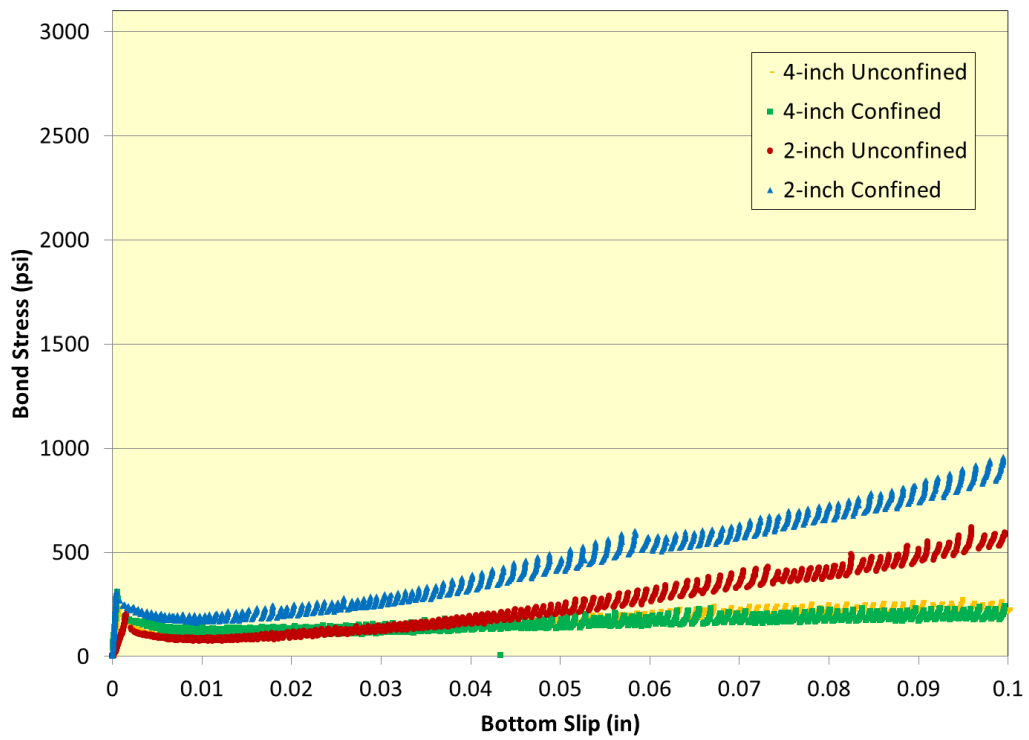


Figure A.1 Confined and unconfined bond stress versus slip relationship for WA



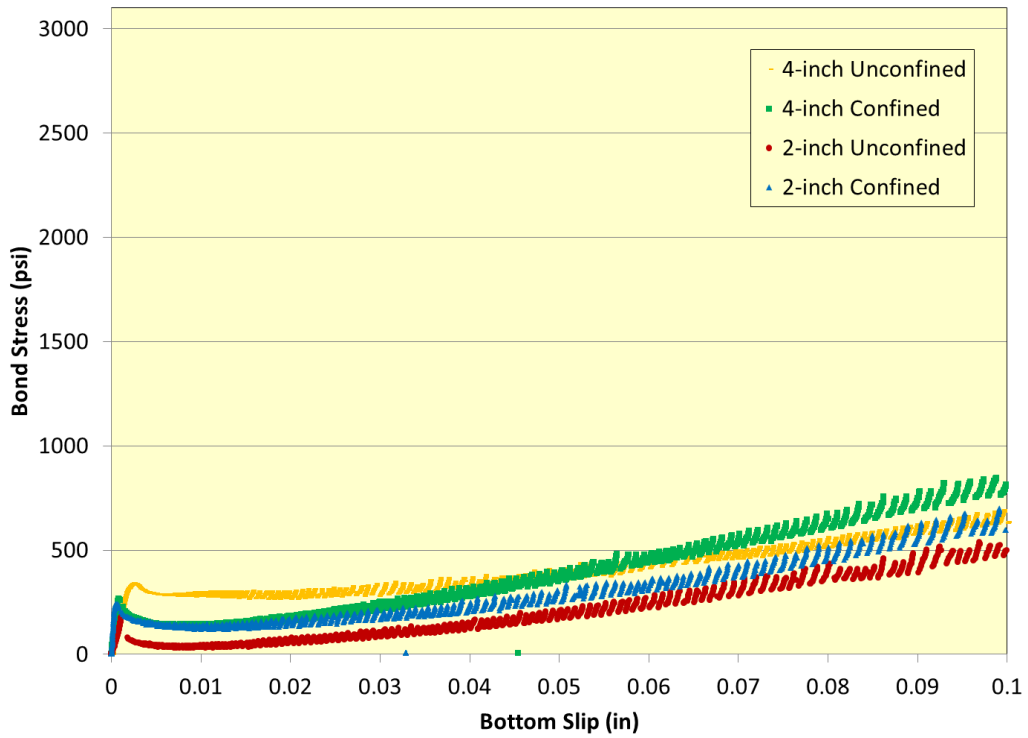


Figure A.2 Confined and unconfined bond stress versus slip relationship for WA

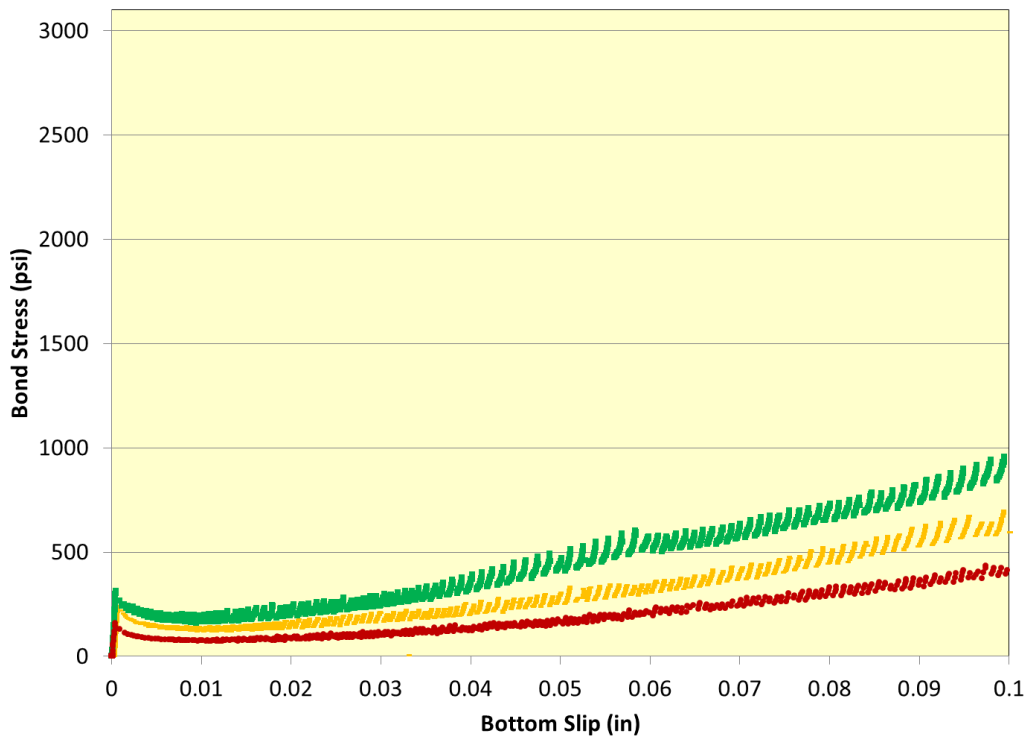
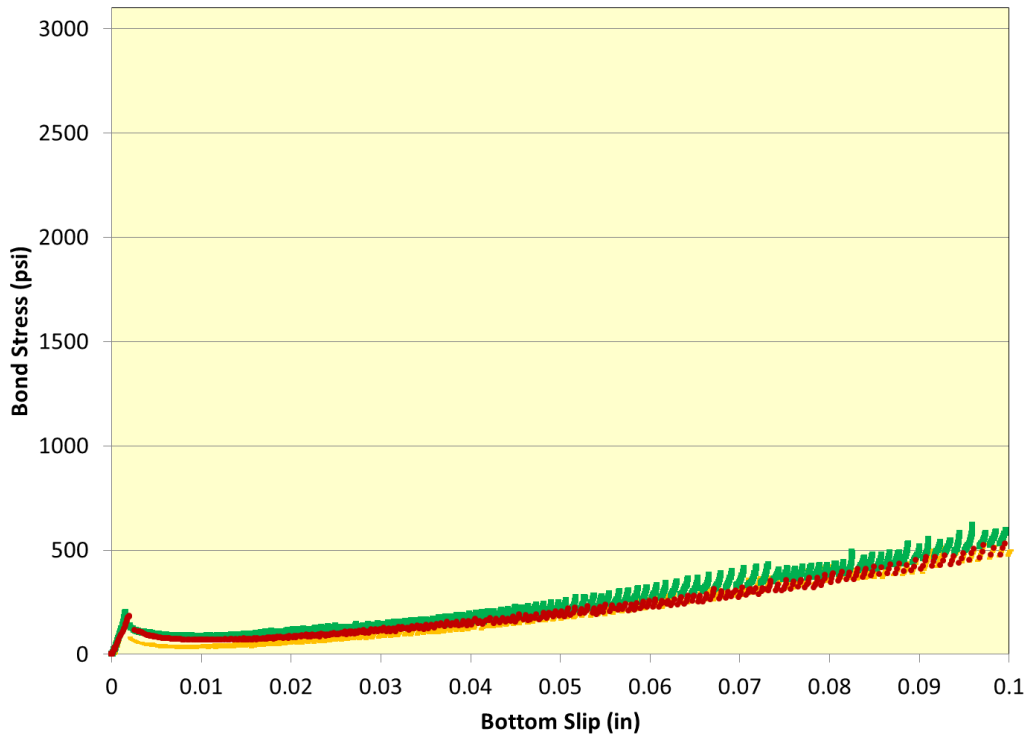
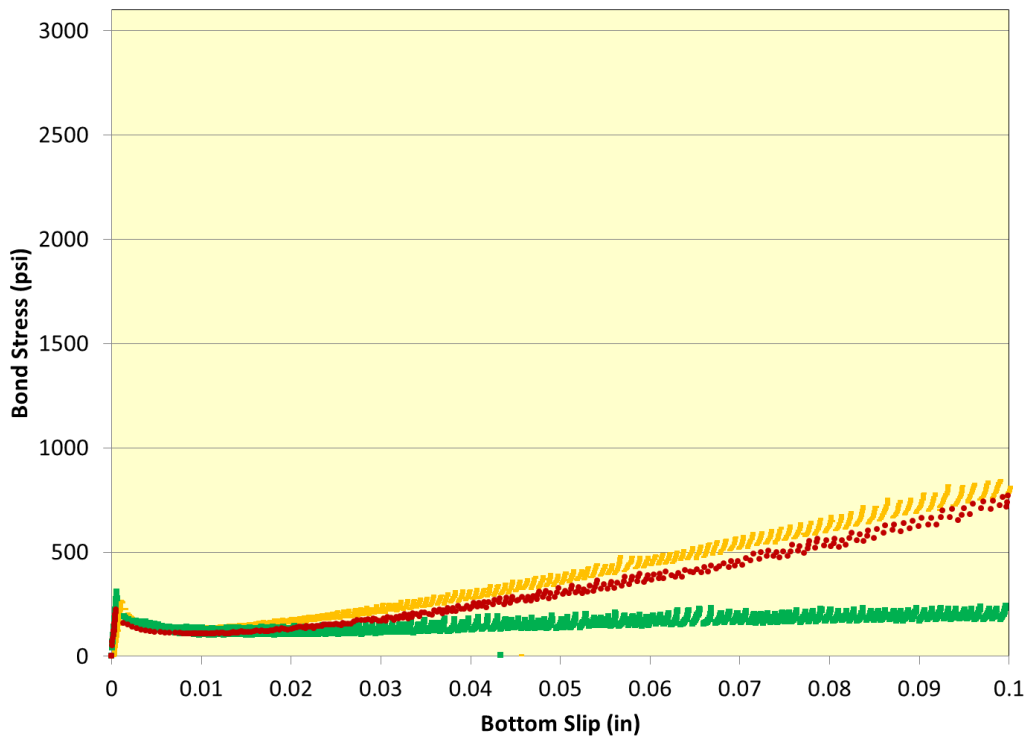


Figure A.3 Bond stress versus slip relationship of confined 2-inch diameter for WA



**Figure A.4 Bond stress versus slip relationship of unconfined 2-inch diameter for WA**



**Figure A.5 Bond stress versus slip relationship of confined 4-inch diameter for WA**

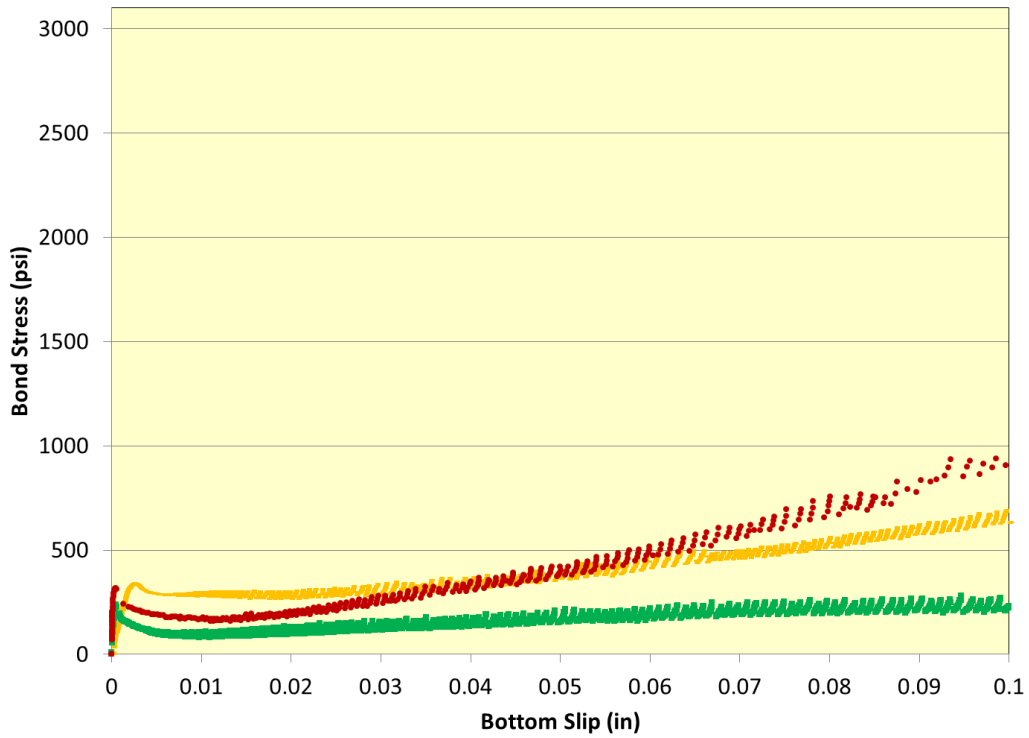


Figure A.6 Bond stress versus slip relationship of unconfined 4-inch diameter for WA

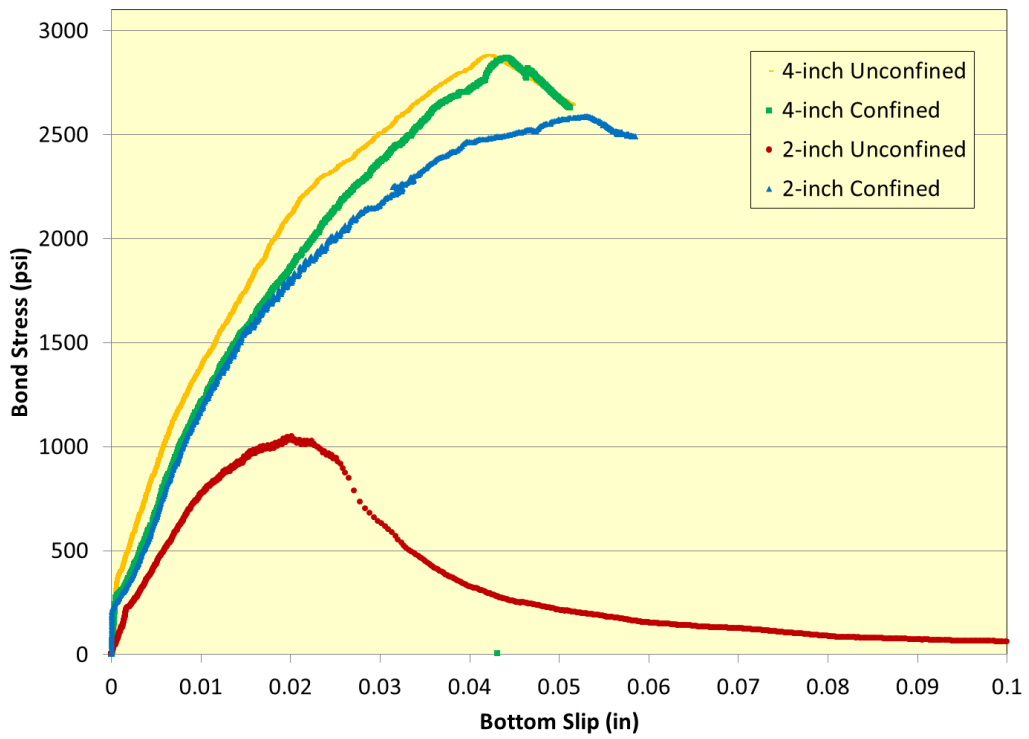
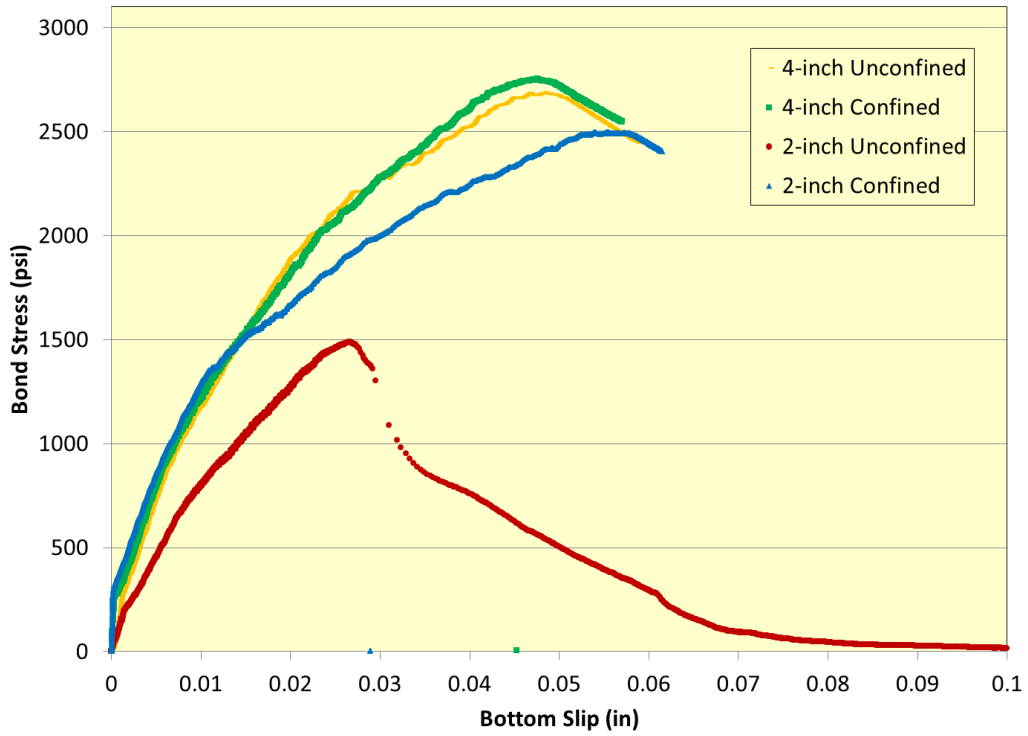
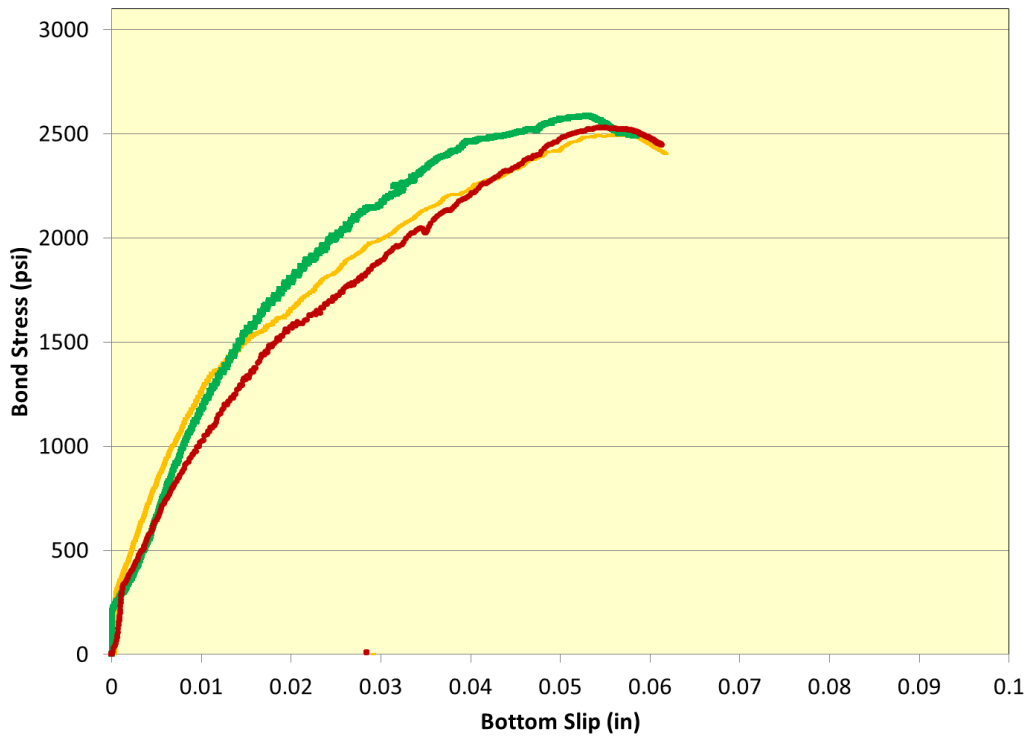


Figure A.7 Confined and unconfined bond stress versus slip relationship for WE



**Figure A.8 Confined and unconfined bond stress versus slip relationship for WE**



**Figure A.9 Bond stress versus slip relationship of confined 2-inch diameter for WE**

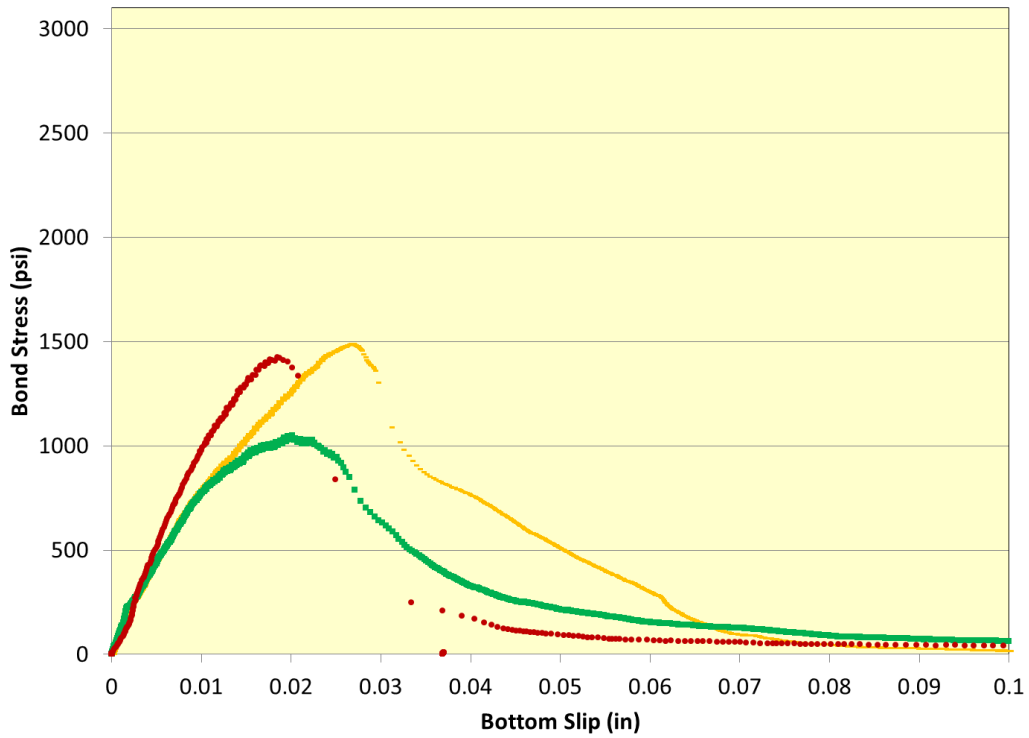


**Figure A.10 Bond stress versus slip relationship of unconfined 2-inch diameter for WE**

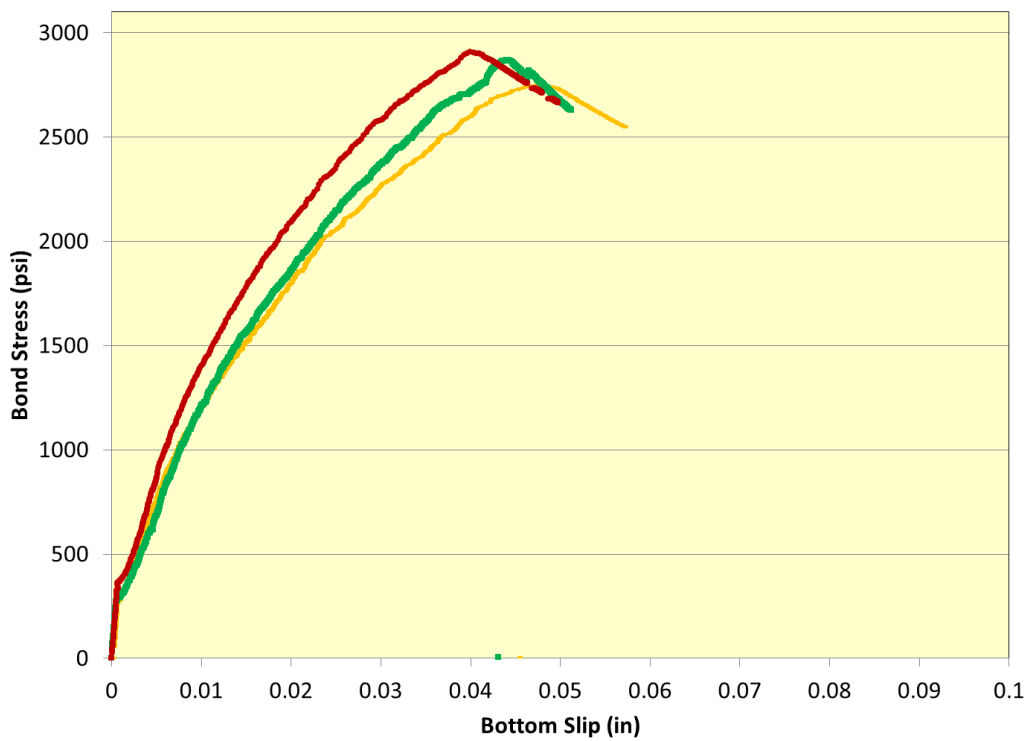


**Figure A.11 Bond stress versus slip relationship of confined 4-inch diameter for WE**

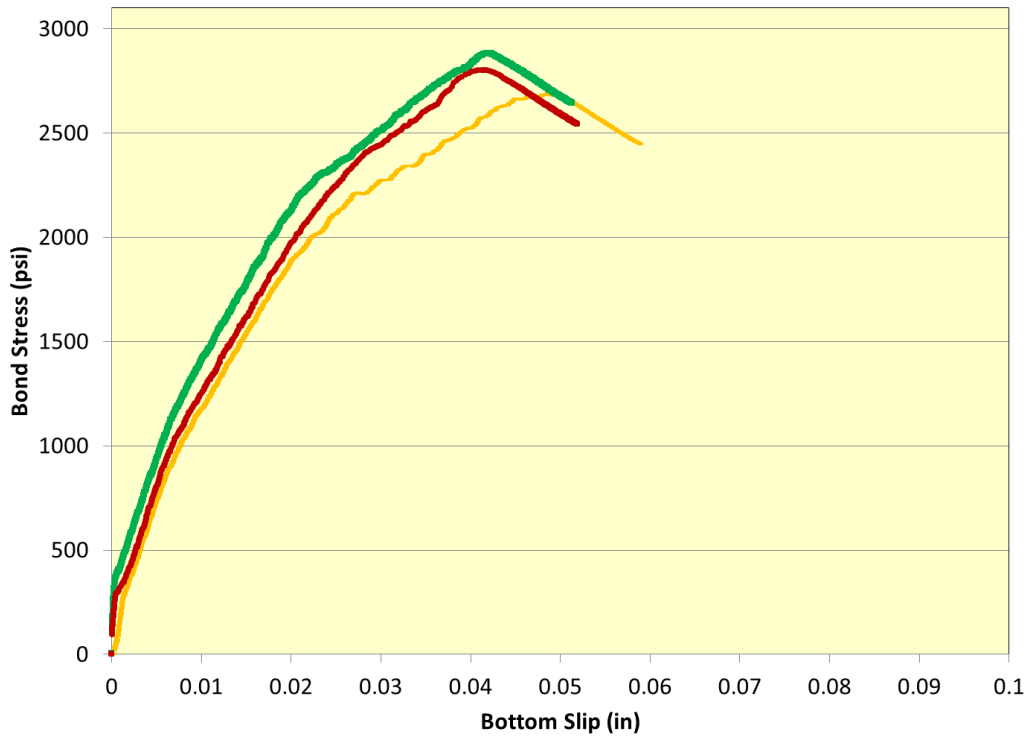


Figure A.12 Bond stress versus slip relationship of unconfined 4-inch diameter for WE

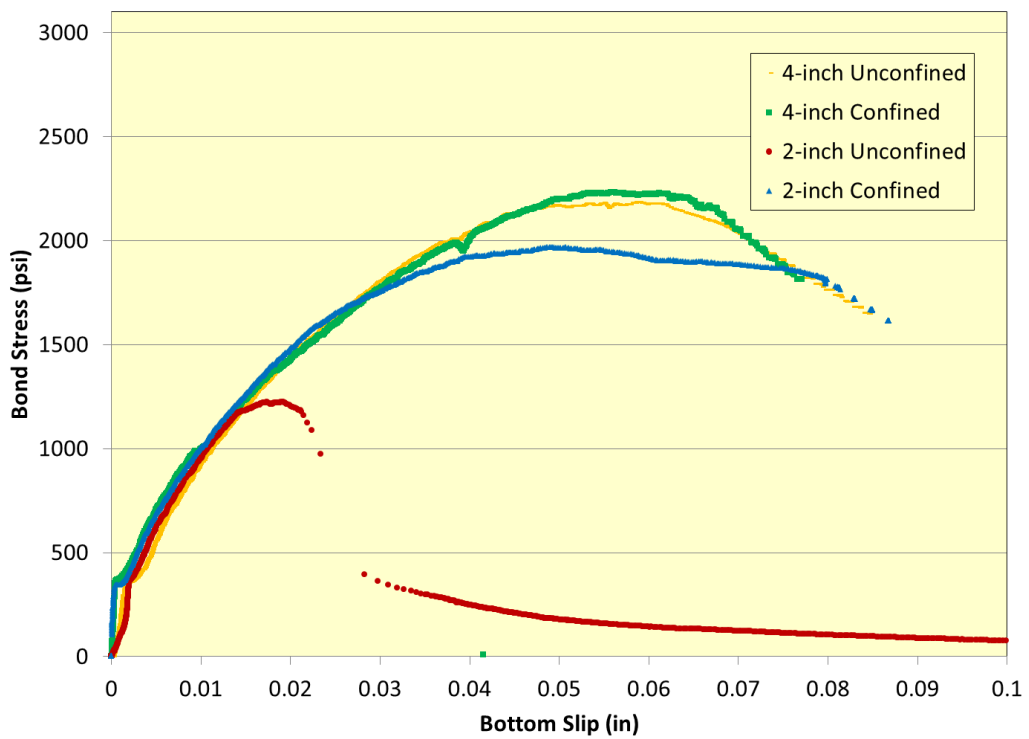


Figure A.13 Confined and unconfined bond stress versus slip relationship for WG (5,500 psi)

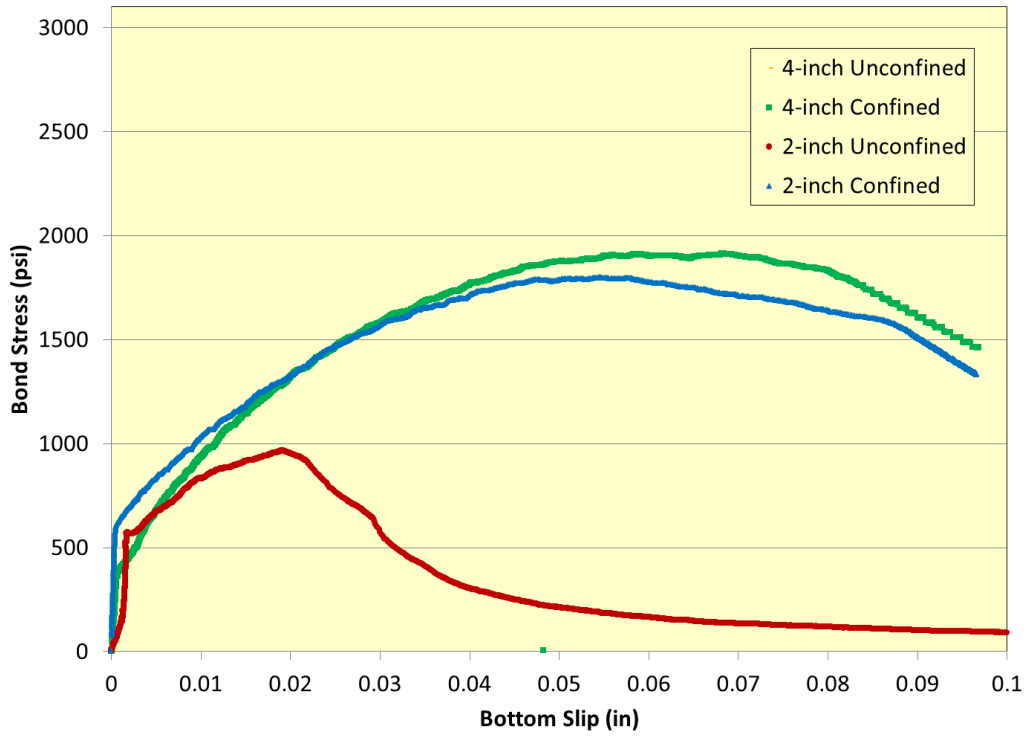


Figure A.14 Confined and unconfined bond stress versus slip relationship for WG

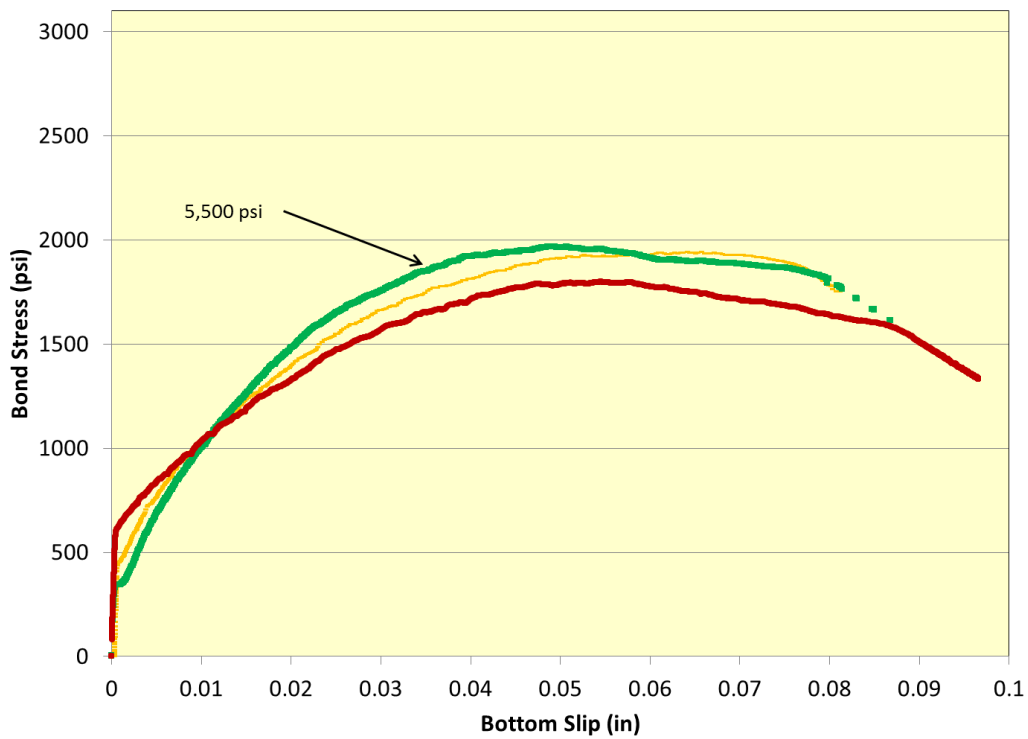
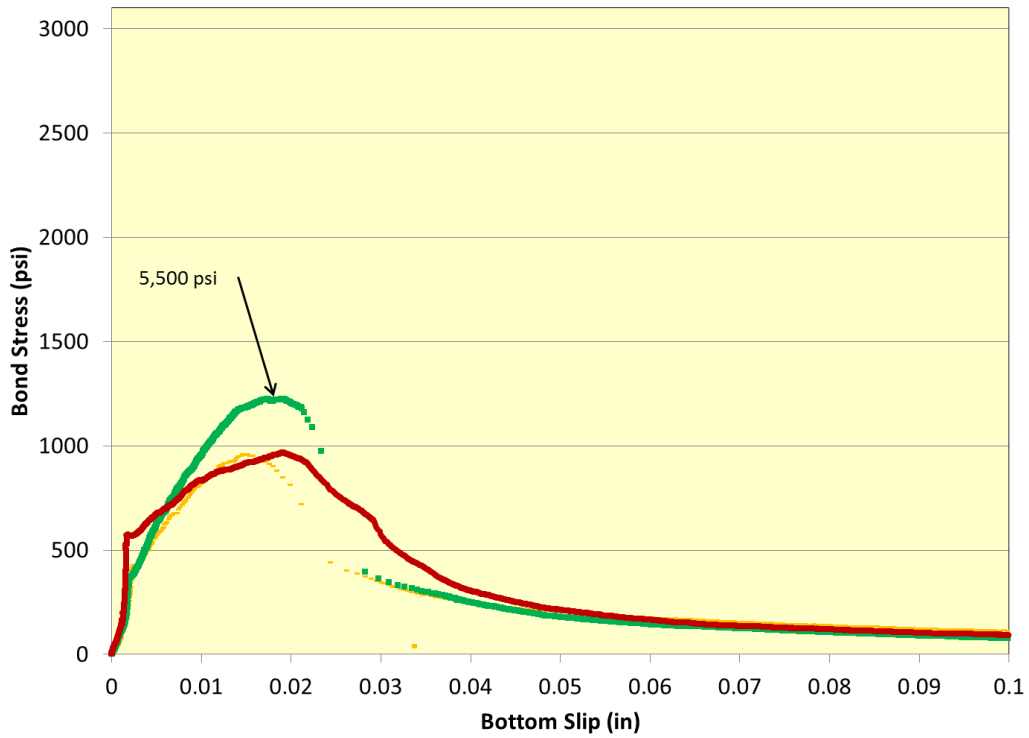
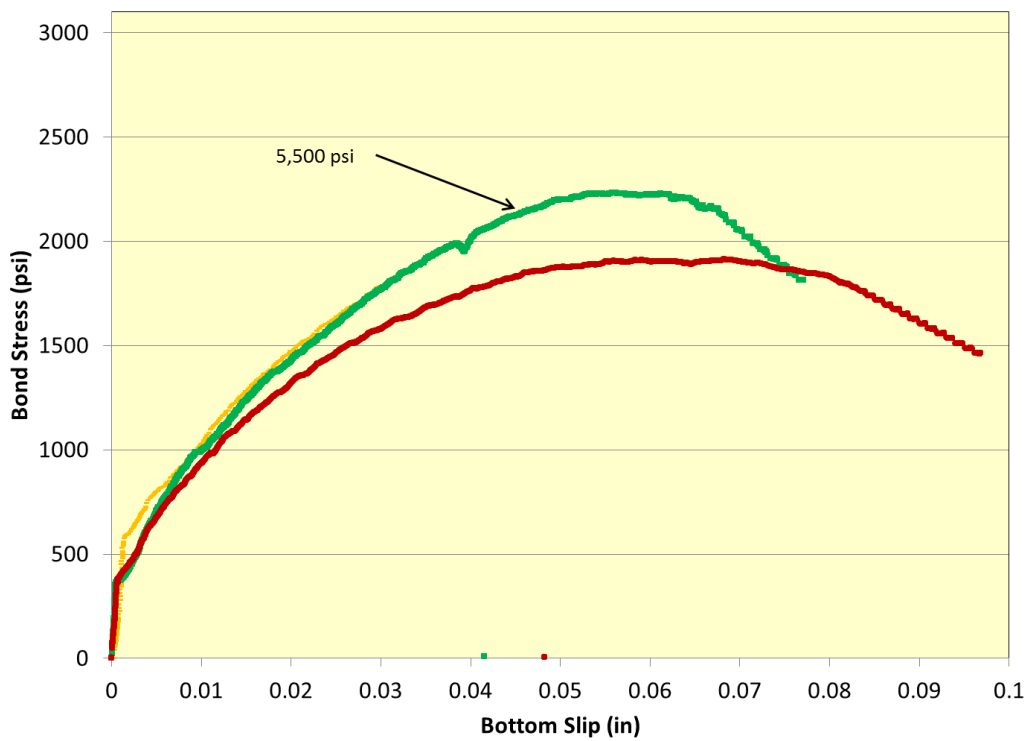


Figure A.15 Bond stress versus slip relationship of confined 2-inch diameter for WG



**Figure A.16 Bond stress versus slip relationship of unconfined 2-inch diameter for WG**



**Figure A.17 Bond stress versus slip relationship of confined 4-inch diameter for WG**



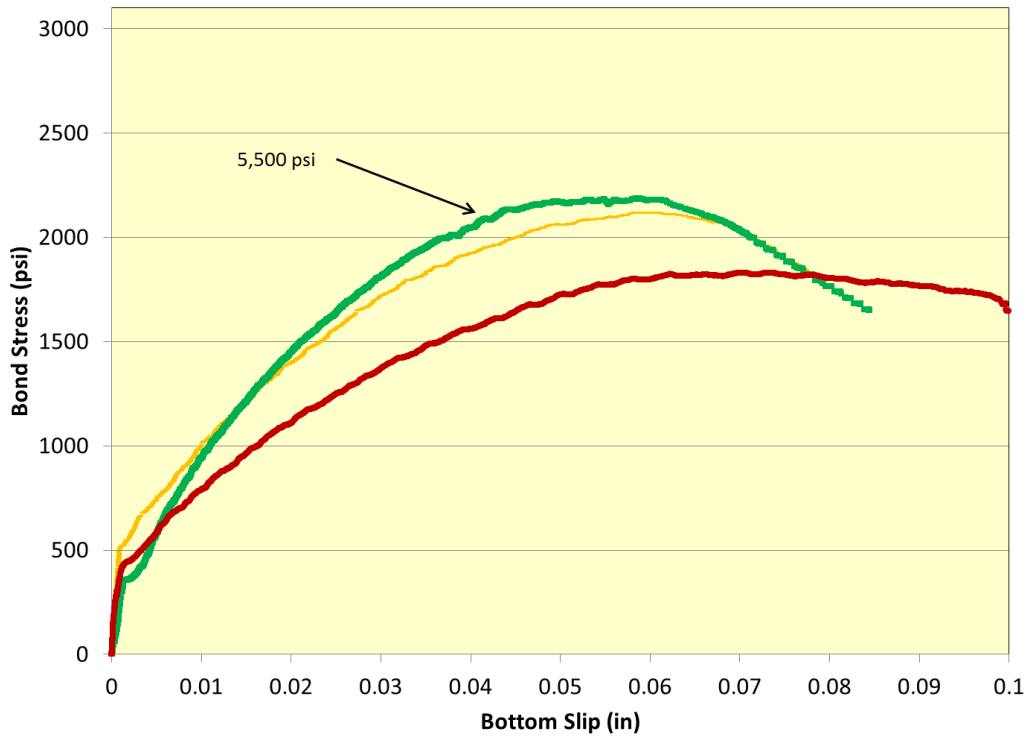


Figure A.18 Bond stress versus slip relationship of unconfined 4-inch diameter for WG

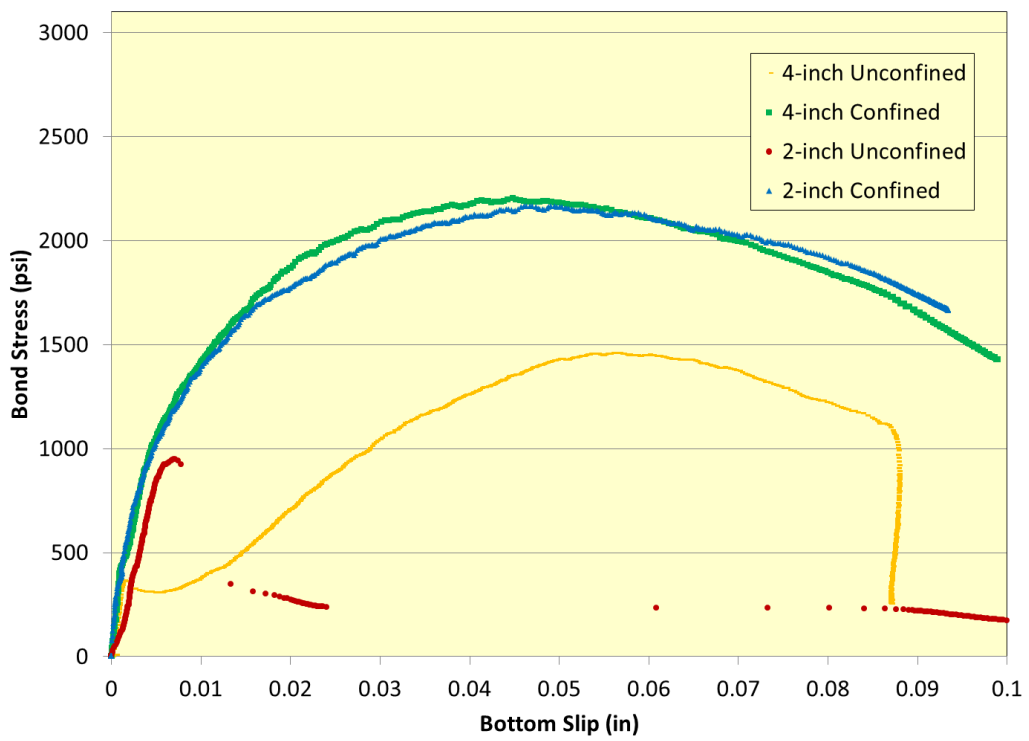


Figure A.19 Confined and unconfined bond stress versus slip relationship for WH

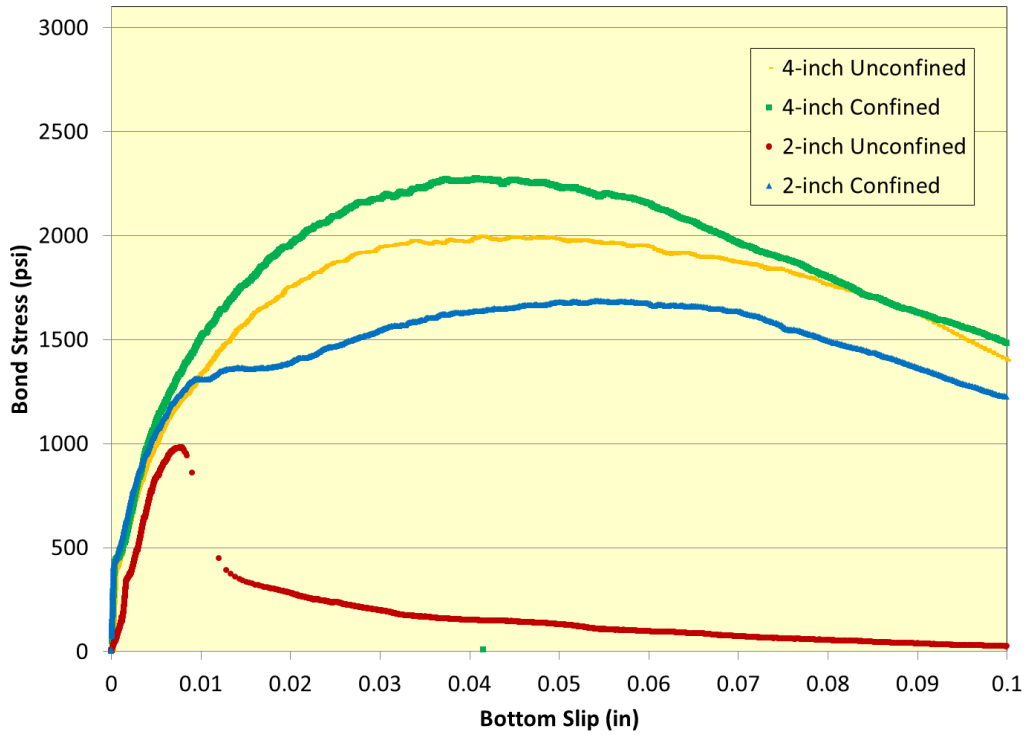


Figure A.20 Confined and unconfined bond stress versus slip relationship for WH

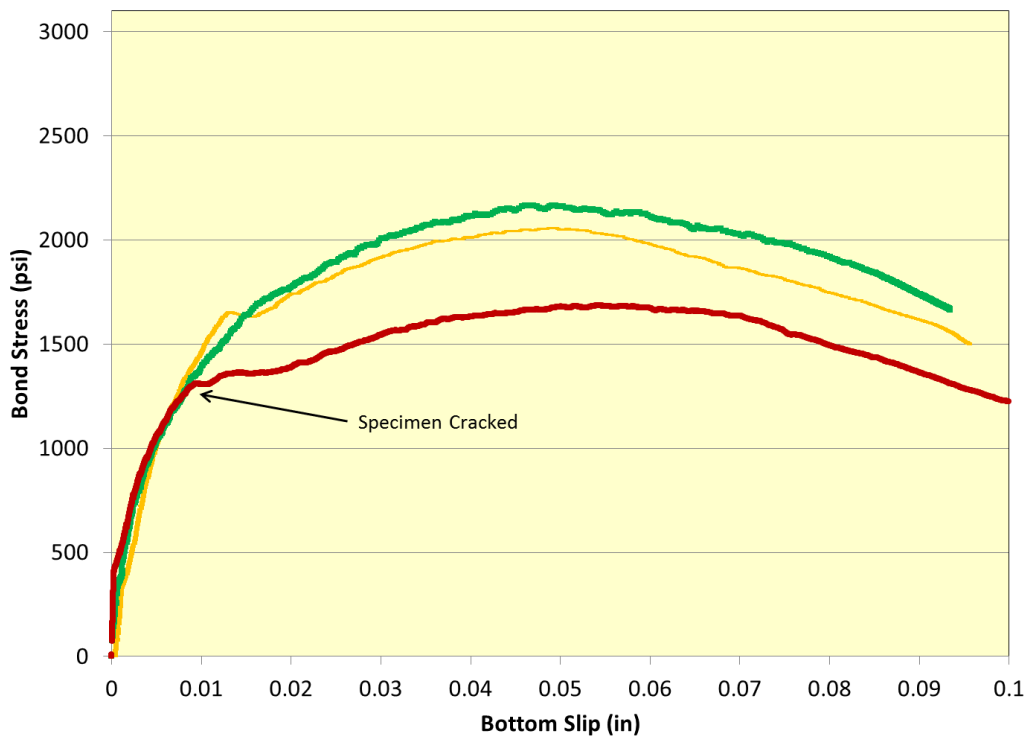


Figure A.21 Bond stress versus slip relationship of confined 2-inch diameter for WH

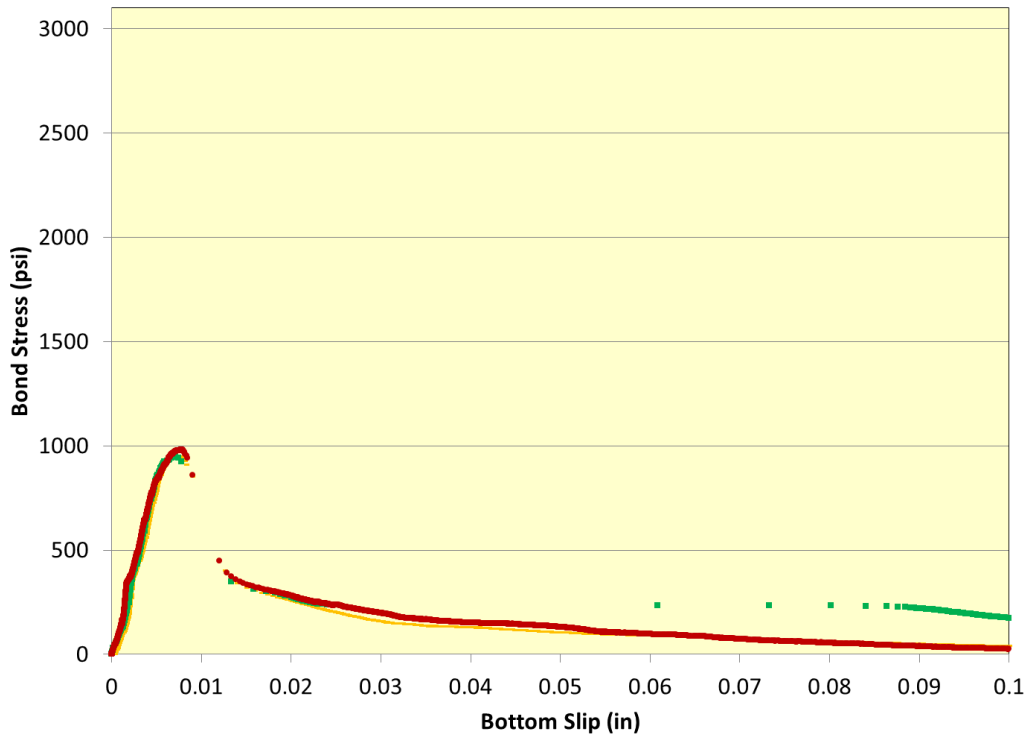


Figure A.22 Bond stress versus slip relationship of unconfined 2-inch diameter for WH

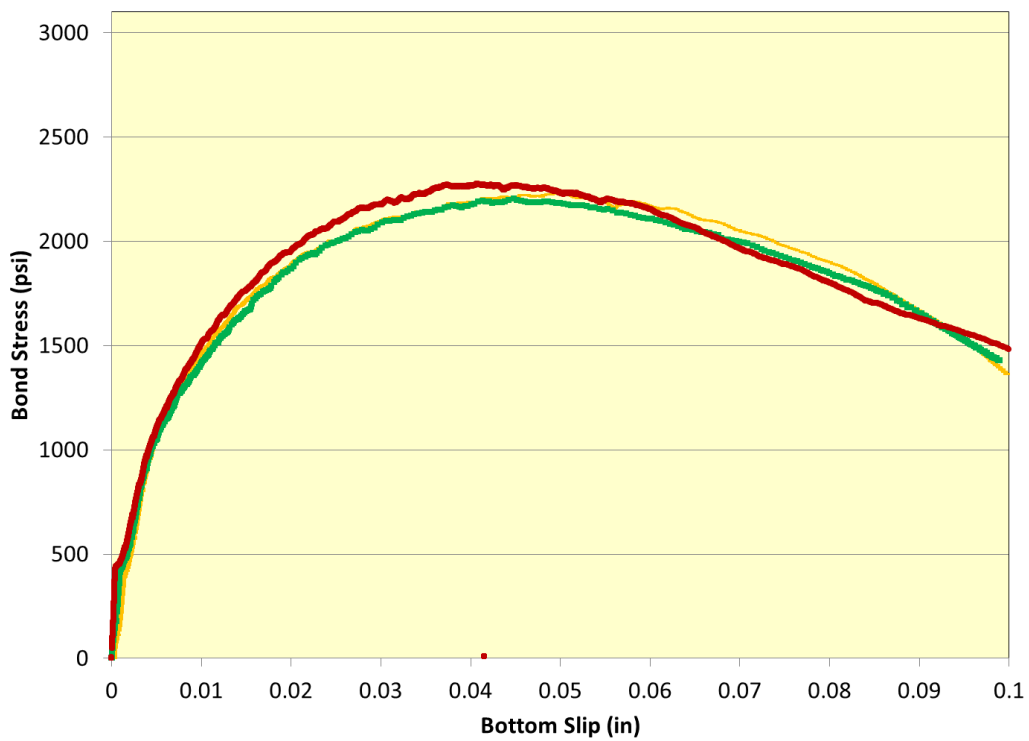


Figure A.23 Bond stress versus slip relationship of confined 4-inch diameter for WH

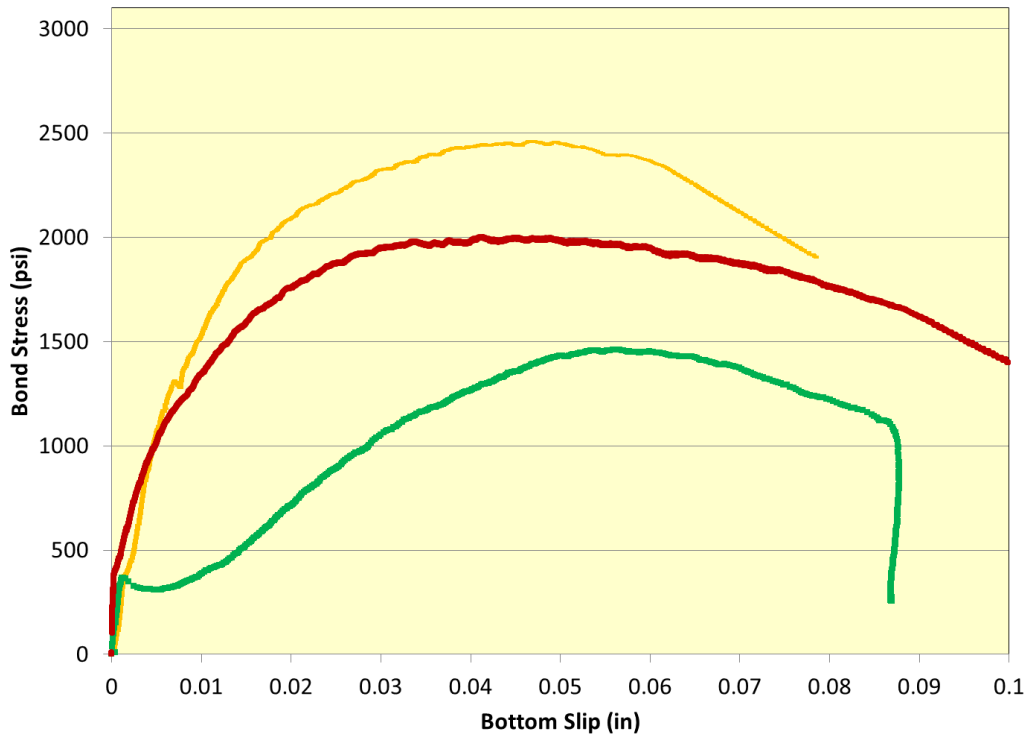


Figure A.24 Bond stress versus slip relationship of unconfined 4-inch diameter for WH

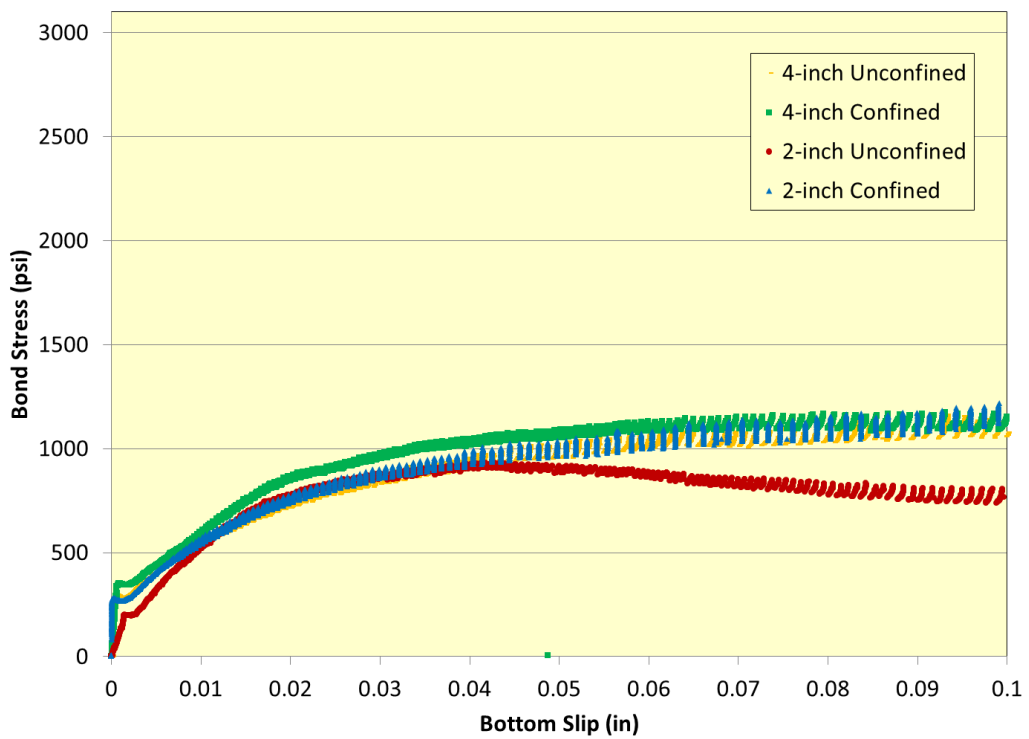


Figure A.25 Confined and unconfined bond stress versus slip relationship for WK

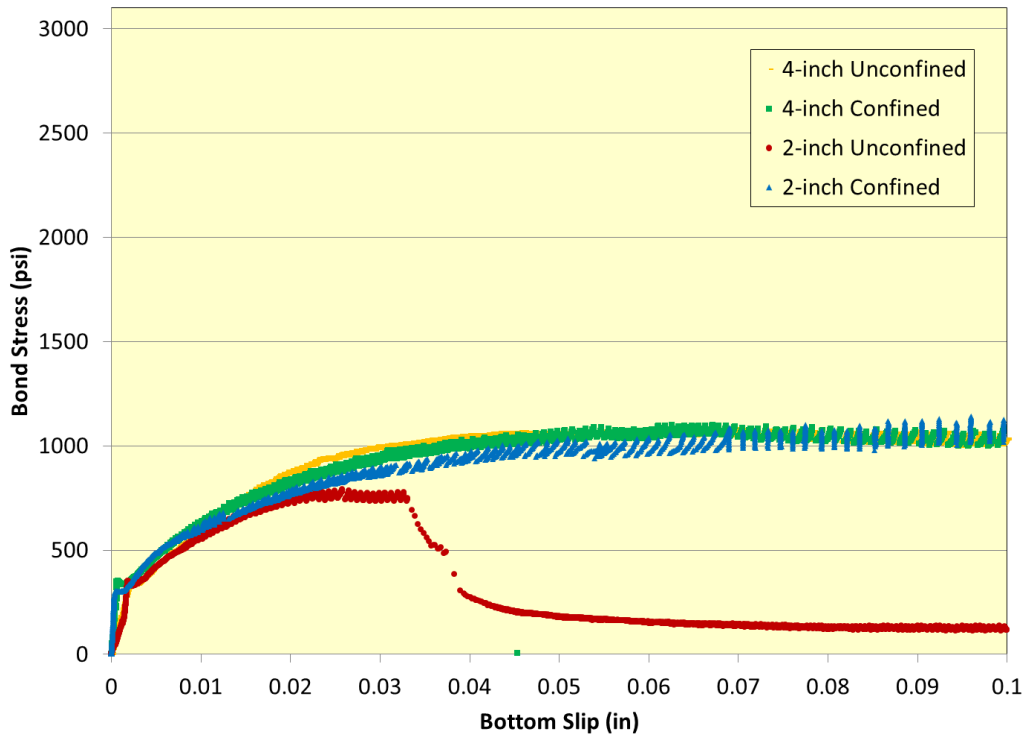


Figure A.26 Confined and unconfined bond stress versus slip relationship for WK

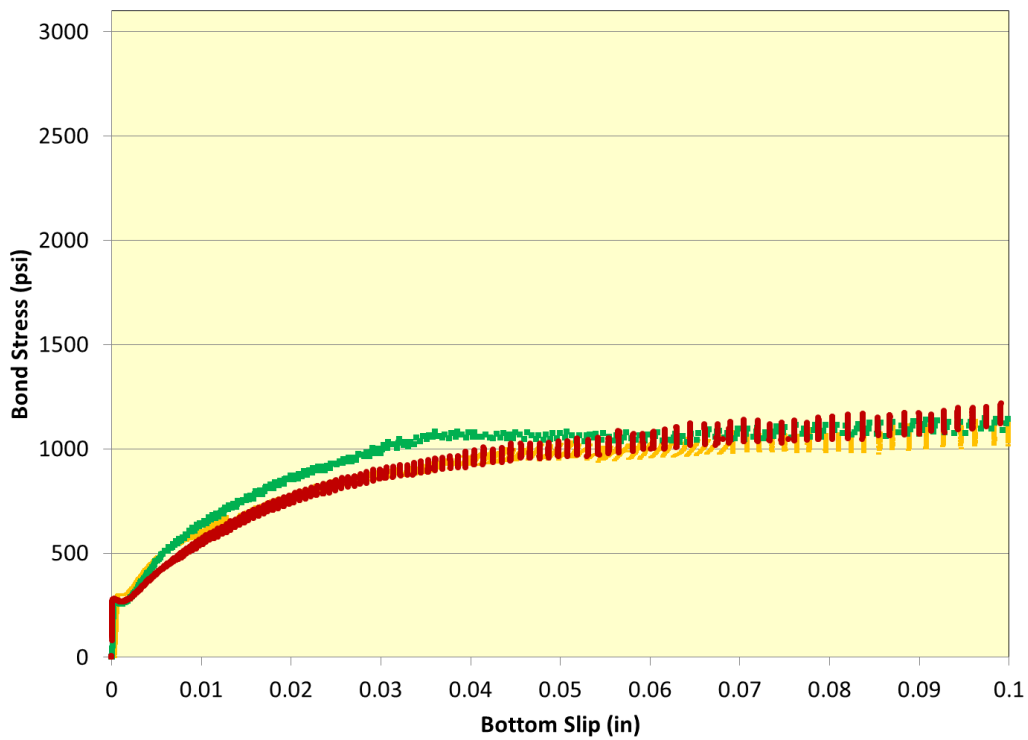


Figure A.27 Bond stress versus slip relationship of confined 2-inch diameter for WK

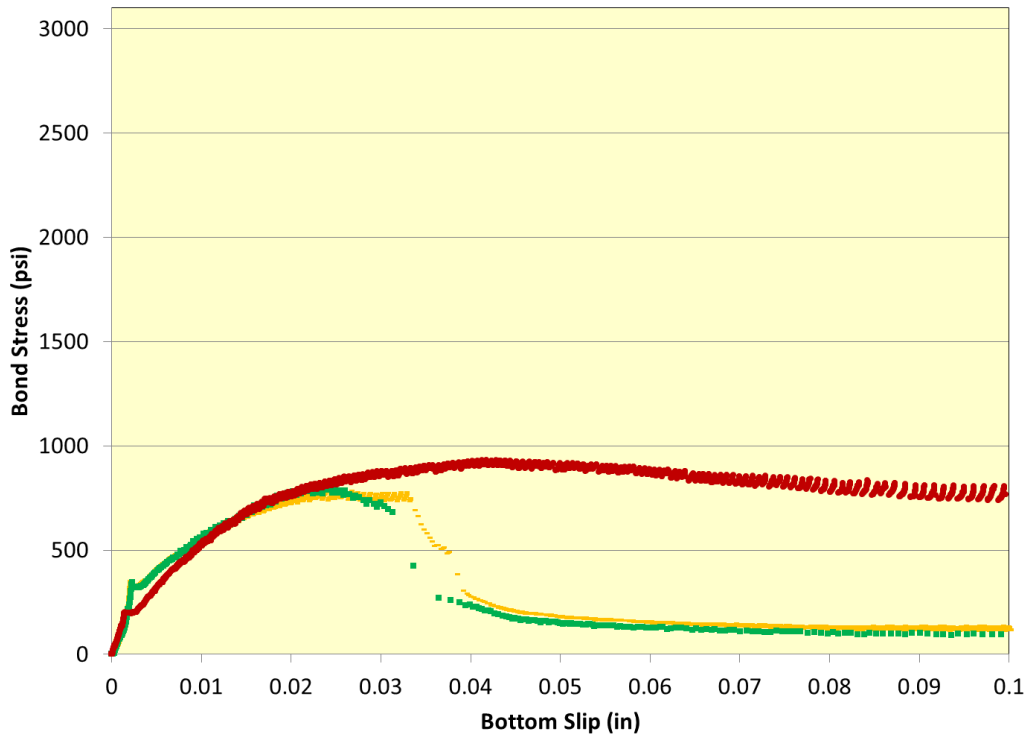


Figure A.28 Bond stress versus slip relationship of unconfined 2-inch diameter for WK

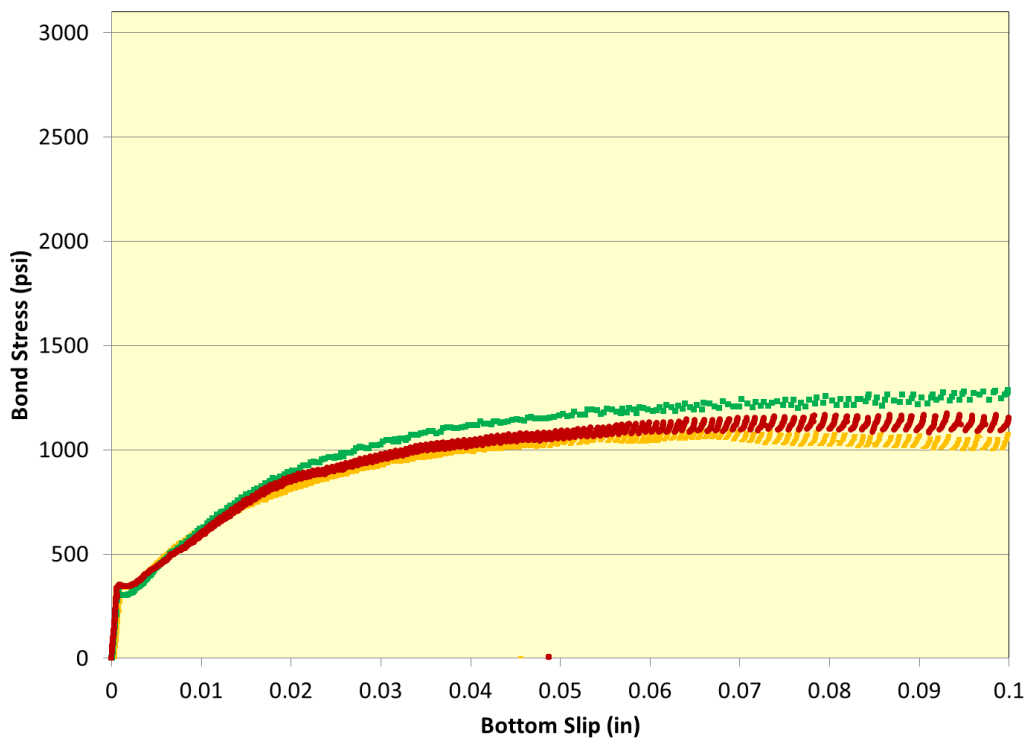
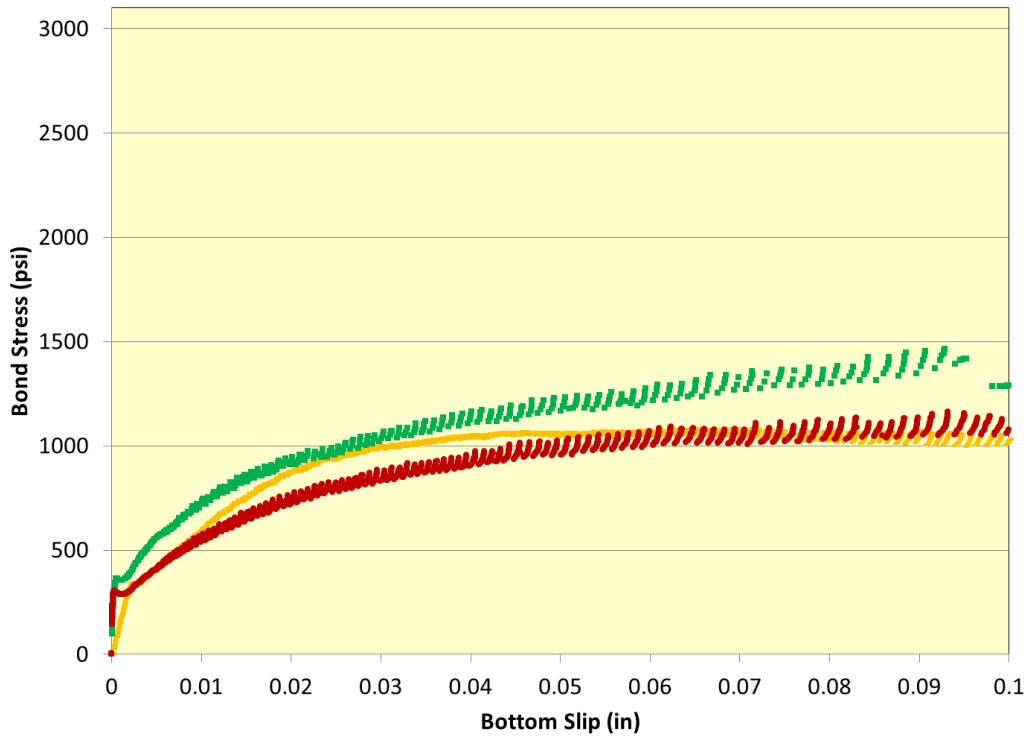


Figure A.29 Bond stress versus slip relationship of confined 4-inch diameter for WK



**Figure A.30 Bond stress versus slip relationship of unconfined 4-inch diameter for WK**

## Appendix B 2-inch Diameter Cylinder Results

Portions of this chapter were originally published here:

Tensioned Pullout Test Used To Investigate Wire Splitting Propensity in Concrete Railroad Ties, by Joseph R. Holste, M.S., Mark Haynes, M.S., Robert J. Peterman, PhD, PE, B. Terry Beck, PhD, Chih-Hang John Wu, PhD, Proceedings of the 2014 Joint Rail Conference, JRC2014-3833, Copyright 2014 American Society of Mechanical Engineers.

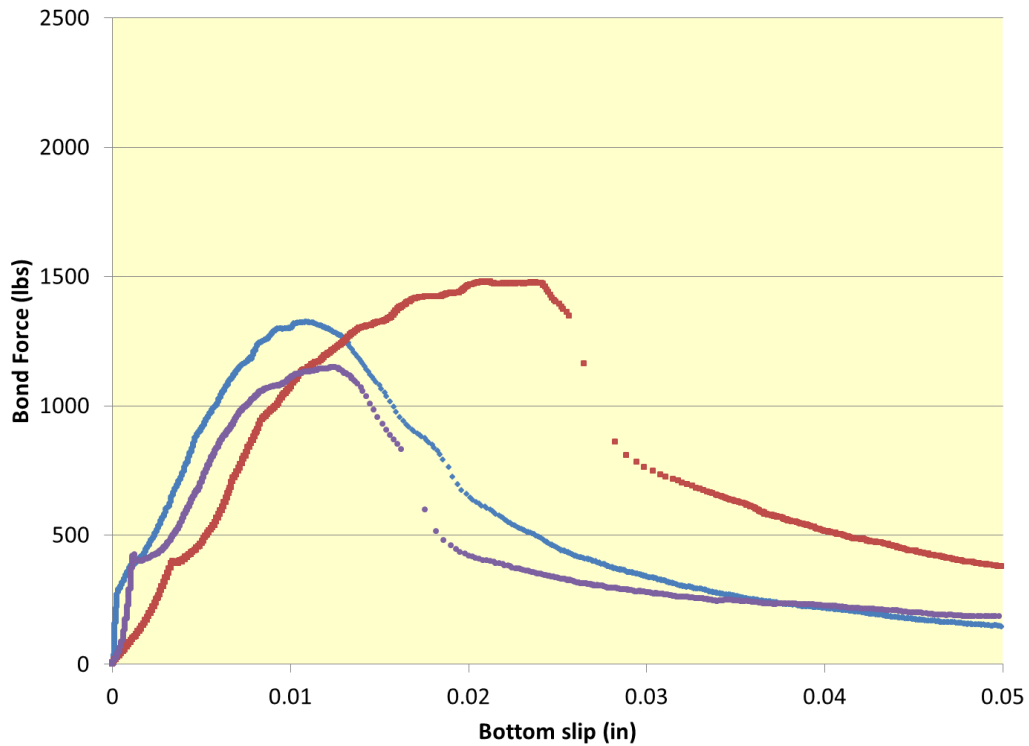
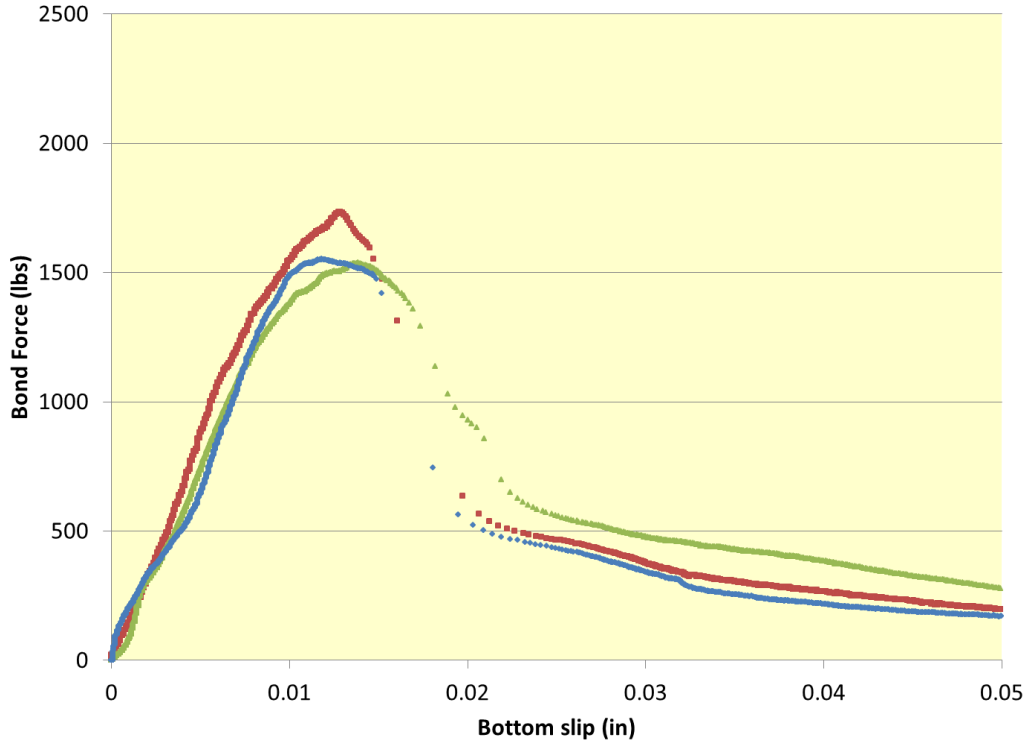
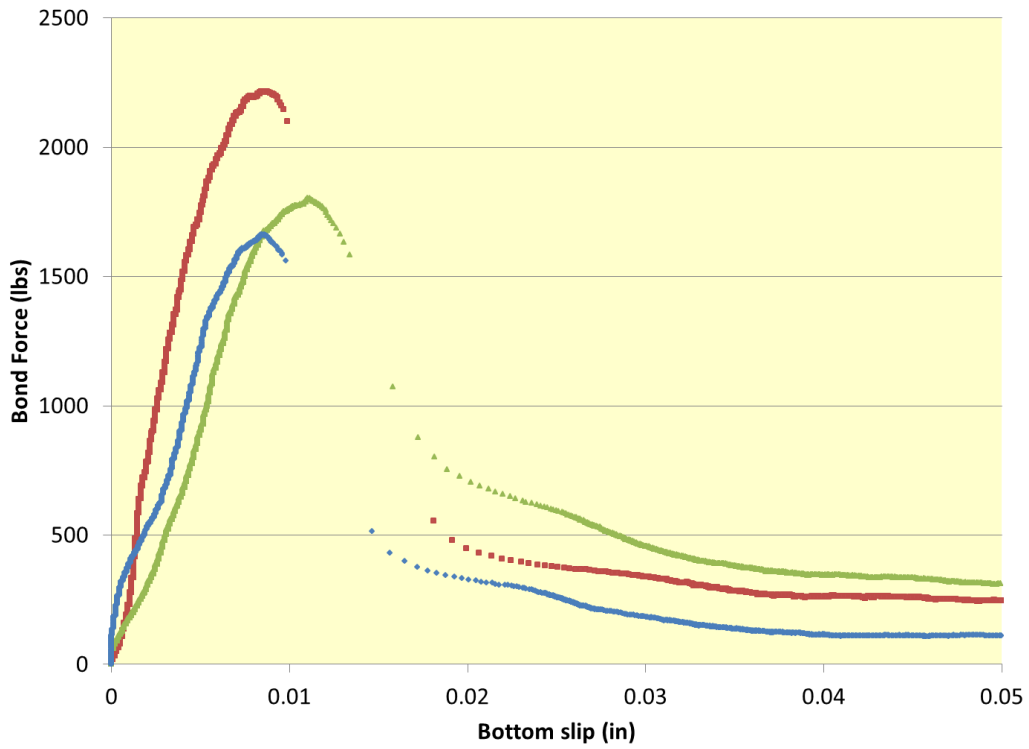


Figure B.1 Bond stress versus slip relationship of 2-inch diameter specimen for WB





**Figure B.2 Bond stress versus slip relationship of 2-inch diameter specimen for WD**



**Figure B.3 Bond stress versus slip relationship of 2-inch diameter specimen for WF**

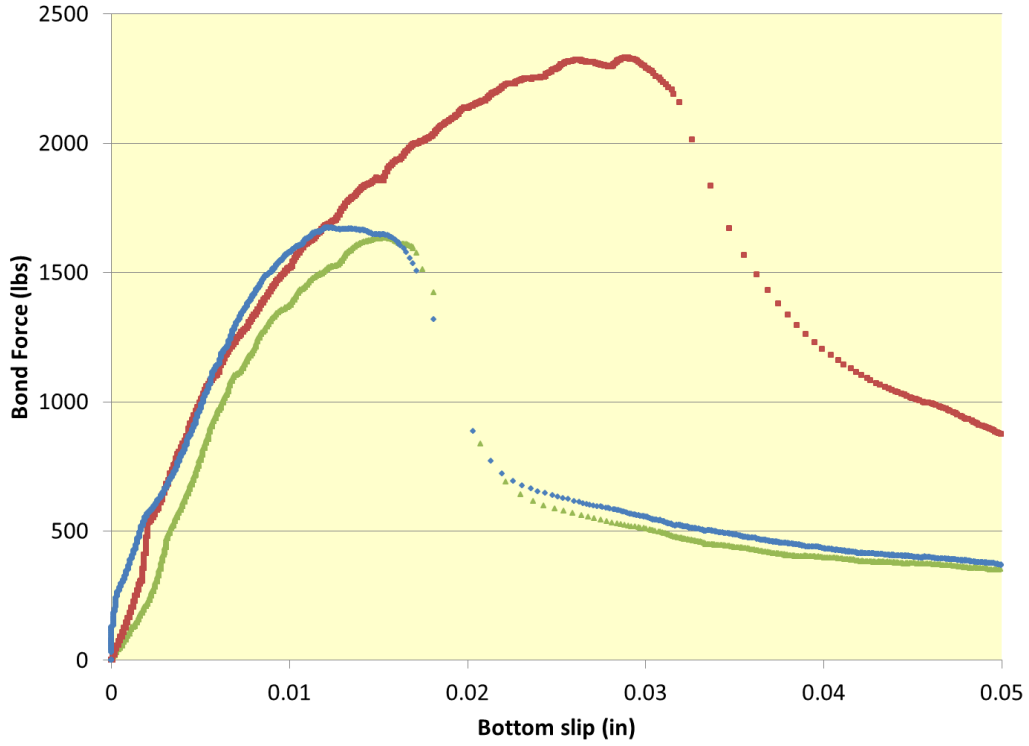


**Figure B.4 Bond stress versus slip relationship of 2-inch diameter specimen for WI**

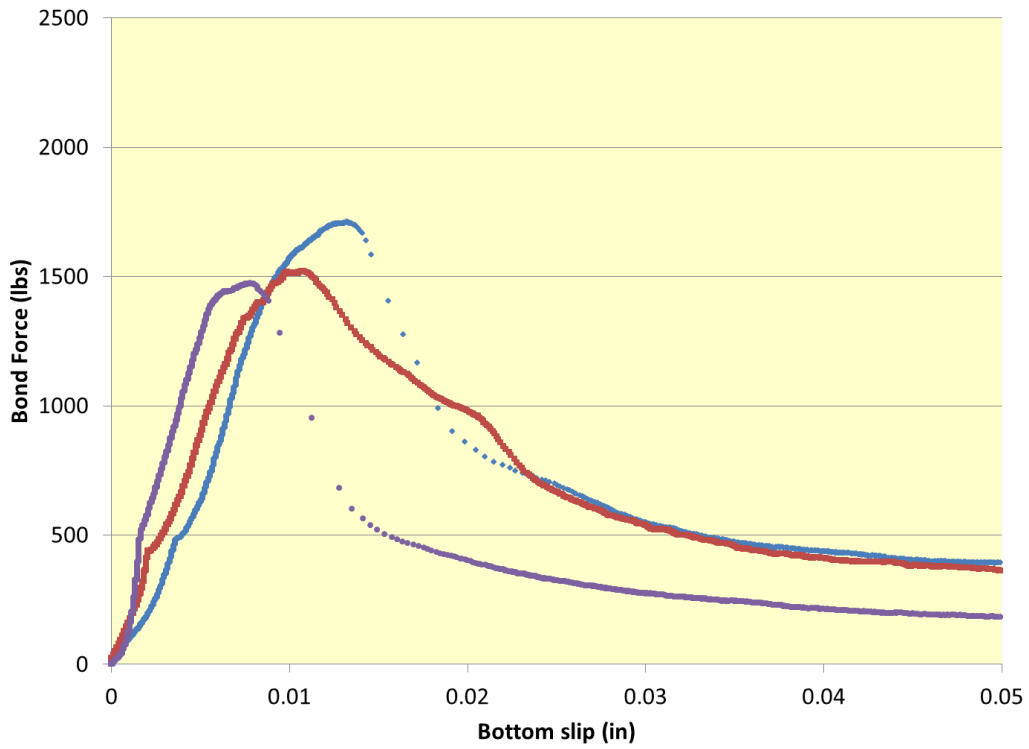


**Figure B.5 Bond stress versus slip relationship of 2-inch diameter specimen for WJ**

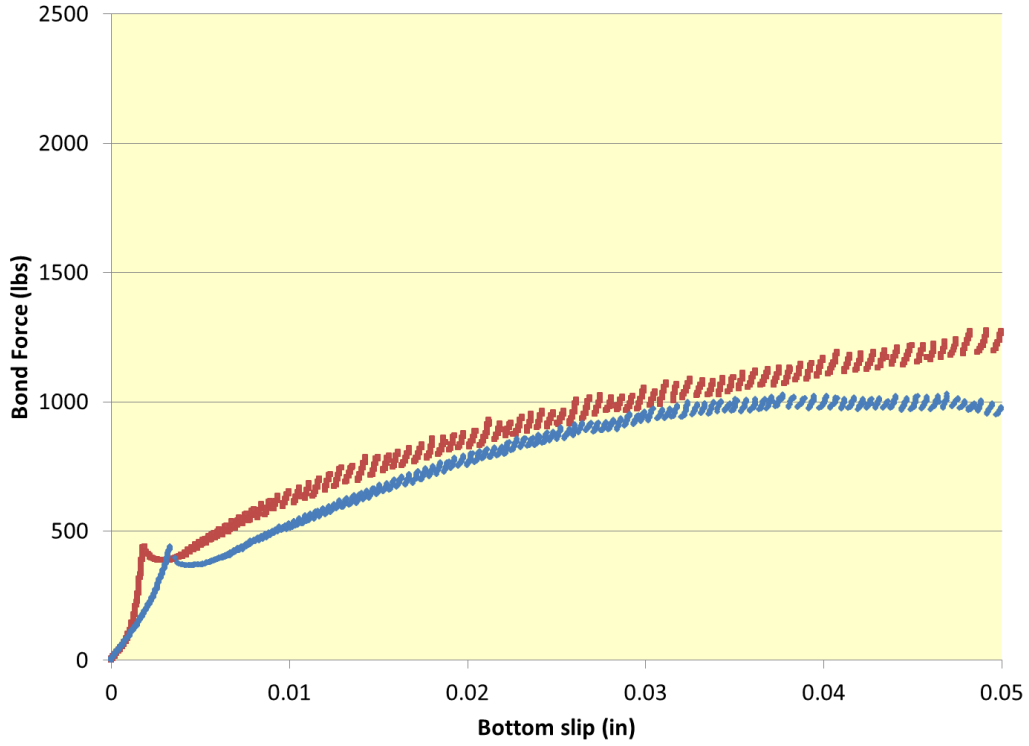


**Figure B.6 Bond stress versus slip relationship of 2-inch diameter specimen for WL**

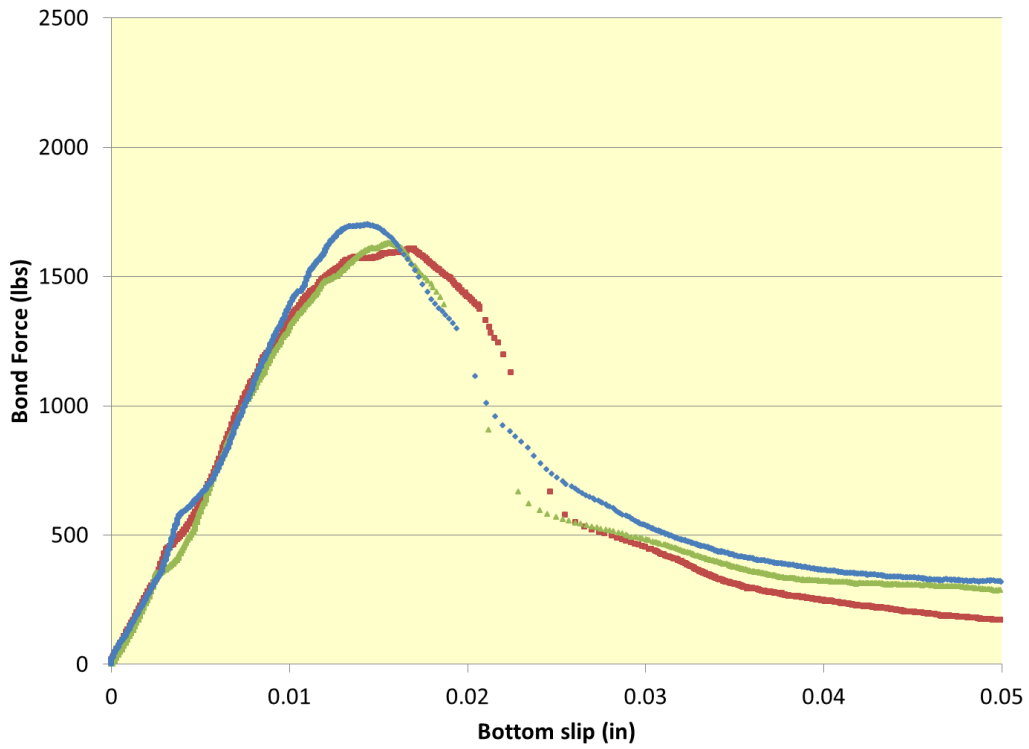


**Figure B.7 Bond stress versus slip relationship of 2-inch diameter specimen for WM**

## Appendix C VWSG Test Graphs

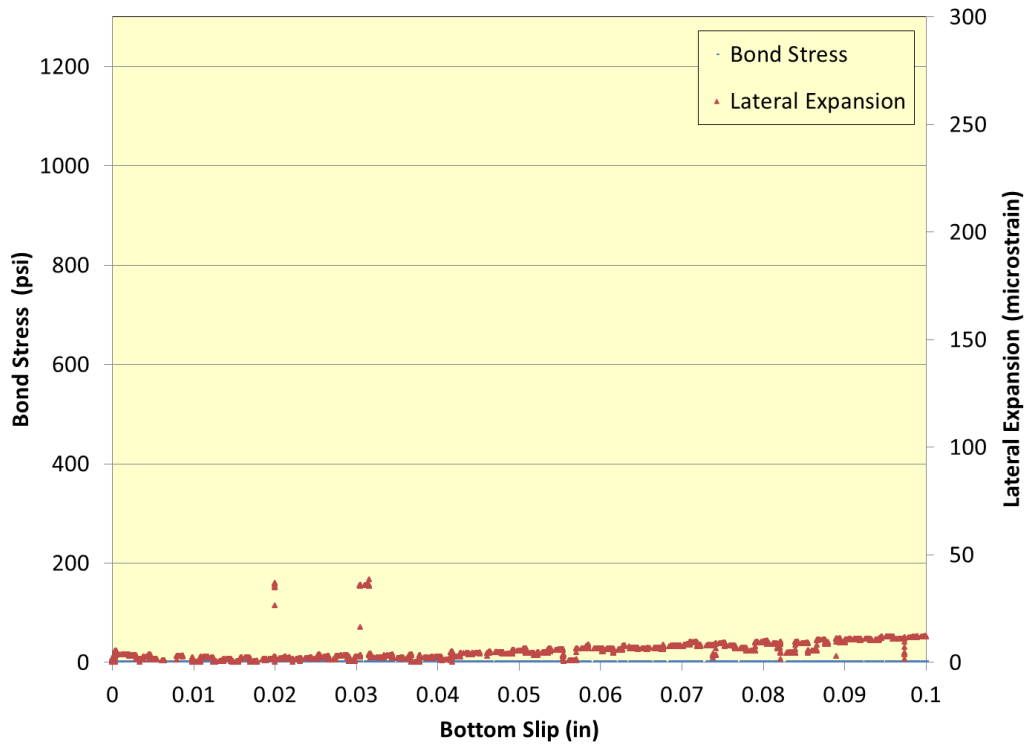
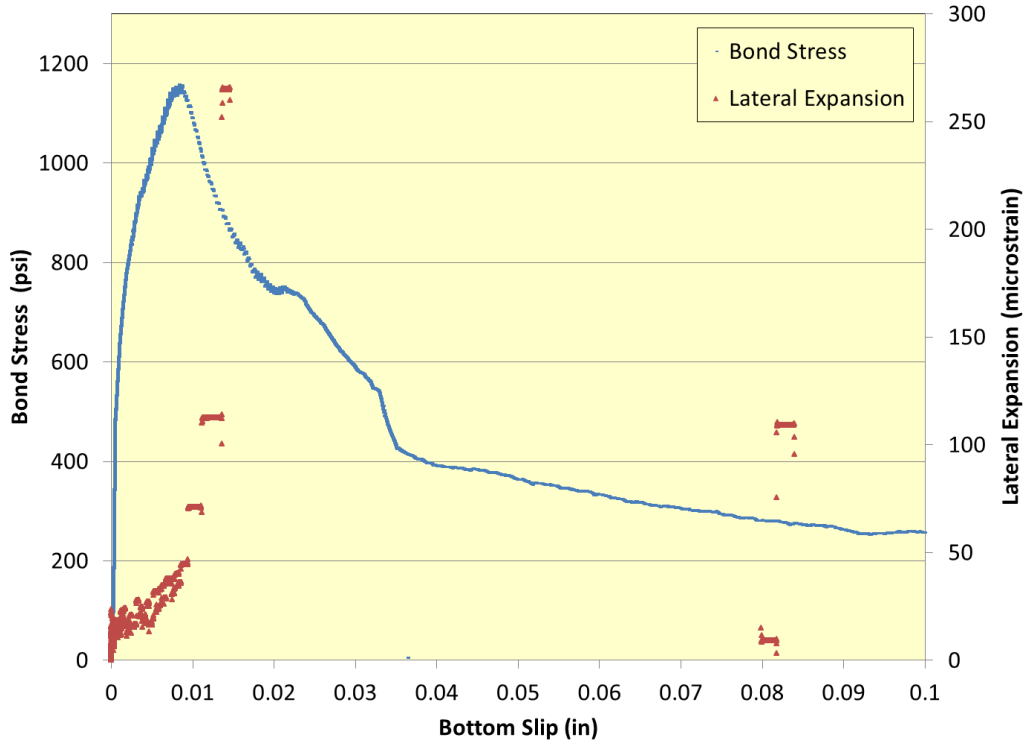
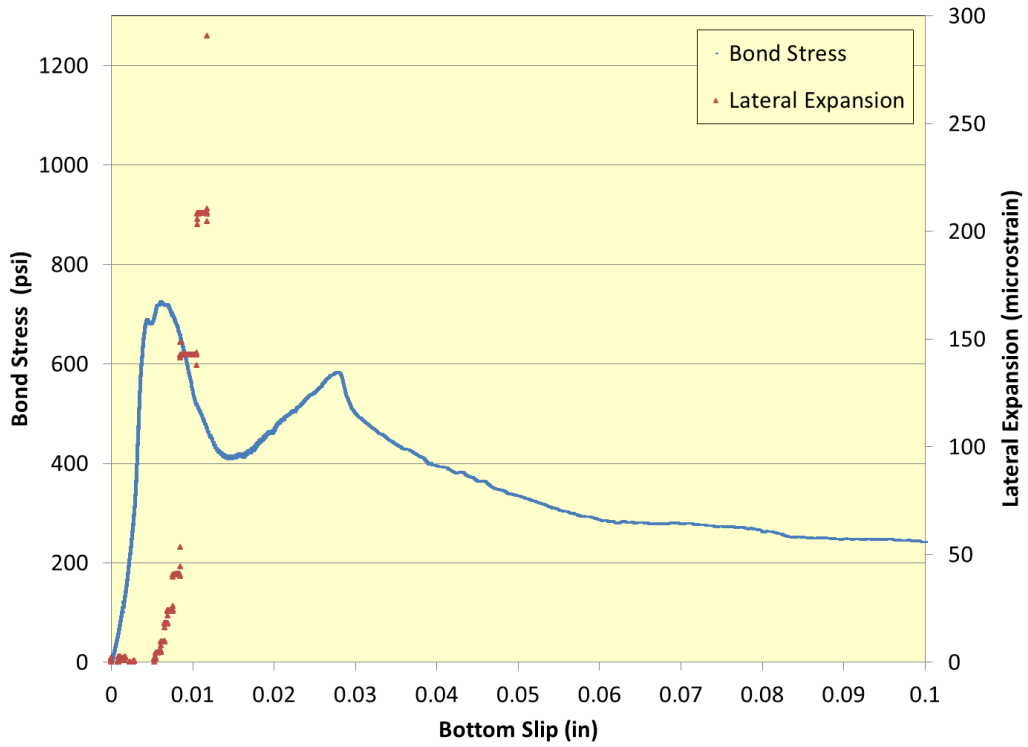


Figure C.1 Bond stress and lateral expansion relationship with bottom slip for WA



**Figure C.2 Bond stress and lateral expansion relationship with bottom slip for WE**



**Figure C.3 Bond stress and lateral expansion relationship with bottom slip for WE**

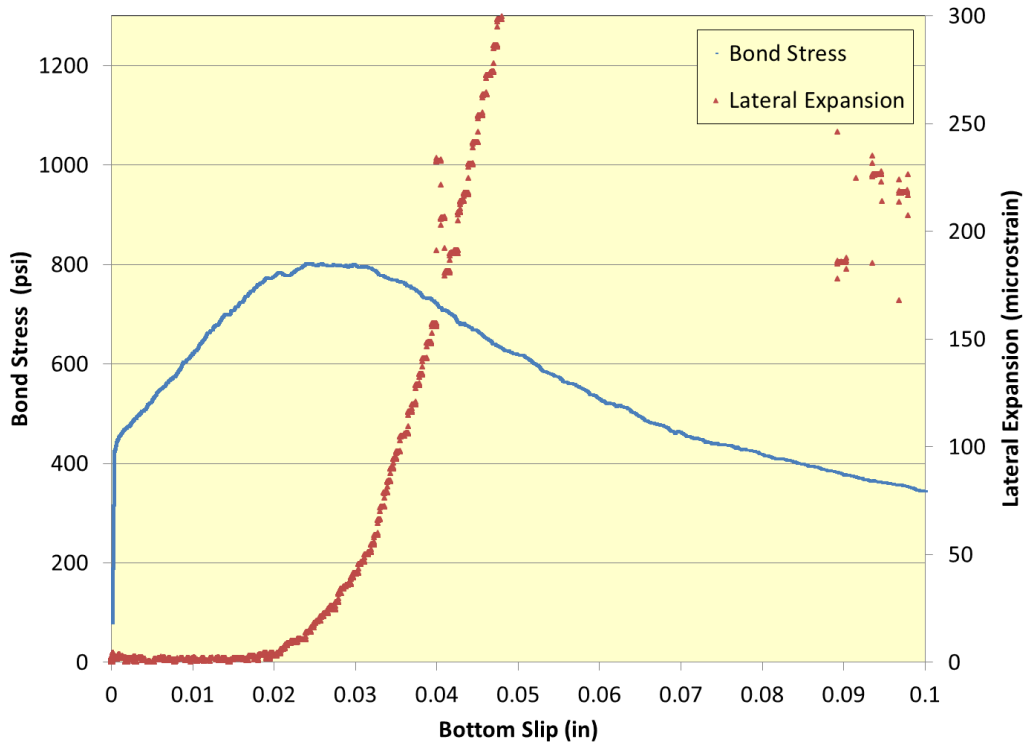


Figure C.4 Bond stress and lateral expansion relationship with bottom slip for WG

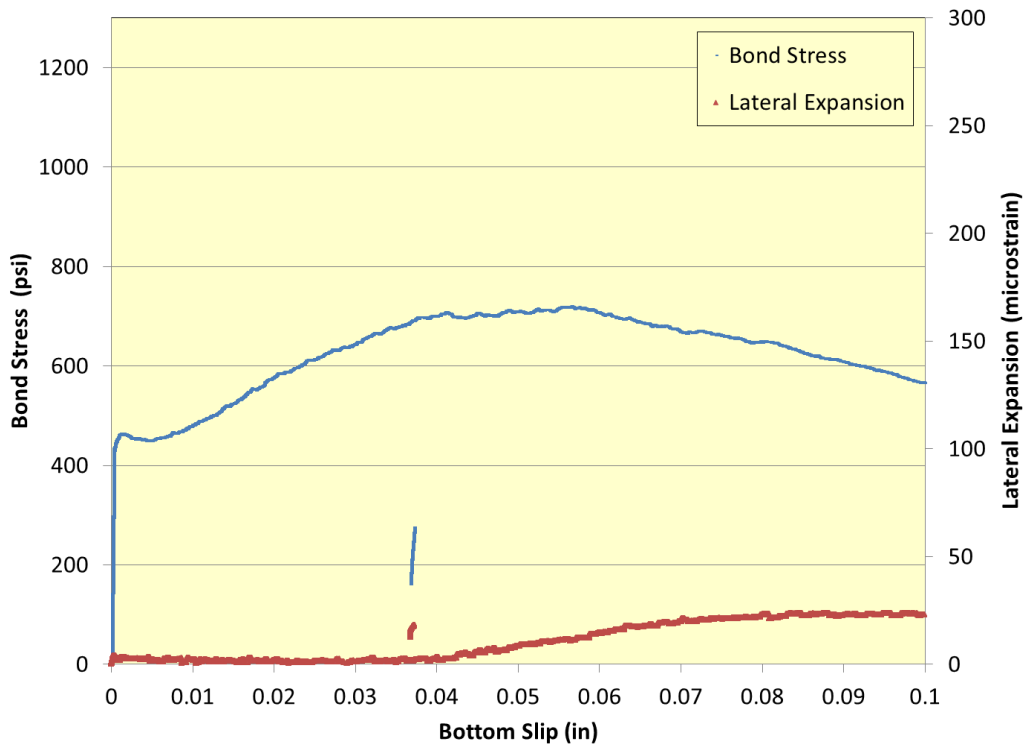
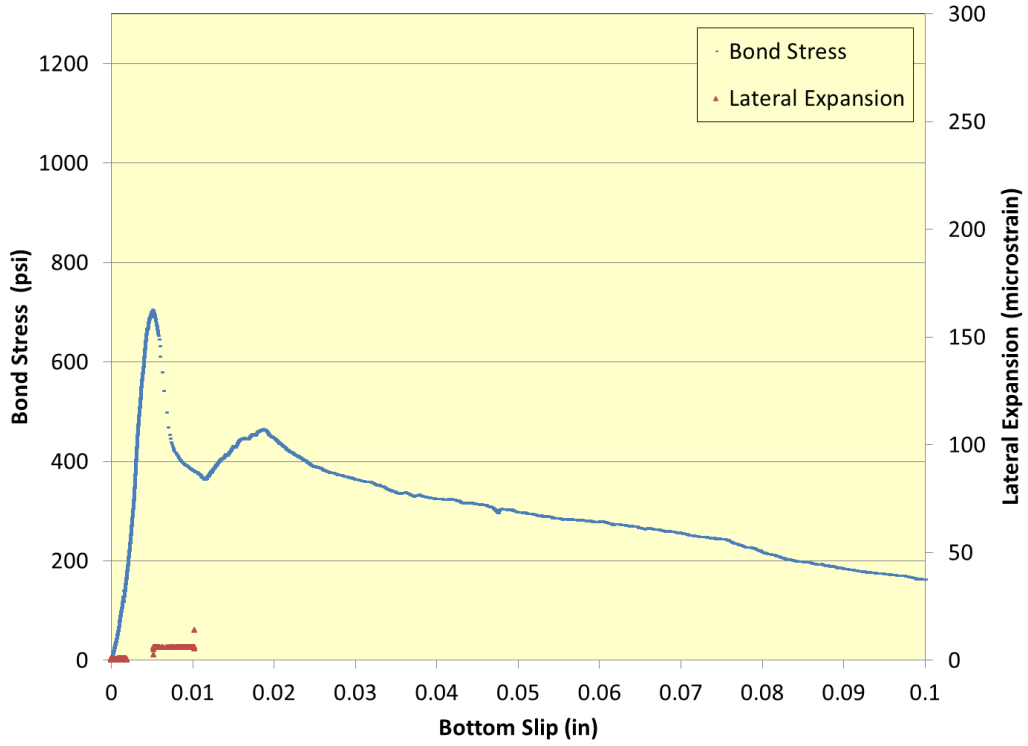
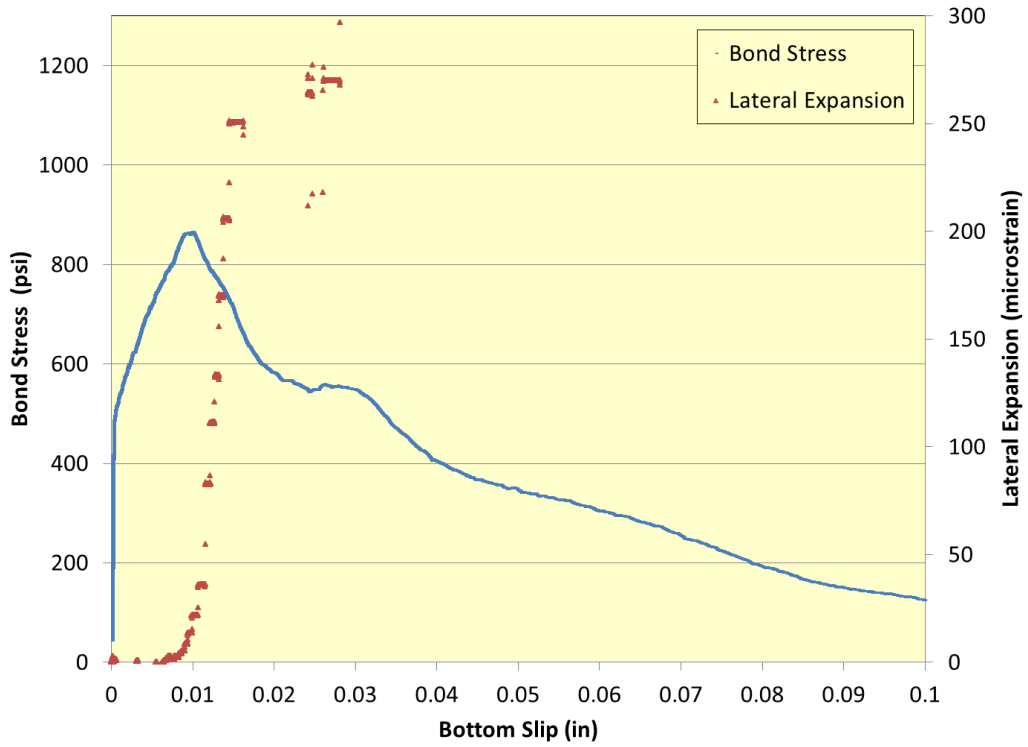


Figure C.5 Bond stress and lateral expansion relationship with bottom slip for WG



**Figure C.6 Bond stress and lateral expansion relationship with bottom slip for WH**



**Figure C.7 Bond stress and lateral expansion relationship with bottom slip for WH**

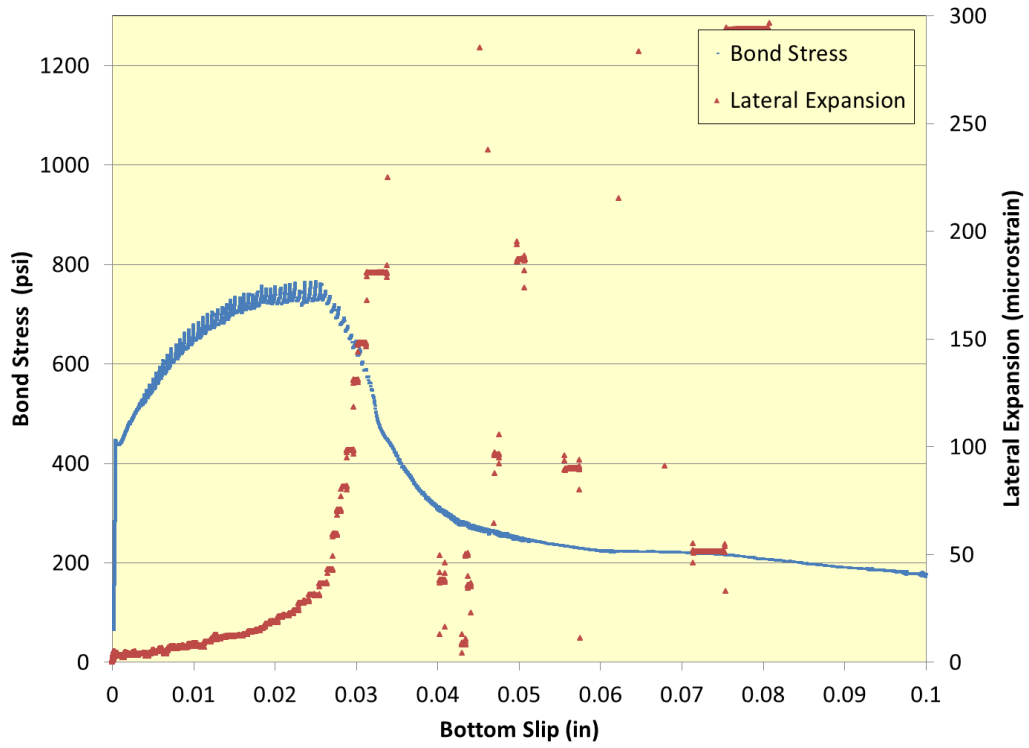


**Figure C.8 Bond stress and lateral expansion relationship with bottom slip for WK**



## Appendix D 4-Wire vs. Single Wire Test Graphs

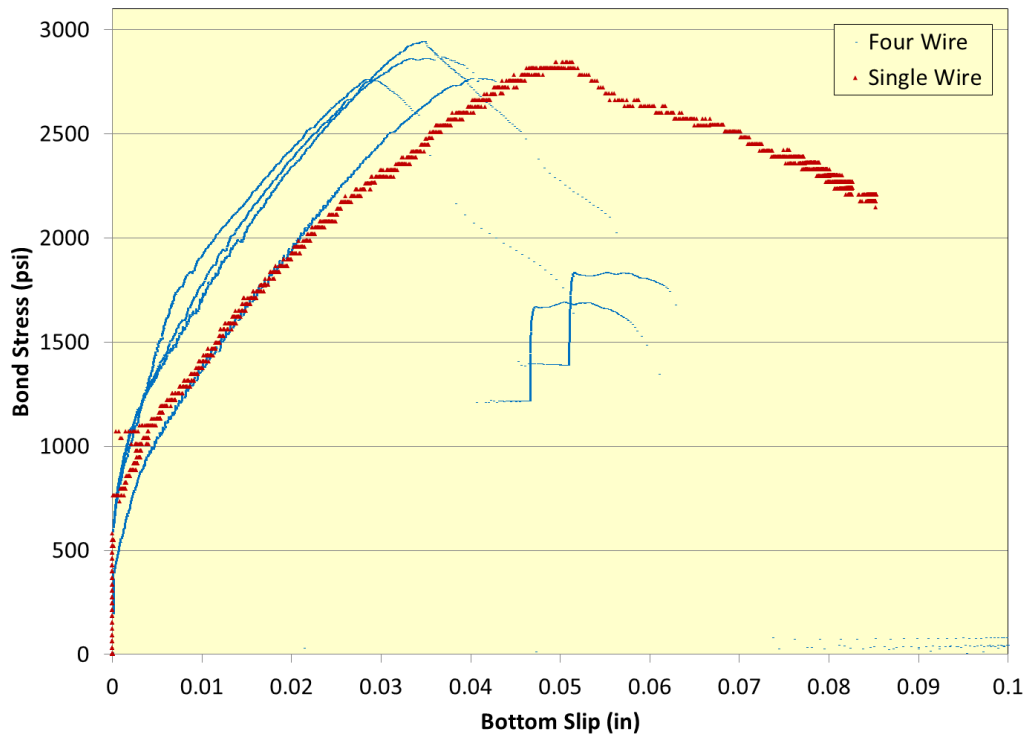
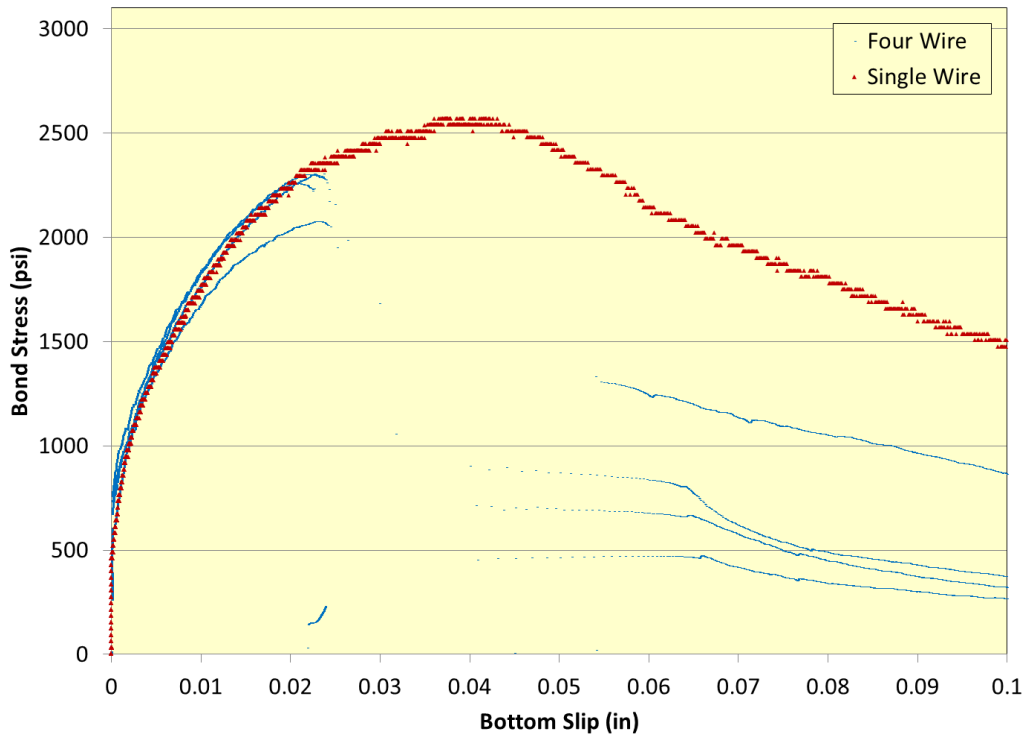


Figure D.1 Bond stress vs. bottom slip comparison for 4-wire and single wire test with WE



**Figure D.2 Bond stress vs. bottom slip comparison for 4-wire and single wire test with WH (single wire specimen had hairline crack)**

## Appendix E Plant readings

**Table E.1 Strain readings for all gauges (in microstrain)**

Gauge	After forms drop	After Detensioning	Before Cutting	After Cutting	Outside on pallets
AD1	-16	39	28	-13	-75
AD2	-4	78	76	13	5
AD3	0	124	129	142	127
AD4	5	7	-2	-9	-55
AL1	21	24	12	-15	-77
AL2	27	10	1	-3	-48
AL3	-3	113	115	140	118
AL4	29	25	17	18	-47
BD1	-15	44	35	18	-40
BD2	-9	97	95	44	1
BD3	0	2	-6	-13	-82
BD4	-3	134	137	160	136
BL1	-4	44	-	15	-38
BL2	16	56	54	26	-21
BL3	-2	139	148	168	148
BL4	13	26	19	6	-55
CD1	-4	66	57	-9	-68
CD2	-3	85	90	13	-20
CD3	0	134	140	162	130
CD4	21	16	-1	-6	-71
CL1	-16	58	49	-7	-62
CL2	-7	101	102	62	31
CL3	-4	143	149	172	146
CL4	7	-8	-27	-17	-80
DD1	-1	60	47	0	-50
DD2	-5	83	83	20	-9
DD3	-3	132	135	165	140
DD4	4	17	3	-14	-77
DL1	10	26	15	-11	-90
DL2	-5	98	100	25	-13
DL3	-1	151	162	175	160
DL4	-17	44	37	-10	-78